**University of Bath**

**PHD**

# A theory of electron-hole pair excitation in the adsorption of simple atoms on metal surfaces

Mizielinski, Matthew

*Award date:*
2007

*Awarding institution:*
University of Bath

Link to publication

## Alternative formats
If you require this document in an alternative format, please contact:
openaccess@bath.ac.uk

Copyright of this thesis rests with the author. Access is subject to the above licence, if given. If no licence is specified above, original content in this thesis is licensed under the terms of the Creative Commons Attribution-NonCommercial 4.0 International (CC BY-NC-ND 4.0) Licence (https://creativecommons.org/licenses/by-nc-nd/4.0/). Any third-party copyright material present remains the property of its respective owner(s) and is licensed under its existing terms.

**Take down policy**
If you consider content within Bath's Research Portal to be in breach of UK law, please contact: openaccess@bath.ac.uk with the details. Your claim will be investigated and, where appropriate, the item will be removed from public view as soon as possible.

Download date: 05. May. 2023

# A THEORY OF ELECTRON-HOLE PAIR EXCITATION IN THE ADSORPTION OF SIMPLE ATOMS ON METAL SURFACES

Matthew Stefan Mizielinski

A thesis submitted for the degree of Doctor of Philosophy

University of Bath

Department of Physics

March 2007

COPYRIGHT

Attention is drawn to the fact that copyright of this thesis rests with its author. This copy of the thesis has been supplied on condition that anyone who consults it is understood to recognise that its copyright rests with its author and no information derived from it may be published without the prior written consent of the author.

This thesis may be made available for consultation within the University library and may be photocopied or lent to other libraries for the purposes of consultation.

# Contents

# Acknowledgements

I would first like to thank my supervisor, Professor David Bird, to whom I am indebted for his support, guidance and enthusiasm throughout the last three and a half years. This thesis has benefited greatly from his comments on early drafts. Our collaborators at the University of Liverpool, Professors Mats Persson and Stephen Holloway have also provided valuable assistance in the development of the work presented here, as well as suggestions for interesting avenues of research.

I would also like to thank the staff and my fellow PhD students in the department of physics who have made working here an enjoyable experience.

Finally, I would like to thank my family; my parents, grandparents and uncles who have supported me throughout my life and sparked my interest in science, and my partner Elizabeth, without whom life would not be as fun.

# Abstract

Recent experiments have provided direct evidence for the excitation of electron-hole pairs during the adsorption of atoms on metal surfaces. The excitation of electron-hole pairs is an inherently non-adiabatic process which is often ignored in standard theoretical treatments of surface phenomena, using tools such as density functional theory (DFT), as the Born-Oppenheimer approximation cannot be used. To obtain a theoretical model for the electronic excitation process it is therefore necessary to go beyond conventional methods. Previous theoretical descriptions have used a nearly-adiabatic approximation to describe electronic excitations. However, these methods have been found to fail in situations where an adsorbing atom undergoes a transition between a spin-polarised and unpolarised state.

In this thesis we develop a fully non-adiabatic theory using a simple description of the adsorbate-metal interaction; the time-dependent, mean-field Newns-Anderson model. This model describes a simple electronic system in which a band of metal states interacts with a single atomic orbital, which can undergo a 'spin-transition'. We derive expressions describing the time-dependent transfer of charge and energy between the adsorbate and surface, as well as the spectrum of electronic excitations generated. Each of these results describe the evolution of the electronic system in terms of a simple set of parameters.

These results are demonstrated using a set of example parameter variations to explore the impact of variables such as adsorbate speed and the temperature of the system. A set of parameter variations describing the interaction of hydrogen isotopes with copper and silver surfaces are obtained from DFT calculations. These parameters are used to drive our model through a single approach of the adsorbate to the surface. We find the results of these calculations to be in good agreement with reported experimental results.

Our conclusions, and some possible directions for further work, are summarised in the final chapter.

# Chapter 1

# Introduction

The field of surface science occupies an important position in the modern world, with significant applications in industrial processes and technology. Heterogeneous catalysis accounts for a significant fraction of the chemical processes used in industry, for example the Haber process[1] and the oxidation of carbon monoxide and nitrous oxides by catalytic converters in the exhaust systems of motor vehicles. Technology such as the integrated circuit and the computer processor is also manufactured through the manipulation of semiconductor surfaces, the study of which has evolved in conjunction with the development of industrial processes [1].

One of the most important theoretical challenges in surface science is to develop a quantitative understanding of the process by which atoms and molecules bond to surfaces [2]. When an atom or molecule approaches a surface it is accelerated by the surface potential well in which it can gain up to a few electron-Volts of kinetic energy. However, to adsorb on a surface the atom or molecule, referred to as the adsorbate hereafter, must lose sufficient energy to prevent it from escaping from the surface potential well. This lost energy can be dissipated into various channels, for example lattice vibrations (phonons), chemiluminescence (photons), exo-electrons (electrons ejected from the surface) and electron-hole pairs (electronic excitations within the surface). Phenomena such as chemiluminescence and exo-electron excitation require substantial amounts of energy to be transferred

[1]The Haber process manufactures ammonia from nitrogen and hydrogen gas using an iron catalyst.

to a single electron or photon and are therefore generally only seen in extremely exothermic reactions such as the oxidation of alkali metal surfaces [3]. The lower energy dissipation channels of phonon and electron-hole pair excitation, however, are expected to be ubiquitous.

The importance of the reactions of diatomic molecules with surfaces to chemistry in general has lead to a large body of literature (see for example the reviews of Darling and Holloway [2] and Groß [4]). A significant fraction of this literature focuses on adsorption dynamics through the use of potential energy surfaces (PES). The PES for an interaction describes the energy gained, or lost, by an adsorbate in moving to a particular position above a surface. For diatomic (and more complicated) molecules properties such as orientation and bond length can also be included in the PES. Forces on the adsorbate are calculated from the gradient of the PES, which can then be used to investigate trajectories of an adsorption reaction. The PES for a particular interaction can be computed using ab-initio methods such as density functional theory (DFT) in combination with interpolation techniques [4]. DFT is a tool by which the electronic structure of a system can be investigated through consideration of the electron density rather than the combination of the wave-functions of the system [5]. However, to perform DFT calculations a number of approximations are commonly used; DFT is inherently a mean-field theory with correlation and exchange effects included through approximate 'exchange-correlation' functionals, the use of which is generally justified by the results obtained for physical systems.

One further approximation which is usually used in DFT, and many other quantum-mechanical calculations, is the Born-Oppenheimer approximation (BOA) [6]. In the BOA the light, fast moving electrons are assumed to react instantaneously to the motion of the much heavier and slower atomic nuclei. The electronic system therefore always remains in the ground, or adiabatic, state. The validity of the BOA is dependent on several factors [7]; (1) the rearrangement of the electronic states associated with a moving atom must be gradual, (2) the electronic states of the system must be widely separated and (3) the velocities of the atoms must be small enough to allow the electronic system to adjust to the changing conditions. In various situations these conditions are not all met, for example in high-energy scattering events or electron transfer reactions. The assumption, in the BOA, that the electronic states of the time-evolving system are the adiabatic states does, however, enable the use of an adiabatic PES to describe surface processes.

This has lead to significant gains in the understanding of adsorption and chemical reactions [4].

For interactions with metal surfaces the band of metal states, filled up to the Fermi level, invalidates the BOA through assumption (2) above. This 'Fermi sea' of electrons provides a means by which *any* amount of energy can be transferred to the surface by promoting an electron from just below the Fermi level to just above, creating an electron-hole pair. This idea that an electronically adiabatic process cannot proceed close to a metal surface is also known as the Anderson orthogonality theorem [8], and is also important in photon emission from metals. Due to this deviation from adiabatic behaviour phenomena such as electron-hole pair excitation or exo-electron emission are commonly referred to as non-adiabatic effects.

Until relatively recently the direct observation of non-adiabatic effects in surface processes has been limited to systems with large energy transfers, such as the oxidation of alkali and alkali-earth metals (see Greber [3] for a review). Such reactions can result in the ejection of exo-electrons or chemiluminescence. An early theoretical treatment of chemiluminescence phenomena in the adsorption of halogens on a sodium surface was reported by Nørskov, Newns and Lundqvist [9]. They treated the halogen-surface interaction in terms of the rapid movement of an unoccupied electronic orbital from above to below the Fermi level. This creates a pair of holes below the Fermi level, which can then be filled by electrons at higher energies through the emission of photons, or exo-electrons through Auger processes[2] [10]. Processes such as this are often described in terms of a set of diabatic states [2,3,11] in which there are multiple potential energy surfaces each representing a particular state of the system. At different positions, i.e. altitudes or bond-lengths, different 'diabats' can be the lowest, ground state. Non-adiabatic behaviour is then described by the system remaining on a diabat that is no longer the ground state as the position changes rapidly. The transition from an excited diabat to a lower energy one (or even the ground state) represents the non-adiabatic release of energy, which can manifest as an excitation of electrons or photons.

There have also been indirect observations of non-adiabatic interactions between

[2]The Auger process involves the 'annihilation' of a hole with an electron, transferring sufficient energy to an electron at or near the Fermi level such that it can escape the surface.

molecules and surfaces. Measurements of the infra-red reflection spectra of carbon monoxide molecules adsorbed on a copper (100) surface showed lifetimes for vibrational states which were several orders of magnitude shorter than would be expected for excitation of phonons in the surface [12]. Persson and Persson [13,14] used a simple model to show that the vibrational lifetime could be accounted for by coupling to the electronic structure of the surface. The mechanism they put forward involves charge flowing between the $2\pi^*$ anti-bonding orbital of the CO molecule and the surface. On interaction with the metal surface this $2\pi^*$ orbital broadens into a resonance, the position of which (relative to the Fermi level) depends on the bond-length. As the C-O bond varies in length during the oscillation a small amount of charge is transferred back and forth between the $2\pi^*$ orbital and the surface, which transfers energy to low-energy electron-hole pairs. Crude calculations of the lifetime of the vibrational state were of the same magnitude as the experimental results.

Another piece of indirect evidence for the transfer of energy to the electronic system during adsorption has been presented by Sitz and co-workers [15–17]. They investigated the rotational and vibrational de-excitation of an $H_2$ molecule as it scattered from the palladium (111) and copper (100) surfaces using pulsed molecular beams and time-resolved laser techniques. This technique allows the populations of the different rotational-vibrational states to be investigated as a function of time, along with measurements of the translational energy. Measurements of molecules de-excited after interacting with the surface show a number of transitions in which significant amounts of energy (50-100 meV) are lost by the adsorbate. It is reasonable to assume that this energy is transferred to the substrate degrees of freedom (electron-hole pairs or phonons) during the scattering event.

Two sets of recent experiments have presented direct observations of low energy ($<$2 eV) electronic excitations. In the first set, performed by Nienhaus and co-workers [18–25] electrons and holes excited to more than 0.5 eV above and below the Fermi level, respectively, have been observed through the use of molecular beams and thin-film Schottky diodes. In the second set, by White, Wodtke and co-workers [26, 27], beams of vibrationally excited NO molecules have been observed to excite substantial yields of exo-electrons from low work-function metal surfaces. These two sets of experiments are reviewed in sections 1.1.1 and 1.1.2.

The experiments of Nienhaus and co-workers have also been the subject of theoretical studies by Trail and co-workers [28, 29], using a combination of DFT and electronic friction models, and Lindenblatt, Pehlke and co-workers [30–34], using time-dependent DFT. The approaches used in these studies, and the results obtained, are discussed in sections 1.2.1 and 1.2.2.

The objective of this thesis is to describe the work we have performed in constructing a model to investigate the non-adiabatic effects in the adsorption of a simple atom (hydrogen) on a metal surface. To gain an insight into the excitation process we have developed a theory based on a simple model Hamiltonian – the Newns-Anderson model [35, 36]. This model contains a basic description of a single orbital interacting with a band of metal states, and has been widely used in the study of adsorption processes. The model itself is described in section 1.2.3 with some discussion of previous applications. An outline of the rest of this thesis is presented in section 1.3.

## 1.1 Experimental observation of electronic excitations

The observation of electronic excitations generated by the adsorption of molecules on surfaces has until recently been limited to high-energy phenomena such as chemiluminescence and exo-electron emission [2], or indirect measurements such as contributions to adsorbate sticking co-efficients and vibrational lifetimes.

However, two recent sets of experiments have directly observed the excitation of electronic states during the adsorption process; the measurement of 'chemicurrents' by Nienhaus and co-workers [18], and the observation of vibrational to electronic energy conversion by White, Wodtke and co-workers [26]. These experiments are reviewed in the following sections.

### 1.1.1 Chemicurrents

In early 1999 Nienhaus and co-workers reported direct observation of low-energy electronic excitations by exposing 'thin-film Schottky diodes' to molecular beams of various species [18]. These thin-film Schottky diodes were initially constructed by depositing around 100 Å of silver or copper on the (111) surface of a doped

silicon wafer, with electrical contacts made to both the metal film and the back of the wafer. These devices were fabricated and operated in ultra-high vacuum conditions and at low temperatures to maximise the sensitivity. At the interface between the metal film and the semiconductor the Fermi-levels of the two materials must match in equilibrium. This forces the valence and conduction bands of the silicon substrate to bend close to the surface to achieve this matching (see Sze [37] page 246), which results in a potential barrier at the interface. For n-doped silicon this leads to a Schottky barrier over which hot-electrons can pass, with p-doping producing a similar barrier for hot-holes. The barrier heights for these devices were determined from current-voltage measurements, yielding typical barrier heights in the range 0.4-0.6 eV for Ag/n-Si and 0.6-0.7 for Cu/n-Si diodes, with slightly lower values for Ag/p-Si devices.

The molecular beams used by Nienhaus and co-workers in their investigations of hydrogen adsorption consisted of a mix of $H_2$ molecules and neutral H-atoms. Typical rates of molecular interaction with the surface of the Schottky diode have been reported to be of order $10^{12}$ cm$^{-2}$ s$^{-1}$, with between 0 and 30% made up of hydrogen atoms. Upon exposure to these beams the maximum closed-loop, 'chemically-induced-reverse-current' (or chemicurrent) through the device was measured to be in the region of 1 nA for Ag/n-Si, 0.2 nA for Ag/p-Si and 20 pA for Cu/n-Si. These chemicurrents imply that the adsorption process must have a non-adiabatic component by which both hot electrons and hot holes are excited.

The mechanism for the generation of this chemicurrent is described in figure 1.1. As an adsorbate atom or molecule approaches the metal surface interactions excite electron-hole pairs which travel ballistically through the metal film. The passage through the metal film will attenuate, through scattering processes, the number of electrons/holes which reach the metal-semiconductor interface. On reaching this interface electron or holes with sufficient energy to cross the Schottky barrier have a certain probability of being detected depending on the characteristics of the interface. This process of excitation, attenuation and transmission has been considered by both Nienhaus et al. [22] and Gadzuk [38]. In this thesis we will be focusing on the excitation process.

The initial report by Nienhaus and co-workers described a number of important results. The measured chemicurrent was observed to peak shortly after the

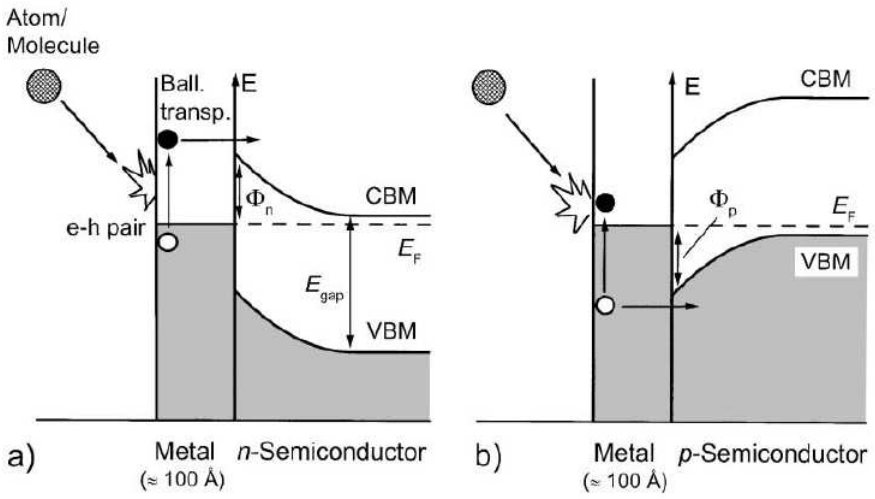


Figure 1.1: Energy level diagram (from Nienhaus [22]) describing the excitation of a current in a thin-film Schottky diode by the adsorption of an atom or molecule. Panels (a) and (b) related to diodes constructed using n- and p-doped silicon respectively. $\Phi$ is the Schottky barrier height of the diode, CBM and VBM denote the conduction band minimum and valence band maximum of the Si substrate, and $E_{\text{gap}}$ is the Si band-gap.

molecular beam is switched on with the chemicurrent decaying to a steady state value after a certain period of time. This time-variation in the chemicurrent can be explained through consideration of the dynamics of the absorption processes. As the metal surface of the device is exposed to the atomic beam the build up of adsorbed atoms reduces the number of available surface sites, limiting the rate of adsorption events, which in turn reduces the magnitude of the measured chemicurrent. Nienhaus and co-workers have also found that the metal surface and the nature of the adsorbate has a significant effect on the magnitude of the observed excitations. The magnitude of the peak chemicurrent in the adsorption of hydrogen was reported [18] to correspond to $4.5 \times 10^{-3}$ and $1.5 \times 10^{-4}$ electrons per H-atom for the Ag/n-Si and Cu/n-Si devices respectively. The differences between the two were attributed to differences in the mean-free-path of electrons in the two metals, which determines the attenuation of the signal, and the formation of scattering centres at the Cu/Si interface.

A significant isotopic effect has been observed in the generation of chemicurrents.

The initial paper published by Nienhaus and co-workers reported that the chemicurrent generated by a beam of deuterium atoms was six times smaller than for hydrogen atoms, when using an Ag/n-Si diode with a barrier height of around 0.5-0.55 eV. Mildner, Hasselbrink and Diesing [39] have also investigated this isotope effect using a metal-insulator-metal device (Au-$TaO_x$-Ta) with a barrier height in the region of 1.6 eV. They reported an isotope ratio of 4.5:1 for H:D atoms in experiments performed at room temperature (the experiments of Nienhaus and co-workers were performed at much lower temperatures). The larger mass of the D-atom, along with similar interaction properties, implies a slower approach to the surface which should generate smaller non-adiabatic effects. Recently Krix, Nünthel and Nienhaus [25] have reported a more thorough analysis of the isotope effect on chemicurrents generated by hole-excitation using Ag/p-Si(111) Schottky diodes. They found a chemicurrent ratio of 3.7±0.7:1 for hydrogen compared to deuterium using a Schottky barrier height of 0.46 eV. In chapter 7 we will compare ratios obtained from model calculations with these experimental data.

In addition to the results discussed above there have been a range of other reports using similar devices to observe electronic excitations with a wide range of different adsorbates. Gergen, Nienhaus and co-workers found a power-law correlation between the adsorption energy of a particular species and the magnitude of the chemicurrent generated [20]. The same group have demonstrated that for NO interactions with an Ag/n-Si diode there is a secondary peak in the variation of the chemicurrent with time, which is consistent with a signal from the reduction of adsorbed NO molecules to form $N_2O$ [21]. Roldan-Cuenya, Nienhaus and McFarland [40] investigated the chemicurrents generated by several molecules with low adsorption energies interacting with a metal-insulator-semiconductor device [Pd/SiO/n-Si (111)]. For molecular beams of Xe, $CO_2$ and $C_2H_4$ a forward current was observed in their devices rather than the reverse chemicurrents found in all other experiments. This they attributed to charging of electronic traps at the metal-insulator interface. Glass and Nienhaus [23, 24] have also investigated the oxidation of magnesium using Schottky diodes. They report that photon mediated excitations have a role to play in the energy transfer process, and that Schottky devices can be used as an accurate oxidation monitor.

To gain an understanding of the trends in these experiments it would be useful to have a model of the behaviour of the electronic system during adsorption. Our approach in this thesis is to consider a simple model of adsorption, the

Newns-Anderson model, to consider the basic physics of the electronic excitation process.

### 1.1.2 Conversion of vibrational to electronic excitation

Study of the interactions between vibrationally excited diatomic molecules and metal surfaces has also yielded significant evidence of non-adiabatic effects. Recently there has been considerable interest in electronic effects in the scattering of NO molecules from metal surfaces. Huang and co-workers [41] reported results for the de-excitation of an NO($\nu$=2)[3] beam on interaction with a gold surface, which could not be explained by adiabatic theory. The same group have also investigated more highly excited NO molecules interacting with Au(111) and LiF surfaces [42]. Substantial vibrational de-excitation of the NO($\nu$=15) beam was observed following the interaction with the gold surface, while for the insulating LiF surface more than 90% of incident molecules remained in their initial state.

A mechanism by which the vibrational energy is transferred to electronic excitations was put forward by Huang et al. [42]. The potential energy of the NO molecule, as constructed from a combination of spectroscopic and ab-initio data (see references in [42]), was compared to that of the $NO^-$ ion as a function of the N-O bond length. At bond-lengths at and above the equilibrium length of around 1.15 Å the NO molecule was found to be the lowest energy state, while below the equilibrium point the $NO^-$ ion was found to be the lower energy state. For an NO molecule vibrating in proximity to a metal surface, electron transfer to the molecule is energetically favourable at one point in the vibration, while half an oscillation later the reverse is true. This process has been considered in terms of the 'diabats' (see the start of this chapter) of the NO and $NO^-$ states by Huang and co-workers. The rapid oscillation of the length of the N-O bond prevents the system from occupying the lowest energy diabat at all times, which leads to high energy non-adiabatic transfers to electronic excitations as the system relaxes. The same process could not take place in the interaction of NO with an insulating surface as there is no Fermi sea of electrons which can easily be transferred to the adsorbate molecule.

Direct observations of electronic excitations during the vibrational de-excitation of NO molecules has recently been reported by White, Wodtke and co-workers

[3] I.e. a beam of molecules each with two vibrational quanta.

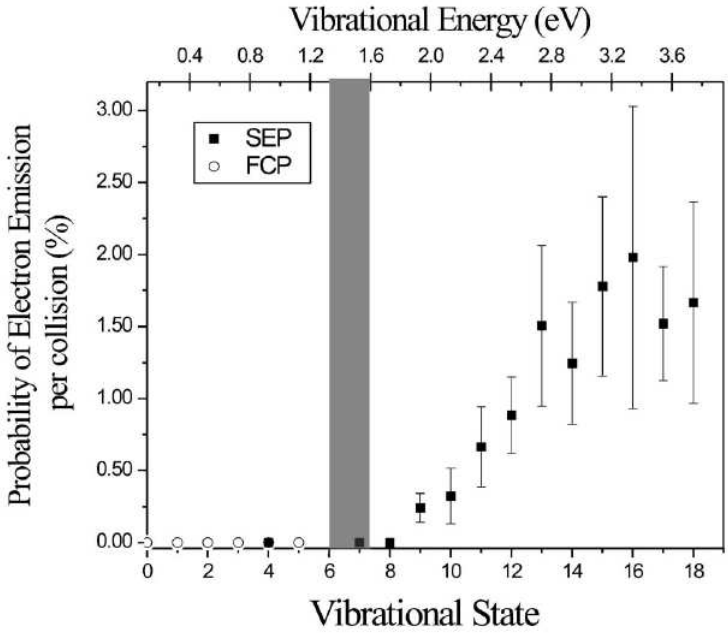


Figure 1.2: The probability of exciting an exo-electron for different vibrational states $\nu$ of an NO molecule from White, Wodtke and co-workers [27]. Open and closed symbols represent data obtained using different vibrational excitation techniques; FCP – Franck-Condon pumping, SEP – stimulated emission pumping.

[26, 27]. By replacing the Au(111) target used by Huang et al. with a low work function caesium doped gold surface[4] White, Wodtke and co-workers were able to detect electrons excited with sufficient energy to escape the surface entirely; exo-electrons. Figure 1.2, from [27], shows experimental measurements of the probability of exciting an exo-electron for different vibrational states of the NO beam. For vibrational states with a greater energy than the surface work function substantial amounts of exo-electron emission is observed. Above this point the electron emission yield per collision displays an approximately linear dependence on the vibrational energy until $\nu$=16, at which point the emission yield saturates at between 1.5 and 2%. This increase in yield with vibrational energy greater than the work-function suggests that direct conversion of vibrational to electronic excitation is occurring.

White, Wodtke and co-workers [27] have considered several different mechanisms by which exo-electron emission, at the magnitude observed, can occur. They spec-

[4]The deposition of sub-monolayer coverages of Cs atoms on an Au surface reduces the work-function to between 1.3 and 1.6 eV – below that of either metal in isolation.

ulate that the most significant contribution to the exo-electron emission comes from a process referred to as "vibrationally promoted auto-detachment". As the neutral and negative ion states of NO are each energetically favourable in different parts of the N-O bond vibration, the NO molecule could gain an electron at one point and eject it half a vibration later. If during the ejection process sufficient energy, i.e. more than the work function, is transferred from the vibrational degrees of freedom to the electron it can escape the surface.

The experimental observations discussed in this section show that electronic excitations can be an important channel for the transfer of energy during molecule-surface interactions. In the next section we consider the theoretical approaches which have been used to investigate the process of electronic excitation.

## 1.2 Theoretical modelling of electronic excitations

In order to theoretically model electronic excitations it is necessary to go beyond adiabatic, ground-state theories, which use the BOA to separate the electronic and nuclear degrees of freedom.

In this section we will discuss two examples of work in which the excitation of electronic systems has been considered. First we introduce an electronic friction based model, used by Trail and co-workers [28, 29] to estimate the probabilities of exciting the chemicurrents discussed in section 1.1.1. Second we look at some recent work by Lindenblatt, Pehlke and co-workers who have used time-dependent DFT techniques to obtain the evolution of the electronic states of the H/Al(111) system [30–34]. The final sub-section will look at the use of the Newns-Anderson model [35, 36] for describing electronic excitations.

### 1.2.1 Electronic friction based models

The evolution of a large time-dependent electronic system of any size is very difficult to compute. Probably the most straightforward way of treating the energy loss of an adsorbate to a surface during adsorption is to define a force, or set of forces, which transfers energy to the appropriate dissipation channel. The lowest order contributions to the force representing this dissipation process

are likely to be proportional to the velocity of the adsorbate, which suggests a friction-like behaviour. This frictional approach was first used by d'Agliano et al. [43] and Blandin, Nourtier and Hone [44] to describe the transfer of energy to electronic degrees of freedom in the motion of adsorbates near metal surfaces.

A friction-like approach to energy-transfer has been used by Trail and co-workers [28, 29, 45] as an approximation to the full non-adiabatic behaviour. A general expression for the non-adiabatic energy transfer is derived by assuming a linear response of the electronic system to a changing potential [29];

$$\dot{E}_{trans}(t) = \dot{s}(t) \int_{-\infty}^{t} dt' \Lambda(t - t', s) s(t'). \tag{1.1}$$

Here $\dot{E}_{trans}$ is the energy transfer rate, $s$ is a coordinate representing the position of the adsorbate and $\Lambda(t - t')$ is referred to as the memory function [29]. This 'memory function' contains information about the evolution of the system to the state occupied at time $t$. In the slow variation limit, i.e small $\dot{s}$, Trail et al. [29] show that the low frequency limit of the response of the electron gas to the adsorbate can be approximated using linear response theory, leading to

$$\tilde{\Lambda}(\omega, s) = -i\eta(s)\omega, \tag{1.2}$$

where $\tilde{\Lambda}(\omega, s)$ is the Fourier transform of $\Lambda(t, s)$ and $\eta(s)$ is a real function. By transforming (1.2) back into the time domain and substituting into (1.1) the energy transfer rate becomes

$$\dot{E}_{trans}(t) = \eta(s(t))\dot{s}(t)^2. \tag{1.3}$$

This expression can easily be shown to be equivalent to the loss of energy due to a friction force $F$;

$$F(t) = -\eta(s(t))\dot{s}(t) = -\frac{dE}{ds}(t), \tag{1.4}$$

from which it follows that

$$dE(t) = \eta(s(t))\dot{s}(t)ds = \eta(s(t))\dot{s}(t)^2 dt. \tag{1.5}$$

The function $\eta(s(t))$ is therefore commonly referred to as an electronic friction coefficient. As the slow-variation approximation for energy transfer rate $\dot{E}_{trans}(t)$

does not depend on the history of the evolution of the system electronic friction theory is commonly referred to as memory-less or Markovian.

This frictional approach to energy transfer has been used by Trail and co-workers [28,29] to model the electronic excitation of a copper (111) surface during the adsorption of hydrogen isotopes for comparison with the chemicurrent experiments discussed in section 1.1.1. They took the slow limit of time-dependent DFT in which the electronic system is assumed to remain close to the adiabatic state at all times, i.e. the system can be represented using standard DFT wave-functions and potentials. From these adiabatic quantities Trail and co-workers were able to calculate the electronic friction coefficient $\eta$ using [29];

$$\eta(s) = \pi\hbar \sum_{\sigma} \sum_{\alpha,\alpha'} \left| \langle \epsilon_F \alpha, \sigma | \frac{dV_\sigma}{ds} | \epsilon_F \alpha', \sigma \rangle \right|^2 , \tag{1.6}$$

where $\sigma$ denotes spin, $|\epsilon_F \alpha, \sigma\rangle$ are states at the Fermi surface and $V_\sigma$ is the effective Kohn-Sham potential for spin $\sigma$. The combination of this approximation with the set of assumptions described above (the slow adsorbate and low-frequency response limits) is referred to as a "nearly-adiabatic" model of electronic friction. This nearly-adiabatic model has been widely used to study damping of vibrations of adsorbed molecules (Hellsing and Persson [46]), molecular dynamics calculations (Head-Gordon and Tully [47]) and vibrational de-excitation in molecular scattering (Luntz, Persson and Sitz [48]).

By using DFT calculations to model the approach of an H-atom to the atop site of the copper (111) system Trail and co-workers [28, 29, 45] obtained the variation of the friction coefficient $\eta$ with altitude. Close to the surface, below 2 Å, calculations show a smooth variation in $\eta$, but at an altitude of $s_0$=2.39 Å the friction co-efficient diverges with an $(s - s_0)^{-1}$ behaviour above $s_0$. This singularity in $\eta$ implies an infinite rate of energy transfer away from the H-atom, and therefore an infinite stopping power, which is clearly unphysical. The altitude at which this breakdown of the nearly-adiabatic friction model occurs was found by Trail and co-workers to correspond to the position of a second-order phase transition in the spin-polarisation of the ground state of the system.

In isolation a neutral hydrogen atom has a single electron in its 1s orbital and therefore has a net spin. As the atom interacts with a metal surface, the hopping of electrons between the metal states and the adsorbate orbital broadens the en-

ergy levels associated with the initially occupied (majority spin) and unoccupied (minority spin) electronic states into resonances. These resonances broaden and converge on one another, until the majority and minority spin resonances become degenerate and the spin-polarisation is lost.

Trail et al. also demonstrated that the singularity in the friction coefficient is a direct result of the failure of the nearly-adiabatic approximation at the spin-transition. This implies that the spin-transition is a fundamentally non-adiabatic phenomenon which cannot be correctly treated by nearly-adiabatic theory. Trail and co-workers [28, 29] forced their calculations to have a particular spin-polarisation, thereby removing the spin-transition and the singularity in $\eta$.

The excitation of the metal surface was modelled by connecting the DFT derived friction co-efficient description of energy transfer with the forced oscillator model, or FOM (see Darling and Holloway [2] for a description). The FOM describes a set of harmonic oscillators driven by a time-dependent force and has been widely used in the description of electronic excitations (see for example Schönhammer and Gunnarsson [49] and Brako and Newns [50]) by assuming that the electron-hole pairs act as a single bosonic entity. This bosonic description has been shown by Schönhammer and Gunnarsson [49] to be consistent with the slow, frictional description of a fermion-based model. In the present case the time-dependent force driving the FOM comes from the motion of the adsorbate.

By making further slow-variation approximations Trail and co-workers [28, 29] related the distribution of excited electron-hole pairs to the friction coefficient, giving

$$P_s(\omega) = \sum_\sigma \frac{1}{\pi\hbar\omega} \left| \int_{-\infty}^{\infty} \eta_\sigma^{1/2}(s(t))\dot{s}(t) \exp[-i\omega t] dt \right|^2 \tag{1.7}$$

where $\hbar\omega$ is the energy of the electron-hole pair. The probability distribution $P_s$ was calculated, for H and D atoms, from the friction coefficient $\eta$ and the motion of the adsorbate during its oscillation in the surface potential well. From $P_s$ the number of electrons excited with sufficient energy to cross a barrier of a given energy was found, yielding figure 1.3 (from ref. 29). By accounting for attenuation and interfacial effects Trail and co-workers made estimates of the magnitude of the chemicurrents detected by Nienhaus and co-workers [18], giving results which agreed reasonably well with the experimental values. Comparison

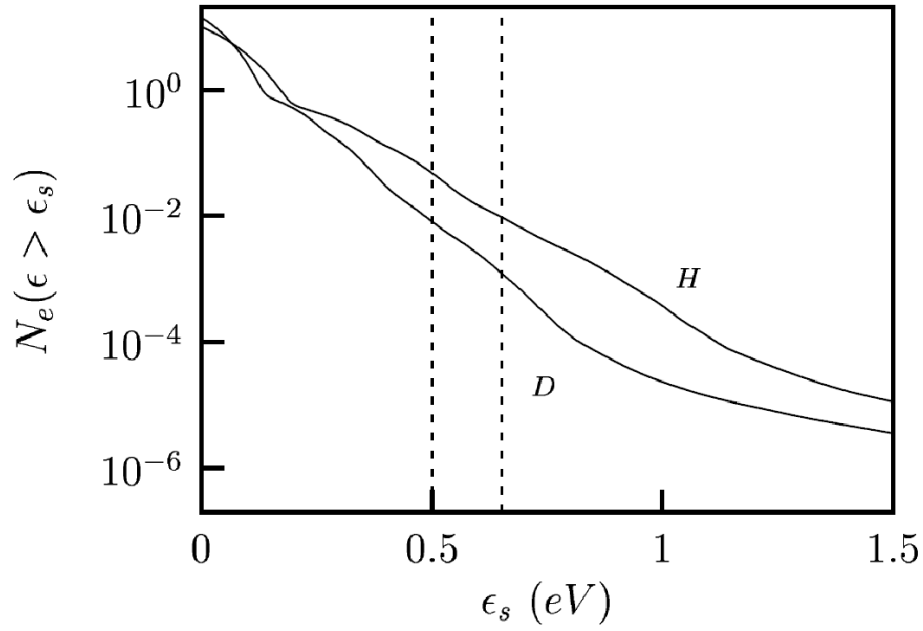


Figure 1.3: The probability of exciting an electron with sufficient energy to cross a Schottky barrier of height $\epsilon_s$ for H and D atoms incident on the top site of a Cu(111) surface (from Trail et al. [29]). The vertical lines denote the range of barrier heights found by Nienhaus et al. [18].

of the results for H and D atoms also showed an isotope effect of a similar size to that reported by Nienhaus and co-workers. It should be noted, however, that the manner in which the singularity in the friction coefficient at the spin-transition is removed is rather arbitrary. A correct treatment of the spin-transition requires a fully non-adiabatic theory – the construction of such a theory is the aim of this thesis.

### 1.2.2 Time-dependent DFT

A more rigorous, but far more computationally expensive, technique for the modelling of electronic excitation is to use a time-dependent theory to directly calculate the evolution of the electronic system. In a series of publications Lindenblatt, Pehlke and co-workers [30–34] have used time-dependent DFT (TD-DFT) to investigate the electronic excitation induced by the approach of a hydrogen atom to an aluminium (111) surface.

The principle behind the TD-DFT method used by Lindenblatt, Pehlke and co-

workers is conceptually relatively straightforward. A conventional DFT calculation is used to obtain the Kohn-Sham wave-functions and the effective potentials for a static adsorbate-surface configuration. The time-dependent Schrödinger equation is then integrated to give the evolution of the wave-functions in time, with the forces on the atomic nuclei dealt with classically using the Ehrenfest approximation. However, a number of computational issues make the application of this method more difficult. In order to consider systems such as H/Ag(111), as used in the chemicurrent experiments of Nienhaus and co-workers (see section 1.1.1), the simulation of a large number of electrons would be necessary (each silver atom has 11 valence electrons which would need to be considered). The variation of the wave-functions as the adsorbate approaches the surface is also rapid, requiring a small integration step size[5], which in turn increases the computational burden of performing a calculation.

To model the electronic excitation process while keeping the computational cost reasonable Lindenblatt, Pehlke and co-workers chose to consider the more simple H/Al(111) system (the aluminium atoms only have three valence electrons) rather than H/Ag(111). They used a $2\sqrt{3} \times 2\sqrt{3}$ supercell containing a 13 layer slab of Al atoms with two hydrogen atoms, one approaching each side of the slab, to model the adsorption process. The Al atoms were represented by pseudopotentials while a Coulomb potential was used for the H-atoms. In order to minimise the computational cost a single special $k$-point was used to perform reciprocal-space calculations, with basis-set cut-offs of 10 Rydberg (136 eV). In early work [30–33] Lindenblatt and co-workers ignored the role of spin, but more recent calculations [34] have included spin-polarisation. They also recognise that the computational parameters used to perform these calculations are substantially smaller than those commonly used to perform static DFT calculations, but state that these limitations are required to achieve reasonable time-scales for computation.

The non-adiabatic energy dissipated at a particular point in the evolution of the adsorbate-metal system was obtained by taking the difference between the energy of the time-dependent system and that obtained from relaxed, ground-state calculations. The distribution of electronic excitations was calculated by projecting the set of time-dependent wave-functions $|\psi_{i\sigma}(k,t)\rangle$ for the $n_{k\sigma}$ electrons of spin $\sigma$ onto the ground-state Kohn-sham wave-functions $|\phi_{j\sigma}(R(t),k)\rangle$ (with energies

[5]Lindenblatt and Pehlke [34] used a step-size of 0.002 fs.

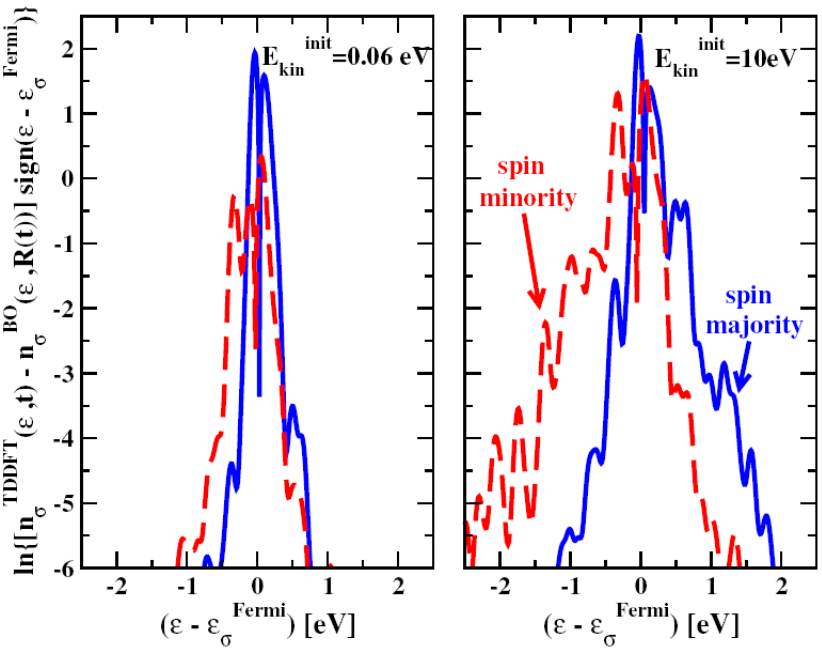


Figure 1.4: Spin-resolved excitation spectra generated by the approach of an H-atom to the Al(111) surface from time-dependent DFT calculations performed by Lindenblatt and Pehlke [34]. The two panels relate to hydrogen atoms with initial kinetic energies of 60 meV and 10 eV. Solid blue lines denote majority-spin excitations with dashed red lines representing the minority-spin component.

$\epsilon_{j\sigma}(R(t),k))$ via

$$n_\sigma(\epsilon,t) = \sum_{jk} w_k \sum_{i=1}^{n_{k\sigma}} |\langle\psi_{i\sigma}(k,t)|\phi_{j\sigma}(R(t),k)\rangle|^2 \,\delta\left(\epsilon - \epsilon_{j\sigma}(R(t),k)\right). \qquad (1.8)$$

In this expression $w_k$ is the weighting for the $k$-points used and $R(t)$ represents the set of co-ordinates of the atomic cores. The ground-state equivalent of this quantity was obtained using the adiabatic wave-functions calculated by relaxing the electronic system at a particular altitude. A similar expression to (1.8) will be used in chapter 4 to construct a model of the electronic excitations induced by the adsorption of a simple atom. However, we will represent the ground-state of the system using the eigenstates of the system at a particular point in time rather than the adiabatic states. The difference between these two representations of the ground-state of the system is discussed on page 88.

The calculations performed by Lindenblatt and Pehlke have produced a number of interesting results. Calculations of the energy lost by an H-atom in a single

round trip show that the spin-transition is important; when including spin the energy loss is approximately 0.18 eV [34] compared to 0.04 eV for unpolarised computations [33]. The excitation spectra calculated were found to be broadly exponential in nature, with some noise due to computational limitations. As might be expected, H-atoms with large amounts of kinetic energy were found to generate larger spectra at high energies; an example of this is shown in figure 1.4. These results, from ref. 34, also show a distinct polarisation of the excitation spectra; the majority-spin spectrum is larger for high-energy electrons than that for minority-spin excitations, with the reverse true for holes. This effect will be explored further in chapter 6.

While the TD-DFT methods used by Lindenblatt, Pehlke and co-workers can give a detailed description of the behaviour of the electronic system, the computational effort involved in performing simulations restricts the accuracy which can be achieved. We have chosen to take an alternative path by describing electronic excitations in the adsorbate-metal system using a simplified model; the Newns-Anderson model. This model is described in the following section, along with a discussion of some previous work which has used it.

### 1.2.3 Newns-Anderson models

One relatively simple model which has been widely used in the past to model the adsorbate-metal interaction is the Newns-Anderson model [35, 36]. This model was initially constructed by Anderson [35] to consider the interaction of magnetic impurities with a non-magnetic, metallic medium, and was later applied to chemisorption by Newns [36]. The model describes the occupied and unoccupied electronic states of a metal surface and an adsorbate orbital, plus the interaction between the two and the Coulomb repulsion energy associated with multiple occupation of the adsorbate orbital. The Newns-Anderson model was originally constructed using a time-independent Hamiltonian;

$$\begin{aligned} \hat{H} &= \sum_{\sigma} \epsilon_a \hat{n}_{a\sigma} + \sum_{k\sigma} \epsilon_{k\sigma} \hat{n}_{k\sigma} + \sum_{k\sigma} \left( V_{ak} \hat{c}^{\dagger}_{a\sigma} \hat{c}_{k\sigma} + \text{H.c} \right) \\ &\quad + U \hat{n}_{a\sigma} \hat{n}_{a-\sigma}, \end{aligned} \tag{1.9}$$

where $a$ and $k$ label the adsorbate and metal states, and $\sigma$ denotes spin. $\hat{c}^{\dagger}_{a\sigma}$ and $\hat{c}^{\dagger}_{k\sigma}$ are the electron creation operators for the adsorbate and metal states respectively, which are used to construct the number operators $\hat{n}_{a\sigma} = \hat{c}^{\dagger}_{a\sigma}\hat{c}_{a\sigma}$,

$\hat{n}_{k\sigma} = \hat{c}^{\dagger}_{k\sigma}\hat{c}_{k\sigma}$. The energies $\epsilon_a$ and $\epsilon_{k\sigma}$ correspond to the adsorbate and metal states respectively. $V_{ak}$ is the interaction energy, representing the coupling between the adsorbate and metal states, and $U$ is the Coulomb repulsion energy associated with having two electrons in the adsorbate orbital. The model has been extended to include time-dependence by allowing $\epsilon_a$ and $V_{ak}$ to be time-dependent (for a review see Brako and Newns [51] and Yoshimori and Makoshi [52]).

The application of (1.9) is complicated by the final term, which contains the product $\hat{n}_{a\sigma}\hat{n}_{a-\sigma} \equiv \hat{c}^{\dagger}_{a\sigma}\hat{c}_{a\sigma}\hat{c}^{\dagger}_{a-\sigma}\hat{c}_{a-\sigma}$. The quantum mechanical expectation value of this four electron operator product is difficult to deal with. Both Anderson and Newns used a mean-field, or Hartree-Fock, approximation to avoid this problem in which the energy level of the adsorbate is renormalised to an effective energy level and the problematic operator product is replaced using expectation values of the operators, i.e. $\langle\langle\hat{n}_{a\sigma}\rangle\rangle\langle\langle\hat{n}_{a-\sigma}\rangle\rangle$. This approximation is also equivalent to the representation of the electronic system by the density of electrons rather than their wave-functions in DFT. The mean-field approximation is described in more detail in chapter 2.

The mean-field approximation is not, however, satisfactory for many situations as it discards all correlated electron behaviour, which leads to phenomena such as the Kondo effect [53]. To avoid this approximation the majority of work which has used the time-dependent Newns-Anderson model has set $U = 0$, which has the effect of neglecting spin [51, 52].

The adsorption process has been investigated within the Newns-Anderson model by Langreth and co-workers [54–56] without using the mean-field approximation. Their model was constructed using a 'slave-boson' approximation in which a fictitious boson is created when an electron hops from the adsorbate to the metal, and is annihilated when it hops back. Langreth and co-workers obtained expressions describing the time-evolution of the charge transfer between multiple adsorbate levels and the metal surface. However, their method is limited to situations in which the Coulomb repulsion energy $U$ is very large, and cannot therefore be applied to 'real' adsorption phenomena.

The mean-field Newns-Anderson model provides a framework within which the spin-transition seen by Trail and co-workers [29] can be described (see section 1.2.1). Anderson [35] originally demonstrated that there are magnetic and non-

magnetic domains in the parameter space of his model. Makoshi, Kawai and Yoshimori [57, 58] used the the time-dependent mean-field model to consider charge transfer in adsorption, focusing on oscillations in the occupations of the adsorbate orbital. More recently Bird, Trail, Persson and Holloway [59] have used a mean-field, time-dependent version of the Newns-Anderson model to consider non-adiabatic behaviour in the region around the spin-transition. In this thesis we extend this work to include a broader description of the adsorbate-metal interaction, from which the excitation process can be studied.

## 1.3 Thesis outline

In the following chapters we derive expressions describing the behaviour of the electronic states of the adsorbate-metal system using the Newns-Anderson model. Chapters 2 to 4 contain derivations of the set of functions which describe the occupied electronic states of the system, the energy lost by an adsorbate during adsorption and the spectrum of electronic excitations generated by the adsorption process.

The following two chapters, 5 and 6, present and discuss numerical results for the charge and energy transfer, and the excitation spectra respectively. In chapter 7 we apply these models to a pair of real systems; through DFT calculations we obtain suitable parameters to describe the adsorption of an H-atom on the copper (111) and silver (111) surfaces. These parameters have been used to drive the model described in chapters 2-4, with the results used to make quantitative comparisons to the experiments of Nienhaus and co-workers discussed above.

The final chapter 8 contains a summary of the work presented here, along with a discussion of the important implications of this work and some directions for further investigation.

Throughout this thesis there are nine appendices containing additional derivations and methods important to our model and its application. To maintain clarity we have chosen to place these appendices immediately following the chapter to which they relate.

The work presented in this thesis has also been published in two papers [60, 61];

- "Electronic nonadiabatic effects in the adsorption of hydrogen atoms on metals" by M. S. Mizielinski, D. M. Bird, M. Persson and S. Holloway, in the Journal of Chemical Physics **122**(8), 084710 (2005).
- "Spectrum of electronic excitations due to the adsorption of atoms on metal surfaces" by M. S. Mizielinski, D. M. Bird, M. Persson and S. Holloway, in the Journal of Chemical Physics **126**(3), 034705 (2007).

Work from parts of chapters 2, 3, 5 and 7 appear in the first paper. The second paper contains a brief description of the work in chapter 4 and some of the results from chapter 6. A number of results from chapters 6 and 7 will be the subject of forthcoming publications.

# Chapter 2

# The Newns-Anderson model and occupation functions

In this chapter we introduce the Newns-Anderson model and use it to derive expressions describing the time-evolution of the occupied electronic states of the system for a simple, single-orbital adsorbate as it interacts with an ideal metal surface.

The Newns-Anderson model was originally constructed by Anderson [35] to explore the properties of magnetic impurities in metals, and was later applied by Newns to the adsorbate-metal system [36]. In both works all time-dependence of the model was ignored, and the results obtained were the adiabatic or ground-state solutions, as discussed in the introduction. In this thesis we are interested in the non-adiabatic behaviour of the adsorbate-metal system and therefore need to consider both the adiabatic and time-evolving systems. Our use of the Newns-Anderson model allows us to analyse the time-evolution of electronic structure of the adsorbate-metal system, whilst being simple enough to study analytically. The model only considers a single adsorbate orbital, the metal states, the interaction between the adsorbate and the metal surface, and the interaction between electrons within the adsorbate orbital. We are therefore ignoring a wide range of phenomena including the motion of the atomic cores of the metal (lattice vibrations and surface deformation) and interactions between electrons within the metal.

The time-dependent Newns-Anderson Hamiltonian can be written in the Heisenberg picture as

$$\begin{aligned}\hat{H}(t) &= \sum_{\sigma} \epsilon_a(t)\hat{n}_{a\sigma}(t) + \sum_{k\sigma} \epsilon_{k\sigma}\hat{n}_{k\sigma}(t) + \sum_{k\sigma} \left( V_{ak}(t)\hat{c}^{\dagger}_{a\sigma}(t)\hat{c}_{k\sigma}(t) + \text{H.c.} \right) \\ &\quad + U\hat{n}_{a\sigma}(t)\hat{n}_{a-\sigma}(t), \end{aligned} \tag{2.1}$$

where $a$ labels the adsorbate state, $k$ the metal states and $\sigma$ represents spin. $\hat{c}^{\dagger}_{a\sigma}(t)$ and $\hat{c}^{\dagger}_{k\sigma}(t)$ are the electron creation operators for the adsorbate and metal states respectively. These operators are used to construct the number operators $\hat{n}_{a\sigma}(t) = \hat{c}^{\dagger}_{a\sigma}(t)\hat{c}_{a\sigma}(t)$ and $\hat{n}_{k\sigma}(t) = \hat{c}^{\dagger}_{k\sigma}(t)\hat{c}_{k\sigma}(t)$, which appear in this Hamiltonian. The energies $\epsilon_a$ and $\epsilon_{k\sigma}$ correspond to the energies of the adsorbate and metal states respectively. $V_{ak}$ is the interaction potential, i.e. the hopping matrix element for the transition between the metal state $k$ and the adsorbate state. $U$ is the intra-adsorbate Coulomb repulsion energy, and represents the energy required to add a second electron into the adsorbate orbital.

The Newns-Anderson model is parameterised by the time-evolution of the energy level $\epsilon_a$ and the interaction potential $V_{ak}$, and the value of the Coulomb repulsion energy $U$. Throughout this work we have chosen for simplicity to ignore the time-dependence of $U$. The energy level $\epsilon_a$ will vary as the adsorbate approaches the surface through image charge and surface barrier effects (Zangwill [10] page 215). $V_{ak}$ will also vary with altitude as the overlap of the adsorbate and metal orbitals change.

The direct solution of (2.1) is difficult due to the four operator product in the final term, $\hat{n}_{a\sigma}\hat{n}_{a-\sigma} = \hat{c}^{\dagger}_{a\sigma}\hat{c}_{a\sigma}\hat{c}^{\dagger}_{a-\sigma}\hat{c}_{a-\sigma}$. The method we use to avoid this problem is the same as that used by both Anderson and Newns; a mean-field approximation. This approximation assumes that each electron 'sees' the average state of the rest of the system, and is used widely in computational techniques such as density functional theory (DFT). The use of the mean-field approximation in electronic structure calculations was discussed in the introduction.

In the mean-field approximation the four operator product is replaced with

$$\hat{n}_{a\sigma}(t)\hat{n}_{a-\sigma}(t) = \hat{n}_{a\sigma}(t)n_{a-\sigma}(t) + n_{a\sigma}(t)\hat{n}_{a-\sigma}(t) - n_{a\sigma}(t)n_{a-\sigma}(t), \tag{2.2}$$

where $n_{a\sigma}(t) = \langle\langle \hat{n}_{a\sigma}(t) \rangle\rangle$ is the thermally averaged expectation value of the ad-

sorbate number operator. We will refer to these thermally averaged expectation values, such as $n_{a\sigma}(t)$, as the "occupation functions" of the system. In section 2.2 expressions describing the evolution of these occupation functions will be derived. The mean-field equivalent of (2.1) therefore becomes

$$\begin{aligned}\hat{H}_{MF}(t) &= \sum_{\sigma} \bar{\epsilon}_{a\sigma}(t)\hat{n}_{a\sigma}(t) + \sum_{k,\sigma} \epsilon_{k\sigma}\hat{n}_{k\sigma}(t) + \sum_{k,\sigma}(V_{ak}(t)\hat{c}^{\dagger}_{a\sigma}(t)\hat{c}_{k\sigma}(t) + \text{H.c.}) \\ &\quad -Un_{a\sigma}(t)n_{a-\sigma}(t), \end{aligned} \tag{2.3}$$

where the effective adsorbate energy level $\bar{\epsilon}_{a\sigma}$ is defined as

$$\bar{\epsilon}_{a\sigma}(t) = \epsilon_a(t) + Un_{a-\sigma}(t). \tag{2.4}$$

The use of the mean-field approximation also allows us to separate the Hamiltonian into single spin components. We choose to rewrite (2.3) as

$$\hat{H}_{MF}(t) = \sum_{\sigma} \hat{H}_{\sigma}(t) - Un_{a\sigma}(t)n_{a-\sigma}(t) \tag{2.5}$$

where $\hat{H}_{\sigma}$ is the single spin Hamiltonian

$$\hat{H}_{\sigma}(t) = \bar{\epsilon}_{a\sigma}(t)\hat{n}_{a\sigma}(t) + \sum_{k} \epsilon_{k\sigma}\hat{n}_{k\sigma}(t) + \sum_{k} \left(V_{ak}(t)\hat{c}^{\dagger}_{a\sigma}(t)\hat{c}_{k\sigma}(t) + \text{H.c}\right). \tag{2.6}$$

This separation implies that we can consider the mean-field Newns-Anderson system as a pair of single spin systems coupled through the mean-field energy level $\bar{\epsilon}_{a\sigma}$. The second term in (2.5) is then only involved when considering the total energy of the system.

We are primarily interested in using this model to describe the interaction of a single orbital, spin-polarised adsorbate, such as a hydrogen atom, with a metal surface. To achieve this we consider an adsorbate with two energy levels corresponding to the spins $\sigma =\uparrow$ and $\sigma =\downarrow$. Before the interaction between the adsorbate and the surface has occurred one of these states will be occupied and the other unoccupied. The choice of spin to assign to the initially occupied level is arbitrary – we choose to define the $\sigma =\uparrow$ level, $\bar{\epsilon}_{a\uparrow}$, to be this level, which will also be referred to as the majority level. The other level with spin $\sigma =\downarrow$, $\bar{\epsilon}_{a\downarrow}$, is therefore the initially unoccupied or minority level.

The adiabatic interaction of the adsorbate resonances with the surface is described

graphically in figure 2.1. For a large adsorbate altitude the adsorbate orbital consists of the energy levels $\bar{\epsilon}_{a\uparrow}$ and $\bar{\epsilon}_{a\downarrow}$ separated by the Coulomb repulsion energy $U$. As the adsorbate approaches the surface the energy levels broaden into resonances, of width $\Gamma$, through interactions with the metal states. The broadening of the resonances causes some charge to be lost from the initially fully occupied majority level to the metal as the tail of the resonance crosses the Fermi level. The same process also broadens the initially unoccupied energy level, which gains charge from the surface. $\epsilon_a$ is also expected to fall due to the image charge effects and surface barrier shifts mentioned previously. From the definition of $\bar{\epsilon}_{a\sigma}$, (2.4), we see that the loss of charge from the majority state causes the minority level to fall. The majority level also rises due to the gain of charge by the minority level. At a particular altitude this transfer of charge between the adsorbate resonances and the surface results in a transition from two distinct energy levels to a degenerate state. This spin-transition was first discussed by Anderson [35] in the context of magnetic impurities in metals. We will derive expressions describing the adiabatic behaviour of the adsorbate in section 2.3

The shape of the adsorbate resonances, or the projected density of states (PDOS) onto the adsorbate orbital, can be calculated using ab-initio methods such as DFT. The mean-field nature of DFT allows us to connect these calculations with the mean-field Newns-Anderson model. These DFT generated PDOS are not perfectly Lorentzian, as we shall show in chapter 7, but this model does broadly describe the observed distributions. From these calculated PDOS we can extract the adiabatic effective energy levels $\bar{\epsilon}^{(ad)}_{a\sigma}$, from which $\epsilon_a$ and $U$ can be found, together with the resonance width $\Gamma$. We will demonstrate the extraction of these parameters in chapter 7 for two systems; a hydrogen atom above the copper and silver surfaces.

In the rest of this chapter we introduce the theory necessary to explore the time-dependent behaviour of the occupations of the various states of the Newns-Anderson system in the region of the spin-transition. In section 2.1, and appendix A, we derive expressions for the electron operators $\hat{c}_{a\sigma}(t)$ and $\hat{c}_{k\sigma}(t)$. These results are then used to derive the time-evolving occupation functions for the Newns-Anderson system in section 2.2. This set of functions will be necessary for the work presented in chapters 3 and 4. An expression for the adiabatic adsorbate occupation function is derived in section 2.3. The important results of this chapter are summarised in section 2.4.

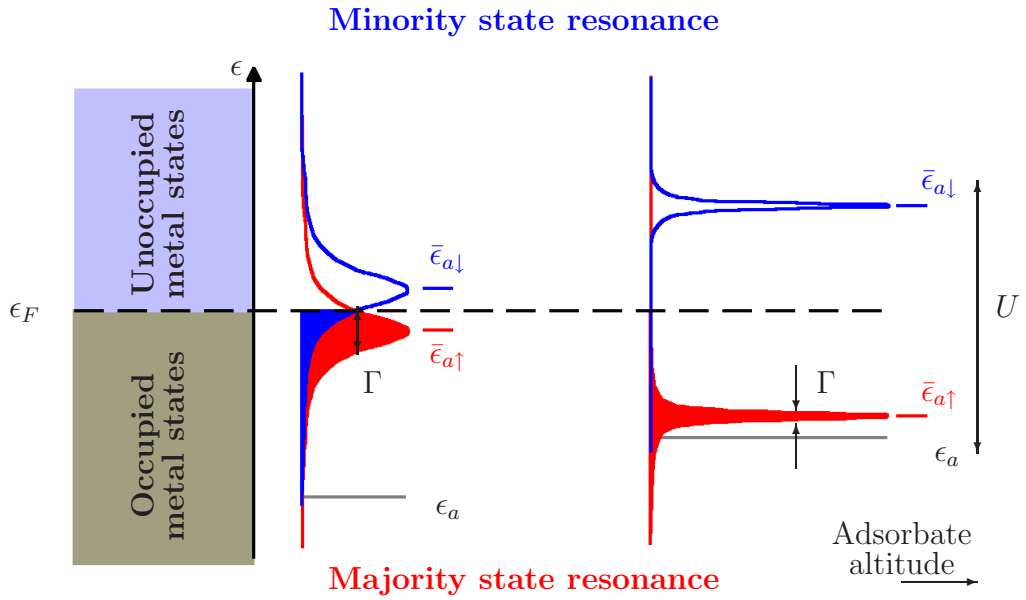


Figure 2.1: Schematic diagram of the behaviour of the energy-levels/resonances of the adsorbate as it interacts with the metal surface. The red line denotes the $\sigma =\uparrow$ majority spin resonance, and the blue line the $\sigma =\downarrow$ minority level. The shaded section of each resonance indicates the occupied states of the adsorbate. The resonances are centred on the effective energy levels $\bar{\epsilon}_{a\uparrow}$ and $\bar{\epsilon}_{a\downarrow}$ as labelled. The adsorbate resonance width is labelled $\Gamma$ and the intra-adsorbate Coulomb repulsion energy $U$ is also indicated. The grey line labelled $\epsilon_a$ denotes the bare adsorbate energy level energy. $\epsilon_F$ is the Fermi level.

## 2.1 Electron operators

In this section we derive expressions for the time-evolution of the electron operators $\hat{c}_{a\sigma}$ and $\hat{c}_{k\sigma}$.

The equations which govern the time-evolution of the operators $\hat{c}_{a\sigma}$ and $\hat{c}_{k\sigma}$ in (2.3) can be found using Heisenberg's equation of motion. These equations are derived in appendix A at the end of this chapter yielding the following differential equations (see (A.7a) and (A.7b) on page 52);

$$i\frac{d}{dt}\hat{c}_{a\sigma}(t) = \bar{\epsilon}_{a\sigma}(t)\hat{c}_{a\sigma}(t) + \sum_k V_{ak}(t)\hat{c}_{k\sigma}(t), \tag{2.7a}$$

$$i\frac{d}{dt}\hat{c}_{k\sigma}(t) = \epsilon_{k\sigma}\hat{c}_{k\sigma}(t) + V^*_{ak}(t)\hat{c}_{a\sigma}(t). \tag{2.7b}$$

In order to solve these equations we make a set of assumptions, commonly referred to as the wide-band approximation [62]. We first assume that $V_{ak}(t)$ can be separated into a complex constant $v_{ak}$ and a real, state-independent, time-dependent function $u(t)$, i.e.

$$V_{ak}(t) = v_{ak}u(t). \tag{2.8}$$

In making this approximation it is assumed that the variation with time of the interaction potential is identical for all metal states $k$, with differences only in the total magnitude and phase. We then assume that the sum

$$\sum_k |v_{ak}|^2\delta(\epsilon - \epsilon_{k\sigma}), \tag{2.9}$$

is independent of energy $\epsilon$. This expression can be interpreted as the distribution of states in the metal which interact with the adsorbate, and by using this approximation we assume that this distribution is flat. We are therefore assuming that the electronic structure of the metal surface consists of a wide band of states without any structure, with which the adsorbate energy levels can interact. This is a significant assumption, but is necessary to allow us to make progress.

The validity of the use of the wide-band approximation has been investigated by Burrows and Amos [62]. They conclude that provided the energy level interacting with the metal is not close to the edge of the band, and the metal density of states is not rapidly varying, then the wide-band approximation is reasonable. However, Plihal and Langreth [63] argue that the restriction in the variation of

the phase of $V_{ak}$ in (2.8) is valid only for motion perpendicular to the surface. The acceleration of the adsorbate in the surface potential well will result in a perpendicular approach to the surface for small initial kinetic energies. Throughout this work we therefore only consider a perpendicular approach of the adsorbate to the surface, so our use of (2.8) should be reasonable.

By using the wide-band approximation the equations of motion for the electron operators can be solved, as shown in appendix A. We find the following expressions for $\hat{c}_{a\sigma}$ and $\hat{c}_{k\sigma}$, see (A.26) and (A.27);

$$\begin{aligned}\hat{c}_{a\sigma}(t) &= -i\int_{t_0}^{t} dt_1 \exp\left[-i\int_{t_1}^{t}\tilde{\epsilon}_{a\sigma}(t')dt'\right]\sum_k V_{ak}(t_1)\exp\left[-i\epsilon_{k\sigma}(t_1-t_0)\right]\hat{c}_{k\sigma}(t_0) \\ &\quad + \exp\left[-i\int_{t_0}^{t}\tilde{\epsilon}_{a\sigma}(t')dt'\right]\hat{c}_{a\sigma}(t_0), \end{aligned} \tag{2.10}$$

$$\begin{aligned}\hat{c}_{k\sigma}(t) &= -\int_{t_0}^{t} dt_1 V_{ak}^*(t_1)\exp\left[-i\epsilon_{k\sigma}(t-t_1)\right]\int_{t_0}^{t_1} dt_2 \exp\left[-i\int_{t_2}^{t_1}\tilde{\epsilon}_{a\sigma}(t')dt'\right] \\ &\qquad \times\sum_{k'} V_{ak'}(t_2)\exp\left[-i\epsilon_{k'\sigma}(t_2-t_0)\right]\hat{c}_{k'\sigma}(t_0) \\ &\quad -i\int_{t_0}^{t} dt_1 V_{ak}^*(t_1)\exp[-i\epsilon_{k\sigma}(t-t_1)]\exp\left[-i\int_{t_0}^{t_1}\tilde{\epsilon}_{a\sigma}(t')dt'\right]\hat{c}_{a\sigma}(t_0) \\ &\quad + \exp[-i\epsilon_{k\sigma}(t-t_0)]\hat{c}_{k\sigma}(t_0), \end{aligned} \tag{2.11}$$

where $t_0$ is an initial reference time, $\tilde{\epsilon}_{a\sigma}$ is defined as

$$\tilde{\epsilon}_{a\sigma}(t) = \bar{\epsilon}_{a\sigma}(t) - i\frac{\Gamma(t)}{2}, \tag{2.12}$$

and $\Gamma$ is defined using (2.9) as

$$\Gamma(t) = 2\pi\sum_k |V_{ak}(t)|^2\delta(\epsilon-\epsilon_{k\sigma}). \tag{2.13}$$

We will show in section 2.3 that $\Gamma(t)$ is the width of the adsorbate resonance.

## 2.2 Occupation functions

In this section we use the results of the previous section to derive expressions for the time-evolving, or dynamical, occupation functions of the Newns-Anderson

system.

It will be shown in later chapters that the required occupation functions for the Newns-Anderson system are defined by

$$n_{a\sigma}(t) = \langle\langle \hat{c}^{\dagger}_{a\sigma}(t)\hat{c}_{a\sigma}(t)\rangle\rangle, \tag{2.14a}$$

$$n_{ak\sigma}(t) = n^{*}_{ka\sigma}(t) = \langle\langle \hat{c}^{\dagger}_{a\sigma}(t)\hat{c}_{k\sigma}(t)\rangle\rangle, \tag{2.14b}$$

$$n_{kk'\sigma}(t) = \langle\langle \hat{c}^{\dagger}_{k\sigma}(t)\hat{c}_{k'\sigma}(t)\rangle\rangle, \tag{2.14c}$$

where (as discussed above) $\langle\langle..\rangle\rangle$ denotes the thermally averaged expectation value of the enclosed operator. Expressions for these functions can be obtained using $\hat{c}_{a\sigma}$ and $\hat{c}_{k\sigma}$, which were derived in the previous section. Before doing this we define the reference time $t_0$, which appears in (2.10) and (2.11), as a point prior to any interaction between the adsorbate and the metal, i.e. $V_{ak}(t_0) \equiv 0$ and therefore $\Gamma(t_0) \equiv 0$. In this case the adsorbate and substrate systems are completely decoupled and the occupation functions at $t_0$ simply become the unperturbed thermal averages

$$n_{a\sigma}(t_0) = f(\bar{\epsilon}_{a\sigma}(t_0)), \qquad n_{ak\sigma}(t_0) = n^{*}_{ka\sigma}(t_0) = 0, \qquad n_{kk'\sigma}(t_0) = \delta_{k,k'} f(\epsilon_{k\sigma}), \tag{2.15}$$

where $f$ denotes the Fermi distribution function at temperature $T$, and $\delta_{k,k'}$ is the Kronecker delta function.

In the following subsections we use these definitions to derive expressions for the occupation functions $n_{a\sigma}$, $n_{ak\sigma}$ and $n_{kk'\sigma}$.

### 2.2.1 The adsorbate occupation function, $n_{a\sigma}(t)$

The dynamical adsorbate occupation function $n_{a\sigma}$ follows easily from the expression for $\hat{c}_{a\sigma}$. By combining (2.10), (2.14a) and (2.15) we find

$$\begin{aligned} n_{a\sigma}(t) = & \int_{t_0}^{t} dt_1 \int_{t_0}^{t} dt_2 \exp\left[i\int_{t_1}^{t} \tilde{\epsilon}^{*}_{a\sigma}(t')dt'\right] \exp\left[-i\int_{t_2}^{t} \tilde{\epsilon}_{a\sigma}(t')dt'\right] \\ & \times \sum_{k,k'} V^{*}_{ak}(t_1)V_{ak'}(t_2)\exp[i\epsilon_{k\sigma}(t_1-t_0) - i\epsilon_{k'\sigma}(t_2-t_0)]\delta_{k,k'} f(\epsilon_{k\sigma}) \\ & + \left|\exp\left[-i\int_{t_0}^{t} \tilde{\epsilon}_{a\sigma}(t')dt'\right]\right|^2 n_{a\sigma}(t_0), \end{aligned} \tag{2.16}$$

which, after simplification and the introduction of an energy integral and corresponding delta function in the first term, gives

$$\begin{aligned} n_{a\sigma}(t) &= \int_{t_0}^{t} dt_1 \int_{t_0}^{t} dt_2 \exp\left[i\int_{t_1}^{t} \tilde{\epsilon}^{*}_{a\sigma}(t')dt'\right] \exp\left[-i\int_{t_2}^{t} \tilde{\epsilon}_{a\sigma}(t')dt'\right] \\ &\qquad \times \int d\epsilon f(\epsilon) \exp[i\epsilon(t_1 - t_2)] \sum_k V^{*}_{ak}(t_1) V_{ak}(t_2) \delta(\epsilon - \epsilon_{k\sigma}) \\ &\quad + n_{a\sigma}(t_0) \exp\left[-\int_{t_0}^{t} \Gamma(t')dt'\right]. \end{aligned} \tag{2.17}$$

The identity (A.14) in appendix A can be used to replace the sum over metal states $k$ in this expression. Equation (2.17) can then be rearranged to give

$$\begin{aligned} n_{a\sigma}(t) &= \int d\epsilon f(\epsilon) \left| \int_{t_0}^{t} dt_1 \sqrt{\frac{\Gamma(t_1)}{2\pi}} \exp\left[-i\epsilon t_1 - i\int_{t_1}^{t} \tilde{\epsilon}_{a\sigma}(t')dt'\right] \right|^2 \\ &\quad + n_{a\sigma}(t_0) \exp\left[-\int_{t_0}^{t} \Gamma(t')dt\right]. \end{aligned} \tag{2.18}$$

We now introduce the phase factor $\exp[i\epsilon t]$ inside the modulus in the first term of (2.18). Our final result for $n_{a\sigma}$ therefore becomes

$$n_{a\sigma}(t) = \int d\epsilon f(\epsilon) |p_\sigma(\epsilon, t)|^2 + n_{a\sigma}(t_0) \exp\left[-\int_{t_0}^{t} \Gamma(t')dt'\right], \tag{2.19}$$

where the quantity $p_\sigma$ is defined as

$$p_\sigma(\epsilon, t) = \int_{t_0}^{t} dt_1 \sqrt{\frac{\Gamma(t_1)}{2\pi}} \exp\left[-i\int_{t_1}^{t} (\tilde{\epsilon}_{a\sigma}(t') - \epsilon)dt'\right]. \tag{2.20}$$

The introduction of the phase factor into (2.18), and consequently $p_\sigma$, is useful in the derivation of the other occupation functions in the following sub-sections. This factor also aids the numerical computation of $p_\sigma$ and hence $n_{a\sigma}$, as will be discussed in chapter 5. It is important to note at this point that $p_\sigma$ depends on the occupation function of opposite spin $n_{a-\sigma}$ through $\tilde{\epsilon}_{a\sigma}$ (see (2.4) and (2.12)). This interdependence requires that when performing numerical computations we maintain consistency between the occupation function $n_{a\sigma}$ and the quantity $p_\sigma$.

The form of $n_{a\sigma}$ has some interesting features. The first term in (2.19) can be interpreted as the integral over the occupied states of a dynamically evolving PDOS. However, from the definition of $p_\sigma$, (2.20), we can see that this dynamical PDOS is initially zero for all energies as $\Gamma(t_0) \equiv 0$. As the width $\Gamma$ increases from

zero the dynamical PDOS evolves as the second, 'transient' term decays from its initial value. This transfer of charge to the PDOS term from the transient term is important for the evolution of the spin-polarisation of the system. If the transient term is neglected the occupation function $n_{a\sigma}$ evolves quickly to a spin-degenerate state. This occurs because the occupation function $n_{a\sigma}$ and the effective energy level $\bar{\epsilon}_{a\sigma}$ are interdependent – if the occupations are identical then the energy levels are degenerate and the system is spin-unpolarised. The transient term is therefore vitally important for the evolution of the spin-polarisation of an adsorbate.

Equivalent expressions to (2.19) for a single level system have been reported previously. Blandin, Nourtier and Hone [44] were the first to derive an equivalent of the PDOS term in (2.19) using a Keldysh formalism. A very similar derivation to that above, except for the explicit inclusion of spin, was developed by Brako and Newns [64], who used their one-level model to consider the ionisation of sodium atoms scattered from a tungsten surface. Langreth and Nordlander [54] have also developed a "master equation" for charge transfer using Green's functions which is equivalent to that developed by Brako and Newns for a single level.

Makoshi, Kawai and Yoshimori [52, 57] used a spin-dependent model to consider charge transfer, based on the work of Blandin et al. However they, as Blandin before them, did not include the transient term in (2.19), and induced a separation of the spin-dependent energy levels through a fictitious magnetic field. More recently Bird et al. [59] derived a spin-polarised model for the occupations, which was driven only by variation in the bare adsorbate energy level $\epsilon_a$. They achieved spin-polarisation by evolving $n_{a\sigma}$ numerically from an initial adiabatic state.

### 2.2.2 Metal state occupation functions I: $n_{ak\sigma}(t)$

We next derive an expression for the dynamical occupation function $n_{ak\sigma}(t)$. By combining (2.10) and (2.11) with (2.14b) we find

$$\begin{aligned} n_{ak\sigma}(t) &= -i\int_{t_0}^{t}dt_1\int_{t_0}^{t}dt_2\int_{t_0}^{t_2}dt_3 V_{ak}^{*}(t_2)\exp[-i\epsilon_{k\sigma}(t_2-t_0)] \\ &\quad\times\exp\left[i\int_{t_1}^{t}\tilde{\epsilon}_{a\sigma}^{*}(t')dt' - i\int_{t_3}^{t_2}\tilde{\epsilon}_{a\sigma}(t')dt'\right] \\ &\quad\times\sum_{k',k''}V_{ak'}^{*}(t_1)V_{ak''}(t_3)\exp[i\epsilon_{k'\sigma}(t_1-t_0)]\exp[-i\epsilon_{k''\sigma}(t_3-t_0)] \\ &\quad\times f(\epsilon_{k'\sigma})\delta_{k',k''} \\ &\quad+i\int_{t_0}^{t}dt_1\exp\left[i\int_{t_1}^{t}\tilde{\epsilon}_{a\sigma}^{*}(t')dt'\right]\sum_{k'}V_{ak'}^{*}(t_1)\exp[i\epsilon_{k'\sigma}(t_1-t_0)] \\ &\quad\times\exp[-i\epsilon_{k\sigma}(t-t_0)]f(\epsilon_{k\sigma})\delta_{k,k'} \\ &\quad-i\int_{t_0}^{t}dt_1 V_{ak}^{*}(t_1)\exp[-i\epsilon_{k\sigma}(t-t_1)]\exp\left[-i\int_{t_0}^{t_1}\tilde{\epsilon}_{a\sigma}(t')dt'\right] \\ &\quad\times\exp\left[i\int_{t_0}^{t}\tilde{\epsilon}_{a\sigma}^{*}(t')dt'\right]n_{a\sigma}(t_0). \end{aligned} \tag{2.21}$$

The sum over metal states $(k', k'')$ in the first term of this equation can be simplified by introducing an energy integral and the delta function $\delta(\epsilon-\epsilon_{k'\sigma})$ to give

$$\int d\epsilon f(\epsilon)\exp[i\epsilon(t_1-t_3)]\sum_{k'}V_{ak'}^{*}(t_1)V_{ak'}(t_3)\delta(\epsilon-\epsilon_{k'\sigma}). \tag{2.22}$$

By using (A.14) this expression can be rewritten as

$$\frac{\sqrt{\Gamma(t_1)\Gamma(t_3)}}{2\pi}\int d\epsilon f(\epsilon)\exp[i\epsilon(t_1-t_3)], \tag{2.23}$$

and (2.21) becomes

$$\begin{aligned} n_{ak\sigma}(t) &= -i\int_{t_0}^{t} dt_2 V_{ak}^*(t_2)\exp[-i\epsilon_{k\sigma}(t-t_2)]\int d\epsilon f(\epsilon) \\ &\quad \times \int_{t_0}^{t} dt_1 \sqrt{\frac{\Gamma(t_1)}{2\pi}}\exp\left[i\int_{t_1}^{t}\tilde{\epsilon}_{a\sigma}^*(t')dt' + i\epsilon t_1\right] \\ &\quad \times \int_{t_0}^{t_2} dt_3 \sqrt{\frac{\Gamma(t_3)}{2\pi}}\exp\left[-i\int_{t_3}^{t_2}\tilde{\epsilon}_{a\sigma}(t')dt' - i\epsilon t_3\right] \\ &\quad + if(\epsilon_{k\sigma})\int_{t_0}^{t} dt_1 V_{ak}^*(t_1)\exp\left[i\int_{t_1}^{t}(\tilde{\epsilon}_{a\sigma}^*(t')-\epsilon_{k\sigma})dt'\right] \\ &\quad - in_{a\sigma}(t_0)\exp\left[-\int_{t_0}^{t}\Gamma(t')dt'\right] \\ &\quad \times \int_{t_0}^{t} dt_1 V_{ak}^*(t_1)\exp\left[i\int_{t_1}^{t}(\tilde{\epsilon}_{a\sigma}(t')-\epsilon_{k\sigma})dt'\right], \end{aligned} \tag{2.24}$$

where we have rewritten $\tilde{\epsilon}_{a\sigma}^*$ in terms of $\tilde{\epsilon}_{a\sigma}$ using $\tilde{\epsilon}_{a\sigma}^* = \bar{\epsilon}_{a\sigma} + i\Gamma/2 = \tilde{\epsilon}_{a\sigma} + i\Gamma$. We now use the definition of $p_\sigma$, (2.20), to obtain our final expression for $n_{ak\sigma}$;

$$\begin{aligned} n_{ak\sigma}(t) &= -i\int_{t_0}^{t} dt_1 V_{ak}^*(t_1)\int d\epsilon f(\epsilon) p_\sigma^*(\epsilon,t)p_\sigma(\epsilon,t_1)\exp[i(\epsilon-\epsilon_{k\sigma})(t-t_1)] \\ &\quad + if(\epsilon_{k\sigma})\int_{t_0}^{t} dt_1 V_{ak}^*(t_1)\exp\left[i\int_{t_1}^{t}(\tilde{\epsilon}_{a\sigma}^*(t')-\epsilon_{k\sigma})dt'\right] \\ &\quad - in_{a\sigma}(t_0)\exp\left[-\int_{t_0}^{t}\Gamma(t')dt'\right] \\ &\quad \times \int_{t_0}^{t} dt_1 V_{ak}^*(t_1)\exp\left[i\int_{t_1}^{t}(\tilde{\epsilon}_{a\sigma}(t')-\epsilon_{k\sigma})dt'\right]. \end{aligned} \tag{2.25}$$

This function is not easy to interpret physically, but it will be necessary to obtain expressions for the non-adiabatic energy transfer rate (chapter 3) and the distribution of occupied electronic states (chapter 4).

### 2.2.3 Metal state occupation functions II: $n_{kk'\sigma}(t)$ and $n_{k\sigma}(t)$

The occupation function $n_{kk'\sigma}$ is derived from (2.11) and (2.14c), yielding

$$
\begin{aligned}
n_{kk'\sigma}(t) = & \\
& \int_{t_0}^{t} dt_1 V_{ak}(t_1) \exp[i\epsilon_{k\sigma}(t-t_1)] \int_{t_0}^{t_1} dt_2 \exp\left[i\int_{t_2}^{t_1} \tilde{\epsilon}^*_{a\sigma}(t')dt'\right] \\
& \quad \times \int_{t_0}^{t} dt_3 V^*_{ak'}(t_3) \exp[-i\epsilon_{k'\sigma}(t-t_3)] \int_{t_0}^{t_3} dt_4 \exp\left[-i\int_{t_4}^{t_3} \tilde{\epsilon}_{a\sigma}(t')dt'\right] \\
& \quad \times \sum_{k'',k'''} V^*_{ak''}(t_2) V_{ak'''}(t_4) \exp[i\epsilon_{k''\sigma}(t_2-t_0)] \exp[i\epsilon_{k'''\sigma}(t_4-t_0)] \\
& \quad \times \delta_{k'',k'''} f(\epsilon_{k''\sigma}) \\
& - \int_{t_0}^{t} dt_1 V_{ak}(t_1) \exp[i\epsilon_{k\sigma}(t-t_1)] \\
& \quad \times \int_{t_0}^{t_1} dt_2 \exp\left[i\int_{t_2}^{t_1} \tilde{\epsilon}^*_{a\sigma}(t')dt'\right] \exp[-i\epsilon_{k'\sigma}(t-t_0)] \\
& \quad \times \sum_{k''} V^*_{ak''}(t_2) \exp[i\epsilon_{k''\sigma}(t_2-t_0)] \delta_{k'',k'} f(\epsilon_{k'\sigma}) \\
& - \int_{t_0}^{t} dt_1 V^*_{ak'}(t_1) \exp[-i\epsilon_{k'\sigma}(t-t_1)] \\
& \quad \times \int_{t_0}^{t_1} dt_2 \exp\left[-i\int_{t_2}^{t_1} \tilde{\epsilon}_{a\sigma}(t')dt'\right] \exp[i\epsilon_{k\sigma}(t-t_0)] \\
& \quad \times \sum_{k''} V_{ak''}(t_2) \exp[-i\epsilon_{k''\sigma}(t_2-t_0)] \delta_{k'',k} f(\epsilon_{k\sigma}) \\
& + n_{a\sigma}(t_0) \int_{t_0}^{t} dt_1 V_{ak}(t_1) \exp[i\epsilon_{k\sigma}(t-t_1)] \exp\left[i\int_{t_0}^{t_1} \tilde{\epsilon}^*_{a\sigma}(t')dt'\right] \\
& \quad \times \int_{t_0}^{t} dt_2 V^*_{ak'}(t_2) \exp[-i\epsilon_{k'\sigma}(t-t_2)] \exp\left[-i\int_{t_0}^{t_2} \tilde{\epsilon}_{a\sigma}(t')dt'\right] \\
& + f(\epsilon_{k\sigma})\delta_{k,k'}.
\end{aligned}
\tag{2.26}
$$

The sum over states $(k'', k''')$ in the first term of this equation can be simplified in an identical manner to the first term in $n_{ak\sigma}$ (see (2.21) to (2.23) in the previous

section and (A.14) in appendix A). Equation (2.26) then becomes

$$
\begin{aligned}
n_{kk'\sigma}(t) = & \\
& \int d\epsilon f(\epsilon) \int_{t_0}^{t} dt_1 V_{ak}(t_1) \exp[i\epsilon_{k\sigma}(t-t_1)] \\
& \quad \times \int_{t_0}^{t_1} dt_2 \sqrt{\frac{\Gamma(t_2)}{2\pi}} \exp\left[ i \int_{t_2}^{t_1} \tilde{\epsilon}^*_{a\sigma}(t')dt' + i\epsilon t_2 \right] \\
& \quad \times \int_{t_0}^{t} dt_3 V^*_{ak'}(t_3) \exp[-i\epsilon_{k'\sigma}(t-t_3)] \\
& \quad \times \int_{t_0}^{t_3} dt_4 \sqrt{\frac{\Gamma(t_4)}{2\pi}} \exp\left[ -i \int_{t_4}^{t_3} \tilde{\epsilon}_{a\sigma}(t')dt' - i\epsilon t_4 \right] \\
& - f(\epsilon_{k'\sigma}) \int_{t_0}^{t} dt_1 V_{ak}(t_1) \exp[i(\epsilon_{k\sigma} - \epsilon_{k'\sigma})(t-t_1)] \\
& \quad \times \int_{t_0}^{t_1} dt_2 V^*_{ak'}(t_2) \exp\left[ i \int_{t_2}^{t_1} (\tilde{\epsilon}^*_{a\sigma}(t') - \epsilon_{k'\sigma})dt' \right] \\
& - f(\epsilon_{k\sigma}) \int_{t_0}^{t} dt_1 V^*_{ak'}(t_1) \exp[i(\epsilon_{k\sigma} - \epsilon_{k'\sigma})(t-t_1)] \\
& \quad \times \int_{t_0}^{t_1} dt_2 V_{ak}(t_2) \exp\left[ -i \int_{t_2}^{t_1} (\tilde{\epsilon}_{a\sigma}(t') - \epsilon_{k\sigma})dt' \right] \\
& + n_{a\sigma}(t_0) \exp[i(\epsilon_{k\sigma} - \epsilon_{k'\sigma})(t-t_0)] \int_{t_0}^{t} dt_1 V_{ak}(t_1) \exp\left[ i \int_{t_0}^{t_1} (\tilde{\epsilon}^*_{a\sigma}(t') - \epsilon_{k\sigma})dt' \right] \\
& \quad \times \int_{t_0}^{t} dt_2 V^*_{ak'}(t_2) \exp\left[ -i \int_{t_0}^{t_2} (\tilde{\epsilon}_{a\sigma}(t') - \epsilon_{k'\sigma})dt' \right] \\
& + f(\epsilon_{k\sigma})\delta_{k,k'}. \qquad (2.27)
\end{aligned}
$$

This expression can be simplified by using the definition of $p_\sigma$, (2.20), in the first term, yielding

$$
\begin{aligned}
n_{kk'\sigma}(t) = & \\
& \int d\epsilon f(\epsilon) \int_{t_0}^{t} dt_1 V_{ak}(t_1) p^*_\sigma(\epsilon, t_1) \exp[-i(\epsilon_{k\sigma} - \epsilon)(t_1 - t)] \\
& \quad \times \int_{t_0}^{t} dt_2 V^*_{ak'}(t_2) p_\sigma(\epsilon, t_2) \exp[i(\epsilon_{k'\sigma} - \epsilon)(t_2 - t)] \\
& - f(\epsilon_{k'\sigma}) \int_{t_0}^{t} dt_1 V_{ak}(t_1) \exp[i(\epsilon_{k\sigma} - \epsilon_{k'\sigma})(t - t_1)] \\
& \quad \times \int_{t_0}^{t_1} dt_2 V^*_{ak'}(t_2) \exp\left[ i \int_{t_2}^{t_1} (\tilde{\epsilon}^*_{a\sigma}(t') - \epsilon_{k'\sigma}) dt' \right] \\
& - f(\epsilon_{k\sigma}) \int_{t_0}^{t} dt_1 V^*_{ak'}(t_1) \exp[i(\epsilon_{k\sigma} - \epsilon_{k'\sigma})(t - t_1)] \\
& \quad \times \int_{t_0}^{t_1} dt_2 V_{ak}(t_2) \exp\left[ -i \int_{t_2}^{t_1} (\tilde{\epsilon}_{a\sigma}(t') - \epsilon_{k\sigma}) dt' \right] \\
& + n_{a\sigma}(t_0) \exp[i(\epsilon_{k\sigma} - \epsilon_{k'\sigma})(t - t_0)] \int_{t_0}^{t} dt_1 V_{ak}(t_1) \exp\left[ i \int_{t_0}^{t_1} (\tilde{\epsilon}^*_{a\sigma}(t') - \epsilon_{k\sigma}) dt' \right] \\
& \quad \times \int_{t_0}^{t} dt_2 V^*_{ak'}(t_2) \exp\left[ -i \int_{t_0}^{t_2} (\tilde{\epsilon}_{a\sigma}(t') - \epsilon_{k'\sigma}) dt' \right] \\
& + f(\epsilon_{k\sigma}) \delta_{k,k'}. \qquad (2.28)
\end{aligned}
$$

The $k' = k$ case of $n_{kk'\sigma}$, $n_{k\sigma}$, is the occupation function for the metal state $k$. $n_{k\sigma}$ can be found from (2.28) to be

$$
\begin{aligned}
n_{k\sigma}(t) \;=\; & \int d\epsilon f(\epsilon) \left| \int_{t_0}^{t} dt_1 V^*_{ak}(t_1) p_\sigma(\epsilon, t_1) \exp[i(\epsilon_{k\sigma} - \epsilon)(t_1 - t)] \right|^2 \\
& - 2 f(\epsilon_{k\sigma}) \mathrm{Re} \Bigg\{ \int_{t_0}^{t} dt_1 V^*_{ak}(t_1) \\
& \qquad \times \int_{t_0}^{t_1} dt_2 V_{ak}(t_2) \exp\left[ -i \int_{t_2}^{t_1} (\tilde{\epsilon}_{a\sigma}(t') - \epsilon_{k\sigma}) dt' \right] \Bigg\} \\
& + n_{a\sigma}(t_0) \left| \int_{t_0}^{t} dt_1 V^*_{ak}(t_1) \exp\left[ -i \int_{t_0}^{t_1} (\tilde{\epsilon}_{a\sigma}(t') - \epsilon_{k\sigma}) dt' \right] \right|^2 \\
& + f(\epsilon_{k\sigma}). \qquad (2.29)
\end{aligned}
$$

The expressions we have derived for $n_{kk'\sigma}$ and $n_{k\sigma}$, like $n_{ak\sigma}$, will be used in chapter 4 to construct an expression for the distribution of occupied electronic

states of the Newns-Anderson system.

## 2.3 Adiabatic occupation functions

In this section we consider the adiabatic, or ground state, equivalent of the time-dependent adsorbate occupation function $n_{a\sigma}^{(ad)}$.

The adiabatic adsorbate occupation function $n_{a\sigma}^{(ad)}$ has historically been derived through the use of Green's Functions. Anderson [35] originally used adiabatic Green's functions to derive expressions for an impurity resonance from which he calculated the occupation of the impurity orbital. Doniach and Sondheimer [65] have used retarded Green's functions to obtain identical expressions. Here we will derive an expression for $n_{a\sigma}^{(ad)}$ from (2.19) by taking the slow limit of the variation in $\epsilon_a$ and $\Gamma$.

We first consider the evolution of the quantity $p_\sigma$, (2.20), which is required for calculation of $n_{a\sigma}$. By differentiating $p_\sigma$ with respect to time $t$ we find[1]

$$\frac{d}{dt}p_\sigma(\epsilon,t) = -i(\tilde{\epsilon}_{a\sigma}(t)-\epsilon)p_\sigma(\epsilon,t) + \sqrt{\frac{\Gamma(t)}{2\pi}}. \tag{2.30}$$

In the adiabatic limit the variation in the parameters driving the behaviour of the system, $\epsilon_a$ and $\Gamma$, will be slow. This implies that the variation in $p_\sigma$ will also be slow and the time-derivative on the left of (2.30) will be small. Assuming that there is no variation in $p_\sigma$, i.e. $dp_\sigma/dt = 0$, we can solve (2.30) to obtain the adiabatic quantity $p_\sigma^{(ad)}$;

$$p_\sigma^{(ad)}(\epsilon,t) = \sqrt{\frac{\Gamma(t)}{2\pi}}\frac{i}{\epsilon - \tilde{\epsilon}_{a\sigma}^{(ad)}(t)}, \tag{2.31}$$

where $\tilde{\epsilon}_{a\sigma}^{(ad)}(t) = \bar{\epsilon}_{a\sigma}^{(ad)}(t) - i\Gamma(t)/2$ and $\bar{\epsilon}_{a\sigma}^{(ad)}(t) = \epsilon_a(t) + Un_{a-\sigma}^{(ad)}(t)$. Combining (2.19) and (2.31) therefore yields the adiabatic occupation

$$n_{a\sigma}^{(ad)}(t) = \int d\epsilon f(\epsilon)\rho_{a\sigma}^{(ad)}(\epsilon,t) \tag{2.32}$$

[1]This expression will also be useful for numerical computations of the evolution of the Newns-Anderson system in chapter 5.

where $\rho_{a\sigma}^{(ad)}$ is the adiabatic PDOS defined as

$$\rho_{a\sigma}^{(ad)}(\epsilon,t) = |p_{\sigma}^{(ad)}(\epsilon,t)|^2 = \frac{\Gamma(t)}{2\pi[(\epsilon - \bar{\epsilon}_{a\sigma}^{(ad)}(t))^2 + \Gamma(t)^2/4]}. \tag{2.33}$$

The adiabatic PDOS is a Lorentzian distribution, centred on $\bar{\epsilon}_{a\sigma}^{(ad)}$, with half-maximum full-width $\Gamma$ as described in figure 2.1. In deriving (2.32) we have ignored the transient term, the second term in (2.19). This omission can be justified by recalling that the variation in the driving parameters is slow, with the exponential in the transient term in $n_{a\sigma}$ tending to zero once $\Gamma$ is greater than zero.

At zero temperature the energy integral in (2.32) can be performed analytically to give an expression equivalent to Anderson's result [35];

$$n_{a\sigma}^{(ad)}(t) = \frac{1}{2} - \frac{1}{\pi}\tan^{-1}\left\{2\frac{\bar{\epsilon}_{a\sigma}^{(ad)}(t) - \epsilon_F}{\Gamma(t)}\right\}, \tag{2.34}$$

As $\bar{\epsilon}_{a\sigma}^{(ad)}$ is also dependent on $n_{a-\sigma}^{(ad)}$, through the adiabatic equivalent of (2.4), this expression must therefore be evaluated in a self-consistent fashion. This self-consistent property makes the behaviour of $n_{a\sigma}^{(ad)}$ difficult to predict at first glance. There are, however, a number of parameter regimes in which the behaviour of $n_{a\sigma}^{(ad)}$ is obvious. In the large $\Gamma$ limit $n_{a\sigma}^{(ad)}$ tends to one half for both spins, provided $|\epsilon_a| \ll \Gamma$ and $|\epsilon_a + U| \ll \Gamma$. In the $\Gamma \to 0$ limit the adsorbate PDOS $\rho_{a\sigma}^{(ad)}$ becomes the delta function $\delta(\epsilon - \bar{\epsilon}_{a\sigma}(t))$, and the occupations are therefore either zero or one.

However when $\epsilon_a$, $U$ and $\Gamma$ are of similar magnitude it is more difficult to predict the behaviour. In this regime there are two phases: one phase in which $n_{a\sigma}^{(ad)}$ has a single solution, i.e. an unpolarised state, and another phase in which there are three possible solutions of (2.34). In this second phase two of the solutions correspond to a spin-polarised state. The third solution, which lies between the spin-polarised pair, is a meta-stable unpolarised state. We will refer in the rest of this section to the meta-stable solution as $n_{a0}^{(ad)}$. These solutions were also noted by Anderson [35]. The stable spin-polarised solutions can be obtained using a simple iterative method, while the meta-stable solution can be found using a binary search algorithm. To demonstrate this we plot the solutions of (2.34) in figure 2.2 for three model systems. In each of the systems the ratio $\Gamma/U$ is varied

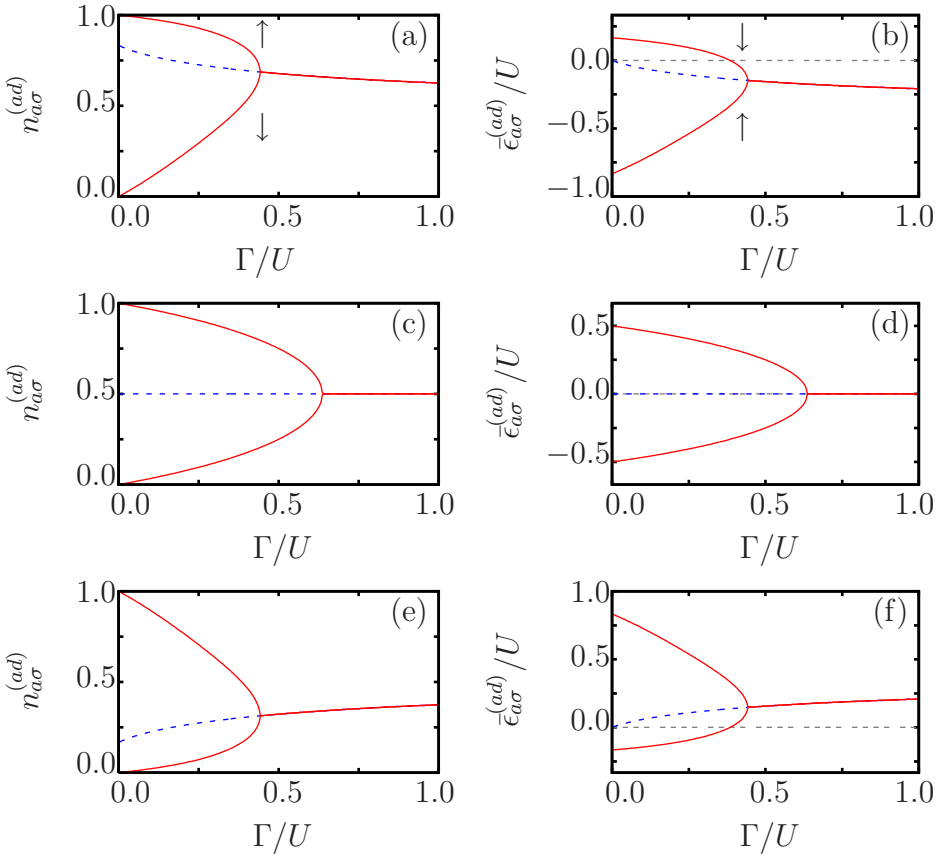


Figure 2.2: Variation of $n_{a\sigma}^{(ad)}$ and $\bar{\epsilon}_{a\sigma}^{(ad)}$ for model systems with $\epsilon_a/U = -5/6$, (a) and (b), $\epsilon_a/U = -1/2$, (c) and (d), and $\epsilon_a/U = -1/6$, (e) and (f). In each case the solid red and dashed blue lines represent the initially spin-polarised and unpolarised solutions of equation (2.34) respectively. The dotted line denotes the Fermi level and the arrows indicate the spin of the polarised solutions. The temperature of the system is set to zero.

from 0 to 1, with the three systems differing in the value of $\epsilon_a/U$, which is held constant. The values used are $\epsilon_a/U = -5/6$ (Fig. 2.2 (a) and (b)), $\epsilon_a/U = -1/2$ (Fig. 2.2 (c) and (d)) and $\epsilon_a/U = -1/6$ (Fig. 2.2 (e) and (f)). The Fermi energy $\epsilon_F$ is taken to be zero.

Each of these model systems display similar characteristic behaviour. As $\Gamma$ is increased from zero the occupations $n_{a\sigma}^{(ad)}$ converge on one another. At a certain point the spin-polarised occupations and the meta-stable solution become degenerate. This point is the adiabatic spin-transition. Close to this transition point the polarisation $n_{a\uparrow}^{(ad)} - n_{a\downarrow}^{(ad)}$ can be described by a square root function of $\Gamma$, i.e. $\sqrt{\Gamma_0 - \Gamma}$ where $\Gamma_0$ is the width at the spin-transition. The meta-stable solution $n_{a0}^{(ad)}$ in each case varies smoothly from an initial energy corresponding to the Fermi level, and becomes degenerate with the spin-polarised solutions at the spin-transition. However, the meta-stable occupation is not of primary importance in this work and we will not discuss it further.

The differences in the model systems can be described by considering the energy level diagrams in figures 2.2 (b), (d) and (f). The $\epsilon_a/U = -5/6$ model system has the majority level well below and the minority level just above the Fermi energy. As the width $\Gamma$ increases the minority level crosses the Fermi energy and the spin-transition therefore occurs at a large occupation. In the $\epsilon_a/U = -1/6$ model the situation is reversed; the majority level is initially just below $\epsilon_F$, while the minority level is well above. In this case it is the majority level which crosses the Fermi level as $\Gamma$ increases, and the spin-transition therefore occurs at a small occupation. The $\epsilon_a/U = -1/2$ model has the energy levels arranged symmetrically about the Fermi energy. The two energy levels therefore approach the Fermi level in an identical manner, with the spin-transition occurring when both levels reach the Fermi energy. It is also interesting to note that the spin-transition for this symmetrical model occurs at larger value of $\Gamma$ than in the $\epsilon_a/U = -1/6$ and $-5/6$ models.

We will revisit these model systems in later chapters to demonstrate the charge and energy transfer behaviour, as well as the spectrum of electronic excitations resulting from the processes, in chapters 5 and 6.

## 2.4 Summary

The time-dependent, mean-field Newns-Anderson model has been used to consider the behaviour of a single orbital adsorbate interacting with a metal surface. The wide-band approximation has been employed to allow expressions for the occupation functions for the different states of the Newns-Anderson system to be obtained. By using this model we have derived the time-dependent adsorbate level occupation function $n_{a\sigma}$, (2.19), which is closely related to the effective energy level $\bar{\epsilon}_{a\sigma}$. The time-dependent occupation functions $n_{ak\sigma}$, $n_{kk'\sigma}$ and $n_{k\sigma}$ (equations (2.25), (2.28) and (2.29)) have also been derived, with results which will be used in chapters 3 and 4. The slow variation limit of the occupation function $n_{a\sigma}$ has been taken to obtain an expression for the adiabatic occupation function $n_{a\sigma}^{(ad)}$, (2.32). We have also obtained an analytic result for $n_{a\sigma}^{(ad)}$ at zero temperature, which has been used to demonstrate the transition between a spin-polarised and an unpolarised ground state.

# Appendix A: Derivation of the electron operator equations of motion

In this appendix we derive expressions for the electron operators $\hat{c}_{k\sigma}$ and $\hat{c}_{a\sigma}$. These expressions can then be used to obtain the occupation functions of the different states of the Newns-Anderson system.

The set of differential equations for the electron operators are derived using Heisenberg's equation of motion [66];

$$\frac{d}{dt}\hat{c}_{b\sigma}(t) = \frac{\partial}{\partial t}\hat{c}_{b\sigma}(t) + \frac{1}{i}\left[\hat{c}_{b\sigma}(t), \hat{H}(t)\right], \tag{A.1}$$

where $\hbar$ has been set to 1 and $b \equiv \{a, k\}$ labels the state (adsorbate or metal). The first term on the right-hand side of this equation can be ignored when considering the electron operators as there is no explicit time-dependence. In order to obtain the equations of motion for the operators $\hat{c}_{a\sigma}$ and $\hat{c}_{k\sigma}$ we require their commutators with each of the first three terms in the mean-field Hamiltonian (2.3). The final term in the mean-field Hamiltonian $\hat{H}_{MF}$ can be ignored for this derivation as it does not contain operators.

We will demonstrate how the commutators are evaluated by considering the term

$$\left[\hat{c}_{a\sigma}(t), \bar{\epsilon}_{a\sigma'}(t)\hat{c}^{\dagger}_{a\sigma'}(t)\hat{c}_{a\sigma'}(t)\right] = \bar{\epsilon}_{a\sigma'}(t)\left(\hat{c}_{a\sigma}(t)\hat{c}^{\dagger}_{a\sigma'}(t)\hat{c}_{a\sigma'}(t) - \hat{c}^{\dagger}_{a\sigma'}(t)\hat{c}_{a\sigma'}(t)\hat{c}_{a\sigma}(t)\right). \tag{A.2}$$

The anti-commutation rules for fermion operators can be used to simplify the operator products in this expression [66];

$$\left[\hat{c}_{b\sigma}(t), \hat{c}_{b'\sigma'}(t)\right]_{+} = \hat{c}_{b\sigma}(t)\hat{c}_{b'\sigma'}(t) + \hat{c}_{b'\sigma'}(t)\hat{c}_{b\sigma}(t) = 0, \tag{A.3a}$$

$$\left[\hat{c}^{\dagger}_{b\sigma}(t), \hat{c}_{b'\sigma'}(t)\right]_{+} = \hat{c}^{\dagger}_{b\sigma}(t)\hat{c}_{b'\sigma'}(t) + \hat{c}_{b'\sigma'}(t)\hat{c}^{\dagger}_{b\sigma}(t) = \delta_{b,b'}\delta_{\sigma,\sigma'}, \tag{A.3b}$$

where the bracket $[...]_+$ denotes the anti-commutator of the enclosed operators. These properties can be used to expand the operator products in (A.2), giving

$$\begin{aligned}
&\hat{c}_{a\sigma}(t)\hat{c}^{\dagger}_{a\sigma'}(t)\hat{c}_{a\sigma'}(t) - \hat{c}^{\dagger}_{a\sigma'}(t)\hat{c}_{a\sigma'}(t)\hat{c}_{a\sigma}(t) \\
&\quad = \hat{c}_{a\sigma}(t)\hat{c}^{\dagger}_{a\sigma'}(t)\hat{c}_{a\sigma'}(t) - \hat{c}^{\dagger}_{a\sigma'}(t)\left(-\hat{c}_{a\sigma}(t)\hat{c}_{a\sigma'}(t)\right) \\
&\quad = \hat{c}_{a\sigma}(t)\hat{c}^{\dagger}_{a\sigma'}(t)\hat{c}_{a\sigma'}(t) + \left(\delta_{\sigma,\sigma'} - \hat{c}_{a\sigma}(t)\hat{c}^{\dagger}_{a\sigma'}(t)\right)\hat{c}_{a\sigma'}(t) \\
&\quad = \delta_{\sigma,\sigma'}\hat{c}_{a\sigma'}(t).
\end{aligned} \tag{A.4}$$

By combining this result with (A.2) we find

$$\left[\hat{c}_{a\sigma}(t), \bar{\epsilon}_{a\sigma'}(t)\hat{c}^{\dagger}_{a\sigma'}(t)\hat{c}_{a\sigma'}(t)\right] = \delta_{\sigma,\sigma'}\bar{\epsilon}_{a\sigma'}(t)\hat{c}_{a\sigma'}(t). \tag{A.5}$$

The Kronecker delta function in this expression implies that the operators for the two different spins do not directly affect one another. The only connection between the two spins is therefore through the definition of the mean-field energy level $\bar{\epsilon}_{a\sigma}$. By using the same procedure for the other terms in $\hat{H}_{MF}$ we find

$$\begin{aligned}
\left[\hat{c}_{a\sigma}(t), \bar{\epsilon}_{a\sigma}(t)\hat{c}^{\dagger}_{a\sigma}(t)\hat{c}_{a\sigma}(t)\right] &= \bar{\epsilon}_{a\sigma}(t)\hat{c}_{a\sigma}(t), & \left[\hat{c}_{a\sigma}(t), \epsilon_{k\sigma}\hat{c}^{\dagger}_{k\sigma}(t)\hat{c}_{k\sigma}(t)\right] &= 0, \\
\left[\hat{c}_{a\sigma}(t), V_{ak}(t)\hat{c}^{\dagger}_{a\sigma}(t)\hat{c}_{k\sigma}(t)\right] &= V_{ak}(t)\hat{c}_{k\sigma}(t), & \left[\hat{c}_{a\sigma}(t), V^{*}_{ak}(t)\hat{c}^{\dagger}_{k\sigma}(t)\hat{c}_{a\sigma}(t)\right] &= 0, \\
\left[\hat{c}_{k\sigma}(t), \epsilon_{k\sigma}\hat{c}^{\dagger}_{k\sigma}(t)\hat{c}_{k\sigma}(t)\right] &= \epsilon_{k\sigma}\hat{c}_{k\sigma}(t), & \left[\hat{c}_{k\sigma}(t), \bar{\epsilon}_{a\sigma}(t)\hat{c}^{\dagger}_{a\sigma}(t)\hat{c}_{a\sigma}(t)\right] &= 0, \\
\left[\hat{c}_{k\sigma}(t), V^{*}_{ak}(t)\hat{c}^{\dagger}_{k\sigma}(t)\hat{c}_{a\sigma}(t)\right] &= V^{*}_{ak}(t)\hat{c}_{a\sigma}(t) & \left[\hat{c}_{k\sigma}(t), V_{ak}(t)\hat{c}^{\dagger}_{a\sigma}(t)\hat{c}_{k\sigma}(t)\right] &= 0,
\end{aligned} \tag{A.6}$$

where we have only included the commutators of operators of the same spin. All commutators involving operators of different spins are zero.

By using the Heisenberg equation of motion, (A.1), and the above commutators, the equations of motion for $\hat{c}_{a\sigma}$ and $\hat{c}_{k\sigma}$ become

$$i\frac{d}{dt}\hat{c}_{a\sigma}(t) = \bar{\epsilon}_{a\sigma}(t)\hat{c}_{a\sigma}(t) + \sum_k V_{ak}(t)\hat{c}_{k\sigma}(t), \tag{A.7a}$$

$$i\frac{d}{dt}\hat{c}_{k\sigma}(t) = \epsilon_{k\sigma}\hat{c}_{k\sigma}(t) + V^*_{ak}(t)\hat{c}_{a\sigma}(t). \tag{A.7b}$$

We wish to solve these coupled differential equations to obtain expressions for $\hat{c}_{a\sigma}$ and $\hat{c}_{k\sigma}$ which only depend on the operators at a single reference time. This dependence on a single reference time allows the initial occupation functions, (2.15), to be used and prevents the derivations in section 2.2 from becoming excessively complicated. To achieve a solution of this form we first solve (A.7b) for $\hat{c}_{k\sigma}$, yielding

$$\begin{aligned}\hat{c}_{k\sigma}(t) = & -i\int_{t_0}^{t} dt_1 V^*_{ak}(t_1)\hat{c}_{a\sigma}(t_1)\exp\left[-i\epsilon_{k\sigma}(t-t_1)\right] \\ & +\hat{c}_{k\sigma}(t_0)\exp\left[-i\epsilon_{k\sigma}(t-t_0)\right],\end{aligned} \tag{A.8}$$

where $t_0$ is the reference time. Substituting (A.8) into (A.7a), we obtain

$$\begin{aligned}i\frac{d}{dt}\hat{c}_{a\sigma}(t) = & \bar{\epsilon}_{a\sigma}(t)\hat{c}_{a\sigma}(t) - i\int_{t_0}^{t} dt_1 \hat{c}_{a\sigma}(t_1)\sum_k V_{ak}(t)V^*_{ak}(t_1)\exp[-i\epsilon_{k\sigma}(t-t_1)] \\ & +\sum_k V_{ak}(t)\hat{c}_{k\sigma}(t_0)\exp[-i\epsilon_{k\sigma}(t-t_0)].\end{aligned} \tag{A.9}$$

The second term on the right-hand side of this equation can be simplified further. We introduce a delta function, $\delta(\epsilon - \epsilon_{k\sigma})$ and a corresponding energy integral, giving

$$-i\int_{t_0}^{t} dt_1 \hat{c}_{a\sigma}(t_1)\int d\epsilon \exp[-i\epsilon(t-t_1)]\sum_k V_{ak}(t)V^*_{ak}(t_1)\delta(\epsilon-\epsilon_{k\sigma}). \tag{A.10}$$

The wide-band approximation, discussed on page 36, allows us to simplify the sum over metal states $k$ in this expression. By using (2.8) this sum can be expanded to give

$$u(t)u(t_1)\sum_k |v_{ak}|^2\delta(\epsilon-\epsilon_{k\sigma}), \tag{A.11}$$

where $u(t)$ is the real, time-dependent, $k$-independent component of $V_{ak}(t)$, and $v_{ak}$ is a complex $k$-dependent constant. This expression is similar to the definition

of $\Gamma$ (2.13) when expanded using (2.8);

$$\Gamma(t) = 2\pi u^2(t) \sum_k |v_{ak}|^2 \delta(\epsilon - \epsilon_{k\sigma}), \tag{A.12}$$

By combining this expression with (A.11) we find

$$\sum_k V_{ak}(t) V_{ak}^*(t_1) \delta(\epsilon - \epsilon_{k\sigma}) = \frac{u(t_1)}{u(t)} . \frac{\Gamma(t)}{2\pi}. \tag{A.13}$$

The ratio $u(t_1)/u(t)$ can be shown to be the square-root of $\Gamma(t_1)/\Gamma(t)$ using (A.12). The sum over $k$ in (A.10) therefore becomes

$$\sum_k V_{ak}(t) V_{ak}^*(t_1) \delta(\epsilon - \epsilon_{k\sigma}) = \frac{\sqrt{\Gamma(t)\Gamma(t_1)}}{2\pi}. \tag{A.14}$$

This expression will be used throughout the derivations presented in chapters 2, 3 and 4.

By using (A.14), (A.10) becomes

$$-i \int_{t_0}^{t} dt_1 \hat{c}_{a\sigma}(t_1) \sqrt{\Gamma(t)\Gamma(t_1)} \int d\epsilon \frac{\exp[-i\epsilon(t-t_1)]}{2\pi}. \tag{A.15}$$

The energy integral in this expression can be recognised as the delta function $\delta(t - t_1)$. However, the time-integral in (A.15) would only cover half of this delta function and its value is therefore not well defined. Expressions with the same form as (A.15) will occur throughout this work, and we will therefore describe the evaluation of the general integral

$$\xi(t) = \int_{t_0}^{t} dt_1 \chi(t_1) \int d\epsilon \frac{\exp[-i\epsilon(t-t_1)]}{2\pi}, \tag{A.16}$$

where $\chi$ is an arbitrary function. We restrict the $\epsilon$ integral to the range $-A$ to $A$ and take the $A \to \infty$ limit at a later stage. The energy integral then gives

$$\int_{-A}^{A} d\epsilon \frac{\exp[-i\epsilon(t-t_1)]}{2\pi} = \frac{1}{\pi} . \frac{\sin(A(t-t_1))}{t-t_1}, \tag{A.17}$$

which is the normalised sinc function. This function is sharply peaked around $t_1 = t$, with a width which will become small in the $A \to \infty$ limit. It is therefore logical to expand the function $\chi(t_1)$ in (A.16) as a Taylor series about $t_1 = t$.

Equation (A.16) then becomes

$$\begin{aligned}\xi(t) &= \frac{1}{\pi}\sum_{m=0}^{\infty}\frac{1}{m!}\frac{d^{(m)}\chi}{dt^{(m)}}\int_{t_0}^{t}dt_1(t_1-t)^m\frac{\sin(A(t-t_1))}{t-t_1} \\ &= -\frac{1}{\pi}\sum_{m=0}^{\infty}\frac{1}{m!}\frac{d^{(m)}\chi}{dt^{(m)}}\int_{t_0}^{t}dt_1(t_1-t)^{(m-1)}\sin(A(t-t_1)), \qquad \text{(A.18)}\end{aligned}$$

which can be simplified by introducing the substitution $x = A(t-t_1)$, giving

$$\begin{aligned}\xi(t) &= -\frac{1}{\pi}\sum_{m=0}^{\infty}\frac{1}{m!}\frac{d^{(m)}\chi}{dt^{(m)}}\int_{A(t-t_0)}^{0}-\frac{dx}{A}\left(\frac{-x}{A}\right)^{(m-1)}\sin(x) \\ &= \frac{1}{\pi}\sum_{m=0}^{\infty}\frac{(-1)^m}{m!}\frac{d^{(m)}\chi}{dt^{(m)}}\frac{1}{A^m}\int_{0}^{A(t-t_0)}dx\ x^{(m-1)}\sin(x). \qquad \text{(A.19)}\end{aligned}$$

The first term in this sum is

$$\frac{\chi(t)}{\pi}\int_0^{A(t-t_0)}dx\frac{\sin(x)}{x} = \frac{\chi(t)}{\pi}\mathrm{Si}(A(t-t_0)), \qquad \text{(A.20)}$$

where Si is the sine integral. The remaining terms in (A.19) contain integrals of the form

$$\frac{1}{A^m}\int_0^{A(t-t_0)}dx\ x^{(m-1)}\sin(x), \qquad \text{(A.21)}$$

where $m \geq 1$. These integrals can be evaluated by performing a series of by-parts integration steps, which can be shown to tend to zero in the $A \to \infty$ limit. This leaves (A.20) as the only contribution to $\xi(t)$, (A.19). In the $A \to \infty$ limit the sine integral in (A.20) will tend to a value of $\pi/2$, and we can therefore rewrite $\xi(t)$ as

$$\xi(t) = \int_{t_0}^{t}dt_1\chi(t_1)\int d\epsilon\frac{\exp[-i\epsilon(t-t_1)]}{2\pi} = \frac{\chi(t)}{2}. \qquad \text{(A.22)}$$

By using (A.22) the time integral in (A.15) can be evaluated, yielding

$$-i\int_{t_0}^{t}dt_1\hat{c}_{a\sigma}(t_1)\sqrt{\Gamma(t)\Gamma(t_1)}\int d\epsilon\frac{\exp[-i\epsilon(t-t_1)]}{2\pi} = -i\frac{\Gamma(t)}{2}\hat{c}_{a\sigma}(t). \qquad \text{(A.23)}$$

The equation of motion for $\hat{c}_{a\sigma}$, (A.9), therefore becomes

$$i\frac{d}{dt}\hat{c}_{a\sigma}(t) = \tilde{\epsilon}_{a\sigma}(t)\hat{c}_{a\sigma}(t) + \sum_k V_{ak}(t)\exp[-i\epsilon_{k\sigma}(t-t_0)]\hat{c}_{k\sigma}(t_0), \tag{A.24}$$

where $\tilde{\epsilon}_{a\sigma}$ is defined as

$$\tilde{\epsilon}_{a\sigma}(t) = \bar{\epsilon}_{a\sigma}(t) - i\Gamma(t)/2. \tag{A.25}$$

Integration of (A.24) yields

$$\begin{aligned}\hat{c}_{a\sigma}(t) &= -i\int_{t_0}^{t} dt_1 \exp\left[-i\int_{t_1}^{t}\tilde{\epsilon}_{a\sigma}(t')dt'\right]\sum_k V_{ak}(t_1)\exp[-i\epsilon_{k\sigma}(t_1-t_0)]\hat{c}_{k\sigma}(t_0) \\ &\quad + \exp\left[-i\int_{t_0}^{t}\tilde{\epsilon}_{a\sigma}(t')dt'\right]\hat{c}_{a\sigma}(t_0),\end{aligned} \tag{A.26}$$

which relates $\hat{c}_{a\sigma}(t)$ to the state of the system at time $t_0$. In order to obtain an expression for $\hat{c}_{k\sigma}(t_0)$ with the same property we substitute (A.26) into (A.8), giving

$$\begin{aligned}\hat{c}_{k\sigma}(t) &= -\int_{t_0}^{t} dt_1 V_{ak}^*(t_1)\exp[-i\epsilon_{k\sigma}(t-t_1)]\int_{t_0}^{t_1} dt_2 \exp\left[-i\int_{t_2}^{t_1}\tilde{\epsilon}_{a\sigma}(t')dt'\right] \\ &\qquad \times\sum_{k'} V_{ak'}(t_2)\exp[-i\epsilon_{k'\sigma}(t_2-t_0)]\hat{c}_{k'\sigma}(t_0) \\ &\quad -i\int_{t_0}^{t} dt_1 V_{ak}^*(t_1)\exp[-i\epsilon_{k\sigma}(t-t_1)]\exp\left[-i\int_{t_0}^{t_1}\tilde{\epsilon}_{a\sigma}(t')dt'\right]\hat{c}_{a\sigma}(t_0) \\ &\quad + \exp[-i\epsilon_{k\sigma}(t-t_0)]\hat{c}_{k\sigma}(t_0).\end{aligned} \tag{A.27}$$

# Chapter 3

# Adsorbate-surface energy transfer

In this chapter we extend the time-dependent mean-field Newns-Anderson model explored in the previous chapter to consider the transfer of energy between an adsorbate and a metal surface.

The rapid transfer of charge from an adsorbate to a metal surface during an interaction will excite the electronic degrees of freedom of the substrate, as the electronic system is unable to react instantaneously to the changing adsorbate position. The total energy of the adsorbate-metal electronic system will therefore consist of two components; the energy due to the configuration of the adsorbate and metal atoms, and the energy of the excitations of the metal electrons. The first of these components, the configuration energy, will be independent of the route by which a given configuration is reached, while the second part will be path dependent. The second, excitation, component will also be dependent on the speed at which the transfer of charge occurs. A slow approach of the adsorbate to the surface gives the electronic system more time to restructure and therefore the excitation component will be smaller. In the limit of infinitely slow adsorbate motion the excitation component disappears and the energy depends entirely on the configuration of system. We define this slow limit of the system to be the adiabatic system we discussed in section 2.3 as there is no transfer of energy to surface excitations. The total energy of the electronic excitations can therefore be calculated by subtracting the energy of the adiabatic system from the total energy

of the system. The energy of the electronic excitations will be referred to as the non-adiabatic energy transferred to the metal surface. In this chapter we will only be considering the *total* energy transfer between the adsorbate and surface - the distribution of excitations generated by this process will be considered in chapter 4.

We choose to investigate the non-adiabatic energy transfer process by deriving an expression for the rate of non-adiabatic energy transfer. An expression for this non-adiabatic energy transfer rate will be derived in section 3.1 and appendix B.

The non-adiabatic energy transfer rate is, however, not a quantity that can easily be understood in a qualitative manner. Therefore, to gain insight into the energy transfer process, we develop a nearly-adiabatic approximation to the non-adiabatic model in section 3.2 and appendix C. This nearly-adiabatic model assumes that the evolving system stays close to the adiabatic state, which is principally valid for slow variation of the driving parameters of our model. This model allows us to make contact with previous work [28, 49, 67], discussed in section 1.2.1, which has considered energy transfer in the nearly-adiabatic limit in terms of a friction coefficient. We also discuss the validity of this nearly-adiabatic approximation for our system.

Numerical methods will be used to calculate the non- and nearly-adiabatic energy transfer rates for a range of systems in chapter 5.

## 3.1 The non-adiabatic energy transfer rate

We derive an expression for the non-adiabatic energy transfer rate by first considering the rate of change of the total energy of the Newns-Anderson system, $\dot{E}$. Dotted quantities, such as $\dot{E}$, will be used throughout this chapter to denote time-derivatives. This rate of change can be found by taking the time derivative of the mean-field Hamiltonian, (2.3), and using the equations of motion for the electron operators to simplify the expression. The thermally averaged expectation value of this expression then gives the rate of change of the total energy of the system. The derivation of $\dot{E}$ through this route is straightforward, but it is long-winded and is therefore presented in appendix B. It is simpler, however, to consider a derivation in the Schrödinger picture for an arbitrary, time-dependent Hamiltonian $\hat{\mathcal{H}}(t)$. The method used here follows that presented by Trail et

al. [29].

The thermally averaged expectation value of the total energy of $\hat{\mathcal{H}}$ in the canonical ensemble can be written (see Baierlein [68]) as

$$E_{\mathcal{H}}(t) \equiv \langle\langle \hat{\mathcal{H}}(t) \rangle\rangle = \sum_{\Phi} P_{\Phi} \langle \Phi(t) | \hat{\mathcal{H}}(t) | \Phi(t) \rangle, \tag{3.1}$$

where $\{|\Phi(t)\rangle\}$ is the set of time-evolving, many-electron states of the system. $P_{\Phi}$ is the canonical probability function defined as [68]

$$P_{\Phi} = \frac{1}{Z} \exp[-\beta \epsilon_{\Phi}(t_0)] \tag{3.2}$$

where $Z$ is the partition function, $\beta = 1/k_B T$ and $\epsilon_{\Phi}(t_0)$ is the energy of the state $|\Phi(t)\rangle$ at time $t = t_0$. By differentiating (3.1) we find

$$\begin{aligned} \dot{E}_{\mathcal{H}}(t) &= \sum_{\Phi} P_{\Phi} \left( \frac{d}{dt} \left\{ \langle \Phi(t) | \right\} \hat{\mathcal{H}}(t) | \Phi(t) \rangle + \langle \Phi(t) | \frac{d\hat{\mathcal{H}}}{dt} | \Phi(t) \rangle \right. \\ &\qquad \left. + \langle \Phi(t) | \hat{\mathcal{H}}(t) \frac{d}{dt} \left\{ | \Phi(t) \rangle \right\} \right). \end{aligned} \tag{3.3}$$

The first and third terms in this expression can be expanded using the time-dependent Schrödinger equation (with $\hbar = 1$), giving

$$\begin{aligned} \dot{E}_{\mathcal{H}}(t) &= \sum_{\Phi} P_{\Phi} \left( i \langle \Phi(t) | \hat{\mathcal{H}}(t) \hat{\mathcal{H}}(t) | \Phi(t) \rangle + \langle \Phi(t) | \frac{d\hat{\mathcal{H}}}{dt} | \Phi(t) \rangle \right. \\ &\qquad \left. - i \langle \Phi(t) | \hat{\mathcal{H}}(t) \hat{\mathcal{H}}(t) | \Phi(t) \rangle \right) \\ &= \sum_{\Phi} P_{\Phi} \langle \Phi(t) | \frac{d\hat{\mathcal{H}}}{dt} | \Phi(t) \rangle, \end{aligned} \tag{3.4}$$

i.e. the time-derivative of the state $|\Phi(t)\rangle$ is not required, only the derivative of the Hamiltonian $\hat{\mathcal{H}}$. An expression for the rate of change of the adiabatic energy of the system can be derived in a similar manner, but noting that the adiabatic many-

electron state $|\Phi^{(ad)}(t)\rangle$ is an eigenstate of the adiabatic Hamiltonian $\hat{\mathcal{H}}^{(ad)}(t)$;

$$\begin{aligned}
\dot{E}^{(ad)}_{\mathcal{H}}(t) &= \sum_{\Phi} P_{\Phi} \left( \frac{d}{dt} \left\{ \langle \Phi^{(ad)}(t)| \right\} \hat{\mathcal{H}}^{(ad)}(t) |\Phi^{(ad)}(t)\rangle \right. \\
&\qquad \left. + \langle \Phi^{(ad)}(t)| \frac{d\hat{\mathcal{H}}^{(ad)}}{dt} |\Phi^{(ad)}(t)\rangle + \langle \Phi^{(ad)}(t)| \hat{\mathcal{H}}^{(ad)}(t) \frac{d}{dt} \left\{ |\Phi^{(ad)}(t)\rangle \right\} \right) \\
&= \sum_{\Phi} P_{\Phi} \left[ \epsilon^{(ad)}_{\Phi}(t) \left( \frac{d}{dt} \left\{ \langle \Phi^{(ad)}(t)| \right\} |\Phi^{(ad)}(t)\rangle \right. \right. \\
&\qquad \left. \left. + \langle \Phi^{(ad)}(t)| \frac{d}{dt} \left\{ |\Phi^{(ad)}(t)\rangle \right\} \right) + \langle \Phi^{(ad)}(t)| \frac{d\hat{\mathcal{H}}^{(ad)}}{dt} |\Phi^{(ad)}(t)\rangle \right] \\
&= \sum_{\Phi} P_{\Phi} \left[ \epsilon^{(ad)}_{\Phi}(t) \frac{d}{dt} \left\{ \langle \Phi^{(ad)}(t)|\Phi^{(ad)}(t)\rangle \right\} + \langle \Phi^{(ad)}(t)| \frac{d\hat{\mathcal{H}}^{(ad)}}{dt} |\Phi^{(ad)}(t)\rangle \right].
\end{aligned} \tag{3.5}$$

where $\epsilon^{(ad)}_{\Phi}(t)$ is the eigenenergy of the adiabatic eigenstate $|\Phi^{(ad)}(t)\rangle$. The first term in this expression contains the derivative of the norm of the adiabatic state, and is therefore zero. This leaves

$$\dot{E}^{(ad)}_{\mathcal{H}}(t) = \sum_{\Phi} P_{\Phi} \langle \Phi^{(ad)}(t)| \frac{d\hat{\mathcal{H}}^{(ad)}}{dt} |\Phi^{(ad)}(t)\rangle. \tag{3.6}$$

The non-adiabatic energy transfer rate is simply the difference between (3.4) and (3.6);

$$\dot{E}^{(non-ad)}_{\mathcal{H}}(t) = \sum_{\Phi} P_{\Phi} \left( \langle \Phi(t)| \frac{d\hat{\mathcal{H}}}{dt} |\Phi(t)\rangle - \langle \Phi^{(ad)}(t)| \frac{d\hat{\mathcal{H}}^{(ad)}}{dt} |\Phi^{(ad)}(t)\rangle \right). \tag{3.7}$$

The equivalent procedure to equations (3.1) to (3.4) in the Heisenberg picture is to take the time derivative of each of the energies $\bar{\epsilon}_{a\sigma}(t)$, $\epsilon_{k\sigma}$ and $V_{ak}(t)$ in the mean-field Hamiltonian (2.3), with the number operators $\hat{n}_{a\sigma}$ and $\hat{n}_{k\sigma}$ and the product $\hat{c}^{\dagger}_{a\sigma}\hat{c}_{k\sigma}$ undifferentiated. The fourth term in the Hamiltonian, the intra-adsorbate Coulomb repulsion term, is directly differentiated as it does not

contain operators. This yields

$$\begin{aligned}\dot{E}(t) &= \sum_{\sigma} \dot{\bar{\epsilon}}_{a\sigma}(t) n_{a\sigma}(t) + \sum_{k,\sigma} \left( \dot{V}_{ak}(t) n_{ak\sigma}(t) + \text{c.c.} \right) \\ &\qquad -U \frac{d}{dt} \left\{ n_{a\sigma}(t) n_{a-\sigma}(t) \right\} \\ &= \sum_{\sigma} \dot{\epsilon}_{a}(t) n_{a\sigma}(t) + \sum_{k,\sigma} \left( \dot{V}_{ak}(t) n_{ak\sigma}(t) + \text{c.c.} \right), \end{aligned} \tag{3.8}$$

where the last step follows using the definition of $\bar{\epsilon}_{a\sigma}$, (2.4). This result can also be obtained using the equations of motion for the electron operators; this derivation is presented in appendix B. Equation (3.8) was first derived by Plihal and Langreth [63] using a density matrix approach.

In the previous chapter we derived expressions for the occupation functions $n_{a\sigma}$ and $n_{ak\sigma}$ which appear in $\dot{E}$ above. The first term in (3.8) can be directly calculated using the definition of $n_{a\sigma}$, (2.19), and the variation of $\epsilon_a$. The second term, however, can be simplified further. We first eliminate the time-derivative $\dot{V}_{ak}$ in $\dot{E}$ using the wide-band limit approximation. This derivative can be expressed as the time-derivative of (2.8), i.e.

$$\dot{V}_{ak}(t) = v_{ak} \dot{u}(t), \tag{3.9}$$

where $u(t)$ is the real, state independent function which contains all the time-dependence of $V_{ak}(t)$. $\dot{u}$ can be related to the adsorbate resonance width $\Gamma$ by differentiating (2.13):

$$\begin{aligned}\dot{\Gamma}(t) &= \frac{d}{dt} \left\{ u^2(t) \right\} 2\pi \sum_{k} |v_{ak}|^2 \delta(\epsilon - \epsilon_{k\sigma}) \\ &= \frac{2\dot{u}(t)}{u(t)} u^2(t) . 2\pi \sum_{k} |v_{ak}|^2 \delta(\epsilon - \epsilon_{k\sigma}) \\ &= 2\Gamma(t) \frac{\dot{u}(t)}{u(t)}. \end{aligned} \tag{3.10}$$

On rearranging this expression, and substituting it into (3.9) for $\dot{u}$, we find

$$\dot{V}_{ak}(t) = v_{ak} u(t) \frac{\dot{\Gamma}(t)}{2\Gamma(t)} = V_{ak}(t) \frac{\dot{\Gamma}(t)}{2\Gamma(t)}. \tag{3.11}$$

The expression for $\dot{E}$ therefore becomes

$$\dot{E}(t) = \sum_{\sigma} \dot{\epsilon}_a(t) n_{a\sigma}(t) + \frac{\dot{\Gamma}(t)}{\Gamma(t)} \mathrm{Re}\left\{ \sum_{k,\sigma} V_{ak}(t) n_{ak\sigma}(t) \right\}. \tag{3.12}$$

where we have recalled that $n_{ka\sigma}(t) = n^*_{ak\sigma}(t)$.

The second term in (3.12) is now in a form that can be simplified by using a similar analysis to that used for the occupation functions in chapter 2. We expand the sum over metal states $k$ using our expression for the occupation function $n_{ak\sigma}$, (2.25), which yields

$$\begin{aligned}
\sum_k V_{ak}(t) n_{ak\sigma}(t) = & \\
& -i \int_{t_0}^{t} dt_1 \int d\epsilon f(\epsilon) p^*_\sigma(\epsilon, t) p_\sigma(\epsilon, t_1) \exp[i\epsilon(t - t_1)] \\
& \qquad \times \sum_k V^*_{ak}(t_1) V_{ak}(t) \exp[-i\epsilon_{k\sigma}(t - t_1)] \\
& + i \int_{t_0}^{t} dt_1 \sum_k V^*_{ak}(t_1) V_{ak}(t) f(\epsilon_{k\sigma}) \exp\left[ i \int_{t_0}^{t} (\tilde{\epsilon}^*_{a\sigma}(t') - \epsilon_{k\sigma}) dt' \right] \\
& - i n_{a\sigma}(t_0) \exp\left[ -\frac{1}{2} \int_{t_0}^{t} \Gamma(t') dt' \right] \\
& \qquad \times \int_{t_0}^{t} dt_1 \sum_k V^*_{ak}(t_1) V_{ak}(t) \exp\left[ i \int_{t_1}^{t} (\tilde{\epsilon}_{a\sigma}(t') - \epsilon_{k\sigma}) dt' \right].
\end{aligned} \tag{3.13}$$

The sums over $k$-states can be simplified by introducing an energy integral and

the delta function $\delta(\epsilon' - \epsilon_{k\sigma})$. By using (A.14) (see page 53), we find

$$\begin{aligned}\sum_k V_{ak}(t) n_{ak\sigma}(t) = & \\ & -i\int_{t_0}^{t} dt_1 \int d\epsilon f(\epsilon) p^*_\sigma(\epsilon,t) p_\sigma(\epsilon,t_1) \exp[i\epsilon(t-t_1)] \\ & \qquad \times \sqrt{\Gamma(t_1)\Gamma(t)} \int d\epsilon' \frac{\exp[-i\epsilon'(t-t_1)]}{2\pi} \\ & +i\int_{t_0}^{t} dt_1 \frac{\sqrt{\Gamma(t_1)\Gamma(t)}}{2\pi} \int d\epsilon' f(\epsilon') \exp\left[i\int_{t_0}^{t} (\tilde{\epsilon}^*_{a\sigma}(t') - \epsilon') dt'\right] \\ & -i n_{a\sigma}(t_0) \exp\left[-\frac{1}{2}\int_{t_0}^{t} \Gamma(t') dt'\right] \\ & \qquad \times \int_{t_0}^{t} dt_1 \sqrt{\Gamma(t_1)\Gamma(t)} \exp\left[i\int_{t_1}^{t} \tilde{\epsilon}_{a\sigma}(t') dt'\right] \int d\epsilon' \frac{\exp[-i\epsilon'(t-t_1)]}{2\pi}.\end{aligned} \tag{3.14}$$

The $\epsilon'$ integrals in the first and third terms in this expression can be evaluated using (A.22) (see page 54). We can therefore simplify (3.14), giving

$$\begin{aligned}\sum_k V_{ak}(t) n_{ak\sigma}(t) &= -\frac{i}{2}\Gamma(t) \int d\epsilon f(\epsilon) |p_\sigma(\epsilon,t)|^2 \\ &\quad + i\sqrt{\frac{\Gamma(t)}{2\pi}} \int d\epsilon' f(\epsilon') p^*_\sigma(\epsilon',t) \\ &\quad - \frac{i}{2} n_{a\sigma}(t_0)\Gamma(t) \exp\left[-\int_{t_0}^{t} \Gamma(t') dt'\right] \\ &= -\frac{i}{2}\Gamma(t) n_{a\sigma}(t) + i\sqrt{\frac{\Gamma(t)}{2\pi}} \int d\epsilon' f(\epsilon') p^*_\sigma(\epsilon',t),\end{aligned} \tag{3.15}$$

where we have used the definitions of $p_\sigma$, (2.20), and $n_{a\sigma}$, (2.19). Substitution of this expression back into (3.12) yields

$$\dot{E}(t) = \sum_\sigma \dot{\epsilon}_a(t) n_{a\sigma}(t) + \frac{\dot{\Gamma}(t)}{\sqrt{2\pi\Gamma(t)}} \sum_\sigma \int d\epsilon f(\epsilon) \mathrm{Im}\left\{p_\sigma(\epsilon,t)\right\}, \tag{3.16}$$

where the first term in (3.15) has been lost as both $\Gamma$ and $n_{a\sigma}$ are real. We note that this expression for the rate of change of the total energy of the system is in a form which we can compute, as we will demonstrate in chapter 5.

To obtain the non-adiabatic energy transfer rate from (3.16) we require the adiabatic equivalent of $\dot{E}$. This follows from (3.16) in a straightforward manner; in

the adiabatic limit the occupation $n_{a\sigma}$ simply becomes $n_{a\sigma}^{(ad)}$ and the quantity $p_\sigma$ tends to $p_\sigma^{(ad)}$, where the adiabatic quantities are defined in chapter 2 (page 46). The non-adiabatic energy transfer rate is therefore given by

$$\dot{E}_{non-ad}(t) = \sum_\sigma \dot{\epsilon}_a(t)\delta n_{a\sigma}(t) + \frac{\dot{\Gamma}(t)}{\sqrt{2\pi\Gamma(t)}} \sum_\sigma \int d\epsilon f(\epsilon) \mathrm{Im}\left\{\delta p_\sigma(\epsilon, t)\right\}. \quad (3.17)$$

where $\delta n_{a\sigma} = n_{a\sigma} - n_{a\sigma}^{(ad)}$ and $\delta p_\sigma = p_\sigma - p_\sigma^{(ad)}$. The rate of non-adiabatic energy transfer between the adsorbate and surface is therefore dependent only on the deviation of $n_{a\sigma}$ and $p_\sigma$ from their adiabatic equivalents and the rate of change of the parameters $\epsilon_a$ and $\Gamma$. By using the expressions for $n_{a\sigma}$ and $p_\sigma$ we derived in chapter 2, $\dot{E}_{non-ad}$ can be calculated. Numerical calculations of $\dot{E}_{non-ad}$ will be presented in chapter 5.

## 3.2 The nearly-adiabatic energy transfer rate

In this section we consider the limit of the non-adiabatic model of energy transfer in which the evolution of the electronic system is slow. This 'nearly-adiabatic' model will help us gain an understanding of the factors affecting adsorbate-metal energy transfer.

For a slow approach of an adsorbate to a surface the system will remain close to the adiabatic state. This adiabatic state of the Newns-Anderson model is described by the parameters $\epsilon_a$, $U$ and $\Gamma$ for a given adsorbate-surface configuration. However, in seeking a nearly-adiabatic approximation we want to include the lowest order features of the time-dependent model. We will introduce time-dependence into the adiabatic model in the most simple manner possible; by using the time-derivatives $\dot{\epsilon}_a$ and $\dot{\Gamma}$, in addition to the parameters $\epsilon_a$, $U$ and $\Gamma$, to describe the nearly-adiabatic state of the system. To obtain the nearly-adiabatic limit of the non-adiabatic energy transfer rate, $\dot{E}_{non-ad}$ (3.17), we will only consider the lowest order terms in the differences $\delta n_{a\sigma}$ and $\delta p_\sigma$, and the derivatives $\dot{\epsilon}_a$ and $\dot{\Gamma}$, all of which will be assumed to be small.

The derivatives $\dot{\Gamma}$ and $\dot{\epsilon}_a$ which appear in (3.17) can be replaced by the product of the derivatives, $d\Gamma/ds$ and $d\epsilon_a/ds$, with the velocity $\dot{s}(t)$, where $s(t)$ is the altitude of the adsorbate. In this section the differences $\delta n_{a\sigma}$ and $\delta p_\sigma$ will be expanded to first order in $\dot{\Gamma}$ and $\dot{\epsilon}_a$. The lowest order terms in the nearly-adiabatic energy

transfer rate will therefore be proportional to the square of the velocity $\dot{s}$, i.e.

$$\dot{E}_{nearly-ad}(t) = \eta(s(t))\dot{s}(t)^2, \tag{3.18}$$

where $\eta$ is a function that describes the nearly-adiabatic behaviour of the system. This expression is similar to the change in energy arising from a classical frictional force, as shown in the introduction (see equations (1.4) to (1.5) on page 20). The function $\eta(s)$ is therefore commonly referred to as an electronic friction coefficient [28, 49, 67]. It is important to note that this friction based model is a 'local' representation of the energy transfer process – the rate of energy transfer depends only on the position of the adsorbate $s$ at a given time $t$ and has no memory of state of the system prior to this point. The non-adiabatic energy transfer model, constructed in the previous section, is not a local theory. The friction coefficient approach has been widely used in the field of surface dynamics to investigate energy transfer processes, as discussed in the introduction.

We now derive nearly-adiabatic expressions for the differences $\delta n_{a\sigma}$ and $\delta p_\sigma$, which are used to obtain a nearly-adiabatic approximation to $\dot{E}_{non-ad}$. To achieve this we first derive a nearly-adiabatic expression for the difference $\delta p_\sigma(\epsilon, t) = p_\sigma(\epsilon, t) - p_\sigma^{(ad)}(\epsilon, t)$. A number of first order expansions are used to obtain this difference. The time-evolving effective energy level $\bar{\epsilon}_{a\sigma}$ is written in terms of difference $\delta n_{a\sigma}$ and the adiabatic level $\bar{\epsilon}_{a\sigma}^{(ad)}$, which is expanded in time as a Taylor series about time $t$. The adsorbate resonance width $\Gamma$ is also Taylor expanded in the same way. These expansions can be written as

$$\begin{aligned}
\bar{\epsilon}_{a\sigma}(t) &= \bar{\epsilon}_{a\sigma}^{(ad)}(t) + U\delta n_{a-\sigma}(t), && (3.19)\\
\bar{\epsilon}_{a\sigma}^{(ad)}(t') &= \bar{\epsilon}_{a\sigma}^{(ad)}(t) + (t'-t)\dot{\bar{\epsilon}}_{a\sigma}^{(ad)}(t). && (3.20)\\
\Gamma(t') &= \Gamma(t) + (t'-t)\dot{\Gamma}(t), && (3.21)
\end{aligned}$$

The time derivatives $\dot{\Gamma}$ and $\dot{\bar{\epsilon}}_{a\sigma}^{(ad)}$ are small quantities and we therefore ignore any higher order derivatives. As the difference $\delta n_{a\sigma}$ is also assumed to be a small quantity we also write

$$\delta n_{a\sigma}(t') = \delta n_{a\sigma}(t). \tag{3.22}$$

By using these expansions we obtain $\delta p_\sigma$ in appendix C.1, yielding (see (C.11))

$$\begin{aligned}\delta p_\sigma(\epsilon,t) &= \sqrt{\frac{\Gamma(t)}{2\pi}}\frac{1}{(\epsilon-\tilde{\epsilon}^{(ad)}_{a\sigma}(t))^2} \\ &\quad\times\left(\frac{\dot{\Gamma}(t)(\epsilon-\tilde{\epsilon}^{(ad)*}_{a\sigma}(t))}{2\Gamma(t)(\epsilon-\tilde{\epsilon}^{(ad)}_{a\sigma}(t))}+iU\delta n_{a-\sigma}(t)+\frac{\dot{\tilde{\epsilon}}^{(ad)}_{a\sigma}(t)}{\epsilon-\tilde{\epsilon}^{(ad)}_{a\sigma}(t)}\right). \quad (3.23)\end{aligned}$$

This expression is then used to obtain an expression for $\delta n_{a\sigma}$ in appendix C.2. We find (see (3.24))

$$\begin{aligned}\delta n_{a\sigma}(t) &= -\pi\int d\epsilon\frac{df}{d\epsilon}\left(\frac{\dot{\Gamma}(t)}{\Gamma(t)}(\epsilon-\bar{\epsilon}^{(ad)}_{a\sigma}(t))+\dot{\bar{\epsilon}}^{(ad)}_{a\sigma}(t)\right)\left[\rho^{(ad)}_{a\sigma}(\epsilon,t)\right]^2 \\ &\quad +U\delta n_{a-\sigma}(t)\int d\epsilon\frac{df}{d\epsilon}\rho^{(ad)}_{a\sigma}(\epsilon,t), \quad (3.24)\end{aligned}$$

where $\rho^{(ad)}_{a\sigma}$ is the adiabatic PDOS defined in (2.33) (page 47). At this point we note that in the derivation of $\delta n_{a\sigma}$ in appendix C.2 we have expanded the integral over a Fermi function by performing a 'by-parts' integration step. This expansion allows us to consider both finite and zero temperature systems as the derivative $df/d\epsilon$, which appears in (3.24), tends to a delta function in the $T\to 0$ limit.

These expressions for $\delta p_\sigma$ and $\delta n_{a\sigma}$ can now be used to obtain the nearly-adiabatic counterparts to the first and second terms in $\dot{E}_{non-ad}$, (3.17). In appendix C.3 we find the contribution to the nearly-adiabatic energy transfer rate from the first term in (3.17), $\dot{E}^{(1)}_{nearly-ad}$, to be (see (C.38))

$$\begin{aligned}\dot{E}^{(1)}_{nearly-ad}(t) &= -\pi\sum_\sigma\dot{\bar{\epsilon}}^{(ad)}_{a\sigma}(t)\int d\epsilon\frac{df}{d\epsilon}\left(\frac{\dot{\Gamma}(t)}{\Gamma(t)}(\epsilon-\bar{\epsilon}^{(ad)}_{a\sigma}(t))+\dot{\bar{\epsilon}}^{(ad)}_{a\sigma}(t)\right)\left[\rho^{(ad)}_{a\sigma}(\epsilon,t)\right]^2 \\ &\quad -\frac{U\dot{\Gamma}(t)}{\Gamma(t)}\sum_\sigma\int d\epsilon\frac{df}{d\epsilon}(\epsilon-\bar{\epsilon}^{(ad)}_{a\sigma}(t))\rho^{(ad)}_{a\sigma}(\epsilon,t)\delta n_{a-\sigma}(t). \quad (3.25)\end{aligned}$$

The contribution from the second term in (3.17), $\dot{E}^{(2)}_{nearly-ad}$, is derived in appendix

C.4, with the result (see (C.52))

$$\begin{aligned}\dot{E}^{(2)}_{nearly-ad}(t) &= -\pi\sum_\sigma\int d\epsilon\frac{df}{d\epsilon}\frac{\dot\Gamma(t)}{\Gamma(t)}(\epsilon-\bar\epsilon^{(ad)}_{a\sigma}(t))\\ &\qquad\times\left(\frac{\dot\Gamma(t)}{\Gamma(t)}(\epsilon-\bar\epsilon^{(ad)}_{a\sigma}(t))+\dot{\bar\epsilon}^{(ad)}_{a\sigma}(t)\right)\left[\rho^{(ad)}_{a\sigma}(\epsilon,t)\right]^2\\ &\quad+\frac{U\dot\Gamma(t)}{\Gamma(t)}\sum_\sigma\int d\epsilon\frac{df}{d\epsilon}(\epsilon-\bar\epsilon^{(ad)}_{a\sigma}(t))\rho^{(ad)}_{a\sigma}(\epsilon,t)\delta n_{a-\sigma}(t). \quad (3.26)\end{aligned}$$

The sum of (3.25) and (3.26) is therefore

$$\dot{E}_{nearly-ad}(t)=-\pi\sum_\sigma\int d\epsilon\frac{df}{d\epsilon}\left(\frac{\dot\Gamma(t)}{\Gamma(t)}(\epsilon-\bar\epsilon^{(ad)}_{a\sigma}(t))+\dot{\bar\epsilon}^{(ad)}_{a\sigma}(t)\right)^2\left[\rho^{(ad)}_{a\sigma}(\epsilon,t)\right]^2, \quad (3.27)$$

where the terms depending on $\delta n_{a-\sigma}$ in $\dot{E}^{(1)}_{nearly-ad}$ and $\dot{E}^{(2)}_{nearly-ad}$ cancel. The speed dependence in the derivatives $\dot\Gamma$ and $\dot{\bar\epsilon}^{(ad)}_{a\sigma}$ can be separated from the altitude dependence allowing us to write the nearly-adiabatic energy transfer rate in terms of the electronic friction coefficient $\eta$ (as in (3.18)). We find

$$\eta(s)=-\pi\sum_\sigma\int d\epsilon\frac{df}{d\epsilon}\left(\frac{d\Gamma}{ds}(s)\frac{(\epsilon-\bar\epsilon^{(ad)}_{a\sigma}(s))}{\Gamma(s)}+\frac{d\bar\epsilon^{(ad)}_{a\sigma}}{ds}(s)\right)^2\left[\rho^{(ad)}_{a\sigma}(\epsilon,s)\right]^2. \quad (3.28)$$

This expression will be used in chapter 5 to compare the non- and nearly-adiabatic models of energy transfer.

It is possible to further simplify our expression for $\dot{E}_{nearly-ad}$ in the zero temperature limit, when the derivative $df/d\epsilon$ becomes a delta function, (see (C.16) on page 77). $\dot{E}_{nearly-ad}$ then becomes

$$\dot{E}_{nearly-ad}(t)=\pi\sum_\sigma\left(\frac{\dot\Gamma(t)}{\Gamma(t)}(\epsilon_F-\bar\epsilon^{(ad)}_{a\sigma}(t))+\dot{\bar\epsilon}^{(ad)}_{a\sigma}(t)\right)^2\left[\rho^{(ad)}_{a\sigma}(\epsilon_F,t)\right]^2. \quad (3.29)$$

By comparing this expression to the zero temperature limit of $\dot{n}^{(ad)}_{a\sigma}$ as derived in appendix C.3, equation (C.34);

$$\dot{n}^{(ad)}_{a\sigma}(t)=-\left(\frac{\dot\Gamma(t)}{\Gamma(t)}(\epsilon_F-\bar\epsilon^{(ad)}_{a\sigma}(t))+\dot{\bar\epsilon}^{(ad)}_{a\sigma}(t)\right)\rho^{(ad)}_{a\sigma}(\epsilon_F,t), \quad (3.30)$$

we find

$$\dot{E}_{nearly-ad}(t) = \pi \sum_{\sigma} \left(\dot{n}^{(ad)}_{a\sigma}(t)\right)^2, \tag{3.31}$$

from which we can extract the friction coefficient;

$$\eta(s) = \pi \sum_{\sigma} \left(\frac{dn^{(ad)}_{a\sigma}}{ds}(s)\right)^2. \tag{3.32}$$

These expressions are remarkably compact, but are only valid at zero temperature.

The zero temperature results, (3.31) and (3.32), allow us to validate our analysis against existing work. Nourtier [67] related the electronic friction to a 'phase-shift' at the Fermi level through Friedel's sum rule;

$$\underline{\eta} = \frac{1}{\pi} \sum_{m} \left(\nabla \phi_m\right)^2, \tag{3.33}$$

where $\underline{\eta}$ represents the diagonal elements of the electronic friction tensor, $\phi$ is the phase-shift at the Fermi level and $m$ labels the various states of the system. This phase-shift is the same as that appearing in scattering theory, and is defined by Schiff [66] (page 121) as the difference between the phase of scattered and unscattered wave functions. In our system the adsorbate can be considered to be the impurity off which the metal electrons scatter. Schönhammer and Gunnarson [49] also related this phase-shift to the total energy transfer in a slowly evolving system by

$$\Delta E = \pi^{-1} \int_{-\infty}^{\infty} dt \left(\dot{\phi}_{\epsilon_F}(t)\right)^2. \tag{3.34}$$

Both the Nourtier, and Schönhammer and Gunnarson results are general and not restricted to the Newns-Anderson model.

To demonstrate the consistency of our model with these prior results we need an expression for $\phi$ within the mean-field Newns-Anderson model. Hewson [53] uses the Friedel sum rule to relate the phase-shift to an impurity density of states;

$$\rho^{(imp)}(\epsilon) = \frac{1}{\pi} \frac{d\phi}{d\epsilon}. \tag{3.35}$$

In our system the impurity is the adsorbate and we can therefore use this expression to relate $\phi$ to the adiabatic adsorbate occupation $n^{(ad)}_{a\sigma}$. By combining (2.32)

and (3.35) we find

$$\begin{aligned} n_{a\sigma}^{(ad)}(t) &= \int d\epsilon f(\epsilon)\rho_{a\sigma}^{(ad)}(\epsilon,t) \\ &= \frac{1}{\pi}\int d\epsilon f(\epsilon)\frac{d\phi_\sigma(\epsilon,t)}{d\epsilon}. \end{aligned} \tag{3.36}$$

Integration by parts then yields

$$\begin{aligned} n_{a\sigma}^{(ad)}(t) &= \frac{1}{\pi}\left[f(\epsilon)\phi_\sigma(\epsilon,t)\right]_{-\infty}^{\infty} - \frac{1}{\pi}\int d\epsilon\frac{df}{d\epsilon}\phi_\sigma(\epsilon,t) \\ &= -\frac{1}{\pi}\int d\epsilon\frac{df}{d\epsilon}\phi_\sigma(\epsilon,t), \end{aligned} \tag{3.37}$$

where we have used $\phi_\sigma(-\infty,t)=0$, which can be found by comparing (2.33) and (3.35). In the zero temperature limit this expression simply becomes

$$n_{a\sigma}^{(ad)}(t) = \frac{\phi_\sigma(\epsilon_F,t)}{\pi}. \tag{3.38}$$

This result allows us to see the equivalence of our nearly-adiabatic energy transfer rate (3.31) with Schönhammer and Gunnarson's result (3.34), and the electronic friction (3.32) with Nourtier's result (3.33). This demonstration of compatibility of the nearly-adiabatic energy transfer rate with previous work in the field also serves as a test of the non-adiabatic expression derived in the previous section.

Our expression for the zero-temperature limit of $\dot{E}_{nearly-ad}$, (3.31), also allows us to consider nearly-adiabatic energy transfer in a qualitative manner. In section 2.3 in the previous chapter we demonstrated the variation in the adsorbate occupation function $n_{a\sigma}^{(ad)}$ as the ratio $\Gamma/U$ is increased from zero. Figures 2.2 (a), (c) and (e) show the occupations of three model systems with different values of $\epsilon_a/U$. In each of the systems demonstrated there is a sharp spin-transition with a square-root like dependency on $\Gamma/U$. The derivative of this dependency will result in a singularity in $\dot{n}_{a\sigma}^{(ad)}$, and hence in the electronic friction coefficient $\eta$, at the spin-transition. This singularity in $\eta$ gives rise to an infinite energy transfer rate, implying that any adsorbate would lose all kinetic energy at the spin-transition altitude and stop. This behaviour is clearly unphysical and indicates a failure of nearly-adiabatic theory. This singularity at the spin-transition has also been observed in DFT calculations of the electronic friction coefficient for H/Cu(111) performed by Trail et al. [28, 29].

## 3.3 Summary

In this chapter we have developed expressions for the non-adiabatic energy transfer rate $\dot{E}_{non-ad}$, (3.17) and the nearly-adiabatic approximation to it, $\dot{E}_{nearly-ad}$, (3.27). In the first section of this chapter $\dot{E}_{non-ad}$ has been related to the differences between the adiabatic and dynamical functions $n_{a\sigma}$ and $p_\sigma$. We have derived an expression for $\dot{E}_{nearly-ad}$ in the second section, with the zero-temperature limit yielding a simple function of the time-derivative $\dot{n}^{(ad)}_{a\sigma}$. This relationship allows us to understand the failure of nearly-adiabatic theory when dealing with a spin-transition. We have also used the nearly-adiabatic model to define an electronic friction coefficient, which allows us to make contact with other nearly-adiabatic theories. The zero-temperature result for $\dot{E}_{nearly-ad}$ has been found to be consistent with previous theoretical work, giving us added confidence in the validity of our analysis.

We present numerical calculations of both the non-adiabatic and nearly-adiabatic energy transfer rates in chapter 5.

# Appendix B: Derivation of $\dot{E}$ for the Newns-Anderson system

In this appendix we demonstrate that the rate of change of the total energy of the mean-field Newns-Anderson system is given by (3.8), as reported by Plihal and Langreth [63]. We will develop an expression for the time-derivative of the mean-field Hamiltonian (2.3) by differentiating each term. The derivative of the first term (ignoring the sum over spin $\sigma$ for simplicity) is

$$\frac{d}{dt}\left\{\bar{\epsilon}_{a\sigma}(t)\hat{n}_{a\sigma}(t)\right\} = \dot{\bar{\epsilon}}_{a\sigma}(t)\hat{n}_{a\sigma}(t) + \bar{\epsilon}_{a\sigma}(t)\left(\frac{d\hat{c}^\dagger_{a\sigma}}{dt}(t)\hat{c}_{a\sigma}(t) + \hat{c}^\dagger_{a\sigma}(t)\frac{d\hat{c}_{a\sigma}}{dt}(t)\right). \quad \text{(B.1)}$$

By using the equations of motion for the electron operator $\hat{c}_{a\sigma}$, (2.7a), this can be expanded to give

$$\begin{aligned}
&\frac{d}{dt}\left\{\bar{\epsilon}_{a\sigma}(t)\hat{n}_{a\sigma}(t)\right\} \\
&\quad = \dot{\bar{\epsilon}}_{a\sigma}(t)\hat{n}_{a\sigma}(t) + \bar{\epsilon}_{a\sigma}(t)\Big(i[\bar{\epsilon}_{a\sigma}(t)\hat{c}^{\dagger}_{a\sigma}(t) + \sum_k V^*_{ak}(t)\hat{c}^{\dagger}_{k\sigma}(t)]\hat{c}_{a\sigma}(t) \\
&\qquad\qquad -i\hat{c}^{\dagger}_{a\sigma}(t)[\bar{\epsilon}_{a\sigma}(t)\hat{c}_{a\sigma}(t) + \sum_k V_{ak}(t)\hat{c}_{k\sigma}(t)]\Big) \\
&\quad = \dot{\bar{\epsilon}}_{a\sigma}(t)\hat{n}_{a\sigma}(t) - i\bar{\epsilon}_{a\sigma}(t)\sum_k \Big(V_{ak}(t)\hat{c}^{\dagger}_{a\sigma}(t)\hat{c}_{k\sigma}(t) - V^*_{ak}(t)\hat{c}^{\dagger}_{k\sigma}(t)\hat{c}_{a\sigma}(t)\Big) \qquad \text{(B.2)}
\end{aligned}$$

For the second term in the Hamiltonian (2.3) we find

$$\frac{d}{dt}\left\{\sum_k \epsilon_{k\sigma}\hat{n}_{k\sigma}(t)\right\} = \sum_k \epsilon_{k\sigma}\left(\frac{d\hat{c}^{\dagger}_{k\sigma}}{dt}(t)\hat{c}_{k\sigma}(t) + \hat{c}^{\dagger}_{k\sigma}(t)\frac{d\hat{c}_{k\sigma}}{dt}(t)\right), \qquad \text{(B.3)}$$

into which we substitute the equation of motion for $\hat{c}_{k\sigma}$, (2.7b). This yields

$$\begin{aligned}
\frac{d}{dt}\left\{\sum_k \epsilon_{k\sigma}\hat{n}_{k\sigma}(t)\right\} &= \sum_k \epsilon_{k\sigma}\big(i[\epsilon_{k\sigma}\hat{c}^{\dagger}_{k\sigma}(t) + V_{ak}(t)\hat{c}^{\dagger}_{a\sigma}(t)]\hat{c}_{k\sigma}(t) \\
&\qquad -i\hat{c}^{\dagger}_{k\sigma}(t)[\epsilon_{k\sigma}\hat{c}_{k\sigma}(t) + V^*_{ak}(t)\hat{c}_{a\sigma}(t)]\big) \\
&= i\sum_k \epsilon_{k\sigma}\left(V_{ak}(t)\hat{c}^{\dagger}_{a\sigma}(t)\hat{c}_{k\sigma}(t) - V^*_{ak}(t)\hat{c}^{\dagger}_{k\sigma}(t)\hat{c}_{a\sigma}(t)\right). \qquad \text{(B.4)}
\end{aligned}$$

The third term in (2.3) becomes

$$\begin{aligned}
&\frac{d}{dt}\left\{\sum_k \left(V_{ak}(t)\hat{c}^{\dagger}_{a\sigma}(t)\hat{c}_{k\sigma}(t) + V^*_{ak}(t)\hat{c}^{\dagger}_{k\sigma}(t)\hat{c}_{a\sigma}(t)\right)\right\} \\
&\qquad = \sum_k \left(\dot{V}_{ak}(t)\hat{c}^{\dagger}_{a\sigma}(t)\hat{c}_{k\sigma}(t) + \dot{V}^*_{ak}(t)\hat{c}^{\dagger}_{k\sigma}(t)\hat{c}_{a\sigma}(t)\right) \\
&\qquad\quad + \sum_k V_{ak}(t)\left(\frac{d\hat{c}^{\dagger}_{a\sigma}}{dt}(t)\hat{c}_{k\sigma}(t) + \hat{c}^{\dagger}_{a\sigma}(t)\frac{d\hat{c}_{k\sigma}}{dt}(t)\right) \\
&\qquad\quad + \sum_k V^*_{ak}(t)\left(\frac{d\hat{c}^{\dagger}_{k\sigma}}{dt}(t)\hat{c}_{a\sigma}(t) + \hat{c}^{\dagger}_{k\sigma}(t)\frac{d\hat{c}_{a\sigma}}{dt}(t)\right). \qquad \text{(B.5)}
\end{aligned}$$

By using both (2.7a) and (2.7b) this expression becomes

$$\begin{aligned}
&\frac{d}{dt}\left\{\sum_k \Big(V_{ak}(t)\hat{c}^\dagger_{a\sigma}(t)\hat{c}_{k\sigma}(t) + V^*_{ak}(t)\hat{c}^\dagger_{k\sigma}(t)\hat{c}_{a\sigma}(t)\Big)\right\} \\
&\quad = \sum_k \Big(\dot{V}_{ak}(t)\hat{c}^\dagger_{a\sigma}(t)\hat{c}_{k\sigma}(t) + \dot{V}^*_{ak}(t)\hat{c}^\dagger_{k\sigma}(t)\hat{c}_{a\sigma}(t)\Big) \\
&\qquad + \sum_k V_{ak}(t)\Big(i[\bar{\epsilon}_{a\sigma}(t)\hat{c}^\dagger_{a\sigma}(t) + \sum_{k'} V^*_{ak'}(t)\hat{c}^\dagger_{k'\sigma}(t)]\hat{c}_{k\sigma}(t) \\
&\qquad\quad -i\hat{c}^\dagger_{a\sigma}(t)[\epsilon_{k\sigma}\hat{c}_{k\sigma}(t) + V^*_{ak}(t)\hat{c}_{a\sigma}(t)]\Big) \\
&\qquad + \sum_k V^*_{ak}(t)\Big(i[\epsilon_{k\sigma}\hat{c}^\dagger_{k\sigma}(t) + V_{ak}(t)\hat{c}_{a\sigma}(t)]\hat{c}_{a\sigma}(t) \\
&\qquad\quad -i\hat{c}^\dagger_{k\sigma}(t)[\bar{\epsilon}_{a\sigma}(t)\hat{c}_{a\sigma}(t) + \sum_{k'} V_{ak'}(t)\hat{c}_{k'\sigma}(t)]\Big),
\end{aligned} \tag{B.6}$$

which can be expanded to give

$$\begin{aligned}
&\frac{d}{dt}\left\{\sum_k \Big(V_{ak}(t)\hat{c}^\dagger_{a\sigma}(t)\hat{c}_{k\sigma}(t) + V^*_{ak}(t)\hat{c}^\dagger_{k\sigma}(t)\hat{c}_{a\sigma}(t)\Big)\right\} \\
&\quad = \sum_k \Big(\dot{V}_{ak}(t)\hat{c}^\dagger_{a\sigma}(t)\hat{c}_{k\sigma}(t) + \dot{V}^*_{ak}(t)\hat{c}^\dagger_{k\sigma}(t)\hat{c}_{a\sigma}(t)\Big) \\
&\qquad + i\bar{\epsilon}_{a\sigma}(t)\sum_k V_{ak}(t)\hat{c}^\dagger_{a\sigma}(t)\hat{c}_{k\sigma}(t) + i\sum_{k,k'} V^*_{ak'}(t)V_{ak}(t)\hat{c}^\dagger_{k'\sigma}(t)\hat{c}_{k\sigma}(t) \\
&\qquad - i\sum_k \epsilon_{k\sigma}V_{ak}(t)\hat{c}^\dagger_{a\sigma}(t)\hat{c}_{k\sigma}(t) - i\hat{n}_{a\sigma}(t)\sum_k |V_{ak}(t)|^2 \\
&\qquad + i\sum_k \epsilon_{k\sigma}V^*_{ak}(t)\hat{c}^\dagger_{k\sigma}(t)\hat{c}_{a\sigma}(t) + i\hat{n}_{a\sigma}(t)\sum_k |V_{ak}(t)|^2 \\
&\qquad - i\bar{\epsilon}_{a\sigma}(t)\sum_k V^*_{ak}(t)n_{ka\sigma}(t) - i\sum_{k,k'} V^*_{ak}(t)V_{ak'}(t)\hat{c}^\dagger_{k\sigma}(t)\hat{c}_{k'\sigma}(t).
\end{aligned} \tag{B.7}$$

The terms in this expression involving $\hat{n}_{a\sigma}$ cancel, as do those containing the product of the metal electron operators. We can therefore rewrite (B.7) as

$$\begin{aligned}
&\frac{d}{dt}\left\{\sum_k \Big(V_{ak}(t)\hat{c}^\dagger_{a\sigma}(t)\hat{c}_{k\sigma}(t) + V^*_{ak}(t)\hat{c}^\dagger_{k\sigma}(t)\hat{c}_{a\sigma}(t)\Big)\right\} \\
&\quad = \sum_k \Big(\dot{V}_{ak}(t)\hat{c}^\dagger_{a\sigma}(t)\hat{c}_{k\sigma}(t) + \dot{V}^*_{ak}(t)\hat{c}^\dagger_{k\sigma}(t)\hat{c}_{a\sigma}(t)\Big) \\
&\qquad + i\bar{\epsilon}_{a\sigma}(t)\sum_k \Big(V_{ak}(t)\hat{c}^\dagger_{a\sigma}(t)\hat{c}_{k\sigma}(t) - V^*_{ak}(t)\hat{c}^\dagger_{k\sigma}(t)\hat{c}_{a\sigma}(t)\Big) \\
&\qquad - i\sum_k \epsilon_{k\sigma}\Big(V_{ak}(t)\hat{c}^\dagger_{a\sigma}(t)\hat{c}_{k\sigma}(t) - V^*_{ak}(t)\hat{c}^\dagger_{k\sigma}(t)\hat{c}_{a\sigma}(t)\Big).
\end{aligned} \tag{B.8}$$

The final term in the Hamiltonian is simply

$$-U\frac{d}{dt}\left\{n_{a\sigma}(t)n_{a-\sigma}(t)\right\}, \tag{B.9}$$

which we do not expand further. The sum of equations (B.2), (B.4), (B.8) and (B.9) gives the time-derivative of the Hamiltonian, which simplifies to

$$\begin{aligned}\frac{d\hat{H}_{MF}}{dt} &= \sum_{\sigma}\dot{\bar{\epsilon}}_{a\sigma}(t)\hat{n}_{a\sigma}(t)+\sum_{k,\sigma}\left(\dot{V}_{ak}(t)\hat{c}^{\dagger}_{a\sigma}(t)\hat{c}_{k\sigma}(t)+\text{H.c}\right)\\ &\quad -U\frac{d}{dt}\left\{n_{a\sigma}(t)n_{a-\sigma}(t)\right\},\end{aligned} \tag{B.10}$$

where all of the imaginary terms have cancelled, and we have reinstated the sum over spin $\sigma$. The rate of change of the total energy of the system, $\dot{E}$, is simply the thermally averaged expectation value of (B.10);

$$\begin{aligned}\dot{E}(t) &= \left\langle\!\!\left\langle \frac{d\hat{H}_{MF}}{dt}\right\rangle\!\!\right\rangle\\ &= \sum_{\sigma}\dot{\bar{\epsilon}}_{a\sigma}(t)n_{a\sigma}(t)+\sum_{k,\sigma}\left(\dot{V}_{ak}(t)n_{ak\sigma}(t)+\text{c.c}\right)\\ &\quad -U\frac{d}{dt}\left\{n_{a\sigma}(t)n_{a-\sigma}(t)\right\}\\ &= \sum_{\sigma}\dot{\epsilon}_{a}(t)n_{a\sigma}(t)+\sum_{k,\sigma}\left(\dot{V}_{ak}(t)n_{ak\sigma}(t)+\text{c.c}\right),\end{aligned} \tag{B.11}$$

where we have used the definitions of the occupation functions (2.14). This expression is used in section 3.1 to obtain the rate of non-adiabatic energy transfer to the metal.

# Appendix C: The nearly-adiabatic energy transfer rate

## C.1: Derivation of a nearly-adiabatic expression for $p_\sigma$

By using (3.19) and the Taylor expansions given in section 3.2, (equations (3.21) to (3.22)), the quantity $p_\sigma$, (2.20), can be expanded to give

$$\begin{aligned} p_\sigma(\epsilon,t) &= \sqrt{\frac{\Gamma(t)}{2\pi}}\int_{t_0}^{t} dt_1 \left(1+(t_1-t)\frac{\dot{\Gamma}(t)}{2\Gamma(t)}\right)\exp\left[i(\tilde{\epsilon}_{a\sigma}^{(ad)}(t)-\epsilon)(t_1-t)\right] \\ &\quad \times \exp\left[iU\delta n_{a-\sigma}(t)(t_1-t)+i\frac{\dot{\tilde{\epsilon}}_{a\sigma}^{(ad)}(t)}{2}(t_1-t)^2\right], \end{aligned} \tag{C.1}$$

where the Taylor expansion of $\sqrt{\Gamma(t_1)}$ about $t_1=t$;

$$\sqrt{\Gamma(t_1)} = \sqrt{\Gamma(t)}\left(1+(t_1-t)\frac{\dot{\Gamma}(t)}{2\Gamma(t)}\right), \tag{C.2}$$

has also been used. The second exponential in (C.1) only contains small quantities, and we therefore Taylor expand this term to give

$$\begin{aligned} p_\sigma(\epsilon,t) &= \sqrt{\frac{\Gamma(t)}{2\pi}}\int_{t_0}^{t} dt_1 \left(1+(t_1-t)\frac{\dot{\Gamma}(t)}{2\Gamma(t)}\right) \\ &\quad \times\left(1+iU\delta n_{a-\sigma}(t)(t_1-t)-i\frac{\dot{\tilde{\epsilon}}_{a\sigma}^{(ad)}(t)}{2}(t_1-t)^2\right) \\ &\quad \times\exp\left[i(\tilde{\epsilon}_{a\sigma}^{(ad)}(t)-\epsilon)(t_1-t)\right] \\ &= \sqrt{\frac{\Gamma(t)}{2\pi}}\int_{t_0}^{t} dt_1 \left(1+(t_1-t)\frac{\dot{\Gamma}(t)}{2\Gamma(t)}+iU\delta n_{a-\sigma}(t)(t_1-t)\right. \\ &\quad \left.+i\frac{\dot{\tilde{\epsilon}}_{a\sigma}^{(ad)}(t)}{2}(t_1-t)^2\right)\exp\left[i(\tilde{\epsilon}_{a\sigma}^{(ad)}(t)-\epsilon)(t_1-t)\right], \end{aligned} \tag{C.3}$$

where products of the small quantities $\dot{\Gamma}$, $\dot{\tilde{\epsilon}}_{a\sigma}$ and $\delta n_{a\sigma}$ have been ignored. By recognising that the evolution of the system is slow, i.e. to reach a given state a long time has passed, we can set $t_0=-\infty$ and introduce the substitution

$\tau = t_1 - t$ so that $p_\sigma$ becomes

$$\begin{aligned} p_\sigma(\epsilon,t) &= \sqrt{\frac{\Gamma(t)}{2\pi}}\int_{-\infty}^{0} d\tau \exp[i(\tilde{\epsilon}^{(ad)}_{a\sigma}(t)-\epsilon)\tau] \\ &+\sqrt{\frac{\Gamma(t)}{2\pi}}\left(\frac{\dot{\Gamma}(t)}{2\Gamma(t)}+iU\delta n_{a-\sigma}(t)\right)\int_{-\infty}^{0} d\tau\ \tau \exp[i(\tilde{\epsilon}^{(ad)}_{a\sigma}(t)-\epsilon)\tau] \\ &+i\frac{\dot{\tilde{\epsilon}}^{(ad)}_{a\sigma}(t)}{2}\int_{-\infty}^{0} d\tau\ \tau^2 \exp[i(\tilde{\epsilon}^{(ad)}_{a\sigma}(t)-\epsilon)\tau]. \end{aligned} \tag{C.4}$$

The first $\tau$ integral in this expression can be evaluated, to give

$$\begin{aligned} \int_{-\infty}^{0} d\tau \exp[i(\tilde{\epsilon}^{(ad)}_{a\sigma}(t)-\epsilon)\tau] &= \left[\frac{i\exp[-i(\tilde{\epsilon}^{(ad)}_{a\sigma}(t)-\epsilon)\tau]}{\epsilon-\tilde{\epsilon}^{(ad)}_{a\sigma}(t)}\right]_{-\infty}^{0} \\ &= \frac{i}{\epsilon-\tilde{\epsilon}^{(ad)}_{a\sigma}(t)}, \end{aligned} \tag{C.5}$$

where the second term vanishes as $\Gamma(t) > 0$. The $\tau$ integrals in the second and third terms of (C.4) can be expressed as $\epsilon$ derivatives of (C.5);

$$\begin{aligned} \int_{-\infty}^{0} d\tau\ \tau \exp[i(\tilde{\epsilon}^{(ad)}_{a\sigma}(t)-\epsilon)\tau] &= i\frac{d}{d\epsilon}\int_{-\infty}^{0} d\tau \exp[i(\tilde{\epsilon}^{(ad)}_{a\sigma}(t)-\epsilon)\tau] \\ &= \frac{1}{(\epsilon-\tilde{\epsilon}^{(ad)}_{a\sigma}(t))^2}, \end{aligned} \tag{C.6}$$

$$\begin{aligned} \int_{-\infty}^{0} d\tau\ \tau^2 \exp[i(\tilde{\epsilon}^{(ad)}_{a\sigma}(t)-\epsilon)\tau] &= -\frac{d^2}{d\epsilon^2}\int_{-\infty}^{0} d\tau \exp[i(\tilde{\epsilon}^{(ad)}_{a\sigma}(t)-\epsilon)\tau] \\ &= \frac{-2i}{(\epsilon-\tilde{\epsilon}^{(ad)}_{a\sigma}(t))^3}. \end{aligned} \tag{C.7}$$

By substituting (C.5), (C.6) and (C.7) into (C.4) we find

$$\begin{aligned} p_\sigma(\epsilon,t) &= \sqrt{\frac{\Gamma(t)}{2\pi}}\frac{i}{\epsilon-\tilde{\epsilon}^{(ad)}_{a\sigma}(t)} \\ &+\sqrt{\frac{\Gamma(t)}{2\pi}}\frac{1}{(\epsilon-\tilde{\epsilon}^{(ad)}_{a\sigma}(t))^2}\left(\frac{\dot{\Gamma}(t)}{2\Gamma(t)}+iU\delta n_{a-\sigma}(t)+\frac{\dot{\tilde{\epsilon}}^{(ad)}_{a\sigma}(t)}{\epsilon-\tilde{\epsilon}^{(ad)}_{a\sigma}(t)}\right). \end{aligned} \tag{C.8}$$

In order to express this concisely in terms of the small quantities $\dot{\Gamma}$, $\delta n_{a\sigma}$ and $\dot{\tilde{\epsilon}}^{(ad)}_{a\sigma}$ we expand the brackets in the final term using the adiabatic equivalent of

the definition of $\tilde{\epsilon}_{a\sigma}$, (A.25), yielding

$$\begin{aligned}\dot{\Gamma}(t)\left(\frac{1}{2\Gamma(t)}-\frac{i}{2(\epsilon-\tilde{\epsilon}^{(ad)}_{a\sigma}(t))}\right)+iU\delta n_{a-\sigma}(t)+\frac{\dot{\tilde{\epsilon}}^{(ad)}_{a\sigma}(t)}{\epsilon-\tilde{\epsilon}^{(ad)}_{a\sigma}(t)}\\ =\frac{\dot{\Gamma}(t)(\epsilon-\tilde{\epsilon}^{(ad)}_{a\sigma}(t)-i\Gamma(t))}{2\Gamma(t)(\epsilon-\tilde{\epsilon}^{(ad)}_{a\sigma}(t))}+iU\delta n_{a-\sigma}(t)+\frac{\dot{\tilde{\epsilon}}^{(ad)}_{a\sigma}(t)}{\epsilon-\tilde{\epsilon}^{(ad)}_{a\sigma}(t)}\\ =\frac{\dot{\Gamma}(t)(\epsilon-\tilde{\epsilon}^{(ad)*}_{a\sigma}(t))}{2\Gamma(t)(\epsilon-\tilde{\epsilon}^{(ad)}_{a\sigma}(t))}+iU\delta n_{a-\sigma}(t)+\frac{\dot{\tilde{\epsilon}}^{(ad)}_{a\sigma}(t)}{\epsilon-\tilde{\epsilon}^{(ad)}_{a\sigma}(t)},\end{aligned} \tag{C.9}$$

where the relation $\tilde{\epsilon}^{(ad)*}_{a\sigma}=\bar{\epsilon}^{(ad)}_{a\sigma}+i\Gamma/2=\tilde{\epsilon}^{(ad)}_{a\sigma}+i\Gamma$ has been used. We therefore find the nearly-adiabatic expansion of $p_\sigma$ to be

$$\begin{aligned}p_\sigma(\epsilon,t) &= \sqrt{\frac{\Gamma(t)}{2\pi}}\frac{i}{\epsilon-\tilde{\epsilon}^{(ad)}_{a\sigma}(t)}+\sqrt{\frac{\Gamma(t)}{2\pi}}\frac{1}{(\epsilon-\tilde{\epsilon}^{(ad)}_{a\sigma}(t))^2}\\ &\quad\times\left(\frac{\dot{\Gamma}(t)(\epsilon-\tilde{\epsilon}^{(ad)*}_{a\sigma}(t))}{2\Gamma(t)(\epsilon-\tilde{\epsilon}^{(ad)}_{a\sigma}(t))}+iU\delta n_{a-\sigma}(t)+\frac{\dot{\tilde{\epsilon}}^{(ad)}_{a\sigma}(t)}{\epsilon-\tilde{\epsilon}^{(ad)}_{a\sigma}(t)}\right).\end{aligned} \tag{C.10}$$

The first term in this expression is $p^{(ad)}_\sigma$ and therefore the nearly-adiabatic component of $p_\sigma$, $\delta p_\sigma=p_\sigma-p^{(ad)}_\sigma$, becomes

$$\begin{aligned}\delta p_\sigma(\epsilon,t) &= \sqrt{\frac{\Gamma(t)}{2\pi}}\frac{1}{(\epsilon-\tilde{\epsilon}^{(ad)}_{a\sigma}(t))^2}\\ &\quad\times\left(\frac{\dot{\Gamma}(t)(\epsilon-\tilde{\epsilon}^{(ad)*}_{a\sigma}(t))}{2\Gamma(t)(\epsilon-\tilde{\epsilon}^{(ad)}_{a\sigma}(t))}+iU\delta n_{a-\sigma}(t)+\frac{\dot{\tilde{\epsilon}}^{(ad)}_{a\sigma}(t)}{\epsilon-\tilde{\epsilon}^{(ad)}_{a\sigma}(t)}\right).\end{aligned} \tag{C.11}$$

This expression will be used in the following section of this appendix to obtain a nearly-adiabatic expansion of $\delta n_{a\sigma}$, and in section C.4 to derive the nearly-adiabatic equivalent of the second term in $\dot{E}_{non-ad}$.

## C.2: Derivation of a nearly-adiabatic expression for $\delta n_{a\sigma}$

In this appendix we derive an expression for the difference $\delta n_{a\sigma}=n_{a\sigma}-n^{(ad)}_{a\sigma}$ using the expression for $\delta p_\sigma$ obtained in the previous section. $\delta n_{a\sigma}$ is needed to calculate the contribution to the nearly-adiabatic energy transfer rate from the first term in (3.17).

We first substitute $p_\sigma=p^{(ad)}_\sigma+\delta p_\sigma$ into the definition of $n_{a\sigma}$, (2.19), yielding to

first order in small quantities (see page 65)

$$\begin{aligned} n_{a\sigma}(t) &= \int d\epsilon f(\epsilon)|p_\sigma^{(ad)}(\epsilon,t)+\delta p_\sigma(\epsilon,t)|^2 + n_{a\sigma}(t_0)\exp\left[-\int_{t_0}^{t}\Gamma(t')dt'\right] \\ &= \int d\epsilon f(\epsilon)\rho_{a\sigma}^{(ad)}(\epsilon,t) + 2\int d\epsilon f(\epsilon)\mathrm{Re}\left\{p_\sigma^{(ad)*}(\epsilon,t)\delta p_\sigma(\epsilon,t)\right\} \\ &\quad + n_{a\sigma}(t_0)\exp\left[-\int_{t_0}^{t}\Gamma(t')dt'\right]. \end{aligned} \tag{C.12}$$

For slow variation of $\Gamma$ the argument of the exponential in the final, transient, term in this equation will be large and negative. This term will approach zero and can therefore be ignored in the nearly-adiabatic approximation. From (C.12), and the definition of $n_{a\sigma}^{(ad)}$ (2.32), we can see that the difference between the nearly-adiabatic and adiabatic occupations $\delta n_{a\sigma} = n_{a\sigma} - n_{a\sigma}^{(ad)}$ is simply

$$\delta n_{a\sigma}(t) = 2\int d\epsilon f(\epsilon)\mathrm{Re}\left\{p_\sigma^{(ad)*}(\epsilon,t)\delta p_\sigma(\epsilon,t)\right\}, \tag{C.13}$$

where the $\epsilon$ integral is over all energies. It is convenient at this point to perform a by-parts integration step of this expression. This yields

$$\begin{aligned} \delta n_{a\sigma}(t) &= 2\left[f(\epsilon)\int^{\epsilon} d\epsilon\ \mathrm{Re}\left\{p_\sigma^{(ad)*}(\epsilon,t)\delta p_\sigma(\epsilon,t)\right\}\right]_{-\infty}^{\infty} \\ &\quad -2\int d\epsilon\ \frac{df}{d\epsilon}\int^{\epsilon} d\epsilon\ \mathrm{Re}\left\{p_\sigma^{(ad)*}(\epsilon,t)\delta p_\sigma(\epsilon,t)\right\}, \end{aligned} \tag{C.14}$$

where we use the notation $\int^{\epsilon} d\epsilon$ to denote an indefinite energy integral evaluated at $\epsilon$. The first term in this equation yields zero as the Fermi function is zero at $\epsilon = \infty$ and the product $p_\sigma^{(ad)*}\delta p_\sigma$ has $\epsilon^{-3}$ and $\epsilon^{-4}$ dependent terms, which tend to zero at $\epsilon = -\infty$. Equation (C.14) therefore becomes

$$\delta n_{a\sigma}(t) = -2\int d\epsilon\ \frac{df}{d\epsilon}\int^{\epsilon} d\epsilon\ \mathrm{Re}\left\{p_\sigma^{(ad)*}(\epsilon,t)\delta p_\sigma(\epsilon,t)\right\}. \tag{C.15}$$

Equation (C.13) has been replaced with (C.15) to allow us to easily consider the nearly-adiabatic transfer at both zero and finite temperatures. In the zero temperature limit the derivative of the Fermi function becomes

$$\lim_{T\to 0}\frac{df}{d\epsilon} = -\delta(\epsilon-\epsilon_F) \tag{C.16}$$

and the energy integral in (C.15) then becomes trivial.

In order to maintain clarity in the rest of this derivation we separate the problem into three parts corresponding to the quantities $\dot{\Gamma}$, $U\delta n_{a-\sigma}$ and $\dot{\tilde{\epsilon}}^{(ad)}_{a\sigma}$ which appear in (C.11). We will derive the contribution of each of these terms to $\delta n_{a\sigma}$ separately.

We start by considering the coefficient of $\dot{\Gamma}$ in the product $p^{(ad)*}_{\sigma}\delta p_{\sigma}$. By using (2.31) and (C.11) we find

$$\begin{aligned}\left\{p^{(ad)*}_{\sigma}(\epsilon,t)\delta p_{\sigma}(\epsilon,t)\right\}_{[\dot{\Gamma}]} &= \frac{\Gamma(t)}{2\pi}.\frac{-i}{(\epsilon-\tilde{\epsilon}^{(ad)*}_{a\sigma}(t))(\epsilon-\tilde{\epsilon}^{(ad)}_{a\sigma}(t))^2}.\frac{\epsilon-\tilde{\epsilon}^{(ad)*}_{a\sigma}(t)}{2\Gamma(t)(\epsilon-\tilde{\epsilon}^{(ad)}_{a\sigma}(t))} \\ &= -i\frac{1}{4\pi}.\frac{1}{(\epsilon-\tilde{\epsilon}^{(ad)}_{a\sigma})^3}. \qquad \text{(C.17)}\end{aligned}$$

The indefinite integral of this expression over energy $\epsilon$ gives

$$\int^{\epsilon} d\epsilon\left\{p^{(ad)*}_{\sigma}(\epsilon,t)\delta p_{\sigma}(\epsilon,t)\right\}_{[\dot{\Gamma}]} = \frac{i}{8\pi}.\frac{1}{(\epsilon-\tilde{\epsilon}_{a\sigma}(t))^2}, \qquad \text{(C.18)}$$

which has the real part

$$\begin{aligned}\mathrm{Re}\left\{\int^{\epsilon} d\epsilon\; p^{(ad)*}_{\sigma}(\epsilon,t)\delta p_{\sigma}(\epsilon,t)\right\}_{[\dot{\Gamma}]} &= \frac{1}{8\pi}.\frac{\Gamma(t)(\epsilon-\bar{\epsilon}^{(ad)}_{a\sigma}(t))}{[(\epsilon-\bar{\epsilon}^{(ad)}_{a\sigma}(t))^2+\Gamma^2(t)/4]^2} \\ &= \frac{\pi}{2\Gamma(t)}(\epsilon-\bar{\epsilon}^{(ad)}_{a\sigma}(t))\left[\rho^{(ad)}_{a\sigma}(\epsilon,t)\right]^2, \qquad \text{(C.19)}\end{aligned}$$

where $\rho^{(ad)}_{a\sigma}$ is defined in (2.33). The contribution to $\delta n_{a\sigma}$ from terms containing $\dot{\Gamma}$ is therefore

$$\{\delta n_{a\sigma}(t)\}_{[\dot{\Gamma}]} = -\pi\frac{\dot{\Gamma}(t)}{\Gamma(t)}\int d\epsilon\;\frac{df}{d\epsilon}(\epsilon-\bar{\epsilon}^{(ad)}_{a\sigma}(t))\left[\rho^{(ad)}_{a\sigma}(\epsilon,t)\right]^2. \qquad \text{(C.20)}$$

The coefficient of $U\delta n_{a-\sigma}$ in the product $p^{(ad)*}_{\sigma}\delta p_{\sigma}$ is

$$\left\{p^{(ad)*}_{\sigma}(\epsilon,t)\delta p_{\sigma}(\epsilon,t)\right\}_{[U\delta n_{a-\sigma}]} = -\frac{\Gamma(t)}{2\pi}.\frac{1}{(\epsilon-\tilde{\epsilon}^{(ad)*}_{a\sigma}(t))(\epsilon-\tilde{\epsilon}^{(ad)}_{a\sigma}(t))^2}. \qquad \text{(C.21)}$$

By taking the real part we find

$$\mathrm{Re}\left\{p^{(ad)*}_{\sigma}(\epsilon,t)\delta p_{\sigma}(\epsilon,t)\right\}_{[U\delta n_{a-\sigma}]} = \frac{\Gamma(t)}{2\pi}.\frac{(\epsilon-\bar{\epsilon}^{(ad)}_{a\sigma}(t))}{[(\epsilon-\bar{\epsilon}^{(ad)}_{a\sigma}(t))^2+\Gamma^2(t)/4]^2}. \qquad \text{(C.22)}$$

On integration this becomes

$$\begin{aligned}\int^{\epsilon} d\epsilon \ \mathrm{Re}\left\{p_{\sigma}^{(ad)*}(\epsilon,t)\delta p_{\sigma}(\epsilon,t)\right\}_{[U\delta n_{a-\sigma}]} &= -\frac{\Gamma(t)}{4\pi}.\frac{1}{[(\epsilon-\bar{\epsilon}_{a\sigma}^{(ad)}(t))^2+\Gamma^2(t)/4]} \\ &= -\frac{1}{2}\rho_{a\sigma}^{(ad)}(\epsilon,t), \end{aligned} \tag{C.23}$$

and the contribution of this term to $\delta n_{a\sigma}$ is therefore

$$\{\delta n_{a\sigma}(t)\}_{[U\delta n_{a-\sigma}]} = U\delta n_{a-\sigma}(t)\int d\epsilon \ \frac{df}{d\epsilon}\rho_{a\sigma}^{(ad)}(\epsilon,t). \tag{C.24}$$

The coefficient of $\dot{\bar{\epsilon}}_{a\sigma}^{(ad)}$ in the product $p_{\sigma}^{(ad)*}\delta p_{\sigma}$ is

$$\left\{p_{\sigma}^{(ad)*}(\epsilon,t)\delta p_{\sigma}(\epsilon,t)\right\}_{[\dot{\bar{\epsilon}}_{a\sigma}^{(ad)}]} = -i\frac{\Gamma(t)}{2\pi}.\frac{1}{(\epsilon-\tilde{\epsilon}_{a\sigma}^{(ad)*}(t))(\epsilon-\tilde{\epsilon}_{a\sigma}^{(ad)}(t))^3}, \tag{C.25}$$

which has the real part

$$\mathrm{Re}\left\{p_{\sigma}^{(ad)*}(\epsilon,t)\delta p_{\sigma}(\epsilon,t)\right\}_{[\dot{\bar{\epsilon}}_{a\sigma}^{(ad)}]} = -\frac{\Gamma^2(t)}{2\pi}.\frac{(\epsilon-\bar{\epsilon}_{a\sigma}^{(ad)}(t))}{[(\epsilon-\bar{\epsilon}_{a\sigma}^{(ad)}(t))^2+\Gamma^2(t)/4]^3}. \tag{C.26}$$

The integral of this equation gives

$$\begin{aligned}\int^{\epsilon} d\epsilon \ \mathrm{Re}\left\{p_{\sigma}^{(ad)*}(\epsilon,t)\delta p_{\sigma}(\epsilon,t)\right\}_{[\dot{\bar{\epsilon}}_{a\sigma}^{(ad)}]} &= \frac{\Gamma^2(t)}{8\pi}.\frac{1}{[(\epsilon-\bar{\epsilon}_{a\sigma}^{(ad)}(t))^2+\Gamma^2(t)/4]^2} \\ &= \frac{\pi}{2}\left[\rho_{a\sigma}^{(ad)}(\epsilon,t)\right]^2, \end{aligned} \tag{C.27}$$

which on combination with (C.14) becomes

$$\{\delta n_{a\sigma}(t)\}_{[\dot{\bar{\epsilon}}_{a\sigma}^{(ad)}]} = -\pi\dot{\bar{\epsilon}}_{a\sigma}^{(ad)}(t)\int d\epsilon \ \frac{df}{d\epsilon}\left[\rho_{a\sigma}^{(ad)}(\epsilon,t)\right]^2. \tag{C.28}$$

The sum of equations (C.20), (C.24) and (C.28) gives our final expression for $\delta n_{a\sigma}$;

$$\begin{aligned}\delta n_{a\sigma}(t) &= -\pi\int d\epsilon \ \frac{df}{d\epsilon}\left(\frac{\dot{\Gamma}(t)}{\Gamma(t)}(\epsilon-\bar{\epsilon}_{a\sigma}^{(ad)}(t))+\dot{\bar{\epsilon}}_{a\sigma}^{(ad)}(t)\right)\left[\rho_{a\sigma}^{(ad)}(\epsilon,t)\right]^2 \\ &\quad +U\delta n_{a-\sigma}(t)\int d\epsilon \ \frac{df}{d\epsilon}\rho_{a\sigma}^{(ad)}(\epsilon,t). \end{aligned} \tag{C.29}$$

By considering this expression as a pair of simultaneous equations for the two

spins $\sigma$ we can write this result in matrix form as

$$\begin{pmatrix} 1 & -U\int d\epsilon \frac{df}{d\epsilon}\rho^{(ad)}_{a\sigma}(\epsilon,t) \\ -U\int d\epsilon \frac{df}{d\epsilon}\rho^{(ad)}_{a-\sigma}(\epsilon,t) & 1 \end{pmatrix} \begin{pmatrix} \delta n_{a\sigma}(t) \\ \delta n_{a-\sigma}(t) \end{pmatrix}$$
$$= -\pi \begin{pmatrix} \int d\epsilon \frac{df}{d\epsilon}\left(\frac{\dot{\Gamma}(t)}{\Gamma(t)}(\epsilon-\bar{\epsilon}^{(ad)}_{a\sigma}(t))+\dot{\bar{\epsilon}}^{(ad)}_{a\sigma}(t)\right)\left[\rho^{(ad)}_{a\sigma}(\epsilon,t)\right]^2 \\ \int d\epsilon \frac{df}{d\epsilon}\left(\frac{\dot{\Gamma}(t)}{\Gamma(t)}(\epsilon-\bar{\epsilon}^{(ad)}_{a-\sigma}(t))+\dot{\bar{\epsilon}}^{(ad)}_{a-\sigma}(t)\right)\left[\rho^{(ad)}_{a-\sigma}(\epsilon,t)\right]^2 \end{pmatrix}. \quad \text{(C.30)}$$

This matrix equation will be used in the following section for the derivation of the nearly-adiabatic equivalent of the first term in $\dot{E}_{non-ad}$.

## C.3: Derivation of $\dot{E}^{(1)}_{nearly-ad}$

In this section we derive the nearly-adiabatic equivalent of the first term in the non-adiabatic energy transfer rate $\dot{E}_{non-ad}$, equation (3.17). We will refer to this term as $\dot{E}^{(1)}_{nearly-ad}$.

In order to derive an expression for $\dot{E}^{(1)}_{nearly-ad}$ we first eliminate the derivative $\dot{\epsilon}_a$. This will allow us to compare terms in $\dot{E}^{(1)}_{nearly-ad}$ with those in $\dot{E}^{(2)}_{nearly-ad}$ when deriving a final expression for the nearly-adiabatic energy transfer rate. This elimination is performed by considering the derivative of $\bar{\epsilon}^{(ad)}_{a\sigma}$;

$$\dot{\bar{\epsilon}}^{(ad)}_{a\sigma}(t) = \dot{\epsilon}_a(t) + U\dot{n}^{(ad)}_{a-\sigma}(t). \quad \text{(C.31)}$$

We therefore require an expression for the time-derivative $\dot{n}^{(ad)}_{a\sigma}$. This can be achieved using (2.32) and the 'by-parts' integration step used in the previous section of this appendix (see (C.13) to (C.15) on page 77). Equation (2.32) is expanded to give

$$n^{(ad)}_{a\sigma}(t) = \left[f(\epsilon)\int^{\epsilon} d\epsilon \rho^{(ad)}_{a\sigma}(\epsilon,t)\right]^{\infty}_{-\infty} - \int d\epsilon\, \frac{df}{d\epsilon}\int^{\epsilon} d\epsilon \rho^{(ad)}_{a\sigma}(\epsilon,t), \quad \text{(C.32)}$$

which can be expanded further using the definition of $\rho^{(ad)}_{a\sigma}$, (2.33), yielding

$$n^{(ad)}_{a\sigma}(t) = \left[f(\epsilon)\frac{1}{\pi}\tan^{-1}\left\{2\frac{\epsilon-\bar{\epsilon}^{(ad)}_{a\sigma}(t)}{\Gamma(t)}\right\}\right]^{\infty}_{-\infty} - \frac{1}{\pi}\int d\epsilon\, \frac{df}{d\epsilon}\tan^{-1}\left\{2\frac{\epsilon-\bar{\epsilon}^{(ad)}_{a\sigma}(t)}{\Gamma(t)}\right\}$$
$$= 1/2 - \frac{1}{\pi}\int d\epsilon\, \frac{df}{d\epsilon}\tan^{-1}\left\{2\frac{\epsilon-\bar{\epsilon}^{(ad)}_{a\sigma}(t)}{\Gamma(t)}\right\}. \quad \text{(C.33)}$$

Differentiating this expression with respect to time gives

$$\begin{aligned}
\dot{n}^{(ad)}_{a\sigma}(t) &= -\frac{1}{\pi}\int d\epsilon\ \frac{df}{d\epsilon}\Bigg(\dot{\Gamma}(t)\frac{d}{d\Gamma}\tan^{-1}\left\{2\frac{\epsilon-\bar{\epsilon}^{(ad)}_{a\sigma}(t)}{\Gamma(t)}\right\} \\
&\qquad\qquad +\dot{\bar{\epsilon}}^{(ad)}_{a\sigma}(t)\frac{d}{d\bar{\epsilon}^{(ad)}_{a\sigma}}\tan^{-1}\left\{2\frac{\epsilon-\bar{\epsilon}^{(ad)}_{a\sigma}(t)}{\Gamma(t)}\right\}\Bigg) \\
&= -\frac{1}{\pi}\int d\epsilon\ \frac{df}{d\epsilon}\Bigg(-\frac{\dot{\Gamma}(t)}{2}.\frac{\epsilon-\bar{\epsilon}^{(ad)}_{a\sigma}(t)}{(\epsilon-\bar{\epsilon}^{(ad)}_{a\sigma}(t))^2+\Gamma(t)^2/4} \\
&\qquad\qquad -\dot{\bar{\epsilon}}^{(ad)}_{a\sigma}(t)\frac{\Gamma(t)}{2[(\epsilon-\bar{\epsilon}^{(ad)}_{a\sigma}(t))^2+\Gamma(t)^2/4]}\Bigg) \\
&= \int d\epsilon\ \frac{df}{d\epsilon}\left(\frac{\dot{\Gamma}(t)}{\Gamma(t)}(\epsilon-\bar{\epsilon}^{(ad)}_{a\sigma}(t))+\dot{\bar{\epsilon}}^{(ad)}_{a\sigma}(t)\right)\rho^{(ad)}_{a\sigma}(\epsilon,t), \qquad \text{(C.34)}
\end{aligned}$$

and we can combine this equation with (C.31) to give

$$\dot{\bar{\epsilon}}^{(ad)}_{a\sigma}(t)=\dot{\epsilon}_a(t)+U\int d\epsilon\ \frac{df}{d\epsilon}\left(\frac{\dot{\Gamma}(t)}{\Gamma(t)}(\epsilon-\bar{\epsilon}^{(ad)}_{a-\sigma}(t))+\dot{\bar{\epsilon}}^{(ad)}_{a-\sigma}(t)\right)\rho^{(ad)}_{a-\sigma}(\epsilon,t). \quad \text{(C.35)}$$

By considering the two values of the spin $\sigma$ this equation can be expressed in matrix form;

$$\begin{aligned}
\begin{pmatrix}\dot{\epsilon}_a(t)\\ \dot{\epsilon}_a(t)\end{pmatrix} &= \begin{pmatrix}1 & -U\int d\epsilon\frac{df}{d\epsilon}\rho^{(ad)}_{a-\sigma}(\epsilon,t)\\ -U\int d\epsilon\frac{df}{d\epsilon}\rho^{(ad)}_{a\sigma}(\epsilon,t) & 1\end{pmatrix}\begin{pmatrix}\dot{\bar{\epsilon}}^{(ad)}_{a\sigma}(t)\\ \dot{\bar{\epsilon}}^{(ad)}_{a-\sigma}(t)\end{pmatrix} \\
&\quad -\frac{U\dot{\Gamma}(t)}{\Gamma(t)}\begin{pmatrix}\int d\epsilon\frac{df}{d\epsilon}(\epsilon-\bar{\epsilon}^{(ad)}_{a-\sigma}(t))\rho^{(ad)}_{a-\sigma}(\epsilon,t)\\ \int d\epsilon\frac{df}{d\epsilon}(\epsilon-\bar{\epsilon}^{(ad)}_{a\sigma}(t))\rho^{(ad)}_{a\sigma}(\epsilon,t)\end{pmatrix}. \qquad \text{(C.36)}
\end{aligned}$$

$\dot{E}^{(1)}_{nearly-ad}$ can now be written as

$$\begin{aligned}
\dot{E}^{(1)}_{nearly-ad}(t) &= \begin{pmatrix}\delta n_{a\sigma}(t) & \delta n_{a-\sigma}(t)\end{pmatrix}\begin{pmatrix}\dot{\epsilon}_a(t)\\ \dot{\epsilon}_a(t)\end{pmatrix} \\
&= \begin{pmatrix}\delta n_{a\sigma}(t) & \delta n_{a-\sigma}(t)\end{pmatrix} \\
&\quad\times\begin{pmatrix}1 & -U\int d\epsilon\frac{df}{d\epsilon}\rho^{(ad)}_{a-\sigma}(\epsilon,t)\\ -U\int d\epsilon\frac{df}{d\epsilon}\rho^{(ad)}_{a\sigma}(\epsilon,t) & 1\end{pmatrix}\begin{pmatrix}\dot{\bar{\epsilon}}^{(ad)}_{a\sigma}(t)\\ \dot{\bar{\epsilon}}^{(ad)}_{a-\sigma}(t)\end{pmatrix} \\
&\quad -\frac{U\dot{\Gamma}(t)}{\Gamma(t)}\sum_\sigma\int d\epsilon\frac{df}{d\epsilon}(\epsilon-\bar{\epsilon}^{(ad)}_{a\sigma}(t))\rho^{(ad)}_{a\sigma}(\epsilon,t)\delta n_{a-\sigma}(t). \qquad \text{(C.37)}
\end{aligned}$$

The first two matrices in the first term of this expression are the transpose of

those derived in the previous section, (C.30). The combination of (C.37) and (C.30) gives our final expression for $\dot{E}^{(1)}_{nearly-ad}$;

$$\begin{aligned}\dot{E}^{(1)}_{nearly-ad}(t) &= -\pi\sum_{\sigma}\dot{\bar{\epsilon}}^{(ad)}_{a\sigma}(t)\int d\epsilon\frac{df}{d\epsilon}\left(\frac{\dot{\Gamma}(t)}{\Gamma(t)}(\epsilon-\bar{\epsilon}^{(ad)}_{a\sigma}(t))+\dot{\bar{\epsilon}}^{(ad)}_{a\sigma}(t)\right)\left[\rho^{(ad)}_{a\sigma}(\epsilon,t)\right]^2 \\ &\quad -\frac{U\dot{\Gamma}(t)}{\Gamma(t)}\sum_{\sigma}\int d\epsilon\frac{df}{d\epsilon}(\epsilon-\bar{\epsilon}^{(ad)}_{a\sigma}(t))\rho^{(ad)}_{a\sigma}(\epsilon,t)\delta n_{a-\sigma}(t). \qquad \text{(C.38)}\end{aligned}$$

## C.4: Derivation of $\dot{E}^{(2)}_{nearly-ad}$

In this section we derive the nearly-adiabatic equivalent of the second term in the non-adiabatic energy transfer rate $\dot{E}_{non-ad}$, (3.17), which will be referred to as $\dot{E}^{(2)}_{nearly-ad}$.

As in section C.2 we first perform a partial integration of $\dot{E}^{(2)}_{nearly-ad}$;

$$\begin{aligned}\dot{E}^{(2)}_{nearly-ad}(t) &= \frac{\dot{\Gamma}(t)}{\sqrt{2\pi\Gamma(t)}}\sum_{\sigma}\left[f(\epsilon)\int^{\epsilon}d\epsilon\ \mathrm{Im}\{\delta p_{\sigma}(\epsilon,t)\}\right]_{-\infty}^{\infty} \\ &\quad -\frac{\dot{\Gamma}(t)}{\sqrt{2\pi\Gamma(t)}}\sum_{\sigma}\int d\epsilon\ \frac{df}{d\epsilon}\mathrm{Im}\left\{\int^{\epsilon}d\epsilon\ \delta p_{\sigma}(\epsilon,t)\right\}. \qquad \text{(C.39)}\end{aligned}$$

The first term in this expression yields zero as the Fermi function is zero at $\epsilon=\infty$ and, as $\delta p_{\sigma}$ contains terms of order $\epsilon^{-3}$ and $\epsilon^{-4}$, $\delta p_{\sigma}$ is zero at $\epsilon=-\infty$. As before we deal with the terms from $\delta p_{\sigma}$ involving $\dot{\Gamma}$, $U\delta n_{a-\sigma}$ and $\dot{\bar{\epsilon}}^{(ad)}_{a\sigma}$ separately. The coefficient of $\dot{\Gamma}$ in $\delta p_{\sigma}$, (C.11), is

$$\{\delta p_{\sigma}(\epsilon,t)\}_{[\dot{\Gamma}]}=\frac{1}{2\sqrt{2\pi\Gamma(t)}}.\frac{\epsilon-\tilde{\epsilon}^{(ad)*}_{a\sigma}(t)}{(\epsilon-\tilde{\epsilon}^{(ad)}_{a\sigma}(t))^3}. \qquad \text{(C.40)}$$

On integration this becomes

$$\begin{aligned}\left\{\int^{\epsilon}d\epsilon\delta p_{\sigma}(\epsilon,t)\right\}_{[\dot{\Gamma}]} &= -\frac{1}{2\sqrt{2\pi\Gamma(t)}}\left(\frac{\epsilon-\tilde{\epsilon}^{(ad)*}_{a\sigma}(t)}{2(\epsilon-\tilde{\epsilon}^{(ad)}_{a\sigma}(t))^2}+\frac{1}{2(\epsilon-\tilde{\epsilon}^{(ad)}_{a\sigma}(t))}\right) \\ &= -\frac{1}{2\sqrt{2\pi\Gamma(t)}}\left(\frac{(\epsilon-\tilde{\epsilon}^{(ad)*}_{a\sigma}(t))+(\epsilon-\tilde{\epsilon}^{(ad)}_{a\sigma}(t))}{2(\epsilon-\tilde{\epsilon}^{(ad)}_{a\sigma}(t))^2}\right) \\ &= -\frac{1}{2\sqrt{2\pi\Gamma(t)}}\frac{\epsilon-\bar{\epsilon}^{(ad)}_{a\sigma}(t)}{(\epsilon-\tilde{\epsilon}^{(ad)}_{a\sigma}(t))^2}, \qquad \text{(C.41)}\end{aligned}$$

which has the imaginary component

$$\begin{aligned}\mathrm{Im}\left\{\int^{\epsilon} d\epsilon\delta p_\sigma(\epsilon,t)\right\}_{[\dot\Gamma]} &= \frac{1}{2}\sqrt{\frac{\Gamma(t)}{2\pi}}\frac{(\epsilon-\bar\epsilon^{(ad)}_{a\sigma}(t))^2}{[(\epsilon-\bar\epsilon^{(ad)}_{a\sigma}(t))^2+\Gamma^2(t)/4]^2} \\ &= \frac{\pi}{\Gamma(t)}\sqrt{\frac{2\pi}{\Gamma(t)}}(\epsilon-\bar\epsilon^{(ad)}_{a\sigma}(t))^2\left[\rho^{(ad)}_{a\sigma}(\epsilon,t)\right]^2. \quad \text{(C.42)}\end{aligned}$$

By substituting this expression into (C.39) we find the $\dot\Gamma$ dependence of $\dot E^{(2)}_{nearly-ad}$ to be

$$\left\{\dot E^{(2)}_{nearly-ad}(t)\right\}_{[\dot\Gamma]} = -\frac{\pi\dot\Gamma^2(t)}{\Gamma^2(t)}\sum_\sigma\int d\epsilon\frac{df}{d\epsilon}(\epsilon-\bar\epsilon^{(ad)}_{a\sigma}(t))^2\left[\rho^{(ad)}_{a\sigma}(\epsilon,t)\right]^2. \quad \text{(C.43)}$$

The coefficient of $U\delta n_{a-\sigma}$ in $\delta p_\sigma$ is

$$\{\delta p_\sigma(\epsilon,t)\}_{[U\delta n_{a-\sigma}]} = \sqrt{\frac{\Gamma(t)}{2\pi}}\frac{i}{(\epsilon-\tilde\epsilon^{(ad)}_{a\sigma}(t))^2}, \quad \text{(C.44)}$$

which on integration yields

$$\left\{\int^{\epsilon} d\epsilon\delta p_\sigma(\epsilon,t)\right\}_{[U\delta n_{a-\sigma}]} = -\sqrt{\frac{\Gamma(t)}{2\pi}}\frac{i}{\epsilon-\tilde\epsilon^{(ad)}_{a\sigma}(t)}. \quad \text{(C.45)}$$

The imaginary part of this expression is

$$\begin{aligned}\mathrm{Im}\left\{\int^{\epsilon} d\epsilon\delta p_\sigma(\epsilon,t)\right\}_{[U\delta n_{a-\sigma}]} &= \sqrt{\frac{\Gamma(t)}{2\pi}}\frac{\epsilon-\bar\epsilon^{(ad)}_{a\sigma}(t)}{(\epsilon-\bar\epsilon^{(ad)}_{a\sigma}(t))^2+\Gamma^2(t)/4} \\ &= -\sqrt{\frac{2\pi}{\Gamma(t)}}(\epsilon-\bar\epsilon^{(ad)}_{a\sigma}(t))\rho^{(ad)}_{a\sigma}(\epsilon,t), \quad \text{(C.46)}\end{aligned}$$

which on combination with (C.39) gives

$$\left\{\dot E^{(2)}_{nearly-ad}(t)\right\}_{U\delta n_{a-\sigma}} = \frac{U\dot\Gamma(t)}{\Gamma(t)}\sum_\sigma\int d\epsilon\frac{df}{d\epsilon}(\epsilon-\bar\epsilon^{(ad)}_{a\sigma}(t))\rho^{(ad)}_{a\sigma}(\epsilon,t)\delta n_{a-\sigma}(t). \quad \text{(C.47)}$$

The coefficient of $\dot{\bar{\epsilon}}^{(ad)}_{a\sigma}$ in $\delta p_\sigma$ is

$$\{\delta p_\sigma(\epsilon,t)\}_{[\dot{\bar{\epsilon}}^{(ad)}_{a\sigma}]} = \sqrt{\frac{\Gamma(t)}{2\pi}}\frac{1}{(\epsilon-\tilde{\epsilon}^{(ad)}_{a\sigma}(t))^3}. \tag{C.48}$$

This integral of this expression is

$$\left\{\int^\epsilon d\epsilon\delta p_\sigma(\epsilon,t)\right\}_{[\dot{\bar{\epsilon}}^{(ad)}_{a\sigma}]} = -\frac{1}{2}\sqrt{\frac{\Gamma(t)}{2\pi}}\frac{1}{(\epsilon-\tilde{\epsilon}^{(ad)}_{a\sigma}(t))^2}, \tag{C.49}$$

which has the imaginary part

$$\begin{aligned}\mathrm{Im}\left\{\int^\epsilon d\epsilon\delta p_\sigma(\epsilon,t)\right\}_{[\dot{\bar{\epsilon}}^{(ad)}_{a\sigma}]} &= \frac{1}{2}\sqrt{\frac{\Gamma(t)}{2\pi}}\frac{\Gamma(t)(\epsilon-\bar{\epsilon}^{(ad)}_{a\sigma}(t))}{[(\epsilon-\bar{\epsilon}^{(ad)}_{a\sigma}(t))^2+\Gamma^2(t)/4]^2} \\ &= \pi\sqrt{\frac{2\pi}{\Gamma(t)}}(\epsilon-\bar{\epsilon}^{(ad)}_{a\sigma}(t))\left[\rho^{(ad)}_{a\sigma}(\epsilon,t)\right]^2. \end{aligned}\tag{C.50}$$

On substitution into (C.39) this yields

$$\left\{\dot{E}^{(2)}_{nearly-ad}(t)\right\}_{[\dot{\bar{\epsilon}}^{(ad)}_{a\sigma}]} = -\frac{\pi\dot{\Gamma}(t)}{\Gamma(t)}\sum_\sigma \dot{\bar{\epsilon}}^{(ad)}_{a\sigma}(t)\int d\epsilon\frac{df}{d\epsilon}(\epsilon-\bar{\epsilon}^{(ad)}_{a\sigma}(t))\left[\rho^{(ad)}_{a\sigma}(\epsilon,t)\right]^2. \tag{C.51}$$

By summing the different contributions to $\dot{E}^{(2)}_{nearly-ad}$ (equations (C.43), (C.47) and (C.51)) we find

$$\begin{aligned}\dot{E}^{(2)}_{nearly-ad}(t) &= -\pi\sum_\sigma\int d\epsilon\frac{df}{d\epsilon}\frac{\dot{\Gamma}(t)}{\Gamma(t)}(\epsilon-\bar{\epsilon}^{(ad)}_{a\sigma}(t)) \\ &\qquad\times\left(\frac{\dot{\Gamma}(t)}{\Gamma(t)}(\epsilon-\bar{\epsilon}^{(ad)}_{a\sigma}(t))+\dot{\bar{\epsilon}}^{(ad)}_{a\sigma}(t)\right)\left[\rho^{(ad)}_{a\sigma}(\epsilon,t)\right]^2 \\ &\quad+\frac{U\dot{\Gamma}(t)}{\Gamma(t)}\sum_\sigma\int d\epsilon\frac{df}{d\epsilon}(\epsilon-\bar{\epsilon}^{(ad)}_{a\sigma}(t))\rho^{(ad)}_{a\sigma}(\epsilon,t)\delta n_{a-\sigma}(t). \end{aligned}\tag{C.52}$$

# Chapter 4

# Excitation spectra

In the previous two chapters we have used the Newns-Anderson model to derive expressions for the occupation functions of the system and the rate of total energy transfer between the adsorbate and the electronic degrees of freedom of the metal surface. We now extend this model to consider the properties of the excitations in the surface generated by the charge and energy transfer processes.

To describe the electronic excitation process in the time-dependent, mean-field Newns-Anderson model we consider the evolution of the occupied states of the system. This evolution will be represented here by the distribution of occupied one-electron states, also referred to as the 'electron distribution function'. This distribution can be separated into two parts; one component which depends upon the instantaneous configuration of the adsorbate relative to the metal, and another which describes the excitations induced by the motion of the adsorbate. It is the derivation of an expression for the second component, the 'excitation spectrum', which is the aim of this chapter.

The derivation of this excitation spectrum is presented here in two parts. In section 4.1 we obtain an expression for the time-evolving electron distribution function using the occupation functions derived in chapter 2. The component of this distribution due to the instantaneous configuration of the system is obtained in section 4.2. The difference between these expressions is the desired excitation spectrum.

The results of this chapter will be used to perform numerical calculations in chapter 6.

## 4.1 The electron distribution function

In this section we introduce the one-electron states of the Newns-Anderson system, which are used to construct an expression for the electron distribution function. This one-electron formalism is used in section 4.1.1 to derive an expression relating the electron distribution function to the occupation functions and a set of Green's functions. These Green's functions are obtained using the Dyson equation in section 4.1.2. The results of these two sections are combined, with the occupation functions from chapter 2, in section 4.1.3. A number of lengthy derivations, which are necessary for the construction of the electron distribution function, are contained in appendix D.

### 4.1.1 The electron distribution function: I

In the previous two chapters the many-electron, mean-field, Newns-Anderson Hamiltonian (2.3) has been used to investigate the variation in the occupation functions and the transfer of energy between adsorbate and surface. Here we are interested in understanding the electronic excitation process, and in particular the energy spectrum of the hot electrons and holes that are created during an adsorption event. For example, to model the generation of chemicurrents (see section 1.1.1) we need to find the probability of exciting an electron to a given energy above the Fermi level. This requires knowledge of the distribution of occupied electronic states of the system. To begin our analysis it is therefore necessary to relate the occupation functions, derived in chapter 2, to the one-electron states of the system.

This connection can be made by writing the occupation functions as elements of the time-dependent, one-electron density matrix $\hat{n}_{1\sigma}(t)$, which is defined through

$$n_{bb'\sigma}(t) = \langle\langle \hat{c}^{\dagger}_{b\sigma}(t)\hat{c}_{b'\sigma}(t)\rangle\rangle \equiv \langle b'_{\sigma}|\hat{n}_{1\sigma}(t)|b_{\sigma}\rangle, \tag{4.1}$$

where $\{|b_{\sigma}\rangle\}$ is the set of one-electron basis states $\{|a_{\sigma}\rangle, |k_{\sigma}\rangle\}$. The time-evolution of $\hat{n}_{1\sigma}$ is determined by considering the one-electron, single-spin Newns-Anderson

Hamiltonian, (2.6), in the Schrödinger picture;

$$\hat{h}_\sigma(t) = \bar{\epsilon}_{a\sigma}(t)|a_\sigma\rangle\langle a_\sigma| + \sum_k \epsilon_{k\sigma}|k_\sigma\rangle\langle k_\sigma| + \sum_k \left(V_{ak}(t)|a_\sigma\rangle\langle k_\sigma| + \text{H.c.}\right). \quad (4.2)$$

We define $\{|\mu_{b\sigma}(t)\rangle\}$ to be the time-dependent states of this Hamiltonian, which evolve from the basis states at time $t_0$, i.e. $|\mu_{b\sigma}(t_0)\rangle \equiv |b_\sigma\rangle$. These states can be used to demonstrate the equivalence of the one-electron description, introduced here, with the many-electron description represented by the electron operators. This equivalence is used in appendix D.1 to expand the electron operators in terms of the one-electron states, yielding

$$\hat{c}_{b\sigma}(t) = \sum_{b'} \langle b_\sigma|\mu_{b'\sigma}(t)\rangle \hat{c}_{b'\sigma}(t_0). \quad (4.3)$$

The occupation function $n_{bb'\sigma}(t)$ can be expanded using (4.3), giving

$$\begin{aligned} n_{bb'\sigma}(t) &= \sum_{b'',b'''} \langle \mu_{b''\sigma}(t)|b_\sigma\rangle\langle b'_\sigma|\mu_{b'''\sigma}(t)\rangle \langle\langle \hat{c}^\dagger_{b''\sigma}(t_0)\hat{c}_{b'''\sigma}(t_0)\rangle\rangle \\ &= \sum_{b''} \langle b'_\sigma|\mu_{b''\sigma}(t)\rangle f(\epsilon_{b''\sigma}(t_0))\langle \mu_{b''\sigma}(t)|b_\sigma\rangle, \end{aligned} \quad (4.4)$$

where the initial occupation functions, (2.15), have been used and the energy $\epsilon_{b''\sigma}(t_0)$ represents $\epsilon_{k\sigma}$ for $b'' = k$ and $\bar{\epsilon}_{a\sigma}(t_0)$ for $b'' = a$. By comparing this expression with (4.1), $\hat{n}_{1\sigma}$ can be recognised as

$$\hat{n}_{1\sigma}(t) = \sum_b |\mu_{b\sigma}(t)\rangle f(\epsilon_{b\sigma}(t_0))\langle \mu_{b\sigma}(t)|. \quad (4.5)$$

This expression has the expected form for a density matrix operator (see Schiff [66] page 378), with the probability of occupation of the $|\mu_{b\sigma}(t)\rangle$ state given by the Fermi function $f(\epsilon_{b\sigma}(t_0))$.

The quantity of interest here is the distribution of occupied one-electron states and the manner in which it evolves with time. To obtain an expression for this distribution we take the diagonal elements of $\hat{n}_{1\sigma}(t)$ with respect to the one-electron eigenstates of $\hat{h}_\sigma$. By defining $\{|\nu_{\sigma t}\rangle\}$ to be this set of eigenstates, with

energies $\epsilon^{\nu}_{\sigma t}$, the electron distribution function can be written as

$$\begin{aligned} n_\sigma(\epsilon,t) &= \sum_\nu \langle \nu_{\sigma t}|\hat{n}_{1\sigma}(t)|\nu_{\sigma t}\rangle \delta(\epsilon-\epsilon^\nu_{\sigma t}) \\ &= \sum_{\nu,b} |\langle \nu_{\sigma t}|\mu_{b\sigma}(t)\rangle|^2 f(\epsilon_{b\sigma}(t_0))\delta(\epsilon-\epsilon^\nu_{\sigma t}). \end{aligned} \tag{4.6}$$

It is important to note here that the eigenstates $|\nu_{\sigma t}\rangle$ are not the usually defined states of the Newns-Anderson system. For a static adsorbate above a surface the system is in an adiabatic state, and the energy level $\bar{\epsilon}^{(ad)}_{a\sigma}$ and occupation $n^{(ad)}_{a\sigma}$ are determined self-consistently by the values of $\epsilon_a$, $U$, $\Gamma$ and the temperature of the system. In the time-dependent system under consideration however, $n_{a\sigma}(t)$ is not the same as the adiabatic solution, but is the occupation of the adsorbate orbital at a given instant. The adsorbate occupation function therefore depends on the history of the evolution of the system. To emphasise this difference from the ground state, we will refer to the states $|\nu_{\sigma t}\rangle$ as the 'instantaneous eigenstates' of the system.

Our use of these instantaneous eigenstates also allows contact to be made between the energy of the one-electron states and that of the many-electron system. The total energy of the electronic system is given by the first moment of the electron distribution function less a factor accounting for the double counting of the intra-adsorbate Coulomb repulsion energy;

$$E(t) = \sum_\sigma \int d\epsilon\ \epsilon n_\sigma(\epsilon,t) - U n_{a\sigma}(t) n_{a-\sigma}(t). \tag{4.7}$$

By substituting (4.6) into this expression we find

$$\begin{aligned} E(t) &= \sum_{\sigma,\nu,b} \langle \mu_{b\sigma}(t)|\nu_{\sigma t}\rangle \epsilon^\nu_{\sigma t} \langle \nu_{\sigma t}|\mu_{b\sigma}(t)\rangle f(\epsilon_{b\sigma}(t_0)) - U n_{a\sigma}(t) n_{a-\sigma}(t) \\ &= \sum_{\sigma,b} \langle \mu_{b\sigma}(t)|\hat{h}_\sigma(t)|\mu_{b\sigma}(t)\rangle f(\epsilon_{b\sigma}(t_0)) - U n_{a\sigma}(t) n_{a-\sigma}(t) \\ &= \sum_\sigma \langle\!\langle \hat{H}_\sigma(t)\rangle\!\rangle - U n_{a\sigma}(t) n_{a-\sigma}(t), \end{aligned} \tag{4.8}$$

i.e. the total energy of the system is simply the expectation value of the mean-field Hamiltonian $\hat{H}_{MF}$, (2.3). These expressions are used in appendix F to verify that the electron distribution function $n_\sigma$ is consistent with the rate of change of total energy derived in chapter 3, (3.16).

The form of the electron distribution function (4.6) is, however, not convenient for numerical computation. To obtain a suitable expression for $n_\sigma$ it is therefore necessary to expand (4.6). This can be performed by introducing the basis states $|b_\sigma\rangle$ into (4.6) and retrieving the occupation functions derived in chapter 2 (using (4.1));

$$\begin{aligned} n_\sigma(\epsilon,t) &= \sum_{\nu,b,b'} \langle \nu_{\sigma t}|b'_\sigma\rangle\langle b'_\sigma|\hat{n}_{1\sigma}(t)|b_\sigma\rangle\langle b_\sigma|\nu_{\sigma t}\rangle \delta(\epsilon-\epsilon^\nu_{\sigma t}) \\ &= \sum_{b,b'} n_{bb'\sigma}(t) \sum_\nu \langle b_\sigma|\nu_{\sigma t}\rangle\langle \nu_{\sigma t}|b'_\sigma\rangle \delta(\epsilon-\epsilon^\nu_{\sigma t}). \end{aligned} \tag{4.9}$$

The remaining projections in this expression can be eliminated by introducing the instantaneous Green's function $G_\sigma$, which we define in a similar manner to Economou [69] (page 40) as

$$G_\sigma(\epsilon,t) = \sum_\nu \frac{|\nu_{\sigma t}\rangle\langle\nu_{\sigma t}|}{\epsilon-\epsilon^\nu_{\sigma t}+i\eta}, \tag{4.10}$$

where $\eta$ is a positive infinitesimal. By combining this definition with (4.9), the electron distribution function becomes

$$\begin{aligned} n_\sigma(\epsilon,t) &= -\frac{1}{\pi}\mathrm{Im}\left\{\sum_{b,b'} n_{bb'\sigma}(t)\langle b_\sigma|G_\sigma(\epsilon,t)|b'_\sigma\rangle\right\} \\ &= -\frac{1}{\pi}\mathrm{Im}\left\{\sum_{b,b'} n_{bb'\sigma}(t) G_{bb'\sigma}(\epsilon,t)\right\}, \end{aligned} \tag{4.11}$$

where $G_{bb'\sigma}(\epsilon,t) = \langle b_\sigma|G_\sigma(\epsilon,t)|b'_\sigma\rangle$.

The expansion of $n_\sigma$ now requires two sets of functions; the occupation functions, derived in chapter 2, and the instantaneous Green's functions. This set of Green's functions is obtained from the Dyson equation in the following subsection, the results of which are used to derive a computable form for $n_\sigma$ in section 4.1.3.

### 4.1.2 Instantaneous Green's functions

The set of Green's functions required to expand $n_\sigma$, (4.11), can be found from the Dyson equation [65],

$$G_\sigma(\epsilon,t) = G^0_\sigma(\epsilon,t) + G^0_\sigma(\epsilon,t)V(t)G_\sigma(\epsilon,t) \tag{4.12}$$

where $V$ is the interaction potential and $G^0_\sigma$ is the unperturbed Green's function, i.e. $G_\sigma$ for $V \equiv 0$. In appendix D.2 the elements of the Green's function $G_\sigma$ for the Newns-Anderson system are obtained, yielding (see (D.18), (D.19), (D.20) and (D.21))

$$
\begin{aligned}
G_{aa\sigma}(\epsilon,t) &= G^0_{aa\sigma}(\epsilon,t) + G^0_{aa\sigma}(\epsilon,t)\sum_k V_{ak}(t)G_{ka\sigma}(\epsilon,t) && (4.13)\\
G_{ak\sigma}(\epsilon,t) &= G^0_{aa\sigma}(\epsilon,t)\sum_{k'} V_{ak'}(t)G_{k'k\sigma}(\epsilon,t) && (4.14)\\
G_{ka\sigma}(\epsilon,t) &= G^0_{kk\sigma}(\epsilon,t)V^*_{ak}(t)G_{aa\sigma}(\epsilon,t) && (4.15)\\
G_{kk'\sigma}(\epsilon,t) &= \delta_{k,k'}G^0_{kk\sigma}(\epsilon,t) + G^0_{kk\sigma}(\epsilon,t)V^*_{ak}(t)G_{ak'\sigma}(\epsilon,t). && (4.16)
\end{aligned}
$$

The unperturbed Green's functions, $G^0_{aa\sigma}$ and $G^0_{kk\sigma}$, are found from the definition of $G_\sigma$, (4.10), to be (see (D.17))

$$
\begin{aligned}
G^0_{aa\sigma}(\epsilon,t) &= \frac{1}{\epsilon - \bar{\epsilon}_{a\sigma}(t) + i\eta} && (4.17a)\\
G^0_{kk\sigma}(\epsilon,t) &= \frac{1}{\epsilon - \epsilon_{k\sigma} + i\eta}. && (4.17b)
\end{aligned}
$$

This set of equations is solved within the wide-band approximation, as discussed in chapter 2 (see page 36), giving (equations (D.27), (D.28), (D.30) and (D.31))

$$
\begin{aligned}
G_{aa\sigma}(\epsilon,t) &= \frac{1}{\epsilon - \tilde{\epsilon}_{a\sigma}(t)} && (4.18)\\
G_{ak\sigma}(\epsilon,t) &= \frac{V_{ak}(t)}{(\epsilon - \epsilon_{k\sigma} + i\eta)}\frac{1}{(\epsilon - \tilde{\epsilon}_{a\sigma}(t))} && (4.19)\\
G_{ka\sigma}(\epsilon,t) &= \frac{V^*_{ak}(t)}{(\epsilon - \epsilon_{k\sigma} + i\eta)}\frac{1}{(\epsilon - \tilde{\epsilon}_{a\sigma}(t))} && (4.20)\\
G_{kk'\sigma}(\epsilon,t) &= \frac{\delta_{k,k'}}{\epsilon - \epsilon_{k\sigma} + i\eta} + \frac{V^*_{ak}(t)}{(\epsilon - \epsilon_{k\sigma} + i\eta)}.\frac{V_{ak'}(t)}{(\epsilon - \epsilon_{k'\sigma} + i\eta)}.\frac{1}{(\epsilon - \tilde{\epsilon}_{a\sigma}(t))}, && (4.21)
\end{aligned}
$$

where $\tilde{\epsilon}_{a\sigma}(t) = \bar{\epsilon}_{a\sigma}(t) - i\Gamma(t)/2$ as defined in (2.12). These Green's functions are very similar to those obtained by Anderson [35], with the exception that the adsorbate level used here is the instantaneous level $\bar{\epsilon}_{a\sigma}(t)$ rather than the adiabatic level $\bar{\epsilon}^{(ad)}_{a\sigma}(t)$.

### 4.1.3 The electron distribution function: II

We now combine the results of the previous two subsections with the occupation functions derived in chapter 2 to obtain the electron distribution function $n_\sigma$.

By substituting the Green's functions, (4.18) to (4.21), into (4.11) the electron distribution function becomes

$$\begin{aligned} n_\sigma(\epsilon,t) &= -\frac{n_{a\sigma}(t)}{\pi}\mathrm{Im}\left\{\frac{1}{\epsilon-\tilde{\epsilon}_{a\sigma}(t)}\right\} \\ &\quad -\frac{2}{\pi}\mathrm{Im}\left\{\frac{1}{\epsilon-\tilde{\epsilon}_{a\sigma}(t)}\sum_k \frac{\mathrm{Re}\left[V_{ak}(t)n_{ak\sigma}(t)\right]}{\epsilon-\epsilon_{k\sigma}+i\eta}\right\} \\ &\quad -\frac{1}{\pi}\mathrm{Im}\left\{\sum_k \frac{n_{k\sigma}(t)}{\epsilon-\epsilon_{k\sigma}+i\eta}\right\} \\ &\quad -\frac{1}{\pi}\mathrm{Im}\left\{\frac{1}{\epsilon-\tilde{\epsilon}_{a\sigma}(t)}\sum_{k,k'} \frac{V^*_{ak}(t)V_{ak'}(t)n_{kk'\sigma}(t)}{(\epsilon-\epsilon_{k\sigma}+i\eta)(\epsilon-\epsilon_{k'\sigma}+i\eta)}\right\}, \end{aligned} \tag{4.22}$$

where the occupation function $n_{ka\sigma}$ has been replaced using $n_{ka\sigma}(t) = n^*_{ak\sigma}(t)$, (2.14b). This expression can be simplified by evaluating the imaginary part of the first and third terms, and introducing delta functions with corresponding energy integrals. This yields

$$\begin{aligned} n_\sigma(\epsilon,t) &= n_{a\sigma}(t)\rho^{(inst)}_{a\sigma}(\epsilon,t) + \sum_k n_{k\sigma}(t)\delta(\epsilon-\epsilon_{k\sigma}) \\ &\quad -\frac{2}{\pi}\mathrm{Im}\left\{\frac{1}{\epsilon-\tilde{\epsilon}_{a\sigma}(t)}\int\frac{d\epsilon'}{\epsilon-\epsilon'+i\eta}.\mathrm{Re}\left[\sum_k V_{ak}(t)n_{ak\sigma}(t)\delta(\epsilon'-\epsilon_{k\sigma})\right]\right\} \\ &\quad -\frac{1}{\pi}\mathrm{Im}\left\{\frac{1}{\epsilon-\tilde{\epsilon}_{a\sigma}(t)}\int\frac{d\epsilon'}{\epsilon-\epsilon'+i\eta}\int\frac{d\epsilon''}{\epsilon-\epsilon''+i\eta}\right. \\ &\qquad \left.\times\sum_{k,k'} V^*_{ak}(t)V_{ak'}(t)n_{kk'\sigma}(t)\delta(\epsilon'-\epsilon_{k\sigma})\delta(\epsilon''-\epsilon_{k'\sigma})\right\}, \end{aligned} \tag{4.23}$$

where $\rho^{(inst)}_{a\sigma}$ is similar to the adiabatic PDOS $\rho^{(ad)}_{a\sigma}$, (2.33), but with the adiabatic level $\bar{\epsilon}^{(ad)}_{a\sigma}$ replaced with the time-evolving level $\bar{\epsilon}_{a\sigma}$;

$$\rho^{(inst)}_{a\sigma}(\epsilon,t) = \frac{\Gamma(t)}{2\pi[(\epsilon-\bar{\epsilon}_{a\sigma}(t))^2+\Gamma(t)^2/4]}. \tag{4.24}$$

The evaluation of (4.11), using the occupation functions, is long-winded, and is therefore performed term by term in appendices D.3 to D.5 for the second, third and fourth terms in (4.23) respectively. The results of these derivations are combined in appendix D.6, yielding our final expression for $n_\sigma$, (D.66);

$$\begin{aligned} n_\sigma(\epsilon,t) &= \int d\epsilon' f(\epsilon') \left| q_\sigma(\epsilon,\epsilon',t) + p_\sigma^{(inst)}(\epsilon,t) p_\sigma(\epsilon',t) \right|^2 - 2f(\epsilon)\mathrm{Re}\left\{ q_\sigma(\epsilon,\epsilon,t) \right\} \\ &\quad + n_{a\sigma}(t_0) \left| r_\sigma(\epsilon,t) + p_\sigma^{(inst)}(\epsilon,t) \exp\left[ -\frac{1}{2}\int_{t_0}^{t} \Gamma(t')dt' \right] \right|^2 \\ &\quad + \sum_k f(\epsilon_{k\sigma})\delta(\epsilon-\epsilon_{k\sigma}) \\ &\quad + \frac{2}{\pi}\int d\epsilon' f(\epsilon') \mathrm{Re}\left\{ \frac{p_\sigma^{(inst)}(\epsilon,t)}{\epsilon-\epsilon'+i\eta} \right\} \mathrm{Im}\left\{ p_\sigma(\epsilon',t) \right\} \\ &\quad - 2\sqrt{\frac{\Gamma(t)}{2\pi}} \int d\epsilon' f(\epsilon') \mathrm{Im}\left\{ \frac{p_\sigma^{(inst)}(\epsilon,t) q_\sigma^*(\epsilon,\epsilon',t)}{\epsilon-\epsilon'+i\eta} \right\} \\ &\quad + \frac{1}{\pi}\sqrt{\frac{\Gamma(t)}{2\pi}} \int d\epsilon' f(\epsilon') \mathrm{Re}\left\{ \frac{p_\sigma^{(inst)}(\epsilon,t)}{(\epsilon-\epsilon'+i\eta)^2} \right\}. \end{aligned} \tag{4.25}$$

where $p_\sigma^{(inst)}$, $q_\sigma$ and $r_\sigma$ are defined as

$$p_\sigma^{(inst)}(\epsilon,t) = \sqrt{\frac{\Gamma(t)}{2\pi}} \frac{i}{(\epsilon-\tilde{\epsilon}_{a\sigma}(t))}, \tag{4.26}$$

$$q_\sigma(\epsilon,\epsilon',t) = \int_{t_0}^{t} dt_1 \sqrt{\frac{\Gamma(t_1)}{2\pi}} p_\sigma(\epsilon',t) \exp[i(\epsilon-\epsilon')(t_1-t)], \tag{4.27}$$

$$r_\sigma(\epsilon,t) = \exp\left[ -\frac{1}{2}\int_{t_0}^{t} \Gamma(t')dt' \right] \int_{t_0}^{t} dt_1 \sqrt{\frac{\Gamma(t_1)}{2\pi}} \exp\left[ i\int_{t_0}^{t} (\tilde{\epsilon}_{a\sigma}(t')-\epsilon)dt' \right], \tag{4.28}$$

and we have used

$$\rho_{a\sigma}^{(inst)}(\epsilon,t) = |p_\sigma^{(inst)}(\epsilon,t)|^2. \tag{4.29}$$

Through the quantities $p_\sigma$, $p_\sigma^{(inst)}$, $q_\sigma$ and $r_\sigma$, we can now calculate the evolution of the distribution of occupied electronic states from the variation of the parameters $\epsilon_a$ and $\Gamma$ and the value of $U$. The methods used to numerically calculate these quantities are described in chapter 6, where results for example systems are also presented.

To validate our result there are two obvious tests which can be performed; conservation of charge and energy. The conservation of charge can be tested by taking the zeroth moment of the electron distribution function, which should be independent of time and yield the number of electrons in the system. The energy of the electron distribution function, given by equation (4.7), should be consistent with the rate of change of total energy (3.16) derived in chapter 3. In appendix E we demonstrate charge conservation, and in appendix F the time-derivative of (4.7) is found to be identical to the rate of change of the total energy of the Newns-Anderson system. We are therefore confident that the distribution function constructed in this section is valid within the mean-field and wide-band approximations.

## 4.2 The spectrum of electronic excitations

In the previous section we obtained the distribution of occupied one-electron states of the Newns-Anderson system. However, the aim of this chapter is to obtain the spectrum of excitations, for which we need to subtract an underlying distribution in which there are no electronic excitations. This underlying distribution can be obtained by constructing an expression for the component due to the instantaneous configuration of the adsorbate relative to the metal. We choose to represent this component by setting $|\mu_{b\sigma}(t)\rangle = |\nu_{\sigma t}\rangle$ in (4.6), yielding the instantaneous electron distribution function $n_{\sigma t}^{(inst)}(\epsilon)$;

$$n_{\sigma t}^{(inst)}(\epsilon) = \sum_{\nu} f(\epsilon_{\sigma t_0}^{\nu})\delta(\epsilon - \epsilon_{\sigma t}^{\nu}). \tag{4.30}$$

The difference between the times in the energies here is important. $f(\epsilon_{\sigma t_0}^{\nu})$ is the initial occupation of the instantaneous eigenstate, while the delta function contains the eigenenergy at time $t$. The two different times make this expression difficult to use in its current form.

The relevance of the different times can be seen if we consider a finite system of $N$ electrons rather than the infinite Newns-Anderson system. In an infinite system a localised perturbation cannot affect the extended electronic eigenvalues. However, in a finite system this is not the case – the eigenenergies of the system can shift an amount $\Delta\epsilon_{\sigma t}^{\nu} = \epsilon_{\sigma t}^{\nu} - \epsilon_{\sigma t_0}^{\nu}$, which will be of order $1/N$. It is therefore possible, in a finite system, to approximate the Fermi function appearing in (4.30) using a Taylor expansion about the eigenenergy $\epsilon_{\sigma t}^{\nu}$. Equation (4.30) then

becomes

$$\begin{aligned} n_{\sigma t}^{(inst)}(\epsilon) &= \sum_{\nu} \left( f(\epsilon_{\sigma t}^{\nu}) - \Delta\epsilon_{\sigma t}^{\nu} \frac{df}{d\epsilon}(\epsilon_{\sigma t}^{\nu}) \right) \delta(\epsilon - \epsilon_{\sigma t}^{\nu}) \\ &= f(\epsilon) \sum_{\nu} \delta(\epsilon - \epsilon_{\sigma t}^{\nu}) - \frac{df}{d\epsilon} \sum_{\nu} \Delta\epsilon_{\sigma t}^{\nu} \delta(\epsilon - \epsilon_{\sigma t}^{\nu}). \end{aligned} \tag{4.31}$$

When integrated to give the charge in the system the first and second terms in this expression yield of order $N$ and 1 electrons respectively (the sum in the second term contains $N$ terms each of order $1/N$). In order to have an instantaneous electron distribution function that conserves charge, the second term in (4.31) cannot be neglected in the $N \to \infty$ limit. Higher order terms in the expansion of the Fermi function yield of order $1/N$ electrons or less, which vanish in the $N \to \infty$ limit.

The first term in (4.31) can be evaluated by introducing the basis states $|b_\sigma\rangle$, projected onto the instantaneous eigenstate $|\nu_{\sigma t}\rangle$, and the Green's function $G_\sigma$, (4.10);

$$\begin{aligned} f(\epsilon) \sum_{\nu} \delta(\epsilon - \epsilon_{\sigma t}^{\nu}) &= f(\epsilon) \sum_{\nu,b} |\langle \nu_{\sigma t} | b_\sigma \rangle|^2 \delta(\epsilon - \epsilon_{\sigma t}^{\nu}) \\ &= -\frac{f(\epsilon)}{\pi} \mathrm{Im} \left\{ \sum_{b} G_{bb\sigma}(\epsilon, t) \right\}. \end{aligned} \tag{4.32}$$

On combination with (4.18) and (4.21) this expression becomes

$$\begin{aligned} & f(\epsilon) \sum_{\nu} \delta(\epsilon - \epsilon_{\sigma t}^{\nu}) \\ &= -\frac{f(\epsilon)}{\pi} \mathrm{Im} \left\{ \frac{1}{\epsilon - \tilde{\epsilon}_{a\sigma}(t)} \right\} - \frac{f(\epsilon)}{\pi} \mathrm{Im} \left\{ \sum_{k} \frac{1}{\epsilon - \epsilon_{k\sigma} + i\eta} \right\} \\ &\quad -\frac{f(\epsilon)}{\pi} \left\{ \sum_{k} \frac{|V_{ak}(t)|^2}{(\epsilon - \epsilon_{k\sigma} + i\eta)^2 (\epsilon - \tilde{\epsilon}_{a\sigma}(t))} \right\} \\ &= f(\epsilon) \rho_{a\sigma}^{(inst)}(\epsilon, t) + \sum_{k} f(\epsilon_{k\sigma}) \delta(\epsilon - \epsilon_{k\sigma}) \\ &\quad -\frac{f(\epsilon)}{\pi} \mathrm{Im} \left\{ \frac{1}{(\epsilon - \tilde{\epsilon}_{a\sigma}(t))} \int \frac{d\epsilon'}{(\epsilon - \epsilon' + i\eta)^2} \sum_{k} |V_{ak}(t)|^2 \delta(\epsilon' - \epsilon_{k\sigma}) \right\}, \end{aligned} \tag{4.33}$$

where $\rho_{a\sigma}^{(inst)}$ is defined in (4.24) and an energy integral and delta function has

been introduced into the final term. The sum over metal states in the final term of (4.33) can be replaced using the definition of $\Gamma$, (2.13). As the width $\Gamma$ is independent of energy the remaining integral can be evaluated yielding zero.

The instantaneous electron distribution function is therefore

$$\begin{aligned} n_{\sigma t}^{(inst)}(\epsilon) &= f(\epsilon)\rho_{a\sigma}^{(inst)}(\epsilon,t) + \sum_k f(\epsilon_{k\sigma})\delta(\epsilon-\epsilon_{k\sigma}) \\ &\quad -\frac{df}{d\epsilon}\sum_\nu \Delta\epsilon_{\sigma t}^\nu \delta(\epsilon-\epsilon_{\sigma t}^\nu). \end{aligned} \tag{4.34}$$

A more convenient, and computable, form for the final term in this expression can be found by considering the charge in this distribution. As for the time-evolving distribution function the zeroth moment of $n_{\sigma t}^{(inst)}$ should give the number of electrons of spin $\sigma$ in the system;

$$\begin{aligned} \int d\epsilon\; n_{\sigma t}^{(inst)}(\epsilon) &= \int d\epsilon f(\epsilon)\rho_{a\sigma}^{(inst)}(\epsilon,t) + \sum_k f(\epsilon_{k\sigma}) \\ &\quad -\int d\epsilon \frac{df}{d\epsilon}\sum_\nu \Delta\epsilon_{\sigma t}^\nu \delta(\epsilon-\epsilon_{\sigma t}^\nu). \end{aligned} \tag{4.35}$$

The second term in this expression is the number of metal electrons and to conserve charge the remaining terms must contain the number of electrons of spin $\sigma$ initially in the adsorbate orbital, i.e.

$$n_{a\sigma}(t_0) = \int d\epsilon f(\epsilon)\rho_{a\sigma}^{(inst)}(\epsilon,t) - \int d\epsilon \frac{df}{d\epsilon}\sum_\nu \Delta\epsilon_{\sigma t}^\nu \delta(\epsilon-\epsilon_{\sigma t}^\nu). \tag{4.36}$$

We now assume that the sum over the eigenstates $|\nu_{\sigma t}\rangle$ in this expression is independent of energy $\epsilon$ over a range of a few $k_BT$ either side of the Fermi level (where the derivative $df/d\epsilon$ is non-negligible). This assumption is consistent with the wide-band approximation discussed in chapter 2 (page 36), and used throughout this thesis. Equation (4.36) can then be rearranged to give

$$\sum_\nu \Delta\epsilon_{\sigma t}^\nu \delta(\epsilon-\epsilon_{\sigma t}^\nu) = n_{a\sigma}(t_0) - \int d\epsilon f(\epsilon)\rho_{a\sigma}^{(inst)}(\epsilon,t), \tag{4.37}$$

and the instantaneous electron distribution function therefore becomes

$$\begin{aligned} n_{\sigma t}^{(inst)}(\epsilon) &= f(\epsilon)\rho_{a\sigma}^{(inst)}(\epsilon,t) + \sum_k f(\epsilon_{k\sigma})\delta(\epsilon-\epsilon_{k\sigma}) \\ &\quad -\frac{df}{d\epsilon}\left[n_{a\sigma}(t_0) - \int d\epsilon' f(\epsilon')\rho_{a\sigma}^{(inst)}(\epsilon',t)\right]. \end{aligned} \tag{4.38}$$

This expression, in contrast to $n_\sigma$ (4.25), is straightforward to interpret. The first term represents the occupied component of the adsorbate resonance, and the second term describes the initially occupied metal states. The final term contains the charge transfered from the adsorbate to the surface, which can be seen as a narrow distribution peaking at the Fermi level.

The difference between this instantaneous distribution and the time-evolving function $n_\sigma$ is the required spectrum of excitations $n_\sigma^{(ex)}(\epsilon,t)$. This spectrum will be calculated numerically in chapter 6 for a set of example parameters.

## 4.3 Summary

In this chapter we have used the Newns-Anderson model to investigate the electronic excitation of the metal due to interactions with an adsorbate orbital. The time-evolving electron distribution function $n_\sigma$, (4.25), and the instantaneous equivalent $n_{\sigma t}^{(inst)}$, (4.38), have been derived in sections 4.1 and 4.2, with additional algebra in appendix D. The difference between these two expressions gives the goal of this chapter; the spectrum of electronic excitations $n_\sigma^{(ex)}$. We have also performed two tests of the electron distribution function. Charge conservation is demonstrated in appendix E, and in appendix F the energy contained in $n_\sigma$ is shown to be consistent with the rate of change of the total energy of the system calculated in chapter 3, (3.16).

# Appendix D: Derivation of the electron distribution function $n_\sigma$

This appendix contains a number of derivations necessary to obtain the final expression for the electron distribution function $n_\sigma$, (4.25), from equation (4.6). In section D.1 the electron operators are related to the states of the one-electron Hamiltonian (4.2), yielding an expression which is used in section 4.1.1 to obtain the one-electron density matrix operator $\hat{n}_{1\sigma}$. The set of instantaneous Green's function which are needed to expand $n_\sigma$ are derived in section D.2.

The remaining sections contain derivations of the second, third and fourth terms in (4.23), labelled $n_\sigma^{(\mathrm{ii})}$, $n_\sigma^{(\mathrm{iii})}$ and $n_\sigma^{(\mathrm{iv})}$ respectively, with the results combined in section D.6 to yield our final expression for $n_\sigma$.

## D.1: Electron operators and one-electron states

In this section we demonstrate that the time-dependent electron operators used to construct the Newns-Anderson model can be related to the time-evolving states of the one-electron Hamiltonian $\hat{h}_\sigma$, (4.2).

The single-spin, many-electron Hamiltonian $\hat{H}_\sigma$, (2.6), can be rewritten in a more compact form as

$$\hat{H}_\sigma(t) = \sum_{b,b'} \epsilon_{bb'\sigma}(t)\hat{c}^\dagger_{b\sigma}(t)\hat{c}_{b'\sigma}(t), \tag{D.1}$$

where $b$ represents the basis states of the system such that the matrix $\epsilon_{bb'\sigma}(t)$ has elements $\epsilon_{aa\sigma}(t) = \bar{\epsilon}_{a\sigma}(t)$, $\epsilon_{kk\sigma}(t) = \epsilon_{k\sigma}$, $\epsilon_{ak\sigma}(t) = V_{ak}(t)$ and $\epsilon_{ka\sigma}(t) = V^*_{ak}(t)$. The remaining elements, $\epsilon_{kk'\sigma}(t)$ for $k \neq k'$, are zero. In this form the equations of motion for the operators $\hat{c}_{a\sigma}(t)$ and $\hat{c}_{k\sigma}(t)$, (2.7a) and (2.7b), can be expressed as a set of linear differential equations (with $\hbar = 1$);

$$i\frac{d}{dt}\hat{c}_{b\sigma}(t) = \sum_{b'} \epsilon_{bb'\sigma}(t)\hat{c}_{b'\sigma}(t). \tag{D.2}$$

This equation has the general solution

$$\hat{c}_{b\sigma}(t) = \sum_{b'} A_{bb'\sigma}(t)\hat{c}_{b'\sigma}(t_0), \tag{D.3}$$

where the time-dependence of the operator $\hat{c}_{b\sigma}(t)$ is now entirely contained in the matrix $A_{bb'\sigma}(t)$. By substituting (D.3) into (D.2) the Heisenberg equation of motion gives

$$i\sum_{b''}\frac{d}{dt}A_{bb''\sigma}(t)\hat{c}_{b''\sigma}(t_0)=\sum_{b',b''}\epsilon_{bb'\sigma}(t)A_{b'b''\sigma}(t)\hat{c}_{b''\sigma}(t_0), \tag{D.4}$$

from which it follows that $A_{bb''\sigma}$ evolves according to

$$i\frac{d}{dt}A_{bb''\sigma}(t)=\sum_{b'}\epsilon_{bb'\sigma}(t)A_{b'b''\sigma}(t), \tag{D.5}$$

with the initial condition

$$A_{bb''\sigma}(t_0)=\delta_{b,b''}. \tag{D.6}$$

The form of equations (D.5) and (D.6) is similar to that of the time-dependent Schrödinger equation. We should therefore be able to connect the matrix $A_{bb'\sigma}$ with the time-evolving states of one-electron Hamiltonian $\hat{h}_\sigma$, (4.2). The evolution of the one-electron states is determined by the Schrödinger equation;

$$i\frac{d}{dt}|\mu_{b''\sigma}(t)\rangle=\hat{h}_\sigma(t)|\mu_{b''\sigma}(t)\rangle \tag{D.7}$$

where the state $|\mu_{b''\sigma}(t)\rangle$ evolves from the initial state $|b''_\sigma\rangle$. The one-electron Hamiltonian (4.2) can be written in a similar compact form to (D.1);

$$\hat{h}_\sigma(t)=\sum_{b,b'}\epsilon_{bb'\sigma}(t)|b_\sigma\rangle\langle b'_\sigma|, \tag{D.8}$$

where $\epsilon_{bb'\sigma}(t)$ is the same matrix as used in the many-electron Hamiltonian $\hat{H}_\sigma$. By combining (D.7) and (D.8) we find

$$i\frac{d}{dt}|\mu_{b''\sigma}(t)\rangle=\sum_{b,b'}\epsilon_{bb'\sigma}(t)|b_\sigma\rangle\langle b'_\sigma|\mu_{b''\sigma}(t)\rangle, \tag{D.9}$$

which, on projection onto the basis state $|b_\sigma\rangle$, yields

$$i\frac{d}{dt}\langle b_\sigma|\mu_{b''\sigma}(t)\rangle=\sum_{b'}\epsilon_{bb'\sigma}(t)\langle b'_\sigma|\mu_{b''\sigma}(t)\rangle. \tag{D.10}$$

The projection $\langle b_\sigma|\mu_{b''\sigma}(t)\rangle$ also has the initial condition

$$\langle b_\sigma|\mu_{b''\sigma}(t_0)\rangle = \delta_{b,b''}. \tag{D.11}$$

Equations (D.10) and (D.11) are identical in form to (D.5) and (D.6), and we can therefore equate the quantity $A_{bb''\sigma}$ in the Heisenberg picture with the projection $\langle b_\sigma|\mu_{b''\sigma}(t)\rangle$. The general solution (D.3) therefore becomes

$$\hat{c}_{b\sigma}(t) = \sum_{b''}\langle b_\sigma|\mu_{b''\sigma}(t)\rangle\hat{c}_{b'\sigma}(t_0), \tag{D.12}$$

which is used in section 4.1.1 to expand the electron distribution function $n_\sigma$.

## D.2: Instantaneous Green's functions

In this section we use the Dyson equation to derive the set of Green's functions required to expand the electron distribution function (4.11).

The Dyson equation is [65];

$$G_\sigma(\epsilon,t) = G^0_\sigma(\epsilon,t) + G^0_\sigma(\epsilon,t)V(t)G_\sigma(\epsilon,t), \tag{D.13}$$

where $V(t)$ is the interaction potential, and $G^0_\sigma$ is the unperturbed Green's function, i.e. $G_\sigma$ for $V \equiv 0$. The Green's function $G_{bb'\sigma}$ is found by taking the elements of (D.13) with respect to the basis states of the system. We demonstrate the derivation of these functions from the Dyson equation by first considering the adsorbate Green's function $G_{aa\sigma}$;

$$\begin{aligned} G_{aa\sigma}(\epsilon,t) &= \langle a_\sigma|G_\sigma(\epsilon,t)|a_\sigma\rangle \\ &= \langle a_\sigma|G^0_\sigma(\epsilon,t)|a_\sigma\rangle + \langle a_\sigma|G^0_\sigma(\epsilon,t)V(t)G_\sigma(\epsilon,t)|a_\sigma\rangle \\ &= \langle a_\sigma|G^0_\sigma(\epsilon,t)|a_\sigma\rangle + \sum_{b,b'}\langle a_\sigma|G^0_\sigma(\epsilon,t)|b_\sigma\rangle\langle b_\sigma|V(t)|b'_\sigma\rangle\langle b'_\sigma|G_\sigma(\epsilon,t)|a_\sigma\rangle, \end{aligned} \tag{D.14}$$

where complete sets of basis states have been introduced on the final line. To expand this expression it is necessary to define the interaction matrix $\langle b_\sigma|V(t)|b'_\sigma\rangle$ and obtain the unperturbed Green's functions. In the Newns-Anderson model

the interaction matrix has the following elements;

$$\begin{aligned} \langle a_\sigma|V(t)|a_\sigma\rangle &= 0, & \langle a_\sigma|V(t)|k_\sigma\rangle &= V_{ak}(t), \\ \langle k_\sigma|V(t)|a_\sigma\rangle &= V^*_{ak}(t), & \langle k_\sigma|V(t)|k'_\sigma\rangle &= 0. \end{aligned} \tag{D.15}$$

The unperturbed Green's functions can be found by considering the definition of $G_\sigma$ (4.10) and the nature of the instantaneous eigenstates $|\nu_{\sigma t}\rangle$. For a non-interacting system the eigenstates of the one-electron Hamiltonian (4.2) are simply the basis states $|b_\sigma\rangle$. The unperturbed Green's function therefore becomes

$$\begin{aligned} G^0_{bb'\sigma}(\epsilon,t) \equiv \langle b_\sigma|G^0_\sigma(\epsilon,t)|b'_\sigma\rangle &= \sum_\nu \frac{\langle b_\sigma|\nu_{\sigma t}\rangle\langle\nu_{\sigma t}|b'_\sigma\rangle}{\epsilon-\epsilon^\nu_{\sigma t}+i\eta} \\ &= \sum_\nu \frac{\delta_{b,\nu}\delta_{\nu,b'}}{\epsilon-\epsilon^\nu_{\sigma t}+i\eta} \\ &= \frac{\delta_{b,b'}}{\epsilon-\epsilon_{b\sigma}(t)+i\eta}. \end{aligned} \tag{D.16}$$

The only non-zero elements of this function are

$$G^0_{aa\sigma}(\epsilon,t) = \frac{1}{\epsilon-\bar{\epsilon}_{a\sigma}(t)+i\eta}, \tag{D.17a}$$

$$G^0_{kk\sigma}(\epsilon,t) = \frac{1}{\epsilon-\epsilon_{k\sigma}+i\eta}. \tag{D.17b}$$

These properties of $G^0_\sigma$ and $V$ allow us to rewrite (D.14) as

$$\begin{aligned} G_{aa\sigma}(\epsilon,t) &= \langle a_\sigma|G^0_\sigma(\epsilon,t)|a_\sigma\rangle + \langle a_\sigma|G^0_\sigma(\epsilon,t)|a_\sigma\rangle\sum_k\langle a_\sigma|V(t)|k_\sigma\rangle\langle k_\sigma|G_\sigma(\epsilon,t)|a_\sigma\rangle \\ &= G^0_{aa\sigma}(\epsilon,t) + G^0_{aa\sigma}(\epsilon,t)\sum_k V_{ak}(t)G_{ka\sigma}(\epsilon,t). \end{aligned} \tag{D.18}$$

The functions $G_{ak\sigma}$, $G_{ka\sigma}$, and $G_{kk'\sigma}$ can be obtained in a similar manner, yielding

$$G_{ak\sigma}(\epsilon,t) = G^0_{aa\sigma}(\epsilon,t)\sum_{k'} V_{ak'}(t)G_{k'k\sigma}(\epsilon,t), \tag{D.19}$$

$$G_{ka\sigma}(\epsilon,t) = G^0_{kk\sigma}(\epsilon,t)V^*_{ak}(t)G_{aa\sigma}(\epsilon,t), \tag{D.20}$$

$$G_{kk'\sigma}(\epsilon,t) = G^0_{kk\sigma}(\epsilon,t)\delta_{k,k'} + G^0_{kk\sigma}(\epsilon,t)V^*_{ak}(t)G_{aa\sigma}(\epsilon,t). \tag{D.21}$$

We now solve equations (D.17) to (D.21) to give expressions in terms of the

energies $\bar{\epsilon}_{a\sigma}$ and $\epsilon_{k\sigma}$ and the interaction potential $V_{ak}$. By substituting (D.20) into (D.18) $G_{aa\sigma}$ becomes

$$\begin{aligned} G_{aa\sigma}(\epsilon,t) &= G^0_{aa\sigma}(\epsilon,t) + G^0_{aa\sigma}(\epsilon,t)G_{aa\sigma}(\epsilon,t)\sum_k |V_{ak}(t)|^2 G^0_{kk\sigma}(\epsilon,t) \\ &= \left[\left(G^0_{aa\sigma}(\epsilon,t)\right)^{-1} - \sum_k |V_{ak}(t)|^2 G^0_{kk\sigma}(\epsilon,t)\right]^{-1}, \end{aligned} \tag{D.22}$$

which, on combination with the definitions (D.17), yields

$$G_{aa\sigma}(\epsilon,t) = \left[\epsilon - \bar{\epsilon}_{a\sigma}(t) + i\eta - \sum_k \frac{|V_{ak}(t)|^2}{\epsilon - \epsilon_{k\sigma} + i\eta}\right]^{-1}. \tag{D.23}$$

The sum over metal states $k$ in this expression can be evaluated by introducing an integral and corresponding delta function, and using the definition of $\Gamma$ (2.13). This gives

$$\begin{aligned} \sum_k \frac{|V_{ak}(t)|^2}{\epsilon - \epsilon_{k\sigma} + i\eta} &= \int \frac{d\epsilon'}{\epsilon - \epsilon' + i\eta} \sum_k |V_{ak}(t)|^2 \delta(\epsilon' - \epsilon_{k\sigma}) \\ &= \frac{\Gamma(t)}{2\pi} \int \frac{d\epsilon'}{\epsilon - \epsilon' + i\eta}, \end{aligned} \tag{D.24}$$

where the $\epsilon'$ integral can be evaluated as follows:

$$\begin{aligned} \int \frac{d\epsilon'}{\epsilon - \epsilon' + i\eta} &= -\left[\ln(\epsilon - \epsilon' + i\eta)\right]_{-\infty}^{\infty} \\ &= -\left[\frac{1}{2}\ln\left|(\epsilon - \epsilon')^2 + \eta^2\right| + i\arg(\epsilon - \epsilon' + i\eta)\right]_{-\infty}^{\infty} \\ &= -\frac{1}{2}\ln\left|\frac{(\epsilon - \infty)^2 + \eta^2}{(\epsilon + \infty)^2 + \eta^2}\right| \\ &\quad -i\left(\arg(\epsilon - \infty + i\eta) - \arg(\epsilon + \infty + i\eta)\right). \end{aligned} \tag{D.25}$$

The first term in this equation vanishes provided that $\epsilon$ is finite and, as $\eta$ is positive, the arguments can be evaluated yielding

$$\int \frac{d\epsilon'}{\epsilon - \epsilon' + i\eta} = -i\pi. \tag{D.26}$$

On combination with (D.23) and (D.24) this gives

$$\begin{aligned} G_{aa\sigma}(\epsilon,t) &= \frac{1}{\epsilon-\bar{\epsilon}_{a\sigma}(t)+i\Gamma(t)/2} \\ &= \frac{1}{\epsilon-\tilde{\epsilon}_{a\sigma}(t)}, \end{aligned} \tag{D.27}$$

where $\eta$ has been neglected and $\tilde{\epsilon}_{a\sigma}$ is defined in chapter 2, (see equation (2.12), page 37). By using this result, and (D.17b), $G_{ka\sigma}$ becomes (from (D.20))

$$G_{ka\sigma}(\epsilon,t) = \frac{V^*_{ak}(t)}{(\epsilon-\epsilon_{k\sigma}+i\eta)}.\frac{1}{(\epsilon-\tilde{\epsilon}_{a\sigma}(t))}. \tag{D.28}$$

To obtain $G_{ak\sigma}$ we substitute (D.21) into (D.19), to give

$$\begin{aligned} G_{ak\sigma}(\epsilon,t) &= G^0_{aa\sigma}(\epsilon,t)V_{ak}(t)G^0_{kk\sigma}(\epsilon,t) \\ &\quad + G^0_{aa\sigma}(\epsilon,t)\sum_{k'}|V_{ak'}(t)|^2 G^0_{k'k'\sigma}(\epsilon,t)G_{ak\sigma}(\epsilon,t) \\ &= \frac{V_{ak}(t)G^0_{kk\sigma}(\epsilon,t)}{\left(G^0_{aa\sigma}(\epsilon,t)\right)^{-1}-\sum_{k'}|V_{ak'}(t)|^2 G^0_{k'k'\sigma}(\epsilon,t)}. \end{aligned} \tag{D.29}$$

The denominator of this fraction is the same as that appearing in the derivation of $G_{aa\sigma}$. By using equation (D.22) $G_{ak\sigma}$ can be rewritten as

$$\begin{aligned} G_{ak\sigma}(\epsilon,t) &= V_{ak}(t)G^0_{kk\sigma}(\epsilon,t)G_{aa\sigma}(\epsilon,t) \\ &= \frac{V_{ak}(t)}{(\epsilon-\epsilon_{k\sigma}+i\eta)}.\frac{1}{(\epsilon-\tilde{\epsilon}_{a\sigma}(t))}. \end{aligned} \tag{D.30}$$

The remaining Green's function required for $n_\sigma$ is $G_{kk'\sigma}$, which can be found by substituting this result for $G_{ak\sigma}$ into (D.21), giving

$$\begin{aligned} G_{kk'\sigma}(\epsilon,t) &= \delta_{k,k'}G^0_{kk\sigma}(\epsilon,t) + G^0_{kk\sigma}(\epsilon,t)V^*_{ak}(t)G^0_{k'k'\sigma}(\epsilon,t)V_{ak'}(t)G_{aa\sigma}(\epsilon,t) \\ &= \frac{\delta_{k,k'}}{\epsilon-\epsilon_{k\sigma}+i\eta} + \frac{V^*_{ak}(t)}{(\epsilon-\epsilon_{k\sigma}+i\eta)}.\frac{V_{ak'}(t)}{(\epsilon-\epsilon_{k'\sigma}+i\eta)}.\frac{1}{(\epsilon-\tilde{\epsilon}_{a\sigma}(t))}. \end{aligned} \tag{D.31}$$

Equations (D.27), (D.28), (D.30) and (D.31) make up the complete set of Green's functions required to expand the electron distribution function (4.11).

## D.3: Derivation of $n_\sigma^{(\mathrm{ii})}$

The second term in (4.23), $n_\sigma^{(\mathrm{ii})}$, can be expanded using the occupation function $n_{k\sigma}$, (2.29), derived in section 2.2.3, yielding

$$\begin{aligned}
n_\sigma^{(\mathrm{ii})}(\epsilon,t) &= \sum_k n_{k\sigma}(t)\delta(\epsilon-\epsilon_{k\sigma}) \\
&= \int d\epsilon' f(\epsilon') \int_{t_0}^{t} dt_1\ p_\sigma(\epsilon',t_1)\exp[i(\epsilon-\epsilon')(t_1-t)] \\
&\qquad \times \int_{t_0}^{t} dt_2\ p_\sigma^*(\epsilon,t_2)\exp[-i(\epsilon-\epsilon')(t_2-t)] \\
&\qquad \times \sum_k V_{ak}(t_1)V_{ak}^*(t_2)\delta(\epsilon-\epsilon_{k\sigma}) \\
&\quad -2f(\epsilon)\mathrm{Re}\Bigg\{ \int_{t_0}^{t} dt_1 \int_{t_0}^{t_1} dt_2 \exp\left[-i\int_{t_2}^{t_1}(\tilde{\epsilon}_{a\sigma}(t')-\epsilon)dt'\right] \\
&\qquad \times \sum_k V_{ak}^*(t_1)V_{ak}(t_2)\delta(\epsilon-\epsilon_{k\sigma})\Bigg\} \\
&\quad +n_{a\sigma}(t_0)\int_{t_0}^{t} dt_1 \exp\left[-i\int_{t_0}^{t_1}(\tilde{\epsilon}_{a\sigma}(t')-\epsilon)dt'\right] \\
&\qquad \times \int_{t_0}^{t} dt_2 \exp\left[i\int_{t_0}^{t_2}(\tilde{\epsilon}_{a\sigma}^*(t')-\epsilon)dt'\right] \\
&\qquad \times \sum_k V_{ak}^*(t_1)V_{ak}(t_2)\delta(\epsilon-\epsilon_{k\sigma}) \\
&\quad +\sum_k f(\epsilon_{k\sigma})\delta(\epsilon-\epsilon_{k\sigma}). \qquad \text{(D.32)}
\end{aligned}$$

This expression can be simplified by using (A.14) to replace the sums over metal states $k$, which appear in the first three terms. This gives

$$\begin{aligned} n_\sigma^{(\mathrm{ii})}(\epsilon,t) &= \int d\epsilon' f(\epsilon') \left| \int_{t_0}^{t} dt_1 \sqrt{\frac{\Gamma(t_1)}{2\pi}} p_\sigma(\epsilon', t_1) \exp[i(\epsilon-\epsilon')(t_1-t)] \right|^2 \\ & -2f(\epsilon)\mathrm{Re}\Bigg\{ \int_{t_0}^{t} dt_1 \sqrt{\frac{\Gamma(t_1)}{2\pi}} \\ & \qquad \times \int_{t_0}^{t_1} dt_2 \sqrt{\frac{\Gamma(t_2)}{2\pi}} \exp\left[ -i \int_{t_2}^{t_1} (\tilde{\epsilon}_{a\sigma}(t') - \epsilon) dt' \right] \Bigg\} \\ & + n_{a\sigma}(t_0) \left| \int_{t_0}^{t} dt_1 \sqrt{\frac{\Gamma(t_1)}{2\pi}} \exp\left[ -i \int_{t_0}^{t_1} (\tilde{\epsilon}_{a\sigma}(t') - \epsilon) dt' \right] \right|^2 \\ & + \sum_k f(\epsilon_{k\sigma}) \delta(\epsilon - \epsilon_{k\sigma}). \end{aligned} \tag{D.33}$$

Numerical computation of this expression would not be straightforward due to the time-integral inside the modulus in the third term in this expression. We therefore rearrange this integral, yielding

$$\begin{aligned} & \int_{t_0}^{t} dt_1 \sqrt{\frac{\Gamma(t_1)}{2\pi}} \exp\left[ -i \int_{t_0}^{t_1} (\tilde{\epsilon}_{a\sigma}(t') - \epsilon) dt' \right] \\ & \quad = \exp\left[ -i \int_{t_0}^{t} (\tilde{\epsilon}_{a\sigma}(t') - \epsilon) dt' \right] \int_{t_0}^{t} dt_1 \sqrt{\frac{\Gamma(t_1)}{2\pi}} \exp\left[ i \int_{t_1}^{t} (\tilde{\epsilon}_{a\sigma}(t') - \epsilon) dt' \right] \\ & \quad = \exp\left[ -i \int_{t_0}^{t} (\bar{\epsilon}_{a\sigma}(t') - \epsilon) dt' \right] \exp\left[ -\frac{1}{2} \int_{t_0}^{t} \Gamma(t') dt' \right] \\ & \qquad \times \int_{t_0}^{t} dt_1 \sqrt{\frac{\Gamma(t_1)}{2\pi}} \exp\left[ i \int_{t_1}^{t} (\tilde{\epsilon}_{a\sigma}(t') - \epsilon) dt' \right]. \end{aligned} \tag{D.34}$$

Equation (D.33) therefore becomes

$$\begin{aligned} n_\sigma^{(\mathrm{ii})}(\epsilon,t) &= \int d\epsilon' f(\epsilon') \left| \int_{t_0}^{t} dt_1 \sqrt{\frac{\Gamma(t_1)}{2\pi}} p_\sigma(\epsilon',t_1) \exp[i(\epsilon-\epsilon')(t_1-t)] \right|^2 \\ &\quad -2f(\epsilon)\mathrm{Re}\left\{ \int_{t_0}^{t} dt_1 \sqrt{\frac{\Gamma(t_1)}{2\pi}} p_\sigma(\epsilon,t_1) \right\} \\ &\quad +n_{a\sigma}(t_0) \left| \exp\left[ -\frac{1}{2}\int_{t_0}^{t} \Gamma(t')dt' \right] \right. \\ &\qquad \left. \times \int_{t_0}^{t} dt_1 \sqrt{\frac{\Gamma(t_1)}{2\pi}} \exp\left[ i\int_{t_1}^{t} (\tilde{\epsilon}_{a\sigma}(t')-\epsilon)dt' \right] \right|^2 \\ &\quad +\sum_k f(\epsilon_{k\sigma})\delta(\epsilon-\epsilon_{k\sigma}), \end{aligned} \tag{D.35}$$

where the definition of $p_\sigma$, (2.20), has been used and the exponential containing a time-integral over $\bar{\epsilon}_{a\sigma}(t)-\epsilon$ from (D.34) has been eliminated. The time integrals in this expression will appear throughout the derivations of $n_\sigma^{(\mathrm{iii})}$ and $n_\sigma^{(\mathrm{iv})}$ and we therefore re-write (D.35) as

$$\begin{aligned} n_\sigma^{(\mathrm{ii})}(\epsilon,t) &= \int d\epsilon' f(\epsilon') \left| q_\sigma(\epsilon,\epsilon',t) \right|^2 - 2f(\epsilon)\mathrm{Re}\left\{ q_\sigma(\epsilon,\epsilon,t) \right\} \\ &\quad +n_{a\sigma}(t_0) \left| r_\sigma(\epsilon,t) \right|^2 + \sum_k f(\epsilon_{k\sigma})\delta(\epsilon-\epsilon_{k\sigma}) \end{aligned} \tag{D.36}$$

where $q_\sigma$ and $r_\sigma$ are defined as

$$q_\sigma(\epsilon,\epsilon',t) = \int_{t_0}^{t} dt_1 \sqrt{\frac{\Gamma(t_1)}{2\pi}} p_\sigma(\epsilon',t_1) \exp[i(\epsilon-\epsilon')(t_1-t)], \tag{D.37}$$

$$r_\sigma(\epsilon,t) = \exp\left[ -\frac{1}{2}\int_{t_0}^{t} \Gamma(t')dt' \right] \int_{t_0}^{t} dt_1 \sqrt{\frac{\Gamma(t_1)}{2\pi}} \exp\left[ i\int_{t_1}^{t} (\tilde{\epsilon}_{a\sigma}(t')-\epsilon)dt' \right]. \tag{D.38}$$

## D.4: Derivation of $n_\sigma^{(\mathrm{iii})}$

The third term in (4.23), $n_\sigma^{(\mathrm{iii})}$, is

$$n_\sigma^{(\mathrm{iii})}(\epsilon,t) = -\frac{2}{\pi}\mathrm{Im}\left\{ \frac{1}{\epsilon-\tilde{\epsilon}_{a\sigma}(t)} \int \frac{d\epsilon'}{\epsilon-\epsilon'+i\eta} \mathrm{Re}\left[ \sum_k V_{ak}(t) n_{ak\sigma}(t) \delta(\epsilon'-\epsilon_{k\sigma}) \right] \right\}. \tag{D.39}$$

We first deal with the sum over states $k$, which by using the expression derived for $n_{ak\sigma}$ in chapter 2 becomes;

$$\begin{aligned}
&\sum_k V_{ak}(t) n_{ak\sigma}(t) \delta(\epsilon' - \epsilon_{k\sigma}) \\
&\quad = \; -i \int d\epsilon'' f(\epsilon'') p^*_\sigma(\epsilon'', t) \int_{t_0}^{t} p_\sigma(\epsilon'', t_1) \exp[i(\epsilon' - \epsilon'')(t_1 - t)] \\
&\qquad\qquad \times \sum_k V^*_{ak}(t_1) V_{ak}(t) \delta(\epsilon' - \epsilon_{k\sigma}) \\
&\qquad + i f(\epsilon') \int_{t_0}^{t} dt_1 \exp\left[ i \int_{t_1}^{t} (\tilde{\epsilon}^*_{a\sigma}(t') - \epsilon') dt' \right] \\
&\qquad\qquad \times \sum_k V^*_{ak}(t_1) V_{ak}(t) \delta(\epsilon' - \epsilon_{k\sigma}) \\
&\qquad - i n_{a\sigma}(t_0) \exp\left[ - \int_{t_0}^{t} \Gamma(t') dt' \right] \int_{t_0}^{t} dt_1 \exp\left[ i \int_{t_1}^{t} (\tilde{\epsilon}_{a\sigma}(t') - \epsilon') dt' \right] \\
&\qquad\qquad \times \sum_k V^*_{ak}(t_1) V_{ak}(t) \delta(\epsilon' - \epsilon_{k\sigma}).
\end{aligned} \tag{D.40}$$

This can be simplified by using (A.14), yielding

$$\begin{aligned}
&\sum_k V_{ak}(t) n_{ak\sigma}(t) \delta(\epsilon' - \epsilon_{k\sigma}) \\
&\quad = \; -i \int d\epsilon'' f(\epsilon'') \sqrt{\frac{\Gamma(t)}{2\pi}} p^*_\sigma(\epsilon'', t) \\
&\qquad\qquad \times \int_{t_0}^{t} \sqrt{\frac{\Gamma(t_1)}{2\pi}} p_\sigma(\epsilon'', t_1) \exp[i(\epsilon' - \epsilon'')(t_1 - t)] \\
&\qquad + i \sqrt{\frac{\Gamma(t)}{2\pi}} f(\epsilon') \int_{t_0}^{t} dt_1 \sqrt{\frac{\Gamma(t_1)}{2\pi}} \exp\left[ i \int_{t_1}^{t} (\tilde{\epsilon}^*_{a\sigma}(t') - \epsilon') dt' \right] \\
&\qquad - i n_{a\sigma}(t_0) \sqrt{\frac{\Gamma(t)}{2\pi}} \exp\left[ - \int_{t_0}^{t} \Gamma(t') dt' \right] \\
&\qquad\qquad \times \int_{t_0}^{t} dt_1 \sqrt{\frac{\Gamma(t_1)}{2\pi}} \exp\left[ i \int_{t_1}^{t} (\tilde{\epsilon}_{a\sigma}(t') - \epsilon') dt' \right].
\end{aligned} \tag{D.41}$$

By using the definitions of $p_\sigma$, (2.20), $q_\sigma$, (D.37), and $r_\sigma$, (D.38), this expression

can be rewritten as

$$\begin{aligned}\sum_k V_{ak}(t)n_{ak\sigma}(t)\delta(\epsilon'-\epsilon_{k\sigma}) \\ &= -i\int d\epsilon'' f(\epsilon'')\sqrt{\frac{\Gamma(t)}{2\pi}}p^*_\sigma(\epsilon'',t)q_\sigma(\epsilon',\epsilon'',t)+i\sqrt{\frac{\Gamma(t)}{2\pi}}f(\epsilon')p^*_\sigma(\epsilon',t) \\ &\quad -in_{a\sigma}(t_0)\sqrt{\frac{\Gamma(t)}{2\pi}}\exp\left[-\frac{1}{2}\int_{t_0}^t\Gamma(t')dt'\right]r_\sigma(\epsilon',t), \qquad \text{(D.42)}\end{aligned}$$

which, on combination with (D.39), gives

$$\begin{aligned}n^{(\mathrm{iii})}_\sigma(\epsilon,t) &= -\frac{2}{\pi}\mathrm{Im}\left\{\sqrt{\frac{\Gamma(t)}{2\pi}}\frac{1}{\epsilon-\tilde{\epsilon}_{a\sigma}(t)}\int\frac{d\epsilon'}{\epsilon-\epsilon'+i\eta}\right. \\ &\qquad \left.\times\int d\epsilon'' f(\epsilon'')\mathrm{Im}\left\{p^*_\sigma(\epsilon'',t)q_\sigma(\epsilon',\epsilon'',t)\right\}\right\} \\ &\quad -\frac{2}{\pi}\mathrm{Im}\left\{\sqrt{\frac{\Gamma(t)}{2\pi}}\frac{1}{\epsilon-\tilde{\epsilon}_{a\sigma}(t)}\int d\epsilon'\frac{f(\epsilon')}{\epsilon-\epsilon'+i\eta}\mathrm{Im}\left\{p_\sigma(\epsilon',t)\right\}\right\} \\ &\quad -\frac{2}{\pi}n_{a\sigma}(t_0)\exp\left[-\frac{1}{2}\int_{t_0}^t\Gamma(t')dt'\right] \\ &\qquad \times\mathrm{Im}\left\{\sqrt{\frac{\Gamma(t)}{2\pi}}\frac{1}{\epsilon-\tilde{\epsilon}_{a\sigma}(t)}\int d\epsilon'\frac{\mathrm{Im}\{r_\sigma(\epsilon,t)\}}{\epsilon-\epsilon'+i\eta}\right\}. \qquad \text{(D.43)}\end{aligned}$$

At this stage it is convenient to define the quantity $p^{(inst)}_\sigma$ to be

$$p^{(inst)}_\sigma(\epsilon,t)=\sqrt{\frac{\Gamma(t)}{2\pi}}\frac{i}{\epsilon-\tilde{\epsilon}_{a\sigma}(t)}. \qquad \text{(D.44)}$$

This quantity is similar to the adiabatic limit of $p_\sigma$, $p^{(ad)}_\sigma$, obtained in section 2.3, but with the adiabatic level $\bar{\epsilon}^{(ad)}_{a\sigma}$ replaced with the time-dependent level $\bar{\epsilon}_{a\sigma}$. By using this substitution, and expanding the inner imaginary part function in the

first and third terms, (D.43) becomes

$$
\begin{aligned}
n_\sigma^{(\mathrm{iii})}(\epsilon,t) &= \frac{2}{\pi}\mathrm{Im}\Bigg\{ip_\sigma^{(inst)}(\epsilon,t)\int d\epsilon'' f(\epsilon'') \\
&\qquad \times\frac{1}{2i}\left[p_\sigma^*(\epsilon'',t)\int d\epsilon'\frac{q_\sigma(\epsilon',\epsilon'',t)}{\epsilon-\epsilon'+i\eta} - p_\sigma(\epsilon'',t)\int d\epsilon'\frac{q_\sigma^*(\epsilon',\epsilon'',t)}{\epsilon-\epsilon'+i\eta}\right]\Bigg\} \\
&\quad +\frac{2}{\pi}\int d\epsilon' f(\epsilon')\mathrm{Im}\left\{\frac{ip_\sigma^{(inst)}(\epsilon,t)}{\epsilon-\epsilon'+i\eta}\right\}\mathrm{Im}\left\{p_\sigma(\epsilon',t)\right\} \\
&\quad +\frac{2}{\pi}n_{a\sigma}(t_0)\exp\left[-\frac{1}{2}\int_{t_0}^t\Gamma(t')dt'\right] \\
&\qquad \times\mathrm{Im}\left\{ip_\sigma^{(inst)}(\epsilon,t)\frac{1}{2i}\left[\int d\epsilon'\frac{r_\sigma(\epsilon',t)}{\epsilon-\epsilon'+i\eta} - \int d\epsilon'\frac{r_\sigma^*(\epsilon',t)}{\epsilon-\epsilon'+i\eta}\right]\right\}, \\
&= \frac{1}{\pi}\mathrm{Im}\left\{p_\sigma^{(inst)}(\epsilon,t)\int d\epsilon'' f(\epsilon'')p_\sigma^*(\epsilon'',t)\int d\epsilon'\frac{q_\sigma(\epsilon',\epsilon'',t)}{\epsilon-\epsilon'+i\eta}\right\} \\
&\quad -\frac{1}{\pi}\mathrm{Im}\left\{p_\sigma^{(inst)}(\epsilon,t)\int d\epsilon'' f(\epsilon'')p_\sigma(\epsilon'',t)\int d\epsilon'\frac{q_\sigma^*(\epsilon',\epsilon'',t)}{\epsilon-\epsilon'+i\eta}\right\} \\
&\quad +\frac{2}{\pi}\int d\epsilon' f(\epsilon')\mathrm{Re}\left\{\frac{p_\sigma^{(inst)}(\epsilon,t)}{\epsilon-\epsilon'+i\eta}\right\}\mathrm{Im}\left\{p_\sigma(\epsilon',t)\right\} \\
&\quad +\frac{1}{\pi}n_{a\sigma}(t_0)\exp\left[-\frac{1}{2}\int_{t_0}^t\Gamma(t')dt'\right]\mathrm{Im}\left\{p_\sigma^{(inst)}(\epsilon,t)\int d\epsilon'\frac{r_\sigma(\epsilon',t)}{\epsilon-\epsilon'+i\eta}\right\} \\
&\quad -\frac{1}{\pi}n_{a\sigma}(t_0)\exp\left[-\frac{1}{2}\int_{t_0}^t\Gamma(t')dt'\right]\mathrm{Im}\left\{p_\sigma^{(inst)}(\epsilon,t)\int d\epsilon'\frac{r_\sigma^*(\epsilon',t)}{\epsilon-\epsilon'+i\eta}\right\}.
\end{aligned}
\tag{D.45}
$$

Contour integration techniques will now be used to evaluate the $\epsilon'$ integrals over $q_\sigma$ and $r_\sigma$ appearing in this expression.

We first consider the $\epsilon'$ integral in the first term in (D.45), which can be expanded using the definition of $q_\sigma$, (D.37), giving

$$
\begin{aligned}
\int d\epsilon'\frac{q_\sigma(\epsilon',\epsilon'',t)}{\epsilon-\epsilon'+i\eta} &= \int_{t_0}^t dt_1\sqrt{\frac{\Gamma(t_1)}{2\pi}}p_\sigma(\epsilon'',t_1)\exp[-i\epsilon''(t_1-t)] \\
&\qquad \times\int d\epsilon'\frac{\exp[i\epsilon'(t_1-t)]}{\epsilon-\epsilon'+i\eta}.
\end{aligned}
\tag{D.46}
$$

The $\epsilon'$ integral on the right-hand side of this expression has a first order pole at $\epsilon'=\epsilon+i\eta$, which is in the upper half of the complex plane. As the time difference $t_1-t$ in the exponential in this integral is negative ($t_1$ is integrated up to time $t$) the contour integral must therefore be closed in the lower half of the complex

plane. This contour does not contain the pole in the integrand and therefore the residue theorem states that the integral is zero, i.e.

$$\int d\epsilon' \frac{q_\sigma(\epsilon', \epsilon'', t)}{\epsilon - \epsilon' + i\eta} = 0. \tag{D.47}$$

The second $\epsilon'$ integral in (D.45) can be expanded in a similar manner, yielding

$$\begin{aligned} \int d\epsilon' \frac{q^*_\sigma(\epsilon', \epsilon'', t)}{\epsilon - \epsilon' + i\eta} &= \int_{t_0}^{t} dt_1 \sqrt{\frac{\Gamma(t_1)}{2\pi}} p^*_\sigma(\epsilon'', t_1) \exp[i\epsilon''(t_1 - t)] \\ &\quad \times \int d\epsilon' \frac{\exp[-i\epsilon'(t_1 - t)]}{\epsilon - \epsilon' + i\eta}. \end{aligned} \tag{D.48}$$

In this integral the exponential containing $\epsilon'$ now requires the integration contour to be closed in the upper half of the complex plane. This contour includes the pole at $\epsilon' = \epsilon + i\eta$ and the integral can be evaluated using the residue theorem. The residue of the $\epsilon'$ integrand at the first order pole $\epsilon' = \epsilon + i\eta$ is

$$\begin{aligned} \mathrm{Res}(\epsilon' = \epsilon + i\eta) &= \lim_{\epsilon' \to \epsilon + i\eta} (\epsilon' - (\epsilon + i\eta)) \frac{\exp[-i\epsilon'(t_1 - t)]}{\epsilon - \epsilon' + i\eta} \\ &= -\exp[-i\epsilon(t_1 - t)] \exp[\eta(t_1 - t)]. \end{aligned} \tag{D.49}$$

In the $\eta \to 0$ limit the second exponential tends to unity, and we can therefore rewrite (D.48) as

$$\begin{aligned} \int d\epsilon' \frac{q^*_\sigma(\epsilon', \epsilon'', t)}{\epsilon - \epsilon' + i\eta} &= \int_{t_0}^{t} dt_1 \sqrt{\frac{\Gamma(t_1)}{2\pi}} p^*_\sigma(\epsilon'', t_1) \exp[i\epsilon''(t_1 - t)] \\ &\quad \times -2\pi i \exp[-i\epsilon(t_1 - t)] \\ &= -2\pi i q^*_\sigma(\epsilon, \epsilon'', t). \end{aligned} \tag{D.50}$$

The contour integrals involving $r_\sigma$ in (D.45) can be evaluated in a similar manner, with the results

$$\int d\epsilon' \frac{r_\sigma(\epsilon', t)}{\epsilon - \epsilon' + i\eta} = 0, \tag{D.51}$$

$$\int d\epsilon' \frac{r^*_\sigma(\epsilon', t)}{\epsilon - \epsilon' + i\eta} = -2\pi i r^*_\sigma(\epsilon, t). \tag{D.52}$$

Equation (D.45) therefore becomes

$$\begin{aligned} n_\sigma^{(\mathrm{iii})}(\epsilon,t) &= -\frac{1}{\pi}\mathrm{Im}\left\{p_\sigma^{(inst)}(\epsilon,t)\int d\epsilon'' f(\epsilon'')p_\sigma(\epsilon'',t). - 2\pi i q_\sigma^*(\epsilon,\epsilon'',t)\right\} \\ &\quad +\frac{2}{\pi}\int d\epsilon' f(\epsilon')\mathrm{Re}\left\{\frac{p_\sigma^{(inst)}(\epsilon,t)}{\epsilon-\epsilon'+i\eta}\right\}\mathrm{Im}\left\{p_\sigma(\epsilon',t)\right\} \\ &\quad -\frac{1}{\pi}n_{a\sigma}(t_0)\exp\left[-\frac{1}{2}\int_{t_0}^{t}\Gamma(t')dt'\right]\mathrm{Im}\left\{p_\sigma^{(inst)}(\epsilon,t). - 2\pi i r_\sigma^*(\epsilon,t)\right\}, \\ &= 2\int d\epsilon' f(\epsilon')\mathrm{Re}\left\{p_\sigma^{(inst)}(\epsilon,t)p_\sigma(\epsilon',t)q_\sigma^*(\epsilon,\epsilon',t)\right\} \\ &\quad +\frac{2}{\pi}\int d\epsilon' f(\epsilon')\mathrm{Re}\left\{\frac{p_\sigma^{(inst)}(\epsilon,t)}{\epsilon-\epsilon'+i\eta}\right\}\mathrm{Im}\left\{p_\sigma(\epsilon',t)\right\} \\ &\quad +2n_{a\sigma}(t_0)\exp\left[-\frac{1}{2}\int_{t_0}^{t}\Gamma(t')dt'\right]\mathrm{Re}\left\{p_\sigma^{(inst)}(\epsilon,t)r_\sigma^*(\epsilon,t)\right\}. \end{aligned} \tag{D.53}$$

## D.5: Derivation of $n_\sigma^{(\mathbf{iv})}$

The final term in (4.23), $n_\sigma^{(\mathrm{iv})}$, is

$$\begin{aligned} n_\sigma^{(\mathrm{iv})}(\epsilon,t) &= -\frac{1}{\pi}\mathrm{Im}\Bigg\{\frac{1}{\epsilon-\tilde{\epsilon}_{a\sigma}(t)}\int\frac{d\epsilon'}{\epsilon-\epsilon'+i\eta}\int\frac{d\epsilon''}{\epsilon-\epsilon''+i\eta} \\ &\qquad \times\sum_{k,k'}V_{ak}^*(t)V_{ak'}(t)n_{kk'\sigma}(t)\delta(\epsilon'-\epsilon_{k\sigma})\delta(\epsilon''-\epsilon_{k'\sigma})\Bigg\}. \end{aligned} \tag{D.54}$$

We expand this term by first considering the sum over metal states $(k,k')$. By using the occupation function $n_{kk'\sigma}$ derived in chapter 2 (see equation 2.28) this

sum becomes

$$
\begin{aligned}
&\sum_{k,k'} V^*_{ak}(t)V_{ak'}(t)n_{kk'\sigma}(t)\delta(\epsilon' - \epsilon_{k\sigma})\delta(\epsilon'' - \epsilon_{k'\sigma}) \\
&\quad = \int d\epsilon''' f(\epsilon''') \int_{t_0}^{t} dt_1 p^*_\sigma(\epsilon''', t_1) \exp[-i(\epsilon' - \epsilon''')(t_1 - t)] \\
&\qquad \times \int_{t_0}^{t} dt_2 p_\sigma(\epsilon''', t_2) \exp[i(\epsilon'' - \epsilon''')(t_2 - t)] \\
&\qquad \times \sum_k V^*_{ak}(t)V_{ak}(t_1)\delta(\epsilon' - \epsilon_{k\sigma}) \sum_{k'} V^*_{ak'}(t_2)V_{ak'}(t)\delta(\epsilon'' - \epsilon_{k\sigma}) \\
&\quad - f(\epsilon'') \int_{t_0}^{t} dt_1 \exp[i(\epsilon' - \epsilon'')(t - t_1)] \\
&\qquad \times \int_{t_0}^{t_1} dt_2 \exp\left[ i \int_{t_2}^{t_1} (\tilde{\epsilon}^*_{a\sigma}(t') - \epsilon'')dt' \right] \\
&\qquad \times \sum_k V^*_{ak}(t)V_{ak}(t_1)\delta(\epsilon' - \epsilon_{k\sigma}) \sum_{k'} V^*_{ak'}(t_2)V_{ak'}(t)\delta(\epsilon'' - \epsilon_{k\sigma}) \\
&\quad - f(\epsilon') \int_{t_0}^{t} dt_1 \exp[i(\epsilon' - \epsilon'')(t - t_1)] \\
&\qquad \times \int_{t_0}^{t_1} dt_2 \exp\left[ -i \int_{t_2}^{t_1} (\tilde{\epsilon}_{a\sigma}(t') - \epsilon')dt' \right] \\
&\qquad \times \sum_{k'} V^*_{ak'}(t_1)V_{ak'}(t)\delta(\epsilon'' - \epsilon_{k'\sigma}) \sum_k V^*_{ak}(t)V_{ak}(t_2)\delta(\epsilon' - \epsilon_{k\sigma}) \\
&\quad + n_{a\sigma}(t_0) \exp[i(\epsilon' - \epsilon'')(t - t_0)] \int_{t_0}^{t} dt_1 \exp\left[ i \int_{t_0}^{t_1} (\tilde{\epsilon}^*_{a\sigma}(t') - \epsilon')dt' \right] \\
&\qquad \times \int_{t_0}^{t} dt_2 \exp\left[ -i \int_{t_0}^{t_2} (\tilde{\epsilon}_{a\sigma}(t') - \epsilon'')dt' \right] \\
&\qquad \times \sum_k V^*_{ak}(t)V_{ak}(t_1)\delta(\epsilon' - \epsilon_{k\sigma}) \sum_{k'} V^*_{ak'}(t_2)V_{ak'}(t)\delta(\epsilon'' - \epsilon_{k\sigma}) \\
&\quad + f(\epsilon') \sum_k |V_{ak}(t)|^2 \delta(\epsilon' - \epsilon_{k\sigma})\delta(\epsilon' - \epsilon''). \qquad \text{(D.55)}
\end{aligned}
$$

As in the preceding subsections this sum can be simplified using (A.14), yielding

$$
\begin{aligned}
&\sum_{k,k'} V^*_{ak}(t)V_{ak'}(t)n_{kk'\sigma}(t)\delta(\epsilon' - \epsilon_{k\sigma})\delta(\epsilon'' - \epsilon_{k'\sigma}) \\
&\quad = \frac{\Gamma(t)}{2\pi}\int d\epsilon'''f(\epsilon''')\int_{t_0}^{t} dt_1\sqrt{\frac{\Gamma(t_1)}{2\pi}}p^*_\sigma(\epsilon''',t_1)\exp[-i(\epsilon' - \epsilon''')(t_1 - t)] \\
&\qquad\quad \times\int_{t_0}^{t} dt_2\sqrt{\frac{\Gamma(t_2)}{2\pi}}p_\sigma(\epsilon''',t_2)\exp[i(\epsilon'' - \epsilon''')(t_2 - t)] \\
&\qquad -f(\epsilon'')\frac{\Gamma(t)}{2\pi}\int_{t_0}^{t} dt_1\sqrt{\frac{\Gamma(t_1)}{2\pi}}\exp[i(\epsilon' - \epsilon'')(t - t_1)] \\
&\qquad\quad \times\int_{t_0}^{t_1} dt_2\sqrt{\frac{\Gamma(t_2)}{2\pi}}\exp\left[i\int_{t_2}^{t_1}(\tilde{\epsilon}^*_{a\sigma}(t') - \epsilon'')dt'\right] \\
&\qquad -f(\epsilon')\frac{\Gamma(t)}{2\pi}\int_{t_0}^{t} dt_1\sqrt{\frac{\Gamma(t_1)}{2\pi}}\exp[i(\epsilon' - \epsilon'')(t - t_1)] \\
&\qquad\quad \times\int_{t_0}^{t_1} dt_2\sqrt{\frac{\Gamma(t_2)}{2\pi}}\exp\left[-i\int_{t_2}^{t_1}(\tilde{\epsilon}_{a\sigma}(t') - \epsilon')dt'\right] \\
&\qquad +n_{a\sigma}(t_0)\frac{\Gamma(t)}{2\pi}\exp[i(\epsilon' - \epsilon'')(t - t_0)] \\
&\qquad\quad \times\int_{t_0}^{t} dt_1\sqrt{\frac{\Gamma(t_1)}{2\pi}}\exp\left[i\int_{t_0}^{t_1}(\tilde{\epsilon}^*_{a\sigma}(t') - \epsilon')dt'\right] \\
&\qquad\quad \times\int_{t_0}^{t} dt_2\sqrt{\frac{\Gamma(t_2)}{2\pi}}\exp\left[-i\int_{t_0}^{t_2}(\tilde{\epsilon}_{a\sigma}(t') - \epsilon'')dt'\right] \\
&\qquad +f(\epsilon')\frac{\Gamma(t)}{2\pi}\delta(\epsilon' - \epsilon''). \qquad\qquad \text{(D.56)}
\end{aligned}
$$

By using the definitions of $p_\sigma$ and $q_\sigma$, (2.20) and (D.37), this expression can be rewritten as

$$\begin{aligned}
&\sum_{k,k'} V^*_{ak}(t)V_{ak'}(t)n_{kk'\sigma}(t)\delta(\epsilon' - \epsilon_{k\sigma})\delta(\epsilon'' - \epsilon_{k'\sigma}) \\
&\quad = \frac{\Gamma(t)}{2\pi}\int d\epsilon''' f(\epsilon''')q^*_\sigma(\epsilon', \epsilon''', t)q_\sigma(\epsilon'', \epsilon''', t) \\
&\quad\quad -f(\epsilon'')\frac{\Gamma(t)}{2\pi}\int_{t_0}^{t} dt_1\sqrt{\frac{\Gamma(t_1)}{2\pi}}p^*_\sigma(\epsilon'', t)\exp[i(\epsilon' - \epsilon'')(t - t_1)] \\
&\quad\quad -f(\epsilon')\frac{\Gamma(t)}{2\pi}\int_{t_0}^{t} dt_1\sqrt{\frac{\Gamma(t_1)}{2\pi}}p_\sigma(\epsilon', t)\exp[i(\epsilon' - \epsilon'')(t - t_1)] \\
&\quad\quad +n_{a\sigma}(t_0)\frac{\Gamma(t)}{2\pi}\exp[i(\epsilon' - \epsilon'')(t - t_0)] \\
&\quad\quad\quad \times\int_{t_0}^{t} dt_1\sqrt{\frac{\Gamma(t_1)}{2\pi}}\exp\left[i\int_{t_0}^{t_1}(\tilde{\epsilon}^*_{a\sigma}(t') - \epsilon')dt'\right] \\
&\quad\quad\quad \times\int_{t_0}^{t} dt_2\sqrt{\frac{\Gamma(t_2)}{2\pi}}\exp\left[-i\int_{t_0}^{t_2}(\tilde{\epsilon}_{a\sigma}(t') - \epsilon'')dt'\right] \\
&\quad\quad +f(\epsilon')\frac{\Gamma(t)}{2\pi}\delta(\epsilon' - \epsilon''), \\
&\quad = \frac{\Gamma(t)}{2\pi}\int d\epsilon''' f(\epsilon''')q^*_\sigma(\epsilon', \epsilon''', t)q_\sigma(\epsilon'', \epsilon''', t) \\
&\quad\quad -f(\epsilon'')\frac{\Gamma(t)}{2\pi}q^*_\sigma(\epsilon', \epsilon'', t) - f(\epsilon')\frac{\Gamma(t)}{2\pi}q_\sigma(\epsilon'', \epsilon', t) \\
&\quad\quad +n_{a\sigma}(t_0)\frac{\Gamma(t)}{2\pi}\exp[i(\epsilon' - \epsilon'')(t - t_0)] \\
&\quad\quad\quad \times\int_{t_0}^{t} dt_1\sqrt{\frac{\Gamma(t_1)}{2\pi}}\exp\left[i\int_{t_0}^{t_1}(\tilde{\epsilon}^*_{a\sigma}(t') - \epsilon')dt'\right] \\
&\quad\quad\quad \times\int_{t_0}^{t} dt_2\sqrt{\frac{\Gamma(t_2)}{2\pi}}\exp\left[-i\int_{t_0}^{t_2}(\tilde{\epsilon}_{a\sigma}(t') - \epsilon'')dt'\right] \\
&\quad\quad +f(\epsilon')\frac{\Gamma(t)}{2\pi}\delta(\epsilon' - \epsilon''). \qquad \text{(D.57)}
\end{aligned}$$

The time integrals in the fourth term in this expression can be expanded to obtain the quantity $r_\sigma$, (D.38). This will be demonstrated for the $t_1$ integral by replacing

the exponential with two terms;

$$\begin{aligned}
&\int_{t_0}^{t} dt_1 \sqrt{\frac{\Gamma(t_1)}{2\pi}} \exp\left[ i \int_{t_0}^{t_1} (\tilde{\epsilon}^*_{a\sigma}(t') - \epsilon') dt' \right] \\
&\quad = \exp\left[ i \int_{t_0}^{t} (\tilde{\epsilon}^*_{a\sigma}(t) - \epsilon') dt' \right] \int_{t_0}^{t} dt_1 \sqrt{\frac{\Gamma(t_1)}{2\pi}} \exp\left[ -i \int_{t_1}^{t} (\tilde{\epsilon}^*_{a\sigma}(t') - \epsilon') dt' \right] \\
&\quad = \exp\left[ i \int_{t_0}^{t} (\bar{\epsilon}_{a\sigma}(t) - \epsilon') dt' \right] \\
&\qquad\qquad \times \exp\left[ -\frac{1}{2} \int_{t_0}^{t} \Gamma(t') dt' \right] \int_{t_0}^{t} dt_1 \sqrt{\frac{\Gamma(t_1)}{2\pi}} \exp\left[ -i \int_{t_1}^{t} (\tilde{\epsilon}^*_{a\sigma}(t') - \epsilon') dt' \right] \\
&\quad = \exp\left[ i \int_{t_0}^{t} (\bar{\epsilon}_{a\sigma}(t) - \epsilon') dt' \right] r^*_\sigma(\epsilon', t). \qquad \text{(D.58)}
\end{aligned}$$

Equation (D.57) therefore becomes

$$\begin{aligned}
&\sum_{k,k'} V^*_{ak}(t) V_{ak'}(t) n_{kk'\sigma}(t) \delta(\epsilon' - \epsilon_{k\sigma}) \delta(\epsilon'' - \epsilon_{k'\sigma}) \\
&\quad = \frac{\Gamma(t)}{2\pi} \int d\epsilon''' f(\epsilon''') q^*_\sigma(\epsilon', \epsilon''', t) q_\sigma(\epsilon'', \epsilon''', t) \\
&\qquad - f(\epsilon'') \frac{\Gamma(t)}{2\pi} q^*_\sigma(\epsilon', \epsilon'', t) - f(\epsilon') \frac{\Gamma(t)}{2\pi} q_\sigma(\epsilon'', \epsilon', t) \\
&\qquad + n_{a\sigma}(t_0) \frac{\Gamma(t)}{2\pi} \exp[i(\epsilon' - \epsilon'')(t - t_0)] \\
&\qquad\qquad \times \exp\left[ i \int_{t_0}^{t} (\bar{\epsilon}_{a\sigma}(t) - \epsilon') dt' \right] r^*_\sigma(\epsilon', t) \\
&\qquad\qquad \times \exp\left[ -i \int_{t_0}^{t} (\bar{\epsilon}_{a\sigma}(t) - \epsilon'') dt' \right] r_\sigma(\epsilon'', t) \\
&\qquad + f(\epsilon') \frac{\Gamma(t)}{2\pi} \delta(\epsilon' - \epsilon''), \\
&\quad = \frac{\Gamma(t)}{2\pi} \int d\epsilon''' f(\epsilon''') q^*_\sigma(\epsilon', \epsilon''', t) q_\sigma(\epsilon'', \epsilon''', t) \\
&\qquad - f(\epsilon'') \frac{\Gamma(t)}{2\pi} q^*_\sigma(\epsilon', \epsilon'', t) - f(\epsilon') \frac{\Gamma(t)}{2\pi} q_\sigma(\epsilon'', \epsilon', t) \\
&\qquad + n_{a\sigma}(t_0) \frac{\Gamma(t)}{2\pi} r^*_\sigma(\epsilon', t) r_\sigma(\epsilon'', t) + f(\epsilon') \frac{\Gamma(t)}{2\pi} \delta(\epsilon' - \epsilon''). \qquad \text{(D.59)}
\end{aligned}$$

When this is substituted into (D.54) we find

$$
\begin{aligned}
n_\sigma^{(\mathrm{iv})}(\epsilon,t) \;=\; & -\frac{\Gamma(t)}{2\pi^2}\mathrm{Im}\Bigg\{\frac{1}{\epsilon-\tilde{\epsilon}_{a\sigma}(t)}\int d\epsilon'''f(\epsilon''') \\
& \qquad \times\int d\epsilon'\frac{q_\sigma^*(\epsilon',\epsilon''',t)}{\epsilon-\epsilon'+i\eta}\int d\epsilon''\frac{q_\sigma(\epsilon'',\epsilon''',t)}{\epsilon-\epsilon''+i\eta}\Bigg\} \\
& +\frac{\Gamma(t)}{2\pi^2}\mathrm{Im}\left\{\frac{1}{\epsilon-\tilde{\epsilon}_{a\sigma}(t)}\int d\epsilon''\frac{f(\epsilon'')}{\epsilon-\epsilon''+i\eta}\int d\epsilon'\frac{q_\sigma^*(\epsilon',\epsilon'',t)}{\epsilon-\epsilon'+i\eta}\right\} \\
& +\frac{\Gamma(t)}{2\pi^2}\mathrm{Im}\left\{\frac{1}{\epsilon-\tilde{\epsilon}_{a\sigma}(t)}\int d\epsilon'\frac{f(\epsilon')}{\epsilon-\epsilon'+i\eta}\int d\epsilon''\frac{q_\sigma(\epsilon'',\epsilon',t)}{\epsilon-\epsilon''+i\eta}\right\} \\
& -\frac{\Gamma(t)}{2\pi^2}n_{a\sigma}(t_0)\mathrm{Im}\left\{\frac{1}{\epsilon-\tilde{\epsilon}_{a\sigma}(t)}\int d\epsilon'\frac{r_\sigma^*(\epsilon',t)}{\epsilon-\epsilon'+i\eta}\int d\epsilon''\frac{r_\sigma(\epsilon'',t)}{\epsilon-\epsilon''+i\eta}\right\} \\
& -\frac{\Gamma(t)}{2\pi^2}\mathrm{Im}\left\{\frac{1}{\epsilon-\tilde{\epsilon}_{a\sigma}(t)}\int d\epsilon'\frac{f(\epsilon')}{\epsilon-\epsilon'+i\eta}\int d\epsilon''\frac{\delta(\epsilon'-\epsilon'')}{\epsilon-\epsilon''+i\eta}\right\}. \qquad \text{(D.60)}
\end{aligned}
$$

The energy integrals in this expression which do not contain the Fermi function were evaluated by contour integration in the previous section of this appendix. By combining equations (D.47), (D.50), (D.51) and (D.52) with (D.60), $n_\sigma^{(\mathrm{iv})}$ becomes

$$
\begin{aligned}
n_\sigma^{(\mathrm{iv})}(\epsilon,t) \;=\; & \frac{\Gamma(t)}{2\pi^2}\mathrm{Im}\left\{\frac{1}{\epsilon-\tilde{\epsilon}_{a\sigma}(t)}\int d\epsilon''\frac{f(\epsilon'')}{\epsilon-\epsilon''+i\eta}.-2\pi i q_\sigma^*(\epsilon,\epsilon'',t)\right\} \\
& -\frac{\Gamma(t)}{2\pi^2}\mathrm{Im}\left\{\frac{1}{\epsilon-\tilde{\epsilon}_{a\sigma}(t)}\int d\epsilon'\frac{f(\epsilon')}{(\epsilon-\epsilon'+i\eta)^2}\right\} \\
= \; & -2\sqrt{\frac{\Gamma(t)}{2\pi}}\int d\epsilon' f(\epsilon')\mathrm{Im}\left\{\frac{p_\sigma^{(inst)}(\epsilon,t)q_\sigma^*(\epsilon,\epsilon',t)}{\epsilon-\epsilon'+i\eta}\right\} \\
& +\frac{1}{\pi}\sqrt{\frac{\Gamma(t)}{2\pi}}\int d\epsilon' f(\epsilon')\mathrm{Re}\left\{\frac{p_\sigma^{(inst)}(\epsilon,t)}{(\epsilon-\epsilon'+i\eta)^2}\right\}, \qquad \text{(D.61)}
\end{aligned}
$$

where the integration variable $\epsilon''$ has been replaced with $\epsilon'$, and $p_\sigma^{(inst)}$ is defined in (D.44).

## D.6: Derivation of $n_\sigma$

We now combine the results of the previous three sections to obtain the final expression for the electron distribution function $n_\sigma$.

The sum of equations (D.36), (D.53) and (D.61), and the first term in (4.23), is

$$\begin{aligned} n_\sigma(\epsilon,t) &= n_{a\sigma}(t)|p_\sigma^{(inst)}(\epsilon,t)|^2 + \int d\epsilon' f(\epsilon') \left|q_\sigma(\epsilon,\epsilon',t)\right|^2 - 2f(\epsilon)\mathrm{Re}\left\{q_\sigma(\epsilon,\epsilon,t)\right\} \\ &\quad + n_{a\sigma}(t_0)\left|r_\sigma(\epsilon,t)\right|^2 + \sum_k f(\epsilon_{k\sigma})\delta(\epsilon-\epsilon_{k\sigma}) \\ &\quad + 2\int d\epsilon' f(\epsilon')\mathrm{Re}\left\{p_\sigma^{(inst)}(\epsilon,t)p_\sigma(\epsilon',t)q_\sigma^*(\epsilon,\epsilon',t)\right\} \\ &\quad + \frac{2}{\pi}\int d\epsilon' f(\epsilon')\mathrm{Re}\left\{\frac{p_\sigma^{(inst)}(\epsilon,t)}{\epsilon-\epsilon'+i\eta}\right\}\mathrm{Im}\left\{p_\sigma(\epsilon',t)\right\} \\ &\quad + 2n_{a\sigma}(t_0)\exp\left[-\frac{1}{2}\int_{t_0}^t \Gamma(t')dt'\right]\mathrm{Re}\left\{p_\sigma^{(inst)}(\epsilon,t)r_\sigma^*(\epsilon,t)\right\} \\ &\quad - 2\sqrt{\frac{\Gamma(t)}{2\pi}}\int d\epsilon' f(\epsilon')\mathrm{Im}\left\{\frac{p_\sigma^{(inst)}(\epsilon,t)q_\sigma^*(\epsilon,\epsilon',t)}{\epsilon-\epsilon'+i\eta}\right\} \\ &\quad + \frac{1}{\pi}\sqrt{\frac{\Gamma(t)}{2\pi}}\int d\epsilon' f(\epsilon')\mathrm{Re}\left\{\frac{p_\sigma^{(inst)}(\epsilon,t)}{(\epsilon-\epsilon'+i\eta)^2}\right\}, \end{aligned} \tag{D.62}$$

where $\rho_{a\sigma}^{(inst)}$ has been replaced with $|p_\sigma^{(inst)}|^2$. This expression can be rewritten in a more concise form by combining a number of terms. Terms which depend on the initial occupation of the adsorbate $n_{a\sigma}(t_0)$ can be found directly from (D.62) and indirectly using the definition of $n_{a\sigma}$, (2.19), giving

$$\begin{aligned} \left\{n_\sigma(\epsilon,t)\right\}_{[n_{a\sigma}(t_0)]} &= n_{a\sigma}(t_0)|p_\sigma^{(inst)}(\epsilon,t)|^2\exp\left[-\int_{t_0}^t \Gamma(t')dt'\right] + n_{a\sigma}(t_0)|r_\sigma(\epsilon,t)|^2 \\ &\quad + 2n_{a\sigma}(t_0)\exp\left[-\frac{1}{2}\int_{t_0}^t \Gamma(t')dt'\right]\mathrm{Re}\left\{p_\sigma^{(inst)}(\epsilon,t)r_\sigma^*(\epsilon,t)\right\}. \end{aligned} \tag{D.63}$$

This can be expressed as a single modulus;

$$\left\{n_\sigma(\epsilon,t)\right\}_{[n_{a\sigma}(t_0)]} = n_{a\sigma}(t_0)\left|r_\sigma(\epsilon,t) + p_\sigma^{(inst)}(\epsilon,t)\exp\left[-\frac{1}{2}\int_{t_0}^t \Gamma(t')dt'\right]\right|^2. \tag{D.64}$$

Equation (D.62) therefore becomes

$$\begin{aligned} n_\sigma(\epsilon,t) &= \int d\epsilon' f(\epsilon')|p_\sigma(\epsilon',t)p_\sigma^{(inst)}(\epsilon,t)|^2 + \int d\epsilon' f(\epsilon')\left|q_\sigma(\epsilon,\epsilon',t)\right|^2 \\ &\quad -2f(\epsilon)\mathrm{Re}\left\{q_\sigma(\epsilon,\epsilon,t)\right\} \\ &\quad +n_{a\sigma}(t_0)\left|r_\sigma(\epsilon,t)+p_\sigma^{(inst)}(\epsilon,t)\exp\left[-\frac{1}{2}\int_{t_0}^{t}\Gamma(t')dt'\right]\right|^2 \\ &\quad +\sum_k f(\epsilon_{k\sigma})\delta(\epsilon-\epsilon_{k\sigma}) \\ &\quad +2\int d\epsilon' f(\epsilon')\mathrm{Re}\left\{p_\sigma^{(inst)}(\epsilon,t)p_\sigma(\epsilon',t)q_\sigma^*(\epsilon,\epsilon',t)\right\} \\ &\quad +\frac{2}{\pi}\int d\epsilon' f(\epsilon')\mathrm{Re}\left\{\frac{p_\sigma^{(inst)}(\epsilon,t)}{\epsilon-\epsilon'+i\eta}\right\}\mathrm{Im}\left\{p_\sigma(\epsilon',t)\right\} \\ &\quad -2\sqrt{\frac{\Gamma(t)}{2\pi}}\int d\epsilon' f(\epsilon')\mathrm{Im}\left\{\frac{p_\sigma^{(inst)}(\epsilon,t)q_\sigma^*(\epsilon,\epsilon',t)}{\epsilon-\epsilon'+i\eta}\right\} \\ &\quad +\frac{1}{\pi}\sqrt{\frac{\Gamma(t)}{2\pi}}\int d\epsilon' f(\epsilon')\mathrm{Re}\left\{\frac{p_\sigma^{(inst)}(\epsilon,t)}{(\epsilon-\epsilon'+i\eta)^2}\right\}. \end{aligned} \tag{D.65}$$

The first, second and sixth terms in this expression can also be combined into a single modulus, yielding our final expression for the electron distribution function $n_\sigma$;

$$\begin{aligned} n_\sigma(\epsilon,t) &= \int d\epsilon' f(\epsilon')\left|q_\sigma(\epsilon,\epsilon',t)+p_\sigma^{(inst)}(\epsilon,t)p_\sigma(\epsilon',t)\right|^2 - 2f(\epsilon)\mathrm{Re}\left\{q_\sigma(\epsilon,\epsilon,t)\right\} \\ &\quad +n_{a\sigma}(t_0)\left|r_\sigma(\epsilon,t)+p_\sigma^{(inst)}(\epsilon,t)\exp\left[-\frac{1}{2}\int_{t_0}^{t}\Gamma(t')dt'\right]\right|^2 \\ &\quad +\sum_k f(\epsilon_{k\sigma})\delta(\epsilon-\epsilon_{k\sigma}) \\ &\quad +\frac{2}{\pi}\int d\epsilon' f(\epsilon')\mathrm{Re}\left\{\frac{p_\sigma^{(inst)}(\epsilon,t)}{\epsilon-\epsilon'+i\eta}\right\}\mathrm{Im}\left\{p_\sigma(\epsilon',t)\right\} \\ &\quad -2\sqrt{\frac{\Gamma(t)}{2\pi}}\int d\epsilon' f(\epsilon')\mathrm{Im}\left\{\frac{p_\sigma^{(inst)}(\epsilon,t)q_\sigma^*(\epsilon,\epsilon',t)}{\epsilon-\epsilon'+i\eta}\right\} \\ &\quad +\frac{1}{\pi}\sqrt{\frac{\Gamma(t)}{2\pi}}\int d\epsilon' f(\epsilon')\mathrm{Re}\left\{\frac{p_\sigma^{(inst)}(\epsilon,t)}{(\epsilon-\epsilon'+i\eta)^2}\right\}. \end{aligned} \tag{D.66}$$

# Appendix E: Electron distribution function test I: conservation of charge

In this appendix we verify that the expression for the electron distribution function $n_\sigma$ derived in section 4.1.3 conserves electrons. This test can be performed analytically by taking the zeroth moment of $n_\sigma$. We will use numerical superscripts to denote the individual terms in $n_\sigma$, (4.25). The integral over the first term in $n_\sigma$, $n_\sigma^{(1)}$, can be expanded yielding

$$\begin{aligned}
&\int d\epsilon n_\sigma^{(1)}(\epsilon,t) \\
&\quad= \int d\epsilon' f(\epsilon') \int d\epsilon \left| q_\sigma(\epsilon,\epsilon',t) + p_\sigma^{(inst)}(\epsilon,t) p_\sigma(\epsilon',t) \right|^2, \\
&\quad= \int d\epsilon' f(\epsilon') \int d\epsilon |q_\sigma(\epsilon,\epsilon',t)|^2 \\
&\qquad +2\mathrm{Re}\left\{ \int d\epsilon p_\sigma^{(inst)}(\epsilon,t) \int d\epsilon' f(\epsilon') p_\sigma(\epsilon',t) q_\sigma^*(\epsilon,\epsilon',t) \right\} \\
&\qquad + \int d\epsilon' f(\epsilon') |p_\sigma(\epsilon',t)|^2 \int d\epsilon |p_\sigma^{(inst)}(\epsilon,t)|^2 \\
&\quad= \int d\epsilon' f(\epsilon') \int_{t_0}^t dt_1 \int_{t_0}^t dt_2 \sqrt{\Gamma(t_1)\Gamma(t_2)} p_\sigma^*(\epsilon',t_2) p_\sigma(\epsilon',t_1) \exp[i\epsilon'(t_2-t_1)] \\
&\qquad\qquad \times \int d\epsilon \frac{\exp[i\epsilon(t_1-t_2)]}{2\pi} \\
&\qquad +2\mathrm{Re}\left\{ i\sqrt{\frac{\Gamma(t)}{2\pi}} \int d\epsilon' f(\epsilon') p_\sigma(\epsilon',t) \int_{t_0}^t dt_1 \sqrt{\frac{\Gamma(t_1)}{2\pi}} p_\sigma^*(\epsilon',t_1) \exp[i\epsilon'(t_1-t)] \right. \\
&\qquad\qquad \left. \times \int d\epsilon \frac{\exp[-i\epsilon(t_1-t)]}{\epsilon - \tilde{\epsilon}_{a\sigma}(t)} \right\} \\
&\qquad + \int d\epsilon' f(\epsilon') \left| p_\sigma(\epsilon',t) \right|^2 \int d\epsilon \frac{\Gamma(t)}{2\pi[(\epsilon-\bar{\epsilon}_{a\sigma}(t))^2 + \Gamma(t)^2/4]},
\end{aligned} \tag{E.1}$$

where the definition of $p_\sigma^{(inst)}$, (4.26), has been used to allow the separation of the $\epsilon$ dependent terms. The $\epsilon$ integral in the first term in this expression is the delta function $\delta(t_1 - t_2)$. Contour integration methods can be used to evaluate the $\epsilon$ integral in the second term of (E.1) with the contour closed in the upper half plane. By the residue theorem this integral is zero as the pole at $\epsilon = \tilde{\epsilon}_{a\sigma} = \bar{\epsilon}_{a\sigma} - i\Gamma/2$ is in the lower half of the complex plane. The remaining $\epsilon$ integral, in the third term in (E.1), is simple to evaluate as it is the integral over a normalised

Lorentzian. Equation (E.1) therefore simplifies to

$$\int d\epsilon\; n_\sigma^{(1)}(\epsilon,t) = \int_{t_0}^{t} dt_1 \Gamma(t_1) \int d\epsilon' f(\epsilon') \left|p_\sigma(\epsilon',t_1)\right|^2 + \int d\epsilon' f(\epsilon') \left|p_\sigma(\epsilon',t)\right|^2 . \quad \text{(E.2)}$$

The integral of the second term in $n_\sigma$, (4.25), results in an expression which cannot be simplified further at this stage;

$$\int d\epsilon\; n_\sigma^{(2)}(\epsilon,t) = -2\int_{t_0}^{t} dt_1 \sqrt{\frac{\Gamma(t_1)}{2\pi}} \int d\epsilon f(\epsilon) \mathrm{Re}\{p_\sigma(\epsilon,t_1)\}. \quad \text{(E.3)}$$

Integration of the third term in $n_\sigma$ yields

$$\begin{aligned}
&\int d\epsilon\; n_\sigma^{(3)}(\epsilon,t) \\
&\quad = n_{a\sigma}(t_0) \int d\epsilon \left| r_\sigma(\epsilon,t) + p_\sigma^{(inst)}(\epsilon,t) \exp\left[-\frac{1}{2}\int_{t_0}^{t}\Gamma(t')dt'\right]\right|^2 \\
&\quad = n_{a\sigma}(t_0) \int d\epsilon |r_\sigma(\epsilon,t)|^2 \\
&\qquad +2\mathrm{Re}\left\{ i n_{a\sigma}(t_0) \exp\left[-\frac{1}{2}\int_{t_0}^{t}\Gamma(t')dt'\right] \sqrt{\frac{\Gamma(t)}{2\pi}} \int d\epsilon \frac{r_\sigma^*(\epsilon,t)}{\epsilon - \tilde{\epsilon}_{a\sigma}(t)} \right\} \\
&\qquad +n_{a\sigma}(t_0) \exp\left[-\int_{t_0}^{t}\Gamma(t')dt'\right] \int d\epsilon \frac{\Gamma(t)}{2\pi[(\epsilon - \bar{\epsilon}_{a\sigma}(t))^2 + \Gamma(t)^2/4]}. \quad \text{(E.4)}
\end{aligned}$$

The first term in this expression can be expanded using the definition of $r_\sigma$, (4.28), giving

$$\begin{aligned}
\int d\epsilon |r_\sigma(\epsilon,t)|^2 &= \exp\left[-\int_{t_0}^{t}\Gamma(t')dt'\right] \int_{t_0}^{t} dt_1 \int_{t_0}^{t} dt_2 \sqrt{\Gamma(t_1)\Gamma(t_2)} \\
&\qquad \times \exp\left[ i\int_{t_2}^{t} \tilde{\epsilon}_{a\sigma}(t')dt' - i\int_{t_1}^{t} \tilde{\epsilon}_{a\sigma}^*(t')dt' \right] \\
&\qquad \times \int d\epsilon \frac{\exp[-i\epsilon(t_1-t_2)]}{2\pi}, \\
&= \exp\left[-\int_{t_0}^{t}\Gamma(t')dt'\right] \int_{t_0}^{t} dt_1 \Gamma(t_1) \exp\left[\int_{t_1}^{t}\Gamma(t')dt'\right], \\
&= \int_{t_0}^{t} dt_1 \Gamma(t_1) \exp\left[-\int_{t_0}^{t_1}\Gamma(t')dt'\right], \quad \text{(E.5)}
\end{aligned}$$

where we have recognised the energy integral in the first line as the delta function $\delta(t_1 - t_2)$. Evaluation of the second term in (E.4) can be performed using the

definition of $r_\sigma$;

$$\begin{aligned}\int d\epsilon \frac{r^*_\sigma(\epsilon,t)}{\epsilon-\tilde{\epsilon}_{a\sigma}(t)} &= \exp\left[-\frac{1}{2}\int_{t_0}^{t}\Gamma(t')dt'\right]\int_{t_0}^{t}dt_1\sqrt{\frac{\Gamma(t_1)}{2\pi}}\exp\left[-i\int_{t_1}^{t}\tilde{\epsilon}^*_{a\sigma}(t')dt'\right] \\ &\quad\times\int d\epsilon\frac{\exp[i\epsilon(t-t_1)]}{\epsilon-\tilde{\epsilon}_{a\sigma}(t)}, \\ &= 0, \end{aligned} \tag{E.6}$$

where the $\epsilon$ integral is the same as that dealt with in the integration of $n^{(1)}_\sigma$.

The final term in (E.4) contains the integral over a normalised Lorentzian and equations (E.4) to (E.6) can be combined to yield

$$\begin{aligned}\int d\epsilon\; n^{(3)}_\sigma(\epsilon,t) &= n_{a\sigma}(t_0)\int_{t_0}^{t}dt_1\Gamma(t_1)\exp\left[-\int_{t_0}^{t_1}\Gamma(t')dt'\right] \\ &\quad+n_{a\sigma}(t_0)\exp\left[-\int_{t_0}^{t}\Gamma(t')dt'\right]. \end{aligned} \tag{E.7}$$

Integration of the fourth term in (4.25) yields the number of electrons initially in the metal, $N_{k\sigma}$;

$$\int d\epsilon\; n^{(4)}_\sigma(\epsilon,t) = \int d\epsilon\sum_k f(\epsilon_{k\sigma})\delta(\epsilon-\epsilon_{k\sigma}) = \sum_k f(\epsilon_{k\sigma}) = N_{k\sigma}. \tag{E.8}$$

The fifth term in the integral of $n_\sigma$ can be expanded using the definition of $p^{(inst)}_\sigma$, (4.26), yielding

$$\begin{aligned}\int d\epsilon\; n^{(5)}_\sigma(\epsilon,t) &= \frac{2}{\pi}\int d\epsilon' f(\epsilon')\mathrm{Im}\{p_\sigma(\epsilon',t)\} \\ &\quad\times\mathrm{Re}\left\{i\sqrt{\frac{\Gamma(t)}{2\pi}}\int d\epsilon\frac{1}{(\epsilon-\epsilon'+i\eta)(\epsilon-\tilde{\epsilon}_{a\sigma}(t))}\right\}, \end{aligned} \tag{E.9}$$

in which the $\epsilon$ integrand has two poles below the real axis. Evaluation of the $\epsilon$ integral can be performed using contour integration methods, with the contour closed in the upper half plane. The zeroth moment of $n^{(5)}_\sigma$ is therefore zero.

We also find the sixth and seventh terms in $n_\sigma$ to be zero via a similar method;

$$\begin{aligned}\int d\epsilon\; n_\sigma^{(6)}(\epsilon,t) &= -2\sqrt{\frac{\Gamma(t)}{2\pi}}\int d\epsilon' f(\epsilon')\mathrm{Im}\Bigg\{\int_{t_0}^{t} dt_1\sqrt{\frac{\Gamma(t_1)}{2\pi}}p_\sigma^*(\epsilon',t)\exp[i\epsilon'(t_1-t)] \\ &\qquad \times i\sqrt{\frac{\Gamma(t)}{2\pi}}\int d\epsilon\frac{\exp[-i\epsilon(t_1-t)]}{(\epsilon-\epsilon'+i\eta)(\epsilon-\tilde{\epsilon}_{a\sigma}(t))}\Bigg\}, \\ &= 0, \end{aligned} \tag{E.10}$$

where the exponential in the $\epsilon$ integral indicates that the contour should be closed in the upper half of the complex plane. The final term in $n_\sigma$ integrates to

$$\begin{aligned}\int d\epsilon\; n_\sigma^{(7)}(\epsilon,t) &= \frac{1}{\pi}\sqrt{\frac{\Gamma(t)}{2\pi}}\int d\epsilon' f(\epsilon')\mathrm{Re}\Bigg\{i\sqrt{\frac{\Gamma(t)}{2\pi}} \\ &\qquad \times\int d\epsilon\frac{1}{(\epsilon-\epsilon'+i\eta)^2(\epsilon-\tilde{\epsilon}_{a\sigma}(t))}\Bigg\}, \\ &= 0, \end{aligned} \tag{E.11}$$

where contour integration methods have again been used. By summing equations (E.2), (E.3), and (E.7) to (E.11) the zeroth moment of $n_\sigma$ becomes

$$\begin{aligned}\int d\epsilon\; n_\sigma(\epsilon,t) &= \int_{t_0}^{t} dt_1\Gamma(t_1)\int d\epsilon' f(\epsilon')\left|p_\sigma(\epsilon',t_1)\right|^2 + \int d\epsilon' f(\epsilon')\left|p_\sigma(\epsilon',t)\right|^2 \\ &\quad -2\int_{t_0}^{t} dt_1\sqrt{\frac{\Gamma(t_1)}{2\pi}}\int d\epsilon f(\epsilon)\mathrm{Re}\{p_\sigma(\epsilon,t_1)\} \\ &\quad +\int_{t_0}^{t} dt_1\Gamma(t_1)n_{a\sigma}(t_0)\exp\left[-\int_{t_0}^{t_1}\Gamma(t')dt'\right] \\ &\quad +n_{a\sigma}(t_0)\exp\left[-\int_{t_0}^{t}\Gamma(t')dt'\right] + N_{k\sigma}. \end{aligned} \tag{E.12}$$

The second and fifth terms in this expression can be combined using the definition of the adsorbate occupation function $n_{a\sigma}$, (2.19), as can the first and fourth terms. Equation (E.12) can therefore be rewritten as

$$\begin{aligned}\int d\epsilon n_\sigma(\epsilon,t) &= \int_{t_0}^{t} dt_1\Gamma(t_1)n_{a\sigma}(t_1) + n_{a\sigma}(t) \\ &\quad -2\int_{t_0}^{t} dt_1\sqrt{\frac{\Gamma(t_1)}{2\pi}}\int d\epsilon f(\epsilon)\mathrm{Re}\left\{p_\sigma(\epsilon,t_1)\right\} + N_{k\sigma}. \end{aligned} \tag{E.13}$$

This expression is not obviously independent of time and we cannot therefore claim conservation of electrons without further simplification. This simplification is performed by considering the time derivative of $n_{a\sigma}(t)$, which can be found from (2.19) using the differential equation for $p_\sigma$, (2.30);

$$\begin{aligned}
\dot{n}_{a\sigma}(t) &= n_{a\sigma}(t_0)\frac{d}{dt}\exp\left[-\int_{t_0}^{t}\Gamma(t')dt'\right] + \int d\epsilon f(\epsilon)\frac{d}{dt}|p_\sigma(\epsilon,t)|^2, \\
&= -n_{a\sigma}(t_0)\Gamma(t)\exp\left[-\int_{t_0}^{t}\Gamma(t')dt'\right] \\
&\quad + \int d\epsilon f(\epsilon)\left(\frac{dp^*_\sigma}{dt}(\epsilon,t)p_\sigma(\epsilon,t) + p^*_\sigma(\epsilon,t)\frac{dp_\sigma}{dt}(\epsilon,t)\right), \\
&= -n_{a\sigma}(t_0)\Gamma(t)\exp\left[-\int_{t_0}^{t}\Gamma(t')dt'\right] \\
&\quad + \int d\epsilon f(\epsilon)\left[\left(i(\tilde{\epsilon}^*_{a\sigma}(t)-\epsilon)p^*_\sigma(\epsilon,t) + \sqrt{\frac{\Gamma(t)}{2\pi}}\right)p_\sigma(\epsilon,t)\right. \\
&\qquad \left. + p^*_\sigma(\epsilon,t)\left(-i(\tilde{\epsilon}_{a\sigma}(t)-\epsilon)p_\sigma(\epsilon,t) + \sqrt{\frac{\Gamma(t)}{2\pi}}\right)\right]. \qquad \text{(E.14)}
\end{aligned}$$

By using the definition of $\tilde{\epsilon}_{a\sigma}$, (2.12), this expression becomes

$$\begin{aligned}
\dot{n}_{a\sigma}(t) &= -n_{a\sigma}(t_0)\Gamma(t)\exp\left[-\int_{t_0}^{t}\Gamma(t')dt'\right] - \Gamma(t)\int d\epsilon f(\epsilon)|p_\sigma(\epsilon,t)|^2 \\
&\quad + 2\sqrt{\frac{\Gamma(t)}{2\pi}}\int d\epsilon f(\epsilon)\mathrm{Re}\{p_\sigma(\epsilon,t)\}, \\
\dot{n}_{a\sigma}(t) &= -\Gamma(t)n_{a\sigma}(t) + 2\sqrt{\frac{\Gamma(t)}{2\pi}}\int d\epsilon f(\epsilon)\mathrm{Re}\{p_\sigma(\epsilon,t)\}. \qquad \text{(E.15)}
\end{aligned}$$

On integration over time from $t_0$ to $t$ this yields

$$\begin{aligned}
n_{a\sigma}(t) - n_{a\sigma}(t_0) &= -\int_{t_0}^{t} dt_1\Gamma(t_1)n_{a\sigma}(t_1) \\
&\quad + 2\int_{t_0}^{t} dt_1\sqrt{\frac{\Gamma(t_1)}{2\pi}}\int d\epsilon f(\epsilon)\mathrm{Re}\{p_\sigma(\epsilon,t_1)\}. \qquad \text{(E.16)}
\end{aligned}$$

This expression can be used to eliminate the remaining time-dependent terms in (E.13), leaving our final expression for the zeroth moment of $n_\sigma$;

$$\int d\epsilon\; n_\sigma(\epsilon,t) = n_{a\sigma}(t_0) + N_{k\sigma}. \qquad \text{(E.17)}$$

This demonstrates that the number of electrons contained in the electron dis-

tribution function $n_\sigma$ is conserved for each spin $\sigma$ independently, and is simply the initial population of the adsorbate orbital plus the initial number of metal electrons.

# Appendix F: Electron distribution function test II: conservation of energy

In this appendix we demonstrate that the energy of the electronic system, calculated from the electron distribution function $n_\sigma$, is consistent with the expression for the rate of change of total energy of the system. The total energy of the electronic system is related to the first moment of the electron distribution function by (see equation (4.7))

$$E(t) = \sum_\sigma \int d\epsilon\ \epsilon n_\sigma(\epsilon,t) - U n_{a\sigma}(t) n_{a-\sigma}(t). \tag{F.1}$$

The rate of change of the total energy of the Newns-Anderson system is therefore the time-derivative of this equation;

$$\dot{E}(t) = \sum_\sigma \frac{d}{dt} \int d\epsilon\ \epsilon n_\sigma(\epsilon,t) - U \frac{d}{dt} \left\{ n_{a\sigma}(t) n_{a-\sigma}(t) \right\}. \tag{F.2}$$

This expression should, if our model conserves energy, be identical to the expression we derived in chapter 3, (3.16). To demonstrate energy conservation the first moment of $n_\sigma$ must be calculated. As in the previous section this derivation will be performed term by term.

The first moment of the first term in $n_\sigma$, (4.25), is

$$\begin{aligned}
\int d\epsilon\ \epsilon n_\sigma^{(1)}(\epsilon,t) &= \int d\epsilon' f(\epsilon') \int d\epsilon\ \epsilon \left| q_\sigma(\epsilon,\epsilon',t) + p_\sigma^{(inst)}(\epsilon,t) p_\sigma(\epsilon',t) \right|^2 \\
&= \int d\epsilon' f(\epsilon') \int d\epsilon\ \epsilon |q_\sigma(\epsilon,\epsilon',t)|^2 \\
&\quad + 2\mathrm{Re}\left\{ i\sqrt{\frac{\Gamma(t)}{2\pi}} \int d\epsilon' f(\epsilon') p_\sigma(\epsilon',t) \int d\epsilon \frac{\epsilon\ q_\sigma^*(\epsilon,\epsilon',t)}{\epsilon - \tilde{\epsilon}_{a\sigma}(t)} \right\} \\
&\quad + \int d\epsilon' f(\epsilon') |p_\sigma(\epsilon',t)|^2 \int d\epsilon \frac{\epsilon\Gamma(t)}{2\pi[(\epsilon - \bar{\epsilon}_{a\sigma}(t))^2 + \Gamma(t)^2/4]}.
\end{aligned} \tag{F.3}$$

The $\epsilon$ integral in the first term in this expression can be expanded using the definition of $q_\sigma$, (4.27), yielding

$$\begin{aligned}\int d\epsilon\ \epsilon|q_\sigma(\epsilon,\epsilon',t)|^2 &= \int_{t_0}^{t} dt_1 \sqrt{\frac{\Gamma(t_1)}{2\pi}} p_\sigma(\epsilon',t_1)\exp[-i\epsilon'(t_1-t)] \\ &\quad\times\int_{t_0}^{t} dt_2 \sqrt{\frac{\Gamma(t_2)}{2\pi}} p^*_\sigma(\epsilon',t_2)\exp[i\epsilon'(t_2-t)] \\ &\quad\times\int d\epsilon\ \epsilon\exp[i\epsilon(t_1-t_2)]. \end{aligned} \tag{F.4}$$

We now perform a 'by-parts' integration step of the $t_2$ integral taking the $\epsilon$ integral as the part to be integrated. The $t_2$ integral becomes

$$\begin{aligned}\int_{t_0}^{t} dt_2 &= \left[\sqrt{\frac{\Gamma(t_2)}{2\pi}} p^*_\sigma(\epsilon',t_2)\exp[i\epsilon'(t_2-t)].2\pi i\int d\epsilon\frac{\exp[i\epsilon(t_1-t_2)]}{2\pi}\right]_{t_2=t_0}^{t_2=t} \\ &\quad -2\pi i\int_{t_0}^{t} dt_2\int d\epsilon\frac{\exp[i\epsilon(t-t_1)]}{2\pi} \\ &\qquad\times\frac{d}{dt_2}\left(\sqrt{\frac{\Gamma(t_1)}{2\pi}} p^*_\sigma(\epsilon',t_2)\exp[i\epsilon'(t_2-t_1)]\right) \\ &= 2\pi i\sqrt{\frac{\Gamma(t)}{2\pi}} p^*_\sigma(\epsilon',t)\int d\epsilon\frac{\exp[i\epsilon(t_1-t)]}{2\pi} \\ &\quad -2\pi i\int_{t_0}^{t} dt_2\frac{\dot\Gamma(t_2)}{2\sqrt{2\pi\Gamma(t_2)}} p^*_\sigma(\epsilon',t_2)\exp[i\epsilon'(t_2-t)]\int d\epsilon\frac{\exp[i\epsilon(t_1-t_2)]}{2\pi} \\ &\quad -2\pi i\int_{t_0}^{t} dt_2\sqrt{\frac{\Gamma(t_2)}{2\pi}}\left(i(\tilde\epsilon^*_{a\sigma}(t_2)-\epsilon')p^*_\sigma(\epsilon',t_2)+\sqrt{\frac{\Gamma(t_2)}{2\pi}}\right) \\ &\qquad\times\exp[i\epsilon'(t_2-t)]\int d\epsilon\frac{\exp[i\epsilon(t_1-t_2)]}{2\pi} \\ &\quad -2\pi i\int_{t_0}^{t} dt_2\sqrt{\frac{\Gamma(t_2)}{2\pi}} p^*_\sigma(\epsilon',t).i\epsilon'\exp[i\epsilon(t_2-t)]\int d\epsilon\frac{\exp[i\epsilon(t_1-t_2)]}{2\pi}, \end{aligned} \tag{F.5}$$

where (2.30) has been used to expand the $t_2$ derivative in the second term. Each of the $\epsilon$ integrals in this expression, with the exception of the first term, can be

replaced by a delta function, giving

$$\begin{aligned}
\int_{t_0}^{t} dt_2 &= i\sqrt{2\pi\Gamma(t)}p^*_\sigma(\epsilon',t)\int d\epsilon \frac{\exp[i\epsilon(t_1-t)]}{2\pi} \\
&\quad -i\pi\int_{t_0}^{t} dt_2 \frac{\dot{\Gamma}(t_2)}{\sqrt{2\pi\Gamma(t_2)}} p^*_\sigma(\epsilon',t_2)\exp[i\epsilon'(t_2-t)]\delta(t_1-t_2) \\
&\quad +\int_{t_0}^{t} dt_2 \sqrt{2\pi\Gamma(t_2)}\tilde{\epsilon}^*_{a\sigma}(t_2)p^*_\sigma(\epsilon',t_2)\exp[i\epsilon'(t_2-t)]\delta(t_1-t_2) \\
&\quad -i\int_{t_0}^{t} dt_2 \Gamma(t_2)\exp[i\epsilon'(t_2-t)]\delta(t_1-t_2), \\
&= i\sqrt{2\pi\Gamma(t)}p^*_\sigma(\epsilon',t)\int d\epsilon\ \frac{\exp[i\epsilon(t_1-t)]}{2\pi} \\
&\quad -i\pi\frac{\dot{\Gamma}(t_1)}{\sqrt{2\pi\Gamma(t_1)}} p^*_\sigma(\epsilon',t_1)\exp[i\epsilon'(t_1-t)] \\
&\quad +\sqrt{2\pi\Gamma(t_1)}\tilde{\epsilon}^*_{a\sigma}(t_1)p^*_\sigma(\epsilon',t_1)\exp[i\epsilon'(t_1-t)] - i\Gamma(t_1)\exp[i\epsilon'(t_1-t)].
\end{aligned} \tag{F.6}$$

Equation (F.4) therefore becomes

$$\begin{aligned}
\int d\epsilon\ \epsilon|q_\sigma(\epsilon,\epsilon',t)|^2 &= i\int_{t_0}^{t} dt_1 \sqrt{\Gamma(t)\Gamma(t_1)}p_\sigma(\epsilon',t_1)p^*_\sigma(\epsilon',t)\exp[i\epsilon'(t_1-t)] \\
&\qquad \times\int d\epsilon\frac{\exp[i\epsilon(t_1-t)]}{2\pi} \\
&\quad -\frac{i}{2}\int_{t_0}^{t} dt_1 \dot{\Gamma}(t_1)|p_\sigma(\epsilon',t_1)|^2 \\
&\quad +\int_{t_0}^{t} dt_1 \bar{\epsilon}_{a\sigma}(t_1)\Gamma(t_1)|p_\sigma(\epsilon',t_1)|^2 + \frac{i}{2}\int_{t_0}^{t} dt_1 \Gamma^2(t_1)|p_\sigma(\epsilon',t_1)|^2 \\
&\quad -i\int_{t_0}^{t} dt_1 \Gamma(t_1)\sqrt{\frac{\Gamma(t_1)}{2\pi}}\mathrm{Re}\{p_\sigma(\epsilon',t_1)\} \\
&\quad +\int_{t_0}^{t} dt_1 \Gamma(t_1)\sqrt{\frac{\Gamma(t_1)}{2\pi}}\mathrm{Im}\{p_\sigma(\epsilon',t_1)\},
\end{aligned} \tag{F.7}$$

where the definition of $\tilde{\epsilon}_{a\sigma}$, (2.12), has also been used. The first term in (F.7) can be expanded using the general expression we derived for an integral of this

form in appendix A, (A.22). This term then becomes

$$i\int_{t_0}^{t} dt_1 \sqrt{\Gamma(t)\Gamma(t_1)} p_\sigma(\epsilon', t_1) p_\sigma^*(\epsilon', t) \exp[i\epsilon'(t_1 - t)] \int d\epsilon \frac{\exp[i\epsilon(t_1 - t)]}{2\pi}$$
$$= \frac{i}{2}\Gamma(t)|p_\sigma(\epsilon', t)|^2. \tag{F.8}$$

As the left hand side of (F.7) is real we expect all imaginary components on the right hand side to cancel. This can be demonstrated by evaluating the second term in (F.7) using the 'by-parts' method, taking $\dot{\Gamma}(t_1)$ as the part to integrate. This yields

$$-\frac{i}{2}\int_{t_0}^{t} dt_1 \dot{\Gamma}(t_1)|p_\sigma(\epsilon', t_1)|^2 = -\frac{i}{2}\Gamma(t)|p_\sigma(\epsilon', t)|^2 - \frac{i}{2}\int_{t_0}^{t} dt_1 \Gamma(t_2)^2 |p_\sigma(\epsilon', t_1)|^2$$
$$+ i\int_{t_0}^{t} dt_1 \Gamma(t_1)\sqrt{\frac{\Gamma(t_1)}{2\pi}}\mathrm{Re}\{p_\sigma(\epsilon', t_1)\}, \tag{F.9}$$

which on combination with (F.8) and (F.7) gives

$$\int d\epsilon\ \epsilon |q_\sigma(\epsilon, \epsilon', t)|^2 = \int_{t_0}^{t} dt_1 \bar{\epsilon}_{a\sigma}(t_1)\Gamma(t_1)|p_\sigma(\epsilon', t_1)|^2$$
$$+ \int_{t_0}^{t} dt_1 \Gamma(t_1)\sqrt{\frac{\Gamma(t_1)}{2\pi}}\mathrm{Im}\{p_\sigma(\epsilon', t_1)\}. \tag{F.10}$$

To evaluate the second term in (F.3) the $\epsilon$ integral is expanded to give

$$\int d\epsilon \frac{\epsilon\ q_\sigma^*(\epsilon, \epsilon', t)}{\epsilon - \tilde{\epsilon}_{a\sigma}(t)} = \int_{t_0}^{t} dt_1 \sqrt{\frac{\Gamma(t_1)}{2\pi}} p_\sigma^*(\epsilon', t_1)\exp[i\epsilon'(t_1 - t)] \int d\epsilon \frac{\epsilon \exp[i\epsilon(t - t_1)]}{\epsilon - \tilde{\epsilon}_{a\sigma}(t)},$$
$$= \int_{t_0}^{t} dt_1 \sqrt{\frac{\Gamma(t_1)}{2\pi}} p_\sigma^*(\epsilon', t_1)\exp[i\epsilon'(t_1 - t)]$$
$$\times \left(2\pi \int d\epsilon \frac{\exp[i\epsilon(t - t_1)]}{2\pi} + \tilde{\epsilon}_{a\sigma}(t)\int d\epsilon \frac{\exp[i\epsilon(t - t_1)]}{\epsilon - \tilde{\epsilon}_{a\sigma}(t)}\right). \tag{F.11}$$

The second energy integral in this expression can be performed by contour methods, yielding zero and the remaining term can be simplified using (A.22), giving

$$\int d\epsilon \frac{\epsilon\ q_\sigma^*(\epsilon, \epsilon', t)}{\epsilon - \tilde{\epsilon}_{a\sigma}(t)} = \pi\sqrt{\frac{\Gamma(t)}{2\pi}} p_\sigma^*(\epsilon', t). \tag{F.12}$$

The second term in (F.3) therefore becomes

$$2\mathrm{Re}\left\{i\frac{\Gamma(t)}{2}\int d\epsilon' f(\epsilon')|p_\sigma(\epsilon',t)|^2\right\}=0 \tag{F.13}$$

The final term in (F.3) can be evaluated by recognising that the $\epsilon$ integral is the first moment of a Lorentzian, which yields the centre of the distribution, i.e. $\bar{\epsilon}_{a\sigma}$. The final term in (F.3) is therefore

$$\bar{\epsilon}_{a\sigma}(t)\int d\epsilon' f(\epsilon')|p_\sigma(\epsilon',t)|^2. \tag{F.14}$$

By combining (F.3), (F.10), (F.13) and (F.14) we find the first moment of $n_\sigma^{(1)}$ to be

$$\begin{aligned}\int d\epsilon\ \epsilon n_\sigma^{(1)}(\epsilon,t) &= \int_{t_0}^{t} dt_1 \bar{\epsilon}_{a\sigma}(t_1)\Gamma(t_1)\int d\epsilon' f(\epsilon')|p_\sigma(\epsilon',t_1)|^2 \\ &\quad +\bar{\epsilon}_{a\sigma}(t)\int d\epsilon' f(\epsilon')|p_\sigma(\epsilon',t)|^2 \\ &\quad +\int_{t_0}^{t} dt_1\Gamma(t_1)\sqrt{\frac{\Gamma(t_1)}{2\pi}}\int d\epsilon' f(\epsilon')\mathrm{Im}\{p_\sigma(\epsilon',t_1)\}.\end{aligned} \tag{F.15}$$

The first moment of the second term in (4.25) is

$$\int d\epsilon\ \epsilon n_\sigma^{(2)}(\epsilon,t)=-2\int_{t_0}^{t} dt_1\sqrt{\frac{\Gamma(t_1)}{2\pi}}\int d\epsilon\ \epsilon f(\epsilon)\mathrm{Re}\{p_\sigma(\epsilon,t_1)\}, \tag{F.16}$$

which we do not attempt to simplify further.

The first moment of the third term in (4.25) is

$$\begin{aligned}\int d\epsilon\ \epsilon n_\sigma^{(3)}(\epsilon,t) &= n_{a\sigma}(t_0)\int d\epsilon\ \epsilon\left|r_\sigma(\epsilon,t)+p_\sigma^{(inst)}(\epsilon,t)\exp\left[-\frac{1}{2}\int_{t_0}^{t}\Gamma(t')dt'\right]\right|^2\\ &= n_{a\sigma}(t_0)\int d\epsilon\ \epsilon|r_\sigma(\epsilon,t)|^2\\ &\quad +2n_{a\sigma}(t_0)\sqrt{\frac{\Gamma(t)}{2\pi}}\exp\left[-\frac{1}{2}\int_{t_0}^{t}\Gamma(t')dt'\right]\mathrm{Re}\left\{i\int d\epsilon\frac{\epsilon r_\sigma^*(\epsilon,t)}{\epsilon-\tilde{\epsilon}_{a\sigma}(t)}\right\}\\ &\quad +n_{a\sigma}(t_0)\exp\left[-\int_{t_0}^{t}\Gamma(t')dt'\right]\int d\epsilon\ \frac{\epsilon\Gamma(t)}{2\pi[(\epsilon-\bar{\epsilon}_{a\sigma}(t))^2+\Gamma(t)^2/4]}\end{aligned} \tag{F.17}$$

The first term in this expression can be expanded, using the definition of $r_\sigma$ (4.28), to give

$$\begin{aligned}\int d\epsilon\ \epsilon|r_\sigma(\epsilon,t)|^2 &= \exp\left[-\int_{t_0}^{t}\Gamma(t')dt'\right]\int_{t_0}^{t}dt_1\sqrt{\frac{\Gamma(t_1)}{2\pi}}\exp\left[i\int_{t_1}^{t}\tilde{\epsilon}_{a\sigma}(t')dt'\right]\\ &\quad\times\int_{t_0}^{t}dt_2\sqrt{\frac{\Gamma(t_2)}{2\pi}}\exp\left[-i\int_{t_2}^{t}\tilde{\epsilon}_{a\sigma}^*(t')dt'\right]\\ &\quad\times\int d\epsilon\ \epsilon\exp[i\epsilon(t_1-t_2)].\end{aligned} \tag{F.18}$$

Again the same method as for (F.6) can be used; a by-parts integration step to expand the $t_2$ integral choosing to differentiate the $\epsilon$ integral. This yields

$$\begin{aligned}\int_{t_0}^{t}dt_2 &= \left[i\sqrt{\frac{\Gamma(t_2)}{2\pi}}\exp\left[-i\int_{t_2}^{t}\tilde{\epsilon}_{a\sigma}^*(t')dt'\right]\int d\epsilon\exp[i\epsilon(t_1-t_2)]\right]_{t_2=t_0}^{t_2=t}\\ &\quad -i\int_{t_0}^{t}dt_2\int d\epsilon\exp[i\epsilon(t_1-t_2)]\frac{d}{dt_2}\left(\sqrt{\frac{\Gamma(t_2)}{2\pi}}\exp\left[-i\int_{t_2}^{t}\tilde{\epsilon}_{a\sigma}^*(t')dt'\right]\right)\\ &= i\sqrt{2\pi\Gamma(t)}\int d\epsilon\frac{\exp[i\epsilon(t_1-t)]}{2\pi}\\ &\quad -i\int_{t_0}^{t}dt_2\frac{\dot{\Gamma}(t_2)}{2\sqrt{2\pi\Gamma(t_2)}}\exp\left[-i\int_{t_2}^{t}\tilde{\epsilon}_{a\sigma}^*(t')dt'\right].2\pi\int d\epsilon\frac{\exp[i\epsilon(t_1-t_2)]}{2\pi}\\ &\quad +\int_{t_0}^{t}dt_2\sqrt{\frac{\Gamma(t_2)}{2\pi}}\tilde{\epsilon}_{a\sigma}^*(t_2)\exp\left[-i\int_{t_2}^{t}\tilde{\epsilon}_{a\sigma}^*(t')dt'\right].2\pi\int d\epsilon\frac{\exp[i\epsilon(t_1-t_2)]}{2\pi},\end{aligned} \tag{F.19}$$

The energy integrals, excluding the first, can be recognised as delta functions and

(F.18) becomes

$$\begin{aligned}\int d\epsilon\ \epsilon|r_\sigma(\epsilon,t)|^2 &= \exp\left[-\int_{t_0}^{t}\Gamma(t')dt'\right]\Bigg(i\int_{t_0}^{t}dt_1\sqrt{\Gamma(t)\Gamma(t_1)}\\ &\qquad\times\exp\left[i\int_{t_1}^{t}(\tilde{\epsilon}_{a\sigma}(t')-\tilde{\epsilon}^*_{a\sigma}(t'))dt'\right]\int d\epsilon\frac{\exp[i\epsilon(t_1-t)]}{2\pi}\\ &\quad-\frac{i}{2}\int_{t_0}^{t}dt_1\dot{\Gamma}(t_1)\exp\left[i\int_{t_1}^{t}(\tilde{\epsilon}_{a\sigma}(t')-\tilde{\epsilon}^*_{a\sigma}(t'))dt'\right]\\ &\quad+\int_{t_0}^{t}dt_1\bar{\epsilon}_{a\sigma}(t_1)\Gamma(t_1)\exp\left[i\int_{t_1}^{t}(\tilde{\epsilon}_{a\sigma}(t')-\tilde{\epsilon}^*_{a\sigma}(t'))dt'\right]\\ &\quad+\frac{i}{2}\int_{t_0}^{t}dt_1\Gamma(t_1)^2\exp\left[i\int_{t_1}^{t}(\tilde{\epsilon}_{a\sigma}(t')-\tilde{\epsilon}^*_{a\sigma}(t'))dt'\right]\Bigg),\\ &= \frac{i}{2}\Gamma(t)\exp\left[-\int_{t_0}^{t}\Gamma(t')dt'\right]\\ &\quad-\frac{i}{2}\int_{t_0}^{t}dt_1\dot{\Gamma}(t_1)\exp\left[-\int_{t_0}^{t_1}\Gamma(t')dt'\right]\\ &\quad+\int_{t_0}^{t}dt_1\bar{\epsilon}_{a\sigma}(t_1)\Gamma(t_1)\exp\left[-\int_{t_0}^{t_1}\Gamma(t')dt'\right]\\ &\quad+\frac{i}{2}\int_{t_0}^{t}dt_1\Gamma^2(t_1)\exp\left[-\int_{t_0}^{t_1}\Gamma(t')dt'\right],\end{aligned}\tag{F.20}$$

where (A.22) is used to evaluate the first $t_1$ integral. As the left hand side of this expression is real we expect all imaginary terms on the right hand side to cancel. This can be demonstrated by evaluating the second term in (F.20), giving

$$\begin{aligned}-\frac{i}{2}\int_{t_0}^{t}dt_1\dot{\Gamma}(t_1)\exp\left[-\int_{t_0}^{t_1}\Gamma(t')dt'\right] &= -\frac{i}{2}\Gamma(t)\exp\left[-\int_{t_0}^{t}\Gamma(t')dt'\right]\\ &\quad-\frac{i}{2}\int_{t_0}^{t}dt_1\Gamma(t_1)^2\exp\left[-\int_{t_0}^{t_1}\Gamma(t')dt'\right],\end{aligned}\tag{F.21}$$

and therefore

$$\int d\epsilon\ \epsilon|r_\sigma(\epsilon,t)|^2=\int_{t_0}^{t}dt_1\bar{\epsilon}_{a\sigma}(t_1)\Gamma(t_1)\exp\left[-\int_{t_0}^{t_1}\Gamma(t')dt'\right].\tag{F.22}$$

The $\epsilon$ integral in the second term in (F.17) can be expanded using the definition

of $r_\sigma$ (4.28);

$$\int d\epsilon \frac{\epsilon r^*_\sigma(\epsilon,t)}{\epsilon-\tilde{\epsilon}_{a\sigma}(t)} = \exp\left[-\frac{1}{2}\int_{t_0}^{t}\Gamma(t')dt'\right]\int_{t_0}^{t}dt_1\sqrt{\frac{\Gamma(t_1)}{2\pi}}\exp\left[-i\int_{t_1}^{t}\tilde{\epsilon}^*_{a\sigma}(t')dt'\right] \times\int d\epsilon\frac{\epsilon\exp[i\epsilon(t-t_1)]}{\epsilon-\tilde{\epsilon}_{a\sigma}(t)}. \quad \text{(F.23)}$$

The $\epsilon$ integral in this equation is the same as that in (F.11) and can be expanded in a similar manner, yielding

$$\int d\epsilon \frac{\epsilon r^*_\sigma(\epsilon,t)}{\epsilon-\tilde{\epsilon}_{a\sigma}(t)} = \exp\left[-\frac{1}{2}\int_{t_0}^{t}\Gamma(t')dt'\right]\int_{t_0}^{t}dt_1\sqrt{\frac{\Gamma(t_1)}{2\pi}}\exp\left[-i\int_{t_1}^{t}\tilde{\epsilon}^*_{a\sigma}(t')dt'\right] \times 2\pi\int d\epsilon\frac{\exp[i\epsilon(t-t_1)]}{2\pi}. \quad \text{(F.24)}$$

This expression can be simplified further using (A.22), giving

$$\int d\epsilon \frac{\epsilon r^*_\sigma(\epsilon,t)}{\epsilon-\tilde{\epsilon}_{a\sigma}(t)} = \pi\exp\left[-\frac{1}{2}\int_{t_0}^{t}\Gamma(t')dt'\right]\sqrt{\frac{\Gamma(t)}{2\pi}}, \quad \text{(F.25)}$$

and the second term in (F.17) therefore becomes

$$2n_{a\sigma}(t_0)\sqrt{\frac{\Gamma(t)}{2\pi}}\exp\left[-\int_{t_0}^{t}\Gamma(t')dt'\right]\mathrm{Re}\left\{i\pi\sqrt{\frac{\Gamma(t)}{2\pi}}\right\} = 0. \quad \text{(F.26)}$$

The energy integral in the final term of (F.17) is the same as dealt with in the final term of (F.3) and can be evaluated to yield $\bar{\epsilon}_{a\sigma}$. We can therefore combine (F.17), (F.22) and (F.26) to give

$$\int d\epsilon\ \epsilon n^{(3)}_\sigma(\epsilon,t) = \int_{t_0}^{t}dt_1\bar{\epsilon}_{a\sigma}(t_1)\Gamma(t_1)n_{a\sigma}(t_0)\exp\left[-\int_{t_0}^{t_1}\Gamma(t')dt'\right] +\bar{\epsilon}_{a\sigma}(t)n_{a\sigma}(t_0)\exp\left[-\int_{t_0}^{t}\Gamma(t')dt'\right]. \quad \text{(F.27)}$$

The first moment of the fourth term in (4.25) simply evaluates to

$$\int d\epsilon\ \epsilon n^{(4)}_\sigma(\epsilon,t) = \sum_k f(\epsilon_{k\sigma})\int d\epsilon\ \epsilon\ \delta(\epsilon-\epsilon_{k\sigma}) = \sum_k \epsilon_{k\sigma}f(\epsilon_{k\sigma}). \quad \text{(F.28)}$$

The first moment of the fifth term in (4.25) is

$$\begin{aligned}\int d\epsilon\ \epsilon n_\sigma^{(5)}(\epsilon,t) &= -\frac{2}{\pi}\sqrt{\frac{\Gamma(t)}{2\pi}}\int d\epsilon' f(\epsilon')\mathrm{Im}\{p_\sigma(\epsilon',t)\} \\ &\quad \times \mathrm{Im}\left\{\int d\epsilon \frac{\epsilon}{(\epsilon-\epsilon'+i\eta)(\epsilon-\tilde{\epsilon}_{a\sigma}(t))}\right\}. \quad \text{(F.29)}\end{aligned}$$

By expanding the fraction in the $\epsilon$ integral this expression can be rewritten as

$$\begin{aligned}\int d\epsilon \frac{\epsilon}{(\epsilon-\epsilon'+i\eta)(\epsilon-\tilde{\epsilon}_{a\sigma}(t))} &= \int d\epsilon \left(1+\frac{\tilde{\epsilon}_{a\sigma}(t)}{\epsilon-\tilde{\epsilon}_{a\sigma}(t)}\right)\frac{1}{\epsilon-\epsilon'+i\eta}, \\ &= \int d\epsilon \frac{1}{\epsilon-\epsilon'+i\eta} \\ &\quad +\tilde{\epsilon}_{a\sigma}(t)\int d\epsilon \frac{1}{(\epsilon-\tilde{\epsilon}_{a\sigma}(t))(\epsilon-\epsilon'+i\eta)}. \quad \text{(F.30)}\end{aligned}$$

The first integral in this expression has been evaluated in appendix D.2, (D.26). Contour integration methods show that the second integral in (F.30) evaluates to zero, as both poles in the integrand are in the same half of the complex plane. Equation (F.29) therefore becomes

$$\int d\epsilon\ \epsilon n_\sigma^{(5)}(\epsilon,t) = 2\sqrt{\frac{\Gamma(t)}{2\pi}}\int d\epsilon' f(\epsilon')\mathrm{Im}\{p_\sigma(\epsilon',t)\}. \quad \text{(F.31)}$$

The first moment of the sixth term in $n_\sigma$ is

$$\int d\epsilon\, \epsilon n_\sigma^{(6)}(\epsilon,t) = -\frac{\Gamma(t)}{\pi}\int d\epsilon' f(\epsilon')\mathrm{Re}\left\{\int d\epsilon \frac{\epsilon q_\sigma^*(\epsilon,\epsilon',t)}{(\epsilon-\epsilon'+i\eta)(\epsilon-\tilde{\epsilon}_{a\sigma}(t))}\right\}. \quad \text{(F.32)}$$

A similar method to that used in the previous term allows the $\epsilon$ integral in this

expression to be expanded, yielding

$$\begin{aligned}
&\int d\epsilon \frac{\epsilon q^*_\sigma(\epsilon,\epsilon',t)}{(\epsilon-\epsilon'+i\eta)(\epsilon-\tilde{\epsilon}_{a\sigma}(t))} \\
&\quad = \int_{t_0}^{t} dt_1 \sqrt{\frac{\Gamma(t_1)}{2\pi}} p^*_\sigma(\epsilon',t_1)\exp[i\epsilon'(t_1-t)] \int d\epsilon \frac{\epsilon\exp[-i\epsilon(t_1-t)]}{(\epsilon-\epsilon'+i\eta)(\epsilon-\tilde{\epsilon}_{a\sigma}(t))}, \\
&\quad = \int_{t_0}^{t} dt_1 \sqrt{\frac{\Gamma(t_1)}{2\pi}} p^*_\sigma(\epsilon',t_1)\exp[i\epsilon'(t_1-t)] \\
&\qquad\qquad \times \left( \int d\epsilon \frac{\exp[-i\epsilon(t_1-t)]}{\epsilon-\epsilon'+i\eta} + \tilde{\epsilon}_{a\sigma}(t) \int d\epsilon \frac{\exp[i\epsilon(t-t_1)]}{(\epsilon-\epsilon'+i\eta)(\epsilon-\tilde{\epsilon}_{a\sigma}(t))} \right).
\end{aligned} \tag{F.33}$$

Both $\epsilon$ integrals in this expression can be performed by contour methods, and as the poles in the integrands are in the lower half plane with the contour closed in the upper plane this leaves $\int d\epsilon\ \epsilon n^{(6)}_\sigma(\epsilon,t) = 0$.

The first moment of the final term in $n_\sigma$ is

$$\int d\epsilon\ \epsilon n^{(7)}_\sigma(\epsilon,t) = -\frac{\Gamma(t)}{2\pi^2} \int d\epsilon' f(\epsilon') \mathrm{Im}\left\{ \int d\epsilon \frac{\epsilon}{(\epsilon-\epsilon'+i\eta)^2(\epsilon-\tilde{\epsilon}_{a\sigma}(t))} \right\}. \tag{F.34}$$

We again expand the fraction in the energy integral, yielding

$$\begin{aligned}
\int d\epsilon \frac{\epsilon}{(\epsilon-\epsilon'+i\eta)^2(\epsilon-\tilde{\epsilon}_{a\sigma}(t))} &= \int d\epsilon \left(1+\frac{\tilde{\epsilon}_{a\sigma}(t)}{\epsilon-\tilde{\epsilon}_{a\sigma}(t)}\right) \frac{1}{(\epsilon-\epsilon'+i\eta)^2}, \\
&= \int d\epsilon \frac{1}{(\epsilon-\epsilon'+i\eta)^2} \\
&\quad + \tilde{\epsilon}_{a\sigma}(t) \int d\epsilon \frac{1}{(\epsilon-\epsilon'+i\eta)^2(\epsilon-\tilde{\epsilon}_{a\sigma}(t))}, \\
&= 0,
\end{aligned} \tag{F.35}$$

where the integrals in the second line have been performed using contour integration methods. Therefore the integral $\int d\epsilon\ \epsilon n^{(7)}_\sigma(\epsilon,t)$ yields zero.

We now sum the non-zero contributions to the first moment of $n_\sigma$, ((F.15), (F.16),

(F.27), (F.28) and (F.31)), yielding

$$\begin{aligned}\int d\epsilon\ \epsilon n_\sigma(\epsilon,t) &= \bar{\epsilon}_{a\sigma}(t)\int d\epsilon' f(\epsilon')|p_\sigma(\epsilon',t)|^2 \\ &+\int_{t_0}^{t} dt_1 \bar{\epsilon}_{a\sigma}(t_1)\Gamma(t_1)\int d\epsilon' f(\epsilon')|p_\sigma(\epsilon',t_1)|^2 \\ &+\int_{t_0}^{t} dt_1 \Gamma(t_1)\sqrt{\frac{\Gamma(t_1)}{2\pi}}\int d\epsilon f(\epsilon)\mathrm{Im}\{p_\sigma(\epsilon,t_1)\} \\ &-2\int_{t_0}^{t} dt_1 \sqrt{\frac{\Gamma(t_1)}{2\pi}}\int d\epsilon\ \epsilon f(\epsilon)\mathrm{Re}\{p_\sigma(\epsilon,t_1)\} \\ &+\bar{\epsilon}_{a\sigma}(t)n_{a\sigma}(t_0)\exp\left[-\int_{t_0}^{t}\Gamma(t')dt'\right] \\ &+\int_{t_0}^{t} dt_1 \bar{\epsilon}_{a\sigma}(t_1)\Gamma(t_1)n_{a\sigma}(t_0)\exp\left[-\int_{t_0}^{t_1}\Gamma(t')dt'\right] \\ &+\sum_k \epsilon_{k\sigma}f(\epsilon_{k\sigma}) + 2\sqrt{\frac{\Gamma(t)}{2\pi}}\int d\epsilon f(\epsilon)\mathrm{Im}\{p_\sigma(\epsilon,t)\}.\end{aligned} \tag{F.36}$$

This expression can be simplified using the definition of $n_{a\sigma}$, (2.19), giving

$$\begin{aligned}&\int d\epsilon\ \epsilon n_\sigma(\epsilon,t) \\ &= \bar{\epsilon}_{a\sigma}(t)n_{a\sigma}(t) + \int_{t_0}^{t} dt_1 \bar{\epsilon}_{a\sigma}(t_1)\Gamma(t_1)n_{a\sigma}(t_1) + \sum_k \epsilon_{k\sigma}f(\epsilon_{k\sigma}) \\ &+2\sqrt{\frac{\Gamma(t)}{2\pi}}\int d\epsilon f(\epsilon)\mathrm{Im}\{p_\sigma(\epsilon,t)\} - 2\int_{t_0}^{t} dt_1 \sqrt{\frac{\Gamma(t_1)}{2\pi}}\int d\epsilon\ \epsilon f(\epsilon)\mathrm{Re}\{p_\sigma(\epsilon,t_1)\} \\ &+\int_{t_0}^{t} dt_1 \Gamma(t_1)\sqrt{\frac{\Gamma(t_1)}{2\pi}}\int d\epsilon f(\epsilon)\mathrm{Im}\{p_\sigma(\epsilon,t_1)\}.\end{aligned} \tag{F.37}$$

To obtain the rate of change of the total energy using (F.2) we need the time-

derivative of this expression. On differentiation (F.37) becomes

$$\begin{aligned}
&\frac{d}{dt}\int d\epsilon\ \epsilon n_\sigma(\epsilon,t) \\
&\quad = \ \dot{\bar{\epsilon}}_{a\sigma}(t)n_{a\sigma}(t) + \bar{\epsilon}_{a\sigma}(t)\dot{n}_{a\sigma}(t) + \bar{\epsilon}_{a\sigma}(t)\Gamma(t)n_{a\sigma}(t) \\
&\qquad + \frac{\dot{\Gamma}(t)}{\sqrt{2\pi\Gamma(t)}}\int d\epsilon f(\epsilon)\mathrm{Im}\left\{p_\sigma(\epsilon,t)\right\} + 2\sqrt{\frac{\Gamma(t)}{2\pi}}\int d\epsilon f(\epsilon)\mathrm{Im}\{\frac{d}{dt}p_\sigma(\epsilon,t)\} \\
&\qquad -2\sqrt{\frac{\Gamma(t)}{2\pi}}\int d\epsilon\ \epsilon f(\epsilon)\mathrm{Re}\{p_\sigma(\epsilon,t)\} + \Gamma(t)\sqrt{\frac{\Gamma(t)}{2\pi}}\int d\epsilon f(\epsilon)\mathrm{Im}\{p_\sigma(\epsilon,t)\}.
\end{aligned} \tag{F.38}$$

The imaginary part of the time-derivative of $p_\sigma$, which appears in the fifth term in this expression, can be expanded using (2.30), yielding

$$\begin{aligned}
\mathrm{Im}\left\{\frac{d}{dt}p_\sigma(\epsilon,t)\right\} &= \mathrm{Im}\left\{-i(\tilde{\epsilon}_{a\sigma}(t)-\epsilon)p_\sigma(\epsilon,t) + \sqrt{\frac{\Gamma(t)}{2\pi}}\right\} \\
&= -(\bar{\epsilon}_{a\sigma}(t)-\epsilon)\mathrm{Re}\{p_\sigma(\epsilon,t)\} + \frac{\Gamma(t)}{2}\mathrm{Im}\{p_\sigma(\epsilon,t)\},
\end{aligned} \tag{F.39}$$

and (F.38) therefore becomes

$$\begin{aligned}
&\frac{d}{dt}\int d\epsilon\ \epsilon n_\sigma(\epsilon,t) \\
&\quad = \ \dot{\bar{\epsilon}}_{a\sigma}(t)n_{a\sigma}(t) + \bar{\epsilon}_{a\sigma}(t)\dot{n}_{a\sigma}(t) + \bar{\epsilon}_{a\sigma}(t)\Gamma(t)n_{a\sigma}(t) \\
&\qquad + \frac{\dot{\Gamma}(t)}{\sqrt{2\pi\Gamma(t)}}\int d\epsilon f(\epsilon)\mathrm{Im}\left\{p_\sigma(\epsilon,t)\right\} - 2\bar{\epsilon}_{a\sigma}(t)\sqrt{\frac{\Gamma(t)}{2\pi}}\int d\epsilon f(\epsilon)\mathrm{Re}\{p_\sigma(\epsilon,t)\} \\
&\qquad + 2\sqrt{\frac{\Gamma(t)}{2\pi}}\int d\epsilon\ \epsilon f(\epsilon)\mathrm{Re}\{p_\sigma(\epsilon,t)\} - \Gamma(t)\sqrt{\frac{\Gamma(t)}{2\pi}}\int d\epsilon f(\epsilon)\mathrm{Im}\{p_\sigma(\epsilon,t)\} \\
&\qquad -2\sqrt{\frac{\Gamma(t)}{2\pi}}\int d\epsilon\ \epsilon f(\epsilon)\mathrm{Re}\{p_\sigma(\epsilon,t)\} + \Gamma(t)\sqrt{\frac{\Gamma(t)}{2\pi}}\int d\epsilon f(\epsilon)\mathrm{Im}\{p_\sigma(\epsilon,t)\} \\
&\quad = \ \dot{\bar{\epsilon}}_{a\sigma}(t)n_{a\sigma}(t) + \frac{\dot{\Gamma}(t)}{\sqrt{2\pi\Gamma(t)}}\int d\epsilon f(\epsilon)\mathrm{Im}\left\{p_\sigma(\epsilon,t)\right\} \\
&\qquad + \bar{\epsilon}_{a\sigma}(t)\left(\dot{n}_{a\sigma}(t) + \Gamma(t)n_{a\sigma}(t) - 2\sqrt{\frac{\Gamma(t)}{2\pi}}\int d\epsilon f(\epsilon)\mathrm{Re}\{p_\sigma(\epsilon,t)\}\right).
\end{aligned} \tag{F.40}$$

The derivative $\dot{n}_{a\sigma}$ can be removed using the expression derived in appendix E, (E.15), giving

$$\frac{d}{dt}\int d\epsilon\ \epsilon n_\sigma(\epsilon,t) = \dot{\bar{\epsilon}}_{a\sigma}(t)n_{a\sigma}(t) + \frac{\dot{\Gamma}(t)}{\sqrt{2\pi\Gamma(t)}}\int d\epsilon f(\epsilon)\mathrm{Im}\left\{p_\sigma(\epsilon,t)\right\}. \tag{F.41}$$

By substituting this expression into (F.2) we find

$$\begin{aligned}\dot{E}(t) &= \sum_{\sigma} \dot{\bar{\epsilon}}_{a\sigma}(t) n_{a\sigma}(t) + \frac{\dot{\Gamma}(t)}{\sqrt{2\pi\Gamma(t)}} \sum_{\sigma} \int d\epsilon f(\epsilon) \mathrm{Im}\left\{p_{\sigma}(\epsilon, t)\right\} \\ &\quad -U \frac{d}{dt}\left\{n_{a\sigma}(t) n_{a-\sigma}(t)\right\} \\ &= \sum_{\sigma} \dot{\epsilon}_{a}(t) n_{a\sigma}(t) + \frac{\dot{\Gamma}(t)}{\sqrt{2\pi\Gamma(t)}} \sum_{\sigma} \int d\epsilon f(\epsilon) \mathrm{Im}\left\{p_{\sigma}(\epsilon, t)\right\}, \quad \text{(F.42)}\end{aligned}$$

which matches the expression we derived in chapter 3 for the rate of change of the total energy of the system. This demonstrates that the change in total energy in the electron distribution function $n_\sigma$ is identical to that calculated directly from the Newns-Anderson Hamiltonian. We have therefore demonstrated that our expression for $n_\sigma$ conserves energy.

# Chapter 5

# Numerical results I: adsorbate level occupations and energy transfer

In this chapter we use numerical methods to explore the behaviour of the time-dependent and adiabatic adsorbate level occupations and the energy transfer rates derived in chapters 2 and 3. The corresponding excitation spectra, as derived in chapter 4, are presented in chapter 6.

In section 5.1 the methods used to perform the calculations presented in this chapter are described. Results for the adsorbate level occupations are presented in section 5.2, with energy transfer considered in section 5.3. In each of these sections we explore the behaviour of three model systems for different approach speeds of the adsorbate and system temperatures. Conclusions are drawn from these results in section 5.4.

## 5.1 Computational methods

In this section we describe the methods used to compute the variation of the adsorbate occupation function and the energy transfer rates derived in chapters 2 and 3.

The time-evolving adsorbate occupation function $n_{a\sigma}$ is calculated from the quantity $p_\sigma$ using (2.19), the variation of the parameters $\epsilon_a$ and $\Gamma$, and the value of $U$. The system temperature, represented by the energy $k_BT$, also has an impact on the behaviour of the system through the Fermi distribution. $p_\sigma$ evolves from zero at time $t_0$, for all energies $\epsilon$, in a fashion governed by the time-derivative $dp_\sigma/dt$, (2.30). However, $dp_\sigma/dt$ depends on the effective energy level $\bar{\epsilon}_{a\sigma}$, through $\tilde{\epsilon}_{a\sigma} = \bar{\epsilon}_{a\sigma} - i\Gamma/2$, which in turn depends on the occupation function $n_{a\sigma}$ (see equation (2.4)). It is therefore necessary to integrate equations (2.19) and (2.30) in parallel to compute the evolution of $n_{a\sigma}$. To perform the time-integration of $p_\sigma$ we use the fourth order Runge-Kutta method [70] on a regular, finite grid of energy values. At each point in the integration at which the derivative $dp_\sigma/dt$ is required the occupation function $n_{a\sigma}$ is computed from (2.19), using Simpson's rule [70] to evaluate the energy integral. Through the use of this method the evolution of $n_{a\sigma}$ can be obtained from the supplied variation of $\epsilon_a$ and $\Gamma$ and the chosen values of $U$ and $k_BT$.

The adiabatic occupation function $n_{a\sigma}^{(ad)}$ is calculated in a self-consistent manner from the values of $\epsilon_a$, $\Gamma$, $U$ and $k_BT$ for a given adsorbate-surface configuration. At each iteration step the occupations from the previous step are used to calculate the adiabatic energy levels $\bar{\epsilon}_{a\sigma}^{(ad)}$ from (2.4). The adiabatic PDOS $\rho_{a\sigma}^{(ad)}(\epsilon, t)$ is then obtained from $\bar{\epsilon}_{a\sigma}^{(ad)}$, and is calculated on the same energy grid as used for the time-dependent calculation. Equation 2.32 then yields $n_{a\sigma}^{(ad)}$, again using Simpson's rule to evaluate the energy integral. This iterative process is stopped when successive steps differ by less than $10^{-12}$. The rate of convergence of this scheme is fast away from the adiabatic spin-transition, but it becomes slower as the spin-transition is approached. Close to the spin-transition the number of steps required to reach convergence is reduced by mixing the occupation $n_{a\sigma}^{(ad)}$ at a given step with that from the previous step.

In the computation of both the time-dependent and adiabatic occupations it is necessary to use two numerical approximations. For the time-dependent model the accuracy of the results depend on the size of the integration time-step used. In both the time-dependent and adiabatic models the range and spacing of the energy grid used to represent $p_\sigma$ and $\rho_{a\sigma}^{(ad)}$ is important. The finite range of the energy grid results in an underestimate of the adsorbate level occupations, which

for the adiabatic model can be approximated by

$$\begin{aligned}\Delta n_{a\sigma}^{(ad)}(t) &= \int_{-\infty}^{\epsilon_{min}} d\epsilon f(\epsilon)\rho_{a\sigma}^{(ad)}(\epsilon) \\ &= \frac{1}{2} - \frac{1}{\pi}\tan^{-1}\left\{2\frac{\bar{\epsilon}_{a\sigma}^{(ad)}(t) - \epsilon_{min}}{\Gamma(t)}\right\}, \end{aligned} \tag{5.1}$$

where $\epsilon_{min}$ is the lower limit of the energy grid and the assumption $|\epsilon_{min} - \epsilon_F| \gg k_B T$ has been made. The upper limit of the energy grid does not affect the occupations provided that the Fermi distribution is sufficiently small at this point. It is reasonable to expect the time-dependent occupation $n_{a\sigma}$ to be underestimated by a similar amount, provided that the difference $\bar{\epsilon}_{a\sigma}(t) - \epsilon_{min}$ is large.

The spacing of the energy grid also needs careful consideration when performing numerical calculations. Too coarse an energy grid results in an erratic result for $n_{a\sigma}$, while an excessively fine grid increases the computational cost of the calculation (in both time and memory) for little gain. The adiabatic occupation function $n_{a\sigma}^{(ad)}$ is also sensitive to the grid spacing for small values of the width $\Gamma$. In practice the iterative scheme described above can only be relied upon when $\Gamma$ is at least five times larger than the energy grid spacing. For smaller values of $\Gamma$ the adsorbate resonance is not well described by the values on the energy grid, and the value obtained for $n_{a\sigma}^{(ad)}$ is not reliable.

As the time-dependent quantities $n_{a\sigma}$ and $p_\sigma$, and their adiabatic equivalents, can be calculated by the methods we have described here, the computation of the non- and nearly-adiabatic energy transfer rates is straightforward. The non-adiabatic energy transfer rate $\dot{E}_{non-ad}$, (3.17), can be directly computed from the differences $\delta p_\sigma(\epsilon, t) = p_\sigma(\epsilon, t) - p_\sigma^{(ad)}(\epsilon, t)$, $\delta n_{a\sigma}(t) = n_{a\sigma}(t) - n_{a\sigma}^{(ad)}(t)$ and the derivatives $\dot{\epsilon}_a$ and $\dot{\Gamma}$. Calculation of the nearly-adiabatic energy transfer rate $\dot{E}_{nearly-ad}$, (3.27), requires the adiabatic quantities used for $\dot{E}_{non-ad}$ plus the derivative $\dot{n}_{a\sigma}^{(ad)}$. This derivative is most easily obtained using a centred finite difference method from values of $n_{a\sigma}^{(ad)}$ a short period before and after the required time.

Before performing calculations of the occupation function and energy transfer behaviour it is convenient to de-dimensionalise the equations governing the evolution of the system. The quantities in equations (2.19), (2.20), (3.17) and (3.27) with units involving time and energy are rescaled using a reference energy $\Gamma_0$.

These dimensionless parameters are denoted by a subscript '$D$';

$$\begin{aligned}
\epsilon_D &= \frac{\epsilon}{\Gamma_0}, & t_D &= \frac{\Gamma_0 t}{\hbar}, & \epsilon_{aD}(t_D) &= \frac{\epsilon_a(t)}{\Gamma_0}, \\
U_D &= \frac{U}{\Gamma_0}, & \Gamma_D(t_D) &= \frac{\Gamma(t)}{\Gamma_0}, & \bar{\epsilon}_{a\sigma D}(t_D) &= \frac{\bar{\epsilon}_{a\sigma}(t)}{\Gamma_0}, \\
\tilde{\epsilon}_{a\sigma D}(t_D) &= \frac{\tilde{\epsilon}_{a\sigma}(t)}{\Gamma_0}, & p_{\sigma D}(\epsilon_D, t_D) &= \sqrt{\Gamma_0} p_\sigma(\epsilon, t), & k_B T_D &= \frac{k_B T}{\Gamma_0}.
\end{aligned} \tag{5.2}$$

Planck's constant, $\hbar$, has been recovered where necessary in the above expressions to clarify the de-dimensionalisation procedure. The adiabatic quantities $\bar{\epsilon}_{a\sigma}^{(ad)}$, $\tilde{\epsilon}_{a\sigma}^{(ad)}$ and $p_\sigma^{(ad)}$ also have equivalent dimensionless counterparts to those defined in (5.2). The energy transfer rates $\dot{E}_{non-ad}$ and $\dot{E}_{nearly-ad}$ have the following dimensionless equivalents;

$$\begin{aligned}
\dot{E}_{non-ad,D}(t_D) &= \frac{\hbar}{\Gamma_0^2} \dot{E}_{non-ad}(t), \\
\dot{E}_{nearly-ad,D}(t_D) &= \frac{\hbar}{\Gamma_0^2} \dot{E}_{nearly-ad}(t).
\end{aligned} \tag{5.3}$$

The electronic friction coefficient $\eta$ has the units $\mathrm{ETD}^{-2}$ (where E, T and D denote units of energy, time and distance respectively). To de-dimensionalise $\eta$ it is therefore necessary to introduce an additional scaling parameter with units of distance. $\eta$ is therefore de-dimensionalised as

$$\eta_D(t_D) = \frac{s_0^2}{\hbar} \eta(t), \tag{5.4}$$

where $s_0$ is a reference length-scale. We will also use a speed $\dot{s}$ to compare calculations with different variations of $\Gamma_D$ in section 5.2.2. This speed can be de-dimensionalised using the reference length $s_0$ and the expression for $t_D$ in (5.2), giving

$$\dot{s}_D = \frac{ds_D}{dt_D} = \frac{\hbar}{\Gamma_0 s_0} \dot{s}. \tag{5.5}$$

Numerical testing of the calculations described in this section has shown that an energy grid of 10,001 points covering the range $\epsilon_D = -100$ to 100 provides a good balance between computational efficiency and accuracy. By using (5.1) and the parameter ranges used in section 5.2 this truncation leads to an underestimate

of $n_{a\sigma}$ of between $4 \times 10^{-3}$ and $5 \times 10^{-3}$. As the variation in $\epsilon_{aD}$ and $\Gamma_D$ is of order unity and occurs over a time range of order tens of dimensionless time units, a dimensionless integration time-step of 0.01 has been used. Convergence tests show that this value again represents a good balance between computational cost and accuracy. Typically the reference energy $\Gamma_0$ is of order 1-3eV, while the length $s_0$ is around 1 Å.

In the rest of this chapter the methods described in this section are used to demonstrate the behaviour of the adsorbate level occupations and energy transfer rates for a number of example systems.

## 5.2 Adsorbate level occupations

In this section we present results for the time-evolution of the adsorbate level occupation $n_{a\sigma}$. In subsection 5.2.1 we introduce three systems with different energy level positions, which will be used throughout the rest of this, and the following, chapter to demonstrate the behaviour of the Newns-Anderson model. The second subsection explores the impact of the speed of variation of the model parameters, and in the final subsection the effect of temperature is considered.

### 5.2.1 Energy level effects

To demonstrate the results of chapters 2 and 3 three model systems will be used. In each system the dimensionless adsorbate resonance width $\Gamma_D$ is increased from zero at $t_D = 0$ to $\Gamma_D = 3$ at $t_D = 50$ using an error function with a maximum gradient of $d\Gamma_D/dt_D = 0.3$ at $t_D = 25$. This variation is shown graphically in figure 5.1(a). The dimensionless intra-adsorbate Coulomb repulsion energy is set to $U_D = 3$. The three model systems differ only in the value of the bare energy level $\epsilon_{aD}$, which is held constant throughout the calculations. The values $\epsilon_{aD} = -2.5$, $-1.5$ and $-0.5$ will be used. Each of these model systems is driven through the spin-transition by the variation in $\Gamma_D$. These parameters are equivalent to those used to demonstrate the analytic expression for the adiabatic occupation function $n_{a\sigma}^{(ad)}$ in chapter 2 (see page 48), with the intra-adsorbate Coulomb repulsion energy set to $U_D = 3$.

The first ($\epsilon_{aD} = -2.5$) system has the minority spin energy level closest to the

Fermi level, the second ($\epsilon_{aD} = -1.5$) has the energy levels equidistant from $\epsilon_F$ and the third ($\epsilon_{aD} = -0.5$) has the majority level closest to $\epsilon_F$. These systems have been chosen to be simple to interpret while being broadly consistent with parameters obtained from DFT calculations, as will be discussed in chapter 7. However, the rate of change of $\Gamma_D$ has been exaggerated by a factor of approximately two to emphasise the non-adiabatic behaviour.

The time-dependent and adiabatic occupations and energy levels are plotted in figures 5.1(c) to (h). The $\epsilon_{aD} = -2.5$ calculations show the minority spin level crossing the Fermi level, gaining occupation and converging on the majority level. The $\epsilon_{aD} = -1.5$ levels converge simultaneously on a final occupation of approximately one half, with small deviations due to the truncation of the energy range in the numerical calculations. The final model system, $\epsilon_{aD} = -0.5$, involves the majority level crossing $\epsilon_F$ and approaching the falling minority level, resulting in a low occupation for the final state. In each of the systems the time-dependent occupations overshoot the adiabatic spin-transition at around $t_D = 25$ and the polarisation, the difference $n_{a\uparrow} - n_{a\downarrow}$, of the adsorbate falls to below 0.01 by $t_D = 35$. The adiabatic spin transition also occurs slightly earlier (by approximately two dimensionless time units) for the $\epsilon_{aD} = -2.5$ and $\epsilon_{aD} = -0.5$ models compared to the $\epsilon_{aD} = -1.5$ system.

It is interesting to note that for all of the model systems described here the first 'transient' term in the adsorbate occupation function $n_{a\sigma}$ (see (2.19) on page 39) does not disappear until the adsorbate reaches the adiabatic spin-transition point. The variation of the exponential governing the evolution of the transient term is shown in panel (b) of figure 5.1. This demonstrates that the transient term has an important role to play in the evolution of the electronic system and should not be neglected.

### 5.2.2 Speed effects

In figure 5.2 the time-dependent adsorbate occupations have been plotted at different speeds of variation for our three model systems. The term 'speed' is used here to refer to the rate of change of the width parameter $\Gamma_D$ which drives the systems through the spin-transition. The $\Gamma_D$ variation shown in figure 5.1 is taken as a reference speed of $\dot{s}_D = 1$. Slower speeds are simulated by reducing the peak gradient of the error function and increasing the time taken to reach

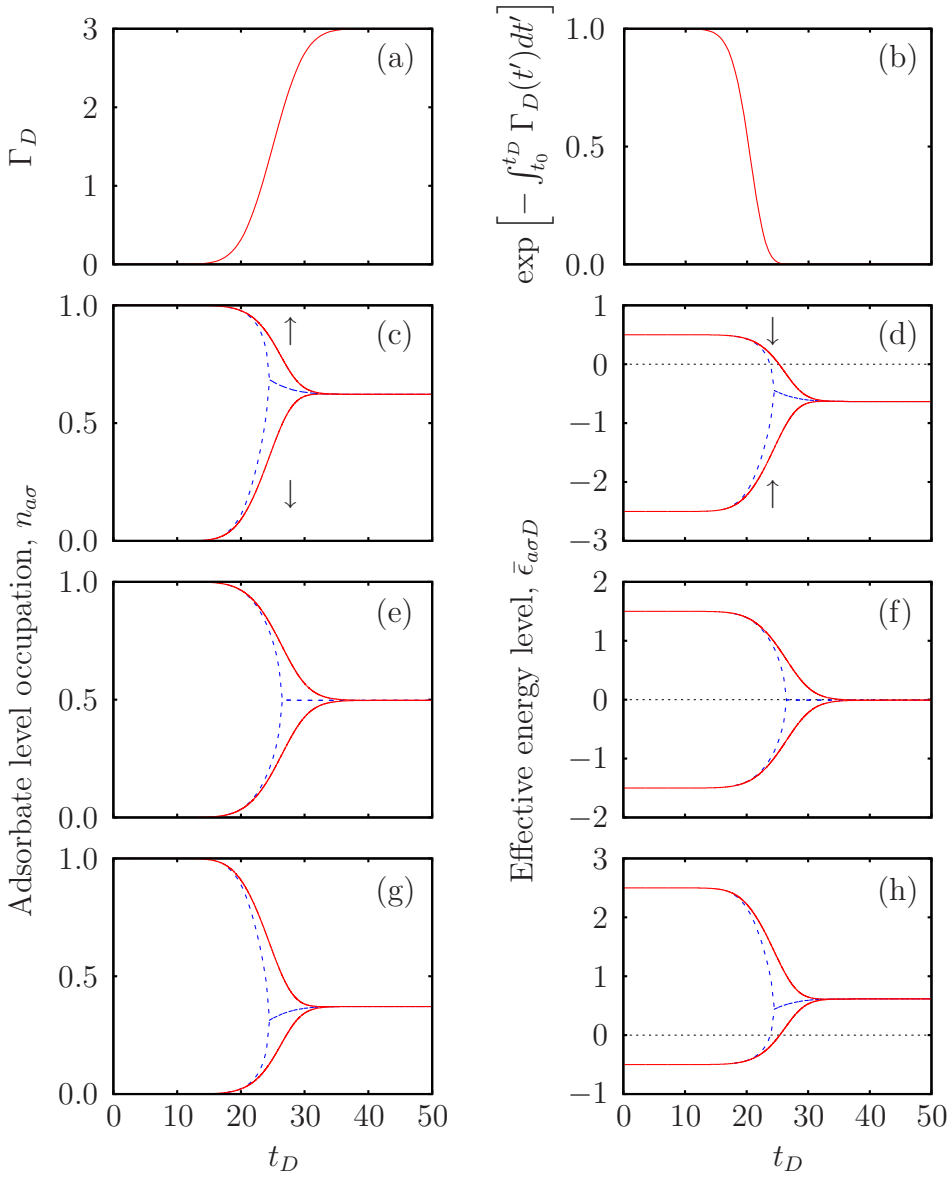


Figure 5.1: Time-evolution of the adsorbate level occupations $n_{a\sigma}$ and effective energy levels $\bar{\epsilon}_{a\sigma}$. (a) shows the variation in the width $\Gamma_D$ with time and (b) the variation of the exponential governing the decay of the transient term in $n_{a\sigma}$ (see (2.19) on page 39). (c), (e) and (g) show the variation of $n_{a\sigma}$ for the $\epsilon_{aD} = -2.5$, $-1.5$ and $-0.5$ model systems. (d), (f) and (h) show the corresponding energy level variation for each of the models. Solid red lines in (c) to (h) represent the time-dependent occupations/energy levels with dashed blue lines showing the adiabatic equivalents. Arrows in (c) and (d) denote the spin of each state; we take the majority state to be spin $\uparrow$.

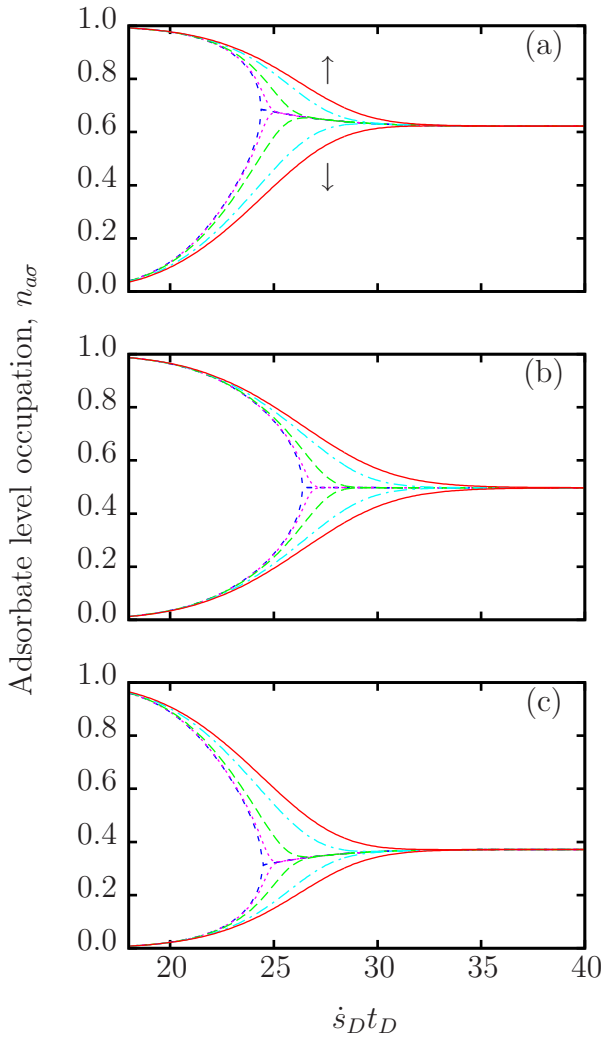


Figure 5.2: Dependence of the time-evolving occupation $n_{a\sigma}$ on the 'speed' of variation of $\Gamma_D$ for the $\epsilon_{aD} = -2.5$, (a), $\epsilon_{aD} = -1.5$, (b), and $\epsilon_{aD} = -0.5$, (c), model systems. Solid red lines show the same results as plotted in figure 5.1, but here we focus on the variation close to the spin-transition. Other lines represent different dimensionless speeds; $\dot{s}_D = 1/2$ (dot-dashed light-blue), $\dot{s}_D = 1/10$ (dashed green) and $\dot{s}_D = 1/100$ (dotted magenta). The dark-blue short-dashed line is the adiabatic occupation $n_{a\sigma}^{(ad)}$. Arrows denote the spin $\sigma$ of the corresponding occupations.

the maximum width[1]. To directly compare calculations performed at different speeds the variation of $n_{a\sigma}$ has been plotted against the product $\dot{s}_D t_D$, which can be interpreted as a displacement of the adsorbate. The different speeds can also be interpreted as calculations for adsorbates of different masses moving in the same potential well. This interpretation will be used in chapter 7 to consider the isotope effect in the adsorption of H/D atoms on copper and silver surfaces.

The impact of changing $\dot{s}_D$ on the evolution of $n_{a\sigma}$, as shown in figure 5.2, is quite dramatic – at slow speeds the adsorbate remains close to the adiabatic state, except for at a small range of displacements around the spin-transition. As the speed is increased the system has less time to react to the changing interaction strength, represented by $\Gamma_D$, which results in the overshoot of the adiabatic occupations beginning earlier. This behaviour results in a larger overshoot at the spin-transition point, and a greater displacement taken to converge to the adiabatic state. One interpretation of this behaviour is that for a particular system there is a maximum rate of charge transfer with distance which can be sustained by the time-dependent model. This maximum rate depends on the speed $\dot{s}_D$. As the adiabatic model exhibits a sharp spin-transition the corresponding rate of charge transfer diverges. The time-dependent model cannot match this divergence and therefore for any non-zero speed of variation there will be an overshoot at the spin-transition. A comparison of the charge transfer rates for the majority spin occupation in the $\epsilon_{aD} = -1.5$ model system is shown in figure 5.3.

The deviation of the occupations from the adiabatic model $\delta n_{a\sigma} = n_{a\sigma} - n_{a\sigma}^{(ad)}$ also yields some interesting insights into the charge transfer process. Figures 5.4, 5.5 and 5.6 show these differences for each spin on both linear and logarithmic scales for the three model systems. In each of the model systems the logarithmic plots show some interesting behaviour. Prior to the spin transition $\delta n_{a\sigma}$ grows roughly exponentially to a maximum value. This growth occurs at a similar rate for the four speeds simulated, with a faster rate of growth in cases where charge transfer is small, i.e. minority spin for the $\epsilon_{aD} = -0.5$ system and majority spin for the $\epsilon_{aD} = -2.5$ system. The growth of $\delta n_{a\sigma}$ for states experiencing greater charge transfer, i.e. majority spin for $\epsilon_{aD} = -0.5$ and minority spin for $\epsilon_{aD} = -2.5$, occurs earlier and increases more slowly.

[1]i.e. for $\dot{s}_D = 1/2$, $\Gamma_D$ is raised to 3 over 100 dimensionless time units, with a peak gradient of $d\Gamma_D/dt_D = 0.15$ at $t_D = 50$.

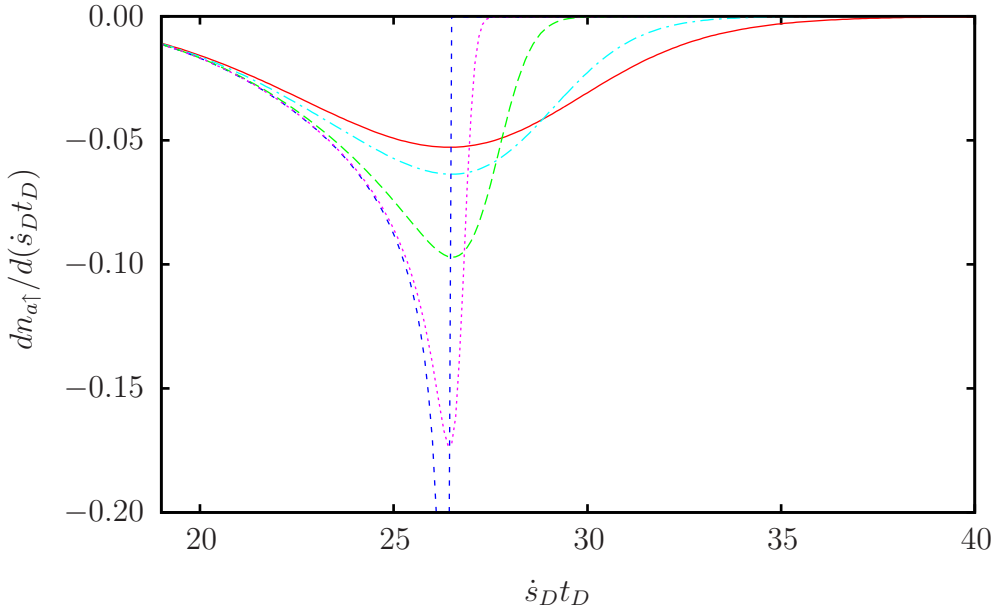


Figure 5.3: Comparison of the rate of change of occupation of the majority state with displacement $\dot{s}_D t_D$ for the $\epsilon_{aD} = -1.5$ system at different speeds. Colours as in figure 5.2.

After the spin-transition the three model systems display different behaviour. The convergence of the symmetric $\epsilon_{aD} = -1.5$ system to the final unpolarised state is shown in figure 5.5 to be approximately exponential in nature, with the magnitude of $\delta n_{a\sigma}$ identical for the two spins. In the other two systems the decay of $\delta n_{a\sigma}$ for the slow speed calculations after the spin-transition shows two domains. Shortly after the spin-transition the differences $\delta n_{a\sigma}$ decay in a similar manner to the $\epsilon_{aD} = -1.5$ system. However, at a certain point the majority difference $\delta n_{a\uparrow}$ in the $\epsilon_{aD} = -2.5$ system (figure 5.4(c)) displays a 'kink' which is sharper for the slower calculations. The modulus of the minority differences for this system show a set of cusps where the difference $\delta n_{a\downarrow}$ changes sign (see figure 5.4(d)).

This behaviour can be explained by recognising that in figure 5.2(a) the adiabatic occupation $n_{a\sigma}^{(ad)}$ varies after the spin-transition. The time-dependent occupations will take a certain amount of time to react to this change and either lag behind (for majority spin) or overshoot (minority spin) the adiabatic occupations. In the $\epsilon_{aD} = -1.5$ system this post-transition charge transfer is not seen and therefore the differences $\delta n_{a\sigma}$ simply decay smoothly (see figure 5.5). The $\epsilon_{aD} = -0.5$ model shows similar behaviour to the $\epsilon_{aD} = -2.5$ system, but with the magnitude of the differences for the two spins reversed.

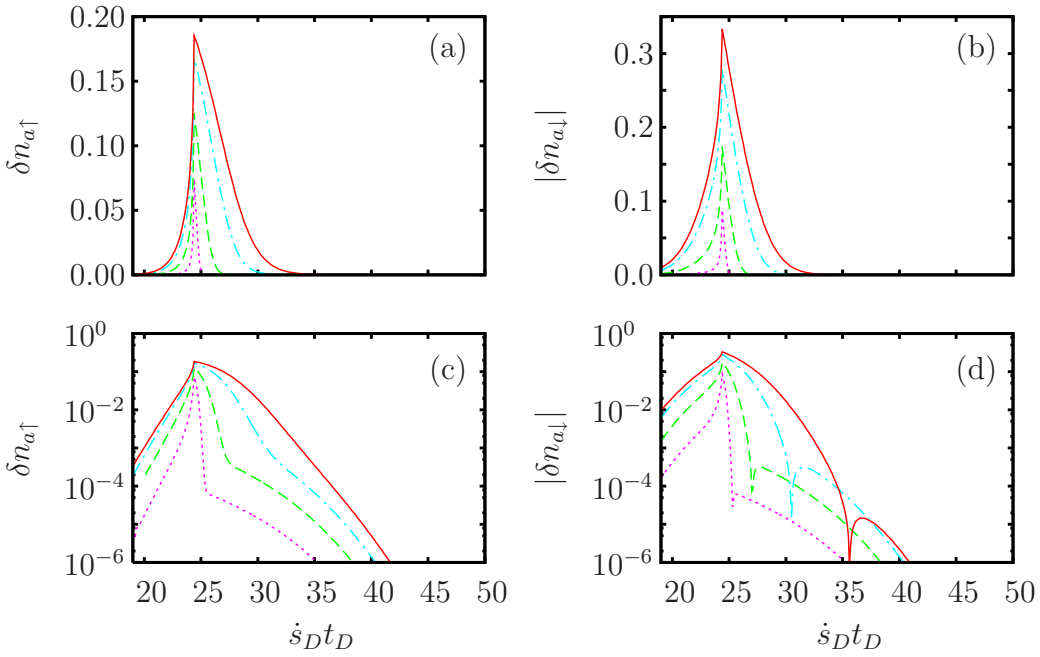


Figure 5.4: Deviation of the adsorbate level occupations $n_{a\sigma}$ from the adiabatic occupation $n_{a\sigma}^{(ad)}$ for the $\epsilon_a = -2.5$ model with displacement $\dot{s}_D t_D$ at different adsorbate speeds. (a) and (c) relate to the majority spin level, while (b) and (d) relate to the minority level. Colours as in figure 5.2.

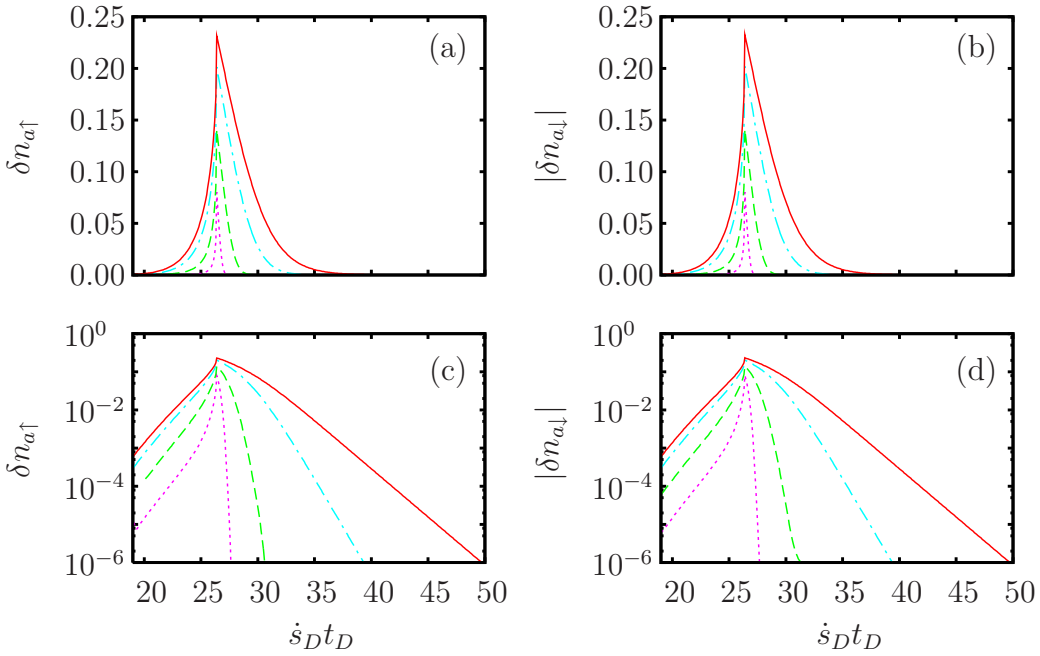


Figure 5.5: As for figure 5.4, but with $\epsilon_{aD} = -1.5$.

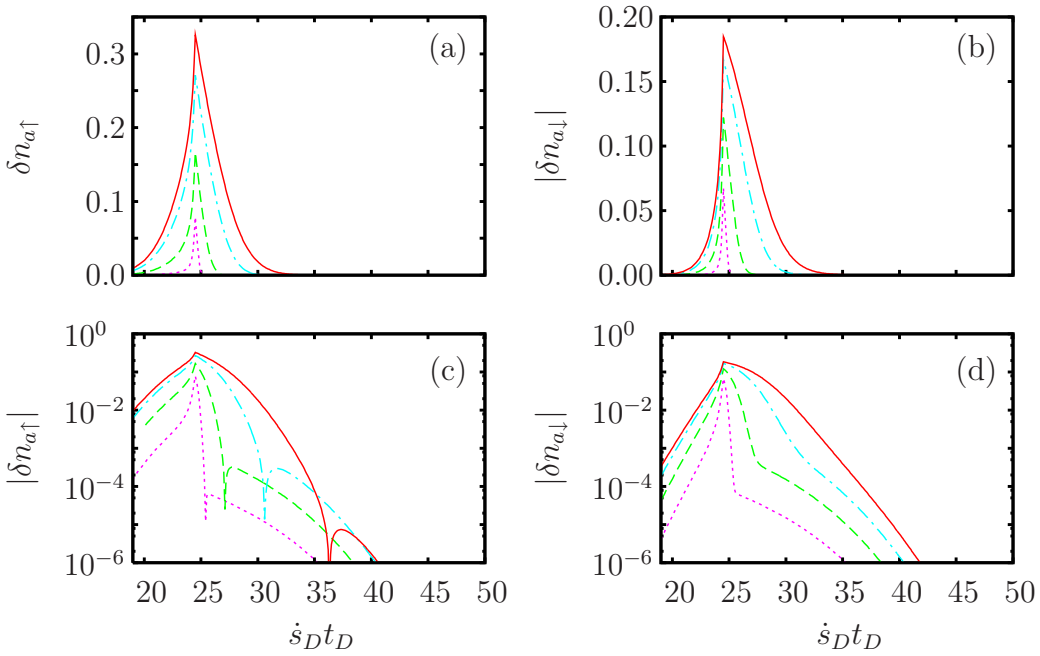


Figure 5.6: As for figure 5.4, but with $\epsilon_{aD} = -0.5$.

One striking feature of figures 5.4 and 5.6 is the similarity between the results for $|\delta n_{a\sigma}|$ for opposite spins in the two models. This reflects the symmetry of the arrangement of the majority and minority energy levels relative to the Fermi level for $\epsilon_{aD} = -2.5$ and $\epsilon_{aD} = -0.5$ when $U_D = 3$. This electron-hole symmetry is well known in condensed matter theory, see Kittel [71] page 206, and our results show that this symmetry is preserved in the Newns-Anderson model for both time-dependent and adiabatic calculations.

It is also interesting to note that the rate of decay of the differences $\delta n_{a\sigma}$ is significantly faster for the $\epsilon_{aD} = -2.5$ and $\epsilon_{aD} = -0.5$ systems than for the $\epsilon_{aD} = -1.5$ model. This, and the fact that the adiabatic spin-transition occurs later in the $\epsilon_{aD} = -1.5$ model, shows that the position of the levels relative to the Fermi level is important in determining the rate at which the system is driven through the spin-transition. The asymmetry of the energy levels in the $\epsilon_{aD} = -2.5$ and $\epsilon_{aD} = -0.5$ models, relative to the Fermi level, reduces the interaction strength required to drive the system through the spin transition. This appears to be correlated with the rate at which the systems converge on their adiabatic equivalents, but we have no explanation for this behaviour.

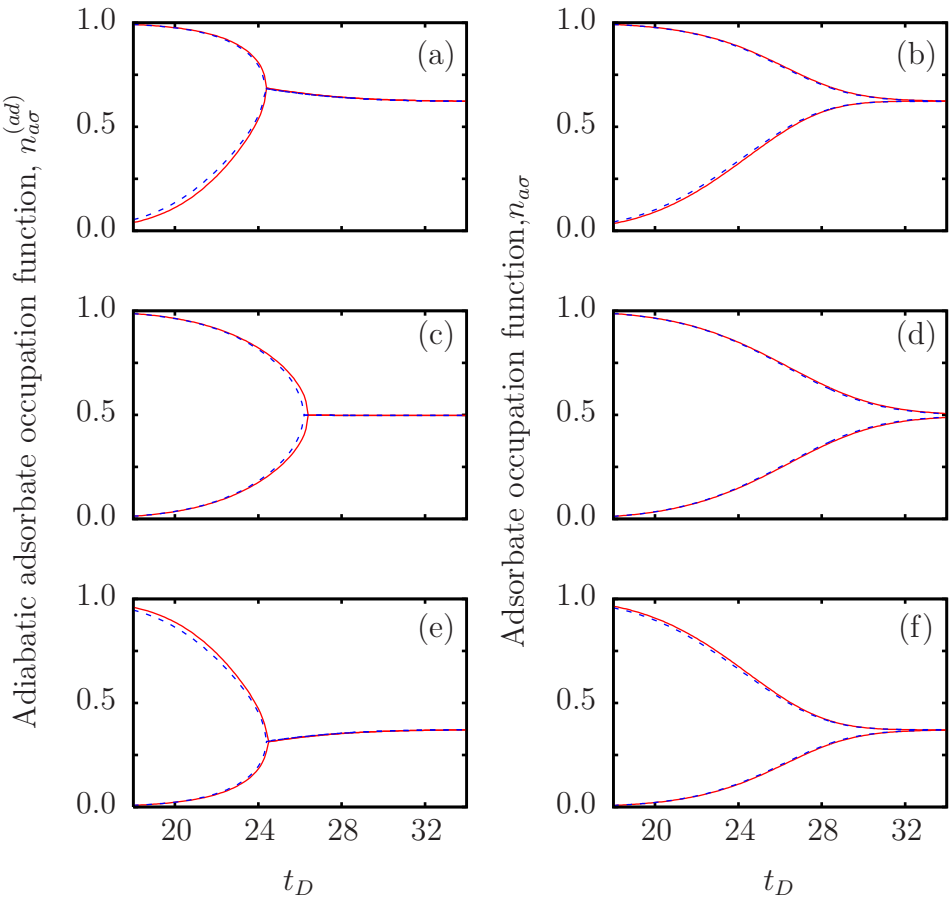


Figure 5.7: Evolution of the adiabatic and time-dependent adsorbate level occupations for the $\epsilon_{aD} = -2.5$, (a) and (b), $\epsilon_{aD} = -1.5$, (c) and (d), and $\epsilon_{aD} = -0.5$, (e) and (f), model systems at two different temperatures. Solid red lines denote results for a thermal energy of $k_B T_D = 0$, while dashed blue lines correspond to $k_B T_D = 0.1$. Calculations are performed at a dimensionless speed of $\dot{s}_D = 1$.

### 5.2.3 Temperature effects

We now consider the effect of the system temperature on the behaviour of the adsorbate occupations in the three model systems.

In figure 5.7 the evolution of $n_{a\sigma}^{(ad)}$ and $n_{a\sigma}$ have been plotted for each of the model systems for two thermal energies; $k_B T_D = 0$ and $k_B T_D = 0.1$. The latter of these values typically corresponds to temperatures between 1150 and 3500 K (for $\Gamma_0$ in the range 1-3 eV). The results for the adiabatic level occupations $n_{a\sigma}^{(ad)}$, panels (a), (c) and (e) in figure 5.7, only show small differences between the results for the two temperatures. For each system the high temperature occupations deviate from the zero temperature results only in the regions during which a level approaches or crosses the Fermi level, see figure 5.1. In the $\epsilon_{aD} = -2.5$ model this appears as a difference in the minority level occupations around $t_D = 20$-$24$, while in the $\epsilon_{aD} = -0.5$ model the majority level shows this effect in the same time-range. The $\epsilon_{aD} = -1.5$ model system has the adiabatic energy levels converging on the Fermi level at the spin-transition, and the deviations due to a finite temperature are therefore seen close to this point.

The differences due to temperature in the time-dependent occupations $n_{a\sigma}$, panels (b), (d) and (f) in figure 5.7, are even smaller than for their adiabatic equivalents. Given that the thermal energy used here, $k_B T_D = 0.1$, corresponds to temperatures of order 1150-3500 Kelvin (for $\Gamma_0 = 1$ to 3 eV), we conclude that in practice thermal effects can be ignored when considering charge transfer in the Newns-Anderson model.

## 5.3 Energy transfer

As in the previous section we will analyse the effect of energy level position, speed and temperature on the non-adiabatic and nearly-adiabatic energy transfer rates derived in chapter 3.

In figure 5.8 the non-adiabatic energy transfer rate $\dot{E}_{non-ad,D}$, as calculated from equation (3.17), is plotted for each of the model systems at four speeds of $\Gamma_D$ variation. Panels (a), (c) and (e) show the evolution of $\dot{E}_{non-ad,D}$ for the $\epsilon_{aD} = -2.5$, $-1.5$ and $-0.5$ models respectively. For each system the rate of energy transfer grows smoothly to a peak at the adiabatic spin-transition point with a

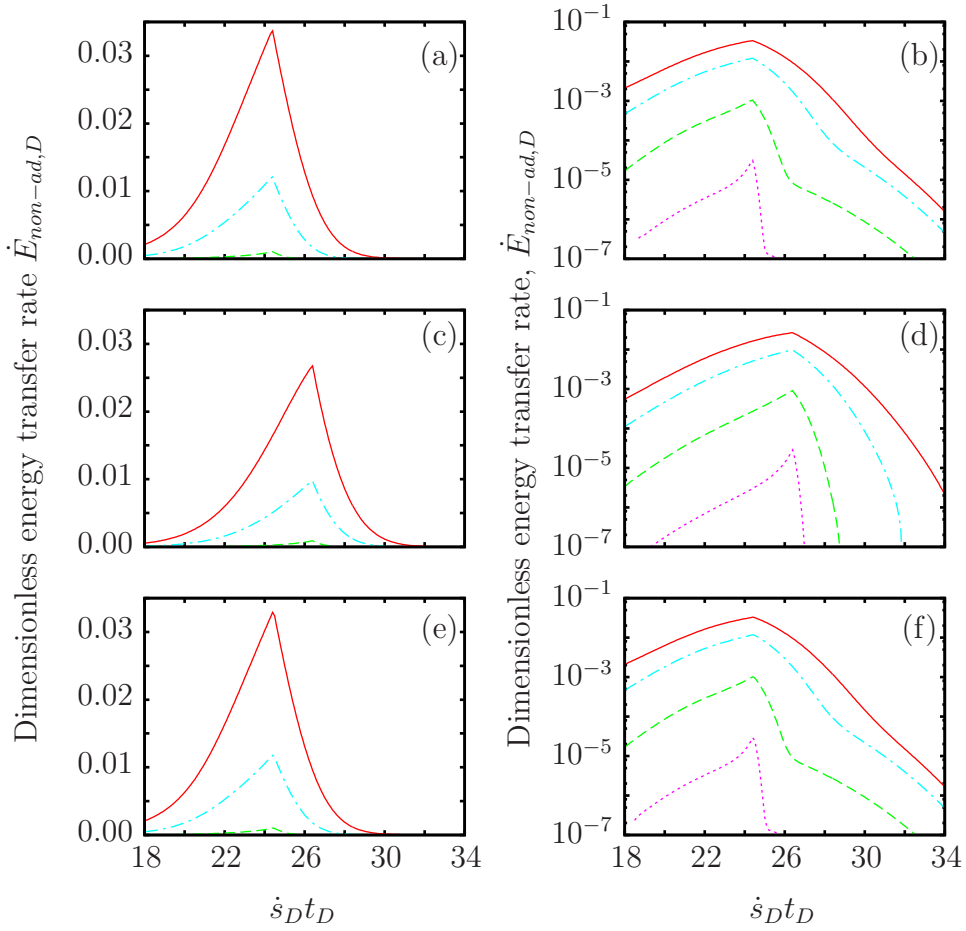


Figure 5.8: Evolution of the non-adiabatic energy transfer rate for the three model systems at different speeds. Panels (a) and (b) show results for the $\epsilon_{aD} = -2.5$ model system, (c) and (d) the $\epsilon_{aD} = -1.5$ system, and (e) and (f) the $\epsilon_{aD} = -0.5$ system. Colours correspond to different speeds of variation; solid red lines – $\dot{s}_D = 1$, dot-dashed light-blue lines – $\dot{s}_D = 1/2$, long-dashed green lines – $\dot{s}_D = 1/10$, dotted magenta lines – $\dot{s}_D = 1/100$. Calculations are performed at zero temperature.

larger and earlier peak for the $\epsilon_{aD} = -2.5$ and $-0.5$ models compared to the $\epsilon_{aD} = -1.5$ system. The peaks in the $\epsilon_{aD} = -2.5$ and $-0.5$ plots for $\dot{s}_D = 1$, solid red lines in figures 5.8(a) and (e), correspond to energy transfer rates in the range 52-465 meV/fs for values of $\Gamma_0$ from 1 to 3 eV. In the $\epsilon_{aD} = -1.5$ system this peak is approximately 20% smaller.

Calculations for slower speeds $\dot{s}_D$, see panels (b), (d) and (f), show significantly smaller energy transfer rates. In each case the rate of energy transfer grows in an approximately exponential manner prior to the spin-transition, with a rapid decay after. These transfer rates can be compared more easily by scaling them according to their dimensionless speeds. In section 3.2 the nearly-adiabatic energy transfer rate was expressed in the general form (see (3.18))

$$\dot{E}_{nearly-ad}(t) = \eta(s(t))\dot{s}(t)^2, \tag{5.6}$$

where the friction coefficient $\eta$ does not directly depend on time. At slower dimensionless speeds the non-adiabatic energy transfer rate approaches its nearly-adiabatic equivalent, and we therefore expect the ratio $\dot{E}_{non-ad,D}/\dot{s}_D^2$ to approach the friction coefficient $\eta_D$. In figure 5.9 these quantities are compared, with panels (a), (c) and (e) showing the energy transfer behaviour for the $\epsilon_{aD} = -2.5$, $\epsilon_{aD} = -1.5$ and $\epsilon_{aD} = -0.5$ models respectively.

The nearly-adiabatic friction coefficient increases steadily as the spin-transition is approached, where the singularity discussed in chapter 3 appears. After the singularity $\eta_D$ is small for each of the model systems; the $\epsilon_{aD} = -2.5$ and $\epsilon_{aD} = -0.5$ systems show a decay with displacement of $\eta_D$ from about $10^{-3}$ in panels (b) and (f) of figure 5.9. The symmetric $\epsilon_{aD} = -1.5$ model, however, does not exhibit the same behaviour – after the spin transition $\eta_D$ is negligible (see figure 5.9(d)). This behaviour can be explained by considering the expression for $\dot{E}_{nearly-ad,D}$, (3.31), or $\eta_D$, (3.32). After the spin-transition the adiabatic occupations in the $\epsilon_{aD} = -2.5$ and $-0.5$ systems change as $\Gamma_D$ is varied. This variation in $n_{a\sigma}^{(ad)}$ gives rise to a finite nearly-adiabatic energy transfer rate, which is absent in the $\epsilon_{aD} = -1.5$ model where $\dot{n}_{a\sigma}^{(ad)} = 0$ after the spin-transition.

The reduction of the speed $\dot{s}_D$ in the non-adiabatic calculations results in the ratio $\dot{E}_{non-ad,D}/\dot{s}_D^2$ approaching the nearly-adiabatic friction coefficient $\eta_D$ away from the spin-transition. As expected the range of displacements for which the nearly-adiabatic model is a good representation of the non-adiabatic energy transfer

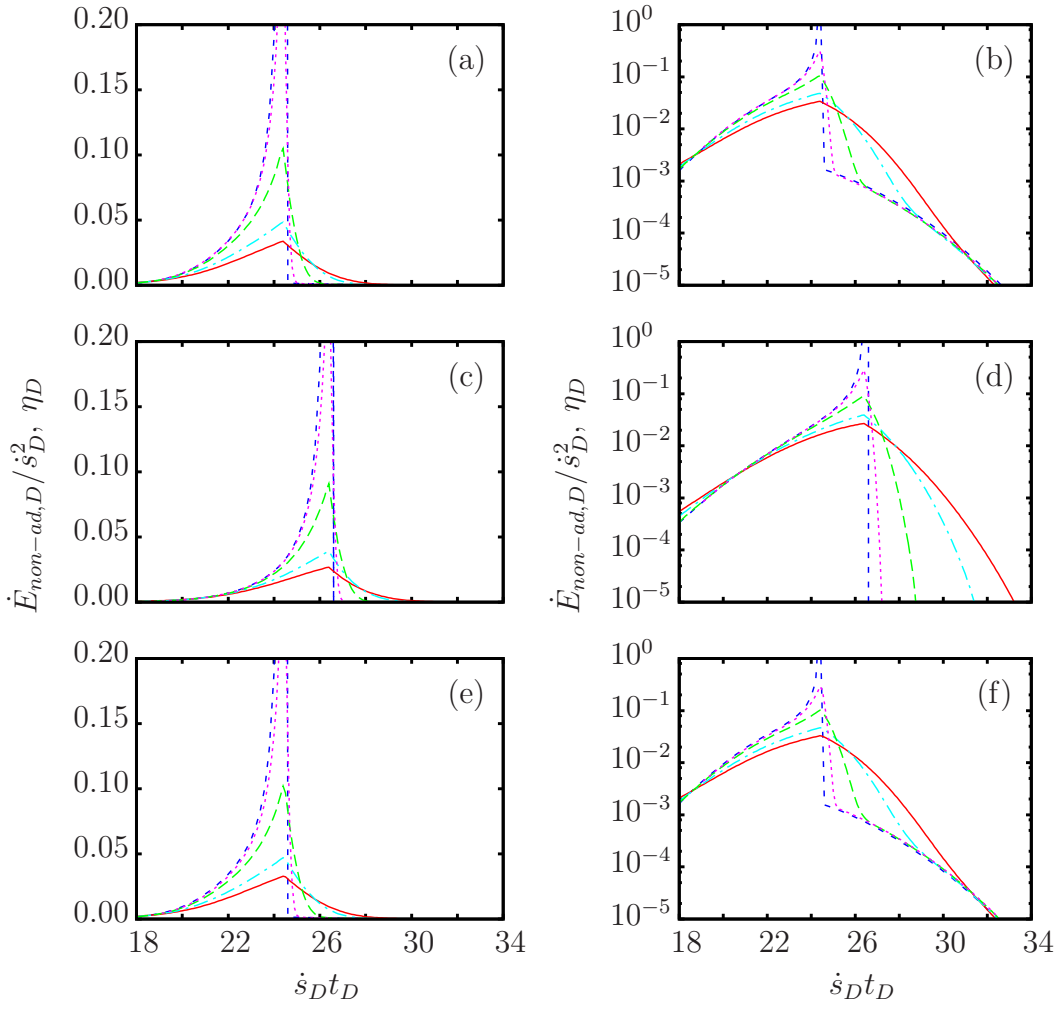


Figure 5.9: Non- and nearly-adiabatic energy transfer variation with displacement, $\dot{s}_D t_D$, for each of the model systems. Panels (a) and (b) relate to the $\epsilon_{aD} = -2.5$ system, (c) and (d) to the $\epsilon_{aD} = -1.5$ system and (e) and (f) to the $\epsilon_{aD} = -0.5$ system. Lines represent calculations performed for different speeds; solid red lines – $\dot{s}_D = 1$, dot-dashed light-blue – $\dot{s}_D = 1/2$, dashed green lines – $\dot{s}_D = 1/10$ and short-dashed magenta lines – $\dot{s}_D = 1/100$. Medium-dashed dark-blue lines denotes the nearly-adiabatic electronic friction coefficient $\eta_D$. Calculations are performed at $k_B T_D = 0$.

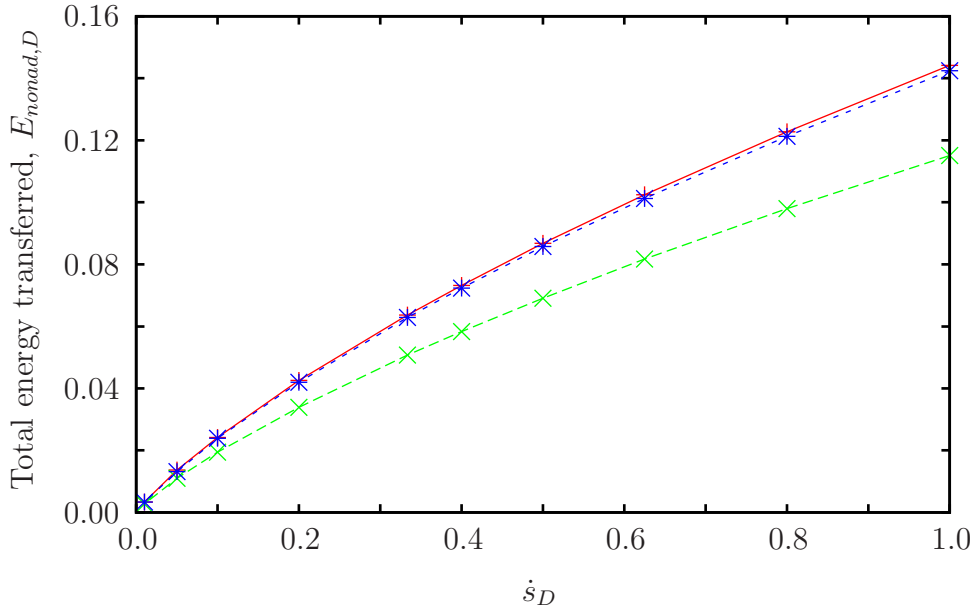


Figure 5.10: The effect of speed on the total energy transferred from an adsorbate to a surface for the $\epsilon_{aD} = -2.5$ (red solid lines), $\epsilon_{aD} = -1.5$ (green dashed lines) and $\epsilon_{aD} = -0.5$ (blue short-dashed lines) models.

process increases as the speed is reduced. Close to the spin-transition the non-adiabatic energy transfer rate remains finite for all speeds, and therefore cannot follow the divergence inherent in the nearly-adiabatic theory.

Another important feature of the energy transfer behaviour shown in figure 5.9 is the similarity of the results for $\epsilon_{aD} = -2.5$ and $\epsilon_{aD} = -0.5$. From figure 5.1 it can be seen that these two models differ significantly in the transfer of electrons to and from the surface; the $\epsilon_{aD} = -2.5$ model contains approximately 1.33 electrons at the end of the calculation, while the $\epsilon_{aD} = -0.5$ model contains 0.67. However, the variation of the magnitude of the total charge transferred is the same for the two systems. This shows that the direction of charge transfer is not as important as the total charge transfer in the deposition of energy to a metal surface by an adsorbate.

The variation of the total non-adiabatic energy transferred $E_{nonad,D}$ with speed, which is plotted in figure 5.10, also shows this electron-hole symmetry. $E_{nonad,D}$ has been calculated by integrating the non-adiabatic energy transfer rate over the full calculation. This integration is performed in two parts; one part covers the period from the time at which the adiabatic calculations become possible (see discussion on page 139) to the end of the calculation. The other part, the early

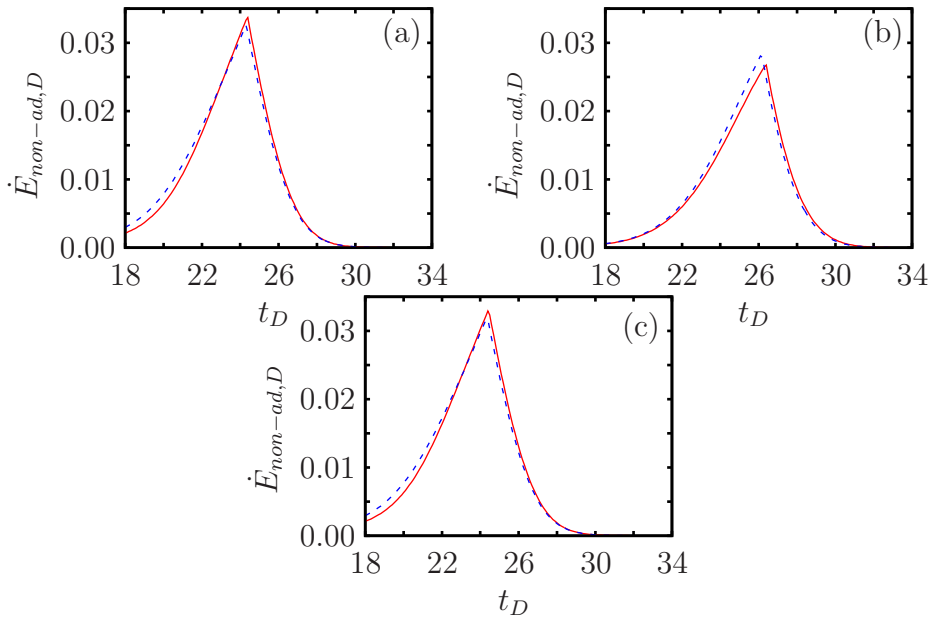


Figure 5.11: The effect of temperature on the non-adiabatic energy transfer rate for the (a) $\epsilon_{aD} = -2.5$, (b) $\epsilon_{aD} = -1.5$ and (c) $\epsilon_{aD} = -0.5$ model systems. Solid red lines denote zero temperature results, while the blue dashed line represents results for a thermal energy of $k_B T_D = 0.1$. All calculations are performed at a dimensionless speed of $\dot{s}_D = 1$

$\dot{E}_{non-ad,D}$ behaviour, is obtained by fitting an exponential to the energy transfer rate in a window a few dimensionless time units long shortly after the adiabatic calculations start. Analytical integration of this exponential provides a correction to the numerical integration, yielding the total energy transferred.

The results presented in figure 5.10 show an approximate power law dependence of the total energy transfer on the speed $\dot{s}_D$. All three of the model systems have $E_{nonad,D}$ roughly proportional to $\dot{s}_D^{4/5}$, with a pre-factor for the $\epsilon_{aD} = -2.5$ and $\epsilon_{aD} = -0.5$ systems 25% larger than that for $\epsilon_{aD} = -1.5$. We have not been able to explain this power law behaviour through analytic consideration of the time-dependent and adiabatic systems. Typical values for the total energy transfer at $\dot{s}_D = 1$ are 115-345 meV and 142-426 meV for the $\epsilon_{aD} = -1.5$ model and $\epsilon_{aD} = -2.5$ and $-0.5$ models respectively, with $\Gamma_0$ in the range 1-3 eV. The total energy transfer for real systems will be compared in chapter 7.

In figure 5.11 the non-adiabatic energy transfer rates are plotted for each model system at two temperatures - zero and 1150-3500 K (for $\Gamma_0$ in the range 1-3 eV). The differences between the energy transfer behaviour at these two temperatures are small – in the $\epsilon_{aD} = -2.5$ and $\epsilon_{aD} = -0.5$ systems the value of $\dot{E}_{non-ad,D}$ at

high temperature is slightly larger prior to the spin-transition. In the $\epsilon_{aD} = -1.5$ model system the energy transfer rates are similar except for the region close to the spin-transition. As expected these differences are confined to regions in which the occupations at the higher temperature, see figure 5.7, deviate from the zero temperature results. By integrating the energy transfer rates in figure 5.11 we find the difference in the total energy transferred is roughly 2-3% larger at the higher temperature. We therefore conclude that the system temperature does not have a significant impact on the non-adiabatic energy transfer behaviour.

## 5.4 Conclusions

In this chapter the methods used to numerically calculate the adsorbate level occupation and energy transfer rates from the results presented in chapters 2 and 3 have been introduced and demonstrated. The impact of the position of the bare-adsorbate energy level $\epsilon_a$, the 'speed' of variation of the width parameter $\Gamma$ and the system temperature on the time-dependent adsorbate level occupations and energy transfer behaviour have been investigated. Calculations of the time-dependent occupations show an overshoot at the adiabatic spin-transition, with slower speeds resulting in non-adiabatic effects being confined to a smaller region close to the spin-transition. The non- and nearly-adiabatic energy transfer rates have been compared and we have shown that in the slow speed limit the two results are consistent away from the spin-transition.

The results presented in this chapter yield a number of important conclusions. First, there is a striking similarity between the results of the $\epsilon_{aD} = -2.5$ and $\epsilon_{aD} = -0.5$ model systems, which is due to a symmetry in the physics of electrons and holes within the Newns-Anderson model. The rate of variation of the driving parameter $\Gamma_D$ has been shown to have a significant effect on the adsorbate level occupations and the non-adiabatic energy transfer rates. This effect suggests that there will be a significant isotope effect, which we will demonstrate for the H/Cu and H/Ag systems in chapter 7. For typical values of the scaling parameter $\Gamma_0$, between 1 and 3 eV, the energy transfer rates for the model systems peak at around 40-460 meV/fs, depending on the system. Integrating these rates yields total energy transfers in the region of 110 to 430 meV depending on the system considered (again for $\Gamma_0$ between 1 and 3 eV). We have also shown that the system temperature has a small effect on the transfer of charge and energy within physically reasonable ranges.

# Chapter 6

# Numerical results II: Electronic excitation spectra

In this chapter we explore the time-dependent evolution of the electronic excitation spectrum, derived in chapter 4, for the set of model systems considered in the previous chapter.

In section 6.1, with additional derivations in appendix G, the methods used to calculate the evolution of the excitation spectrum are presented. Results demonstrating the behaviour of this spectrum are presented in 6.2, with the three model systems compared in section 6.2.1. We then investigate the effect of the speed of parameter variation in section 6.2.2, with system temperature effects considered in section 6.2.3. Conclusions are drawn from these results in section 6.3.

## 6.1 Computational methods

In this section we describe the methods used to obtain the excitation spectrum numerically. We first consider the computation of the electron distribution function $n_\sigma(\epsilon, t)$, (4.25), which requires the quantities $q_\sigma(\epsilon, \epsilon', t)$, (4.27), and $r_\sigma$, (4.28), in addition to $p_\sigma$ and $n_{a\sigma}$, as discussed in section 5.1.

$q_\sigma$ can in principle be calculated in the same manner as $p_\sigma$; through the Runge-Kutta integration of the time-derivative $\partial q_\sigma / \partial t$. However, due to the large num-

ber of grid points required to accurately compute the last three terms in equation (4.25) this method becomes uneconomical in both time and memory. Instead we rewrite $q_\sigma$, (4.27), as

$$\begin{aligned} q_\sigma(\epsilon,\epsilon',t) &= \exp[-i(\epsilon-\epsilon')(t-t_0)] \\ &\quad \times \int_{t_0}^{t} dt_1 \sqrt{\frac{\Gamma(t_1)}{2\pi}} p_\sigma(\epsilon',t_1)\exp[i(\epsilon-\epsilon')(t_1-t_0)]. \end{aligned} \quad (6.1)$$

The separation of the exponential in (4.27) into the two terms in this equation has been performed to allow the evolution of $q_\sigma$ to be computed. As $p_\sigma$ also evolves in time equation (6.1) must be integrated simultaneously with $p_\sigma$, and $n_{a\sigma}$, to obtain the correct behaviour of $q_\sigma$. Simpson's rule is used to perform the time-integral in (6.1), and $q_\sigma$ can therefore be obtained at regular intervals.

The quantity $r_\sigma$ is calculated in a similar fashion to $p_\sigma$; the fourth-order Runge-Kutta method is used to integrate the time-derivative

$$\begin{aligned} \frac{\partial r_\sigma}{\partial t}(\epsilon,t) &= -\frac{\Gamma(t)}{2} r_\sigma(\epsilon,t) + i(\tilde{\epsilon}_{a\sigma}(t)-\epsilon) r_\sigma(\epsilon,t) + \sqrt{\frac{\Gamma(t)}{2\pi}} \exp\left[-\frac{1}{2}\int_{t_0}^{t}\Gamma(t')dt'\right] \\ &= -i(\bar{\epsilon}_{a\sigma}(t)-\epsilon) r_\sigma(\epsilon,t) + \sqrt{\frac{\Gamma(t)}{2\pi}} \exp\left[-\frac{1}{2}\int_{t_0}^{t}\Gamma(t')dt'\right]. \end{aligned} \quad (6.2)$$

As the coefficient of $r_\sigma$ in the first term on the right-hand side of this equation does not have a real component the growth of the magnitude of $r_\sigma$ is determined by the final term in (6.2). This term is governed by an exponential which is similar in form to the transient term in $n_{a\sigma}$, (2.19), and the growth in the magnitude of $r_\sigma$ therefore stops once the transient term is small. The third term in $n_\sigma$, which is the only place where $r_\sigma$ appears, will therefore evolve on a similar time-scale to the transient term in $n_{a\sigma}$.

By using (6.1) and (6.2), along with $p_\sigma$ (2.20) and $n_{a\sigma}$ (2.19), the first three terms in the electron distribution function can be evaluated. The fourth term in (4.25), which describes the initially occupied metal states, cancels with a similar term in the instantaneous electron distribution function, (4.38), on calculation of the excitation spectrum and is therefore ignored. The final three terms in $n_\sigma$ require further work due to the presence of singularities in their integrands in the $\eta \to 0^+$ limit.

We evaluate these three terms using a method in which the $\epsilon'$ integrals are sepa-

rated into three components; a window of width $2\alpha$ around $\epsilon' = \epsilon$, a section below $\epsilon' = \epsilon - \alpha$ and a section above $\epsilon' = \epsilon + \alpha$. The sum of the outer two sections is similar to a principle value integral, and we therefore use the notation $\mathrm{PV}_\alpha$ to denote this sum. The integral of the window around $\epsilon' = \epsilon$ is calculated by Taylor expanding the integrand to first order in $\alpha$ and evaluating this component analytically. In appendix G this expansion is performed, giving (see equations (G.5), (G.10) and (G.13))

$$\begin{aligned} n_\sigma^{(5)}(\epsilon,t) &= 2\sqrt{\frac{\Gamma(t)}{2\pi}}\rho_{a\sigma}^{(inst)}(\epsilon,t)\mathrm{PV}_\alpha\int d\epsilon'\frac{f(\epsilon')}{\epsilon-\epsilon'}\mathrm{Im}\left\{p_\sigma(\epsilon',t)\right\} \\ &\quad +2\sqrt{\frac{2\pi}{\Gamma(t)}}(\epsilon-\bar{\epsilon}_{a\sigma}(t))\rho_{a\sigma}^{(inst)}(\epsilon,t)f(\epsilon)\mathrm{Im}\{p_\sigma(\epsilon,t)\} \\ &\quad -4\alpha\sqrt{\frac{\Gamma(t)}{2\pi}}\rho_{a\sigma}^{(inst)}(\epsilon,t)\left(\frac{df}{d\epsilon}\,\mathrm{Im}\{p_\sigma(\epsilon,t)\}+f(\epsilon)\mathrm{Im}\left\{\frac{\partial p_\sigma}{\partial\epsilon}(\epsilon,t)\right\}\right), \end{aligned} \tag{6.3}$$

$$\begin{aligned} n_\sigma^{(6)}(\epsilon,t) &= -2\sqrt{\frac{\Gamma(t)}{2\pi}}\mathrm{PV}_\alpha\int d\epsilon'\frac{f(\epsilon')}{\epsilon-\epsilon'}\mathrm{Im}\left\{q_\sigma^*(\epsilon,\epsilon',t)p_\sigma^{(inst)}(\epsilon,t)\right\} \\ &\quad +\left(2\pi-4\alpha(t-t_0)\right)\sqrt{\frac{\Gamma(t)}{2\pi}}f(\epsilon)\mathrm{Re}\left\{q_\sigma^*(\epsilon,\epsilon,t)p_\sigma^{(inst)}(\epsilon,t)\right\} \\ &\quad +4\alpha\sqrt{\frac{\Gamma(t)}{2\pi}}\frac{df}{d\epsilon}\,\mathrm{Im}\left\{q_\sigma^*(\epsilon,\epsilon,t)p_\sigma^{(inst)}(\epsilon,t)\right\} \\ &\quad +4\alpha\sqrt{\frac{\Gamma(t)}{2\pi}}f(\epsilon)\mathrm{Im}\left\{p_\sigma^{(inst)}(\epsilon,t)\right. \\ &\qquad \left.\times\int_{t_0}^{t}dt_1\sqrt{\frac{\Gamma(t_1)}{2\pi}}\left(\frac{\partial p_\sigma^*}{\partial\epsilon}(\epsilon,t_1)+i(t_1-t_0)p_\sigma^*(\epsilon,t_1)\right)\right\}, \end{aligned} \tag{6.4}$$

$$\begin{aligned} n_\sigma^{(7)}(\epsilon,t) &= -\frac{\Gamma(t)}{2\pi}.\frac{\rho_{a\sigma}^{(inst)}(\epsilon,t)}{(\epsilon-\epsilon'_-)}-\frac{\Gamma(t)}{2\pi}\rho_{a\sigma}^{(inst)}(\epsilon,t)\mathrm{PV}_\alpha\int d\epsilon'\frac{df}{d\epsilon'}\frac{1}{\epsilon-\epsilon'} \\ &\quad -(\epsilon-\bar{\epsilon}_{a\sigma}(t))\frac{df}{d\epsilon}\rho_{a\sigma}^{(inst)}(\epsilon,t)+\frac{\alpha\Gamma(t)}{\pi}\frac{d^2f}{d\epsilon^2}\rho_{a\sigma}^{(inst)}(\epsilon,t), \end{aligned} \tag{6.5}$$

where $n_\sigma^{(5)}$, $n_\sigma^{(6)}$ and $n_\sigma^{(7)}$ are the fifth, sixth and seventh terms in the electron distribution function (4.25) and the expansions used are correct to order $\alpha$. In the expression for $n_\sigma^{(7)}$ the values of the Fermi function at the upper and lower edges of the $\epsilon'$ integration range have been assumed to be zero and one respectively. $\epsilon'_-$, which appears in $n_\sigma^{(7)}$, is the lower limit of the $\epsilon'$ range used to evaluate the energy integrals.

It is important to note here that the quantity $q_\sigma(\epsilon, \epsilon', t)$, which appears in three terms in $n_\sigma$, grows with time for energies $\epsilon \approx \epsilon'$. As the electron distribution function should stabilise for constant values of the driving parameters it is reasonable to expect these growing terms to cancel each other out. However, numerical testing suggests that in using an approximation to obtain values for $n_\sigma^{(6)}$ we have slightly disturbed this balance resulting in changes in the high-energy hole spectrum with time. As expected the magnitude of these changes also depends on the size of the analytic half-width $\alpha$. To minimise the impact of these convergence issues $\alpha$ is set to the smallest value possible, the $\epsilon'$ grid spacing, and by trial-and-error the number of grid points over a given range required to maintain accuracy for a given time has been found.

$n_{\sigma t}^{(inst)}$, the instantaneous electron distribution function, is more straightforward to calculate than its time-evolving counterpart. The first term in $n_{\sigma t}^{(inst)}$, (4.38), can be calculated directly from the parameters of the system and the time-dependent occupation $n_{a\sigma}$ using the definition of $\rho_{a\sigma}^{(inst)}$, (4.24). The second term in (4.38) can be ignored as it cancels with the fourth term in $n_\sigma$ as mentioned previously. The final term in $n_{\sigma t}^{(inst)}$ cannot be used directly due to the truncation of the $\epsilon'$ range over which the numerical integrals are performed. To maintain charge conservation in the instantaneous system we modify the final term in (4.38) to

$$
\begin{aligned}
&-\frac{df}{d\epsilon}\left[n_{a\sigma}(t_0) - \int_{-\infty}^{\infty} d\epsilon f(\epsilon)\rho_{a\sigma}^{(inst)}(\epsilon, t)\right] \\
&\quad = -\frac{df}{d\epsilon}\left[n_{a\sigma}(t_0) - \int_{\epsilon'_-}^{\epsilon'_+} d\epsilon' f(\epsilon')\rho_{a\sigma}^{(inst)}(\epsilon') - \int_{-\infty}^{\epsilon'_-} d\epsilon \rho_{a\sigma}^{(inst)}(\epsilon, t)\right] \\
&\quad = -\frac{df}{d\epsilon}\Bigg[n_{a\sigma}(t_0) - \int_{\epsilon'_-}^{\epsilon'_+} d\epsilon' f(\epsilon')\rho_{a\sigma}^{(inst)}(\epsilon', t) \\
&\qquad\qquad - \left(\frac{1}{2} - \frac{1}{\pi}\tan^{-1}\left\{2\frac{\bar{\epsilon}_{a\sigma}(t) - \epsilon'_-}{\Gamma(t)}\right\}\right)\Bigg],
\end{aligned}
\tag{6.6}
$$

where we have assumed that the Fermi function is zero at the upper limit of the integration range, $\epsilon'_+$, and the integral over $\epsilon'$ up to $\epsilon'_-$ has been performed analytically.

As in the methodology described for the computation of $n_{a\sigma}$ and $\dot{E}_{non-ad}$, see section 5.1, we de-dimensionalise all parameters before performing numerical calculations. In addition to the dimensionless quantities defined in (5.2) the dimensionless electron distribution functions, excitation spectra and the analytic

window half-width are defined as

$$\begin{aligned} n_{\sigma D}(\epsilon_D, t_D) &= \Gamma_0 n_\sigma(\epsilon, t), & n^{(inst)}_{\sigma t,D}(\epsilon_D) &= \Gamma_0 n^{(inst)}_{\sigma t}(\epsilon), \\ n^{(ex)}_{\sigma D}(\epsilon_D, t_D) &= \Gamma_0 n^{(ex)}_{\sigma}(\epsilon, t), & \alpha_D &= \frac{\alpha}{\Gamma_0}, \end{aligned} \tag{6.7}$$

where $\Gamma_0$ is the scaling energy.

Numerical testing of the calculations described here has shown that for calculations running for up to 200 dimensionless time units a 160,001 point $\epsilon'_D$ grid covering the range $\epsilon'_D = -20$ to 20 provides a stable result. For the longer calculations used in this chapter a 320,001 point grid over the same energy range is necessary to avoid convergence issues resulting from the analytic window approximation as discussed above. Our use of a smaller energy range here than in the previous chapter is due to the need for a small value for the analytic window half-width $\alpha_D$, while having a reasonable number of energy grid points. The dimensionless window half-width $\alpha_D$ is set to a single $\epsilon'_D$ grid spacing; $2.5 \times 10^{-4}$ for the 160,001 point grid.

The truncation of the energy grid used here leads to a larger underestimate of the occupation $n_{a\sigma}$ than reported in the previous chapter; from equation (5.1) this truncation reduces $n_{a\sigma}$ by approximately 0.02. This underestimate in turn also has an impact on the excitation spectra, which will be discussed later.

Numerical integration of the final excitation spectra over energy demonstrates that charge is conserved to within $10^{-5}$ of an electron. The total energy contained in the electronic excitations, calculated from the first moment of $n^{(ex)}_{\sigma}(\epsilon, t)$, agrees with the total non-adiabatic energy transfer calculated in section 5.3 to within a few percent.

## 6.2 Excitation Spectra

In this section we present results for the time-evolution of the electron distribution function $n_{\sigma D}$, its instantaneous equivalent $n^{(inst)}_{\sigma t,D}$ and the difference $n^{(ex)}_{\sigma D}$ derived in chapter 4. To demonstrate the behaviour of the electronic system the three model systems introduced in the previous chapter are again used. The evolution of the excitation spectra is investigated in section 6.2.1, with speed and system temperature effects considered in sections 6.2.2 and 6.2.3 respectively.

### 6.2.1 Model systems

The same three model systems introduced in section 5.2.1 are used here to demonstrate the calculation of the time-evolving and instantaneous electron distribution functions, from which the excitation spectrum in obtained. In each of these systems the dimensionless width $\Gamma_D$ is increased from zero to three over 50 dimensionless time units with a peak gradient of $d\Gamma_D/dt_D = 0.3$ at $t_D = 25$. $U_D$ is set to 3 and the three systems differ only in the constant values of the bare adsorbate energy level used; $\epsilon_{aD} = -2.5$, $-1.5$ and $-0.5$. As demonstrated in the previous chapter each system is driven through the spin transition by the variation in $\Gamma_D$. A thermal energy of $k_B T_D = 0.02$ is used to improve computational efficiency and to allow the variation close to the Fermi level to be easily considered. This energy corresponds to temperatures in the range 230-700 K for $\Gamma_0$ in the range 1 to 3 eV.

Before we consider the behaviour of the electron distribution function and its instantaneous equivalent it is informative to look at the contributions from the different terms in $n_\sigma$, (4.25). In figure 6.1 the magnitude of the contributions from these terms for the $\epsilon_{aD} = -1.5$ model system at the end of the calculation are compared, with the exception of the fourth term in $n_\sigma$ which cancels with an identical term in $n_{\sigma t}^{(inst)}$. This figure shows that most of the terms have a magnitude between $10^{-2}$ and 100 over the range $\epsilon_D = -2$ to 2. However, the electronic excitation spectrum is several orders of magnitude smaller at these energies demonstrating that there is a very delicate balance between the different terms in $n_\sigma$ from which $n_\sigma^{(ex)}$ is extracted. As a result of this balance we are unable to attribute the behaviour of any particular section of the excitation spectrum to a given physical process, and are therefore unable to determine the origins of the various features of our spectra. Equivalent plots to figure 6.1 can be produced for the $\epsilon_{aD} = -2.5$ and $\epsilon_{aD} = -0.5$ model systems, but these do not show any qualitatively different behaviour – the balance between the different terms changes slightly.

The cancellation between the electron distribution function and its instantaneous counterpart away from the Fermi level can be seen most clearly in the early evolution of our model systems. In figure 6.2 a snapshot of $n_{\sigma D}$, $n_{\sigma t,D}^{(inst)}$ and $n_{\sigma D}^{(ex)}$ at $t_D = 23$ is presented for each spin of the $\epsilon_{aD} = -1.5$ system. The two distribution functions are dominated by two features; a broad distribution below

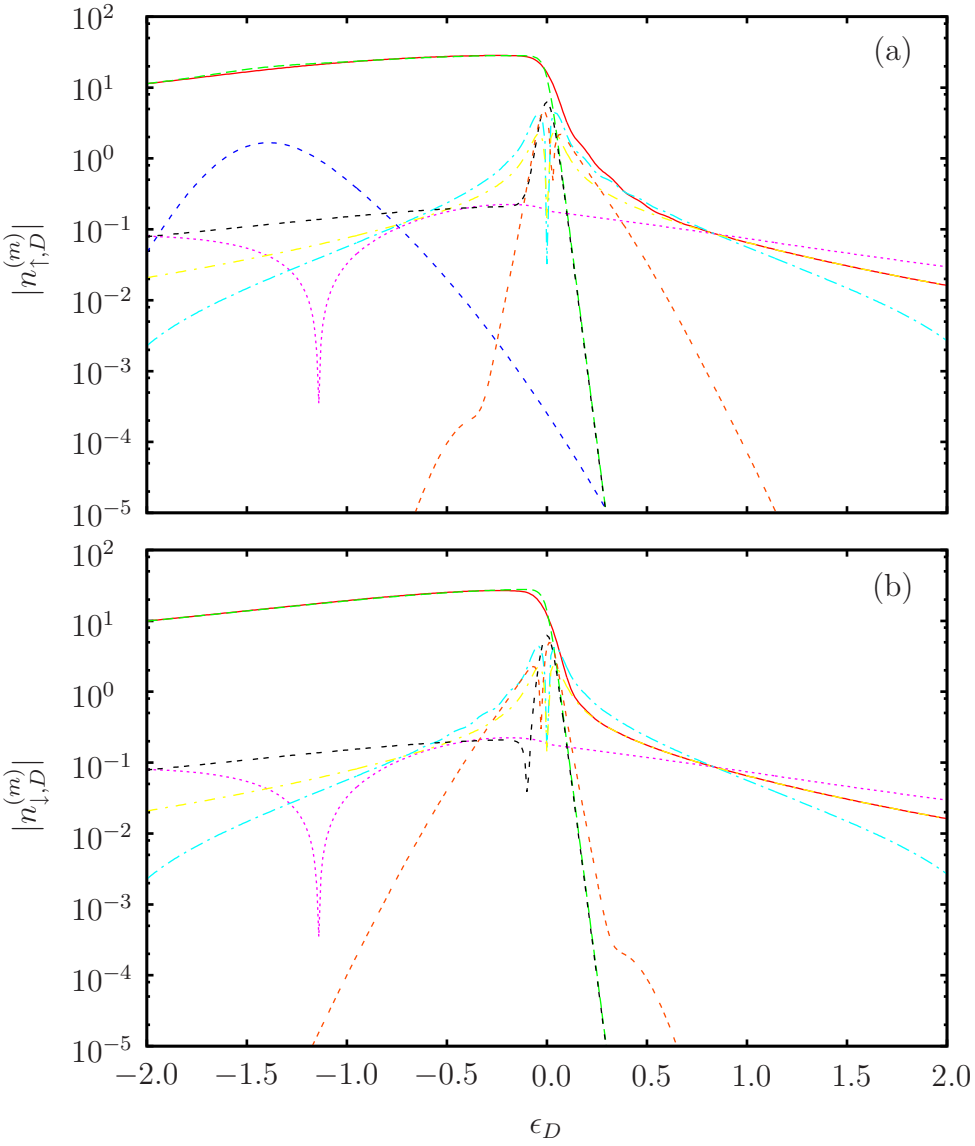


Figure 6.1: Comparison of the magnitude of the separate terms contributing to the final ($t_D = 50$) excitation spectrum of the $\epsilon_{aD} = -1.5$ system for (a) majority spin and (b) minority spin. Lines represent different contributions to $n^{(ex)}_{\sigma D}$; $n^{(1)}_{\sigma,D}$ (solid red lines) [+/+], $n^{(2)}_{\sigma,D}$ (long-dashed green lines) [−/−], $n^{(3)}_{\sigma,D}$ (medium-dashed dark-blue lines) [+/+], $n^{(5)}_{\sigma,D}$ (short-dashed magenta lines) [+/−], $n^{(6)}_{\sigma,D}$ (light-blue long-dash dotted lines) [+/−], $n^{(7)}_{\sigma,D}$ (yellow short-dash dotted lines) [−/+], $n^{(inst)}_{\sigma t,D}$ (black double-dashed lines [+/+ (a), +/− (b)] and $n^{(ex)}_{\sigma D}$ (orange triple-dashed lines) [−/+]. $n^{(4)}_{\sigma,D}$, which describes the initially occupied metal states, is not plotted here as it cancels exactly with a term in $n^{(inst)}_{\sigma t,D}$. Cusps denote points where a term changes sign and symbols in square brackets denote the sign of the term on the left and right-hand edges of the plot.

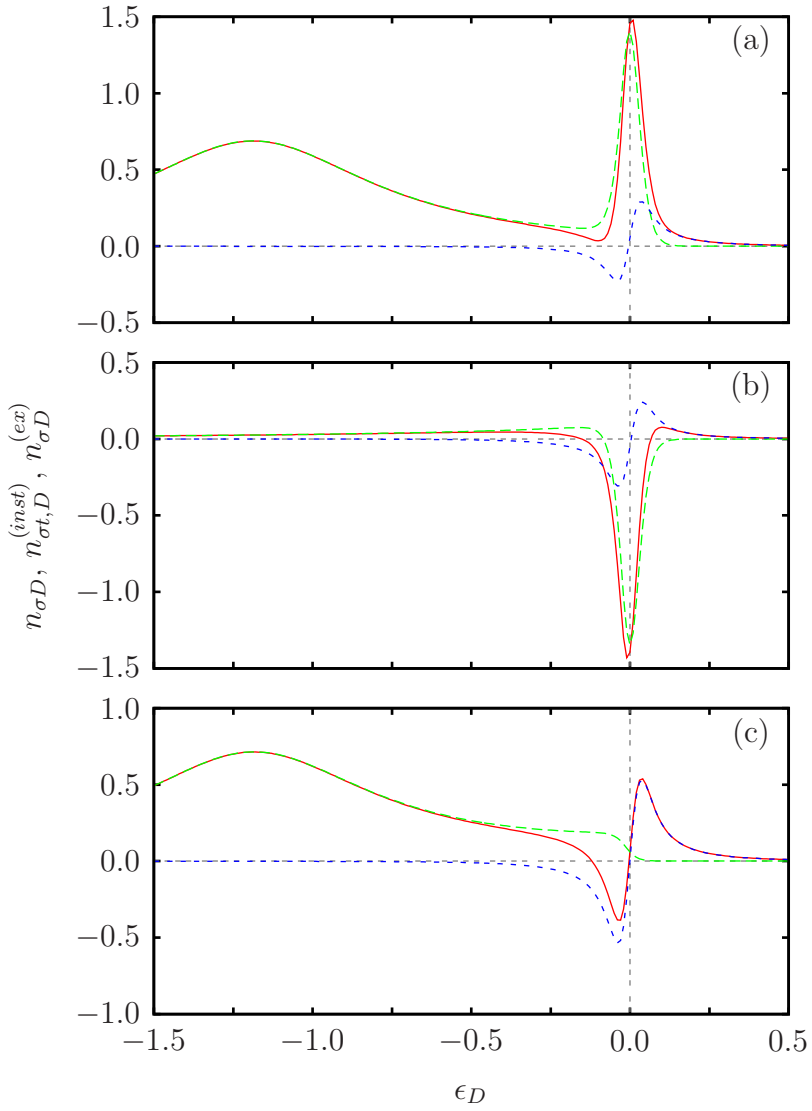


Figure 6.2: The electron distribution function $n_{\sigma D}$, its instantaneous equivalent $n^{(inst)}_{\sigma t,D}$ and the excitation spectrum $n^{(ex)}_{\sigma D}$ of the $\epsilon_{aD} = -1.5$ model system at $t_D = 23$ for (a) majority spin, (b) minority spin and (c) the sum of the two. Solid red lines denote $n_{\sigma D}$, long-dashed green lines $n^{(inst)}_{\sigma t,D}$ and medium-dashed blue lines $n^{(ex)}_{\sigma D}$. In both $n_{\sigma D}$ and $n^{(inst)}_{\sigma t,D}$ the term relating to the initially occupied metal states has been neglected.

$\epsilon_F$ (most obvious for majority spin, panel (a)) and a peak or trough at the Fermi level. Far below the Fermi level, particularly for majority spin, there is an almost exact cancellation between $n_{\sigma D}$ and the contribution to $n^{(inst)}_{\sigma t,D}$ from the adsorbate resonance $\rho^{(inst)}_{a\sigma}$. Close to the Fermi level both distribution functions show a large peak or trough (for majority or minority spin respectively) with $n^{(ex)}_{\sigma D}$, the difference between the two, substantially smaller. This similarity between $n_{\sigma D}$ and $n^{(inst)}_{\sigma t}$ at this early time, when the adsorbate occupations are close to the adiabatic state ($|\delta n_{a\sigma}| \approx 0.014$ for both spins), gives us confidence that our derivation is correct. The cancellation between the distributions for the other two model systems is similar, with differences in the position of the peak in the majority spin distributions and the magnitude of the peaks and troughs at the Fermi level.

In the rest of this chapter we will focus on the properties of the excitation spectrum. Figures 6.3, 6.4 and 6.5 show a series of snapshots, i.e. the excitation spectra at selected points in their evolution, for the three model systems. Each figure shows that the majority of the evolution of the electronic system occurs during the period in which the rate of change of $\Gamma_D$ is largest. The snapshots of the $\epsilon_{aD} = -2.5$ system, figure 6.3, show early evolution in the minority spin spectrum with the majority spin spectrum evolving later. In the $\epsilon_{aD} = -0.5$ system, figure 6.5, this behaviour is reversed; the early evolution primarily occurs in the majority spectrum with the minority spectrum again evolving later. The $\epsilon_{aD} = -1.5$ model system, figure 6.4, has both spin states evolving in a symmetrical manner – the spectra for majority spin electrons and minority spin-holes are almost identical. This similarity will be investigated further at the end of this section.

Each of the model systems exhibit a number of similar features in their spectra, with the balance between them determined by the parameters of the system. Below the Fermi level the majority spin spectra consists of a peak of low energy holes with small high energy tails, while the minority excitation spectra are broader with large high energy tails. Above the Fermi level this behaviour is reversed; the majority spin spectra show a broad distribution of electrons with large high energy tails, while the minority spin excitations are confined to peaks close to $\epsilon_F$. However, the magnitude of these components is different in each of the model systems. In the $\epsilon_{aD} = -2.5$ model the spectrum of holes below the Fermi level is larger than electron excitations above, with the minority spin

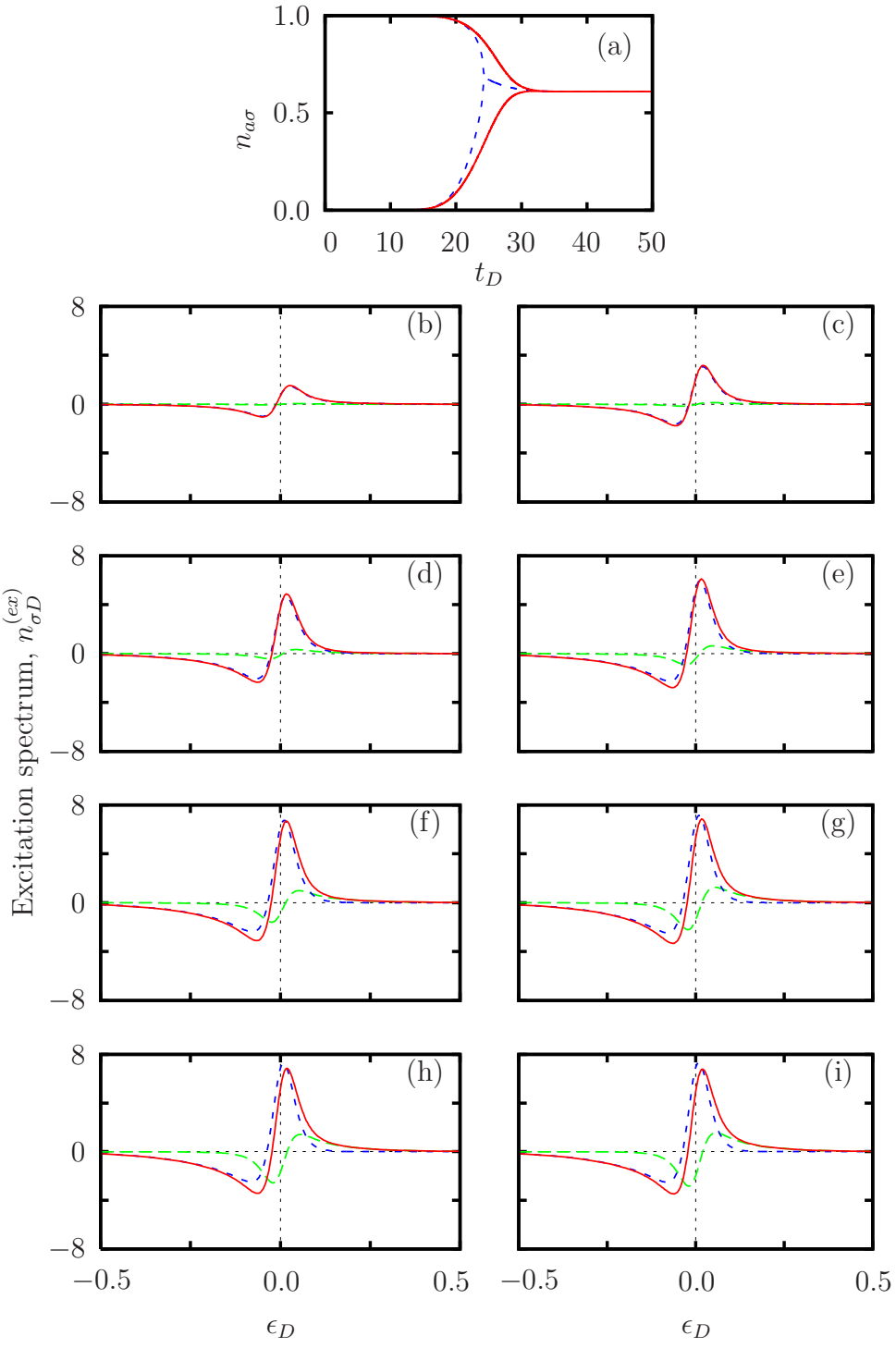


Figure 6.3: Excitation spectra snapshots for the $\epsilon_{aD} = -2.5$ model at times (b) $t_D = 22.00$, (c) $t_D = 23.25$, (d) $t_D = 24.50$, (e) $t_D = 25.75$, (f) $t_D = 27.00$, (g) $t_D = 28.25$, (h) $t_D = 29.50$, and (i) after $\Gamma_D$ variation has finished ($t_D = 50.00$). Panel (a) shows $n_{a\sigma}$ (solid red lines) and $n^{(ad)}_{a\sigma}$ (medium-dashed blue lines). In panels (b) to (i) solid red lines denote the total electronic excitation spectrum, long-dashed green line the majority ($\sigma =\uparrow$) component and medium-dashed blue lines the minority ($\sigma =\downarrow$) component.

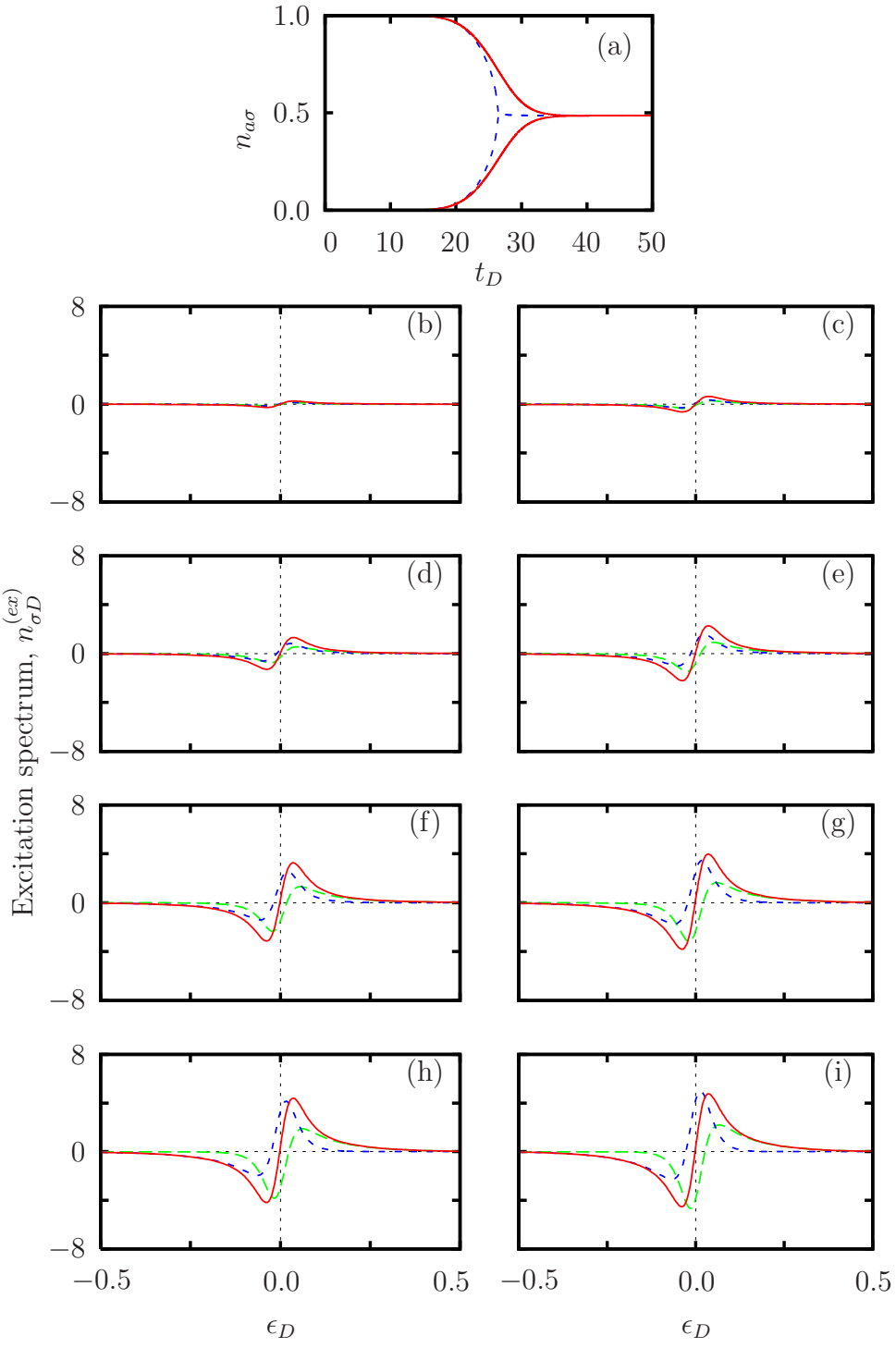


Figure 6.4: Excitation spectra snapshots for the $\epsilon_{aD} = -1.5$ model at times (b) $t_D = 22.00$, (c) $t_D = 23.25$, (d) $t_D = 24.50$, (e) $t_D = 25.75$, (f) $t_D = 27.00$, (g) $t_D = 28.25$, (h) $t_D = 29.50$, and (i) after $\Gamma_D$ variation has finished ($t_D = 50.00$). Panel (a) shows $n_{a\sigma}$ (solid red lines) and $n^{(ad)}_{a\sigma}$ (medium-dashed blue lines). In panels (b) to (i) solid red lines denote the total electronic excitation spectrum, long-dashed green line the majority ($\sigma =\uparrow$) component and medium-dashed blue lines the minority ($\sigma =\downarrow$) component.

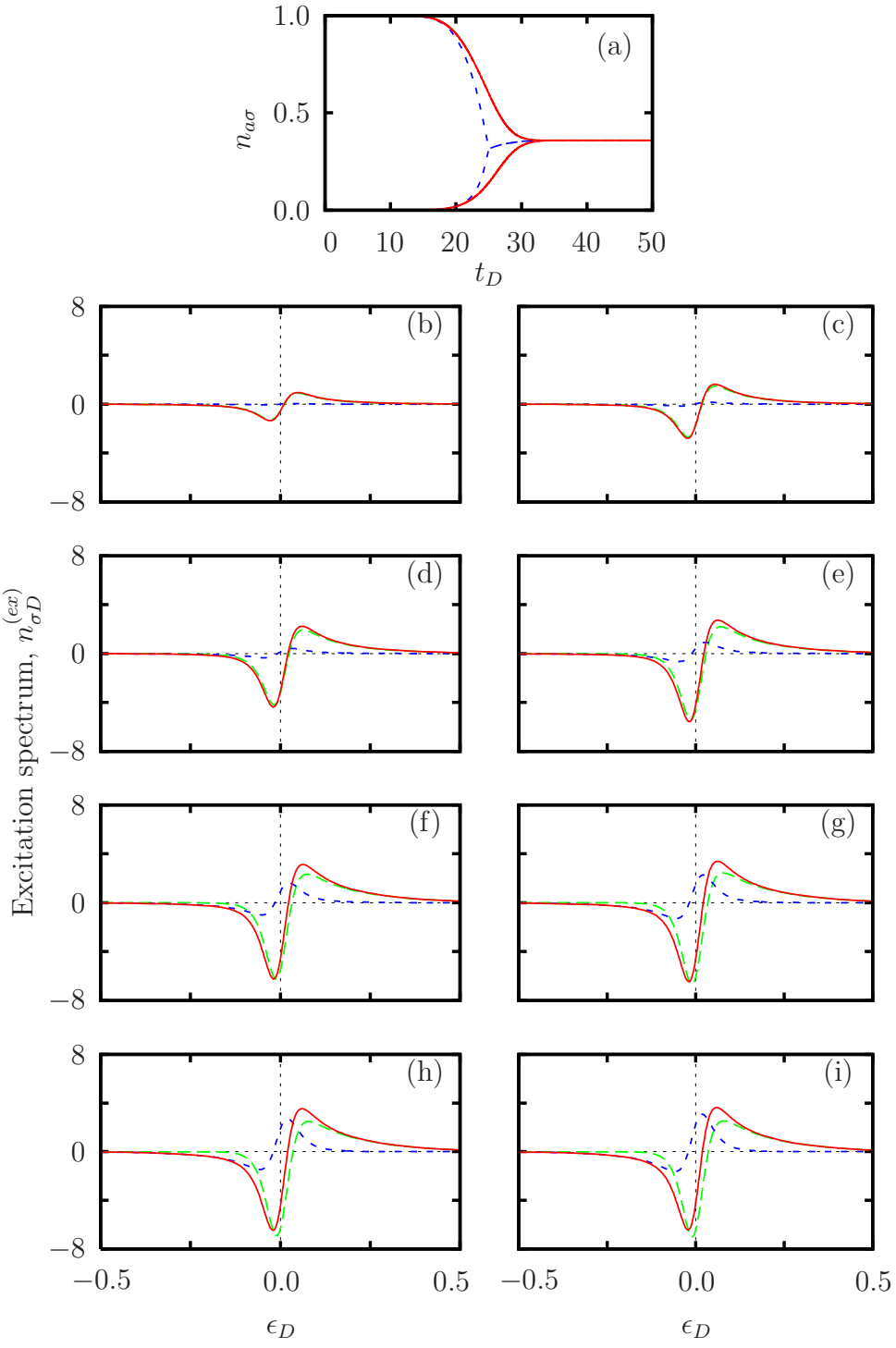


Figure 6.5: Excitation spectra snapshots for the $\epsilon_{aD} = -0.5$ model at times (b) $t_D = 22.00$, (c) $t_D = 23.25$, (d) $t_D = 24.50$, (e) $t_D = 25.75$, (f) $t_D = 27.00$, (g) $t_D = 28.25$, (h) $t_D = 29.50$, and (i) after $\Gamma_D$ variation has finished ($t_D = 50.00$). Panel (a) shows $n_{a\sigma}$ (solid red lines) and $n^{(ad)}_{a\sigma}$ (medium-dashed blue lines). In panels (b) to (i) solid red lines denote the total electronic excitation spectrum, long-dashed green line the majority ($\sigma =\uparrow$) component and medium-dashed blue lines the minority ($\sigma =\downarrow$) component.

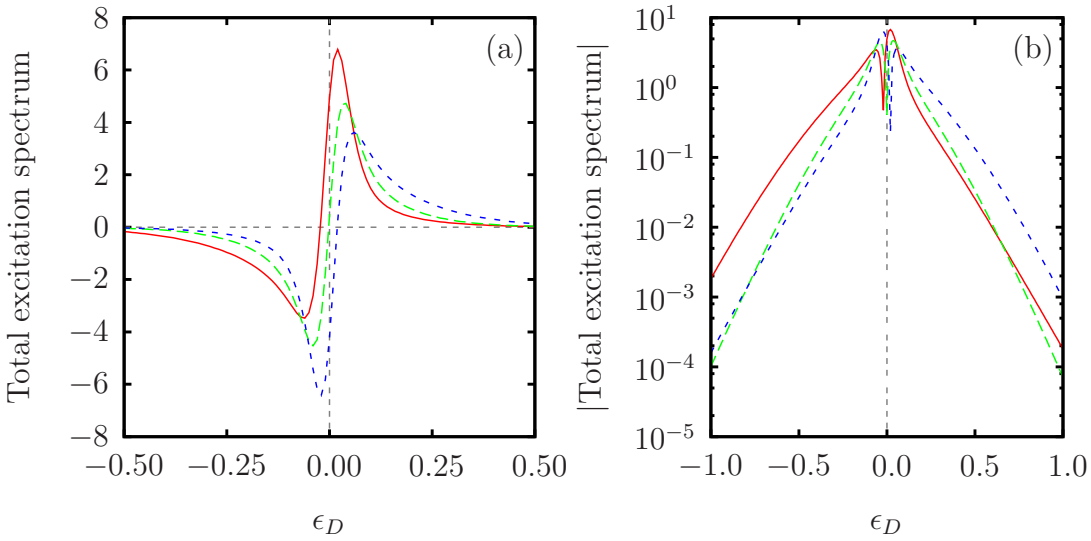


Figure 6.6: Comparison of the final total excitation spectra for the three model systems on (a) linear and (b) logarithmic scales. Solid red lines, long-dashed green lines and medium-dashed blue lines denote the $\epsilon_{aD} = -2.5$, $-1.5$ and $-0.5$ model systems respectively.

component more exaggerated than for majority spin. The $\epsilon_{aD} = -1.5$ model system has similar spectra of electrons above and holes below the Fermi level, with the minority spin component similar to a 180° rotation of the majority spin component. The $\epsilon_{aD} = -0.5$ system is similar to the reverse of the $\epsilon_{aD} = -2.5$ model; the spectrum of electrons above the Fermi level is larger than the hole excitations below, with the majority spin component more exaggerated than the minority component.

We can connect this behaviour to the variation in the occupations of the adsorbate energy levels. The excitation spectra for the $\epsilon_{aD} = -2.5$ and $\epsilon_{aD} = -0.5$ systems are dominated by the minority and majority spin components respectively, and it is these states which experience the largest change in occupation. In the $\epsilon_{aD} = -1.5$ system the magnitude of the charge transfer is similar for both spins, and the excitation spectra is evenly balanced between electrons and holes. This suggests that the spectra for any given system will be larger for the state with the greatest change in population, and that a net transfer of charge to the surface excites more high-energy electrons than holes, with the reverse true for charge transfer to the adsorbate.

Figure 6.6(a) shows the final ($t_D = 50$) total excitation spectra for the three model systems in the region around the Fermi level. This plot shows explicitly the differences between the three model systems – as $\epsilon_{aD}$ is moved closer to the Fermi energy, for example in the $\epsilon_{aD} = -0.5$ system, the high-energy electron tail becomes larger with a smaller peak close to $\epsilon_F$. Below the Fermi level this trend is reversed for the excited hole distribution.

Another interesting feature of this figure is the movement of the 'node' of the spectrum, the point at which the total excitation spectrum crosses zero. We might expect the excitation spectra for all systems to pass through zero at the Fermi level. However, this need only be true at zero system temperature. At finite temperature the Fermi function changes from one to zero over a range of several $k_B T_D$ around the Fermi level. As the Fermi function governs the initial occupation of the sea of metal states there will be some states immediately below $\epsilon_F$ which are not fully occupied, and some states just above $\epsilon_F$ which have a small occupation. It is therefore possible for electrons to be promoted to states just below and for holes to be excited just above the Fermi level. In the model calculations presented in this section a thermal energy of $k_B T_D = 0.02$ has been used, for which the variation in the Fermi function occurs primarily within the range $\epsilon_D = -0.1$ to 0.1. The nodes in our three model systems occur at $\epsilon_D = -0.022$, $-0.002$, and 0.019 (for $\epsilon_{aD} = -2.5$, $-1.5$ and $-0.5$ respectively) which is well within the range of variation of the Fermi function. Both the speed of variation $\dot{s}_D$ and the temperature of the system have an impact on the position of this node – this will be explored in sections 6.2.2 and 6.2.3.

Panel (b) of figure 6.6 shows the final total excitation spectrum for the three systems on a logarithmic scale. A number of features of these excitation spectra should be noted at this point. First, the spectra for all three systems away from the Fermi level are roughly exponential in nature for both electrons and holes. The electron spectrum at $\epsilon_D = 0.5$ is approximately 5.4 times larger for the $\epsilon_{aD} = -0.5$ system than for the $\epsilon_{aD} = -2.5$ model. For the hole spectra the reverse is true; at $\epsilon_D = -0.5$ the $\epsilon_{aD} = -2.5$ result is 6 times larger than for the $\epsilon_{aD} = -0.5$ system. In the $\epsilon_{aD} = -1.5$ system the gradients of the excitation spectra are similar for both electrons and holes, and are steeper than for either of the other model systems.

The excitation spectra for each of the systems are also spin-polarised, as shown

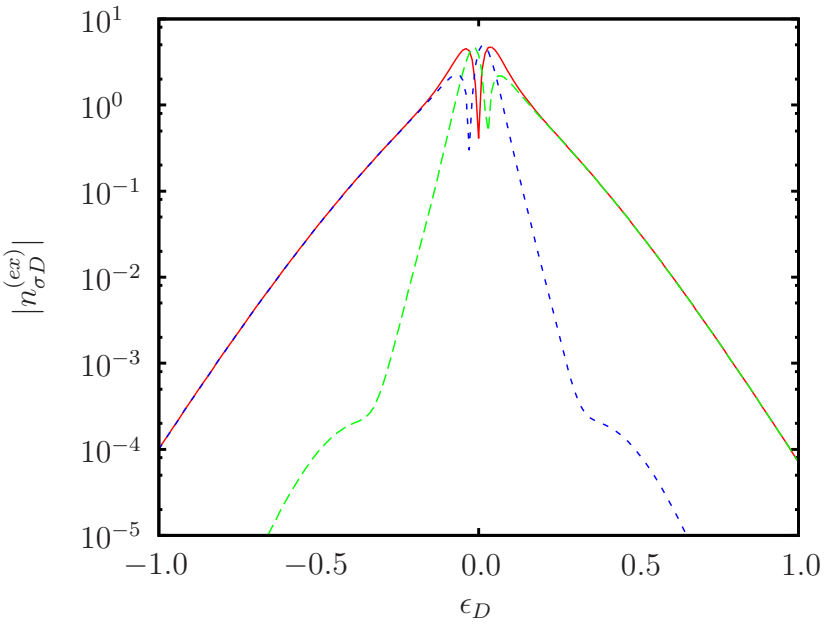


Figure 6.7: Breakdown of the excitation spectra for the $\epsilon_{aD} = -1.5$ model system into spin components on a logarithmic scale. Solid red lines denote the total excitation spectrum, long-dashed green lines the majority spin component and medium-dashed blue lines the minority spin component.

in figure 6.7. Above the Fermi level the excitation spectrum is dominated by the majority spin components; above $\epsilon_D = 0.2$ the excitations are comprised of at least 95% majority spin electrons. Below $\epsilon_F$ the minority spin dominates the hole spectra with less than 5% of the excitation spectra made up of majority spin excitations. We are unsure of the origin of the 'lumps' which can be seen in the minority excitation spectra in figure 6.7 at $\epsilon_D = 0.5$, and in the majority spectra at $\epsilon_D = -0.5$.

In section 5.2.2 we noted that the results for $\delta n_{a\sigma}$ for the $\epsilon_{aD} = -2.5$ and $\epsilon_{aD} = -0.5$ systems show a symmetry between the behaviour of electrons and holes within the Newns-Anderson model. This symmetry is also apparent in the excitation spectra presented in this chapter. To emphasise this the electron and hole spectra for the three systems are compared in figure 6.8. Panel (a) shows the electron spectra for the $\epsilon_{aD} = -2.5$ model system compared to the hole spectra for the $\epsilon_{aD} = -0.5$ model, with the reverse comparison in panel (b). The electron and hole spectra for the $\epsilon_{aD} = -1.5$ model system are compared in panel (c). In each of these figures there is a striking similarity between the hole spectra of one spin with the electron spectra of the opposite spin. We attribute the symmetry

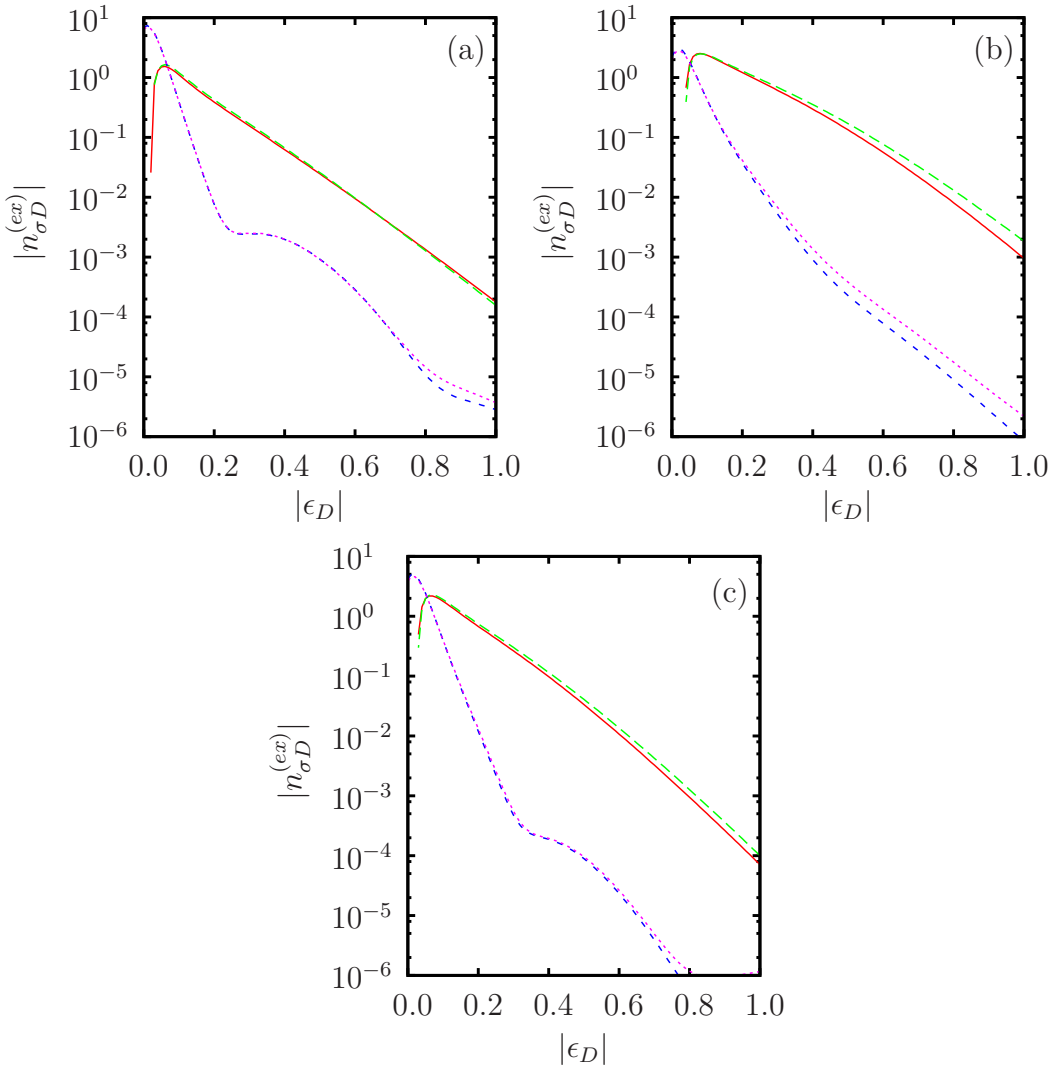


Figure 6.8: Demonstration of equivalence of electron and hole excitation spectra for the three model systems. In each panel the colours denote different electron/hole spin components; solid red lines = majority spin electrons, long-dashed green lines = minority spin holes, medium-dashed blue lines = minority spin electrons and short-dashed magenta lines = majority spin holes. In panel (a) the $\epsilon_{aD} = -2.5$ model electron excitations are compared to the $\epsilon_{aD} = -0.5$ hole excitations. Panel (b) shows the $\epsilon_{aD} = -0.5$ electron spectra compared to the $\epsilon_{aD} = -2.5$ hole spectra. The final panel, (c), shows a comparison of the electron and hole excitation spectra for the $\epsilon_{aD} = -1.5$ system.

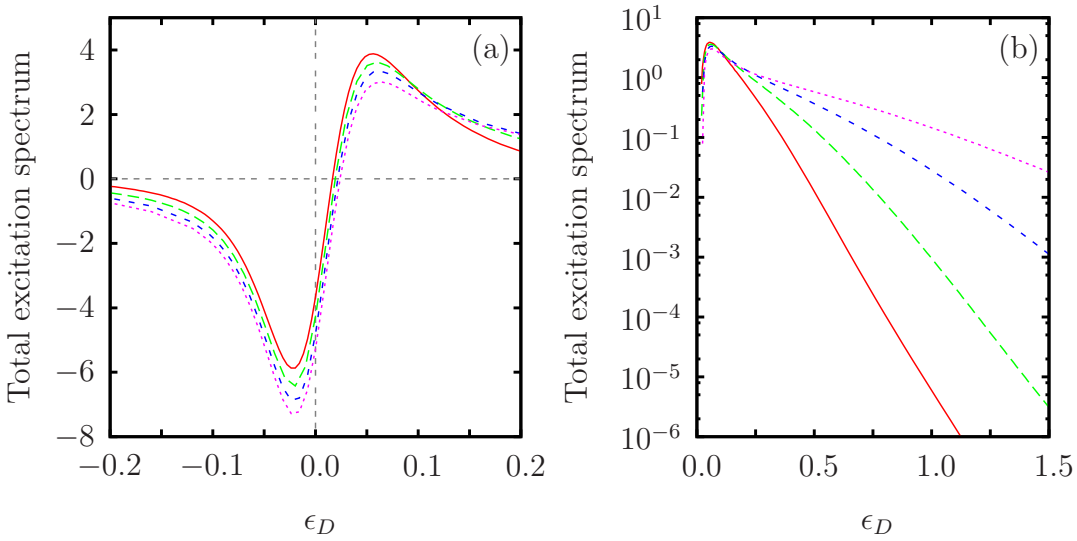


Figure 6.9: Final electron excitation spectra for the $\epsilon_{aD} = -0.5$ system at various speeds on (a) a linear scale and (b) a logarithmic scale. Colours represent different dimensionless speeds $\dot{s}_D$; $\dot{s}_D = 1/2$ (solid red lines), $\dot{s}_D = 1$ (long-dashed green lines), $\dot{s}_D = 2$ (medium-dashed blue lines) and $\dot{s}_D = 4$ (short-dashed magenta lines).

breaking which can be seen, particularly in figure 6.8(b), to the finite $\epsilon'_D$ range used in the calculations. Calculations with larger $\epsilon'_D$ grid ranges show smaller differences between the spectra of opposite spin and charge.

### 6.2.2 Effects of varying speed

As in the previous chapter (see section 5.2.2) we now consider the impact of the rate of $\Gamma_D$ variation on the evolution of the excitation spectrum. The variation in $\Gamma_D$ used in the previous section is again defined as corresponding to the dimensionless speed $\dot{s}_D = 1$. Different speeds are represented by a larger peak gradient $d\Gamma_D/dt_D$, and a shorter time over which $\Gamma_D$ is raised to a maximum.

Figure 6.9 shows the changes in the excitation spectra for the $\epsilon_{aD} = -0.5$ model system for four dimensionless speeds. As the speed is increased panel (a) shows the final electron spectrum changing; the peak in the electron spectrum close to $\epsilon_D = 0.05$ shrinks, while the high-energy tail grows. Below the node the magnitude of the hole spectrum also increases with speed, but with a larger

number of holes excited at all energies, rather than the shift in excitations seen for the electrons. The position of node of the excitation spectra also shifts away from the Fermi level as $\dot{s}_D$ is increased, implying that for higher speeds more electrons are excited from above, as well as below, $\epsilon_F$. Similar behaviour is seen in the $\epsilon_{aD} = -2.5$ system, but with the electron and hole spectra reversed. In the $\epsilon_{aD} = -1.5$ system both the electron and hole spectra are exaggerated at higher speeds, with little movement seen in the position of the node.

In figure 6.9(b) the excitation spectrum above the Fermi level is plotted for the same system on a logarithmic scale. The effect of $\dot{s}_D$ on the high-energy electron excitations is quite dramatic – as the speed is increased the rate of decay of the spectra with energy rapidly decreases. As these distributions are broadly exponential in nature, above around $\epsilon_D = 0.2$, the spectrum can be fitted to an exponential of the form $\exp(\lambda_D \epsilon_D)$. Here $\lambda_D$ is a dimensionless parameter describing the decay of the excitation spectrum at high energies.

By performing this fitting procedure on calculations performed at different speeds the dependence of $\lambda_D$ on $\dot{s}$ can be extracted, and is plotted for the three model systems in figure 6.10. In panel (a) of this figure the decay parameter $\lambda_D$ is plotted for the three model systems. These results show very similar values for the $\epsilon_{aD} = -2.5$ and $\epsilon_{aD} = -0.5$ systems, with a larger value for the $\epsilon_{aD} = -1.5$ model. At slow speeds the excitations become more confined to the region around the Fermi level, and this is seen as a sharp increase in the magnitude of $\lambda_D$ as zero velocity is approached. Above a dimensionless speed of around $\dot{s}_D = 1$ fitting results suggest that $\lambda_D$ is approximately inversely proportional to $\dot{s}_D$, while below this point a $\dot{s}_D^{-1/2}$ variation appears to be appropriate. These two domains are not obvious from figure 6.10(a) and we will therefore re-plot this data in a different form as described below.

Recent work by Nienhaus and co-workers [24,25] and Lindenblatt and Pehlke [33] has described the high-energy excitation spectra using an 'effective temperature' $T_{\text{eff}}$, by fitting their results to an $\exp(-\epsilon/k_B T_{\text{eff}})$ variation. The decay parameter used in figure 6.10(a) can be related to this effective temperature using

$$T_{\text{eff}} = -\frac{\Gamma_0}{k_B \lambda_D}, \tag{6.8}$$

where the scaling energy $\Gamma_0$ has been included to allow $T_{\text{eff}}$ to be expressed in

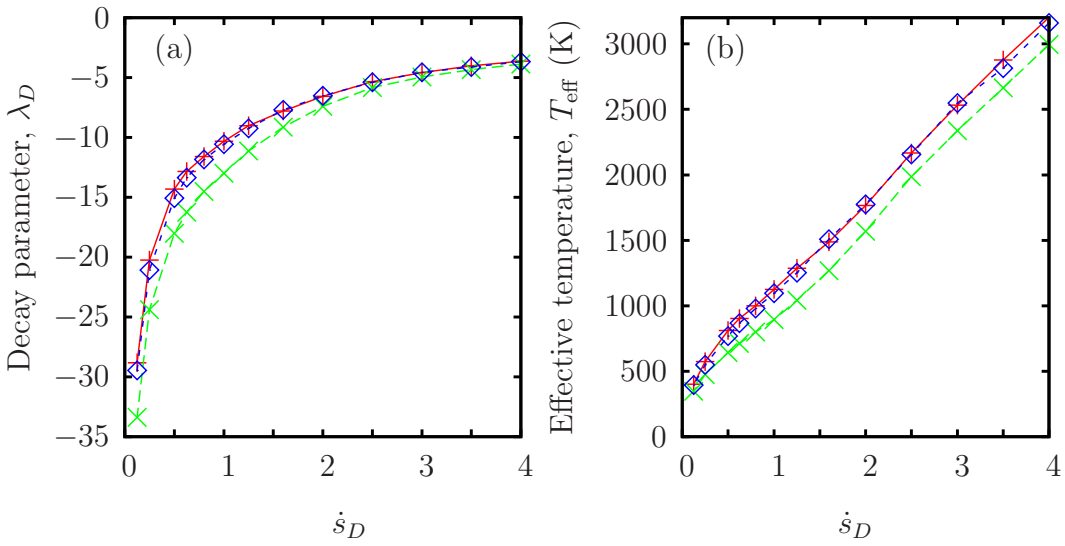


Figure 6.10: (a) Variation of the dimensionless decay parameter $\lambda_D$ with dimensionless speed $\dot{s}_D$. Solid red lines with '+' symbols denote results for the $\epsilon_{aD} = -2.5$ system, long-dashed green lines with '×' symbols relate to the $\epsilon_{aD} = -1.5$ system and medium-dashed blue lines with '◇' symbols correspond to the $\epsilon_{aD} = -0.5$ system. (b) the same data as (a), but re-expressed in terms of an 'effective temperature', $T_{\text{eff}}$, defined in (6.8), and $\Gamma_0$ has been taken to be one electron-Volt.

Kelvin. Figure 6.10(b) shows the dependence of $T_{\text{eff}}$ on the dimensionless speed $\dot{s}_D$ for the three model systems, with $\Gamma_0$ taken to be 1 eV. At high speeds the effective temperature is roughly linearly dependent on temperature, with results for the $\epsilon_{aD} = -1.5$ system approximately 200 K smaller than for the other models.

The results reported by Lindenblatt and Pehlke [33] describe a linear scaling between the effective temperature and $m^{-1/2}$ where $m$ is the mass of the hydrogen like adsorbate used in their calculations. As the potential well with which their hydrogenic atom is interacting is not affected by the adsorbate mass, the observed mass scaling is equivalent to $T_{\text{eff}} \propto \dot{s}_D$, i.e. the same behaviour as reported above. Lindenblatt and Pehlke also note that this variation is consistent with the friction based approach used by Trail and co-workers [28, 29].

However, at slow speeds $T_{\text{eff}}$ is roughly proportional to the square root of the speed, equivalent to a $m^{-1/4}$ scaling. This 'transition' is shown most clearly on the log-log plot in figure 6.11, where the three model systems show a 'kink' in

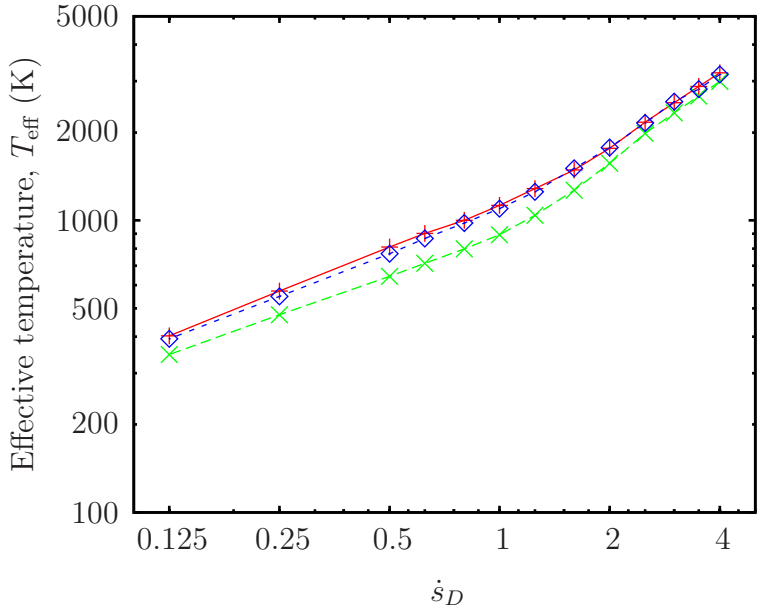


Figure 6.11: Effective temperature $T_{\text{eff}}$ as a function of speed as shown in figure 6.10(b), but on logarithmic axes.

their effective temperatures at around $\dot{s}_D = 1$. We are unable to explain this change in behaviour at this time.

### 6.2.3 Effects of varying temperature

In chapter 5, sections 5.2.3 and 5.3, we demonstrated that the system temperature has little impact on the adsorbate level occupations and energy transfer rates. We now consider the impact of the system temperature on the excitation process for each of the model systems. Experience suggests that some of the high-temperature effects only become important when the effective temperature and the system temperature are comparable. To make the temperature effects on the excitation process more obvious we therefore use a dimensionless speed of $\dot{s}_D = 1/2$ for each calculation presented in this section.

Figure 6.12 shows the total excitation spectrum for each system at five system temperatures. A number of features in these plots require comment. Close to the Fermi level there are significant differences between the calculations; at high temperatures the spectra have relatively shallow peaks of electrons and holes above and below $\epsilon_F$. As the temperature is reduced these peaks move towards the Fermi level and grow in size. For thermal energies below $k_B T_D = 0.005$ the peaks are very close to $\epsilon_F$ and the spectrum resembles a $1/(\epsilon_D - \epsilon_F)$ function.

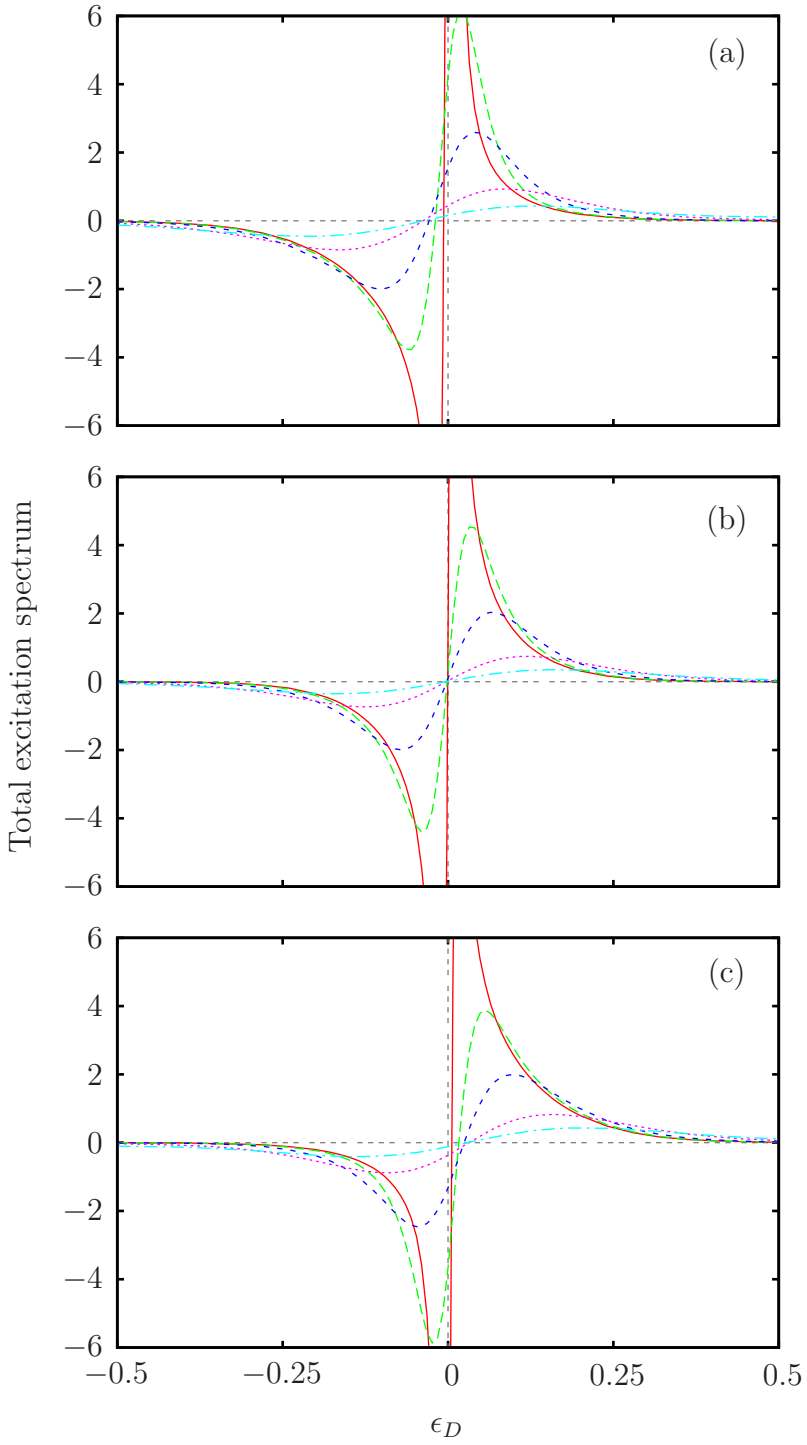


Figure 6.12: The impact on temperature on the final total excitation spectra for the (a) $\epsilon_{aD} = -2.5$, (b) $\epsilon_{aD} = -1.5$ and (c) $\epsilon_{aD} = -0.5$ model system. Different lines represent different thermal energies; solid red line - $k_B T_D = 0.005$ (58 K), long-dashed green line - $k_B T_D = 0.02$ (232 K), medium-dashed dark-blue line - $k_B T_D = 0.04$ (464 K), short-dashed magenta line - $k_B T_D = 0.08$ (928 K), dot-dashed light-blue line - $k_B T_D = 0.12$ (1391 K). Numbers in brackets denote the corresponding system temperatures assuming $\Gamma_0 = 1$ eV. All calculations are performed for a dimensionless speed of $\dot{s}_D = 1/2$.

The node of the spectra, discussed in the previous sections, shifts away from the Fermi level with increasing temperature for the $\epsilon_{aD} = -2.5$ and $-0.5$ systems.

To consider the impact of temperature on the high-energy tails of the excitation spectra more clearly, figure 6.12 has been re-plotted on a logarithmic scale in figure 6.13. Two high-energy effects of temperature can be seen in the electron and hole spectra for the three model systems. For thermal energies up to $k_B T_D = 0.04$, the tails of the electronic spectra become larger while the effective temperature remains approximately constant. This effect results in tails with a magnitude roughly 2.2 times larger for the $k_B T_D = 0.04$ spectra than for $k_B T_D = 0.005$, for both electrons and holes in the $\epsilon_{aD} = -1.5$ system. In order to interpret this behaviour we recall that at temperatures above zero there is a small population of electrons in the states just above the Fermi level. This population can be excited to high energies more easily, leading to an enhancement of the tail of the electron excitation spectrum. An equivalent argument can be made for the enhancement of the spectrum of excited holes.

At higher temperatures the effective temperature of the excitation spectra change, with the $k_B T_D = 0.12$ spectra in figure 6.13 noticeably different from those for lower temperatures. In the high temperature $\epsilon_{aD} = -2.5$ and $\epsilon_{aD} = -0.5$ plots there are 'lumps' in the spectra close to $\epsilon_D = 0.5$ and $-0.5$ respectively. Analysis of the contributions from the different terms in the electron distribution function (see equation (4.25) on page 92) suggests that the feature in the $\epsilon_{aD} = -2.5$ model is due to the adsorbate minority state having a significant occupation ($n_{a\downarrow}(t_0) = 0.0152$) at the start of the calculation. As the initial energy level for the minority state in the $\epsilon_{aD} = -2.5$ model is at $\epsilon_D = 0.5$ there is an extra contribution to the excitation spectrum in this region. As expected by electron hole-symmetry, the same feature in the $\epsilon_{aD} = -0.5$ model is due to the deviation of the initial majority spin occupation from one electron ($n_{a\uparrow}(t_0) = 0.985$).

By fitting the excitation spectra above $\epsilon_D = 0.5$ to an exponential of the form $\exp(-\epsilon_D / k_B T_{eff,D})$ the variation of effective temperature with system temperature can be obtained. This variation has been plotted in figure 6.14 with the scaling energy $\Gamma_0$ taken to be 1 eV to allow real units to be used. Figure 6.14 shows two domains; below around 400K the effective temperature is independent of the system temperature and is roughly constant. Above $T \approx T_{\text{eff}}$, 700 K for the $\epsilon_{aD} = -1.5$ model, and 800-900 K for the $\epsilon_{aD} = -2.5$ and $-0.5$ models, the vari-

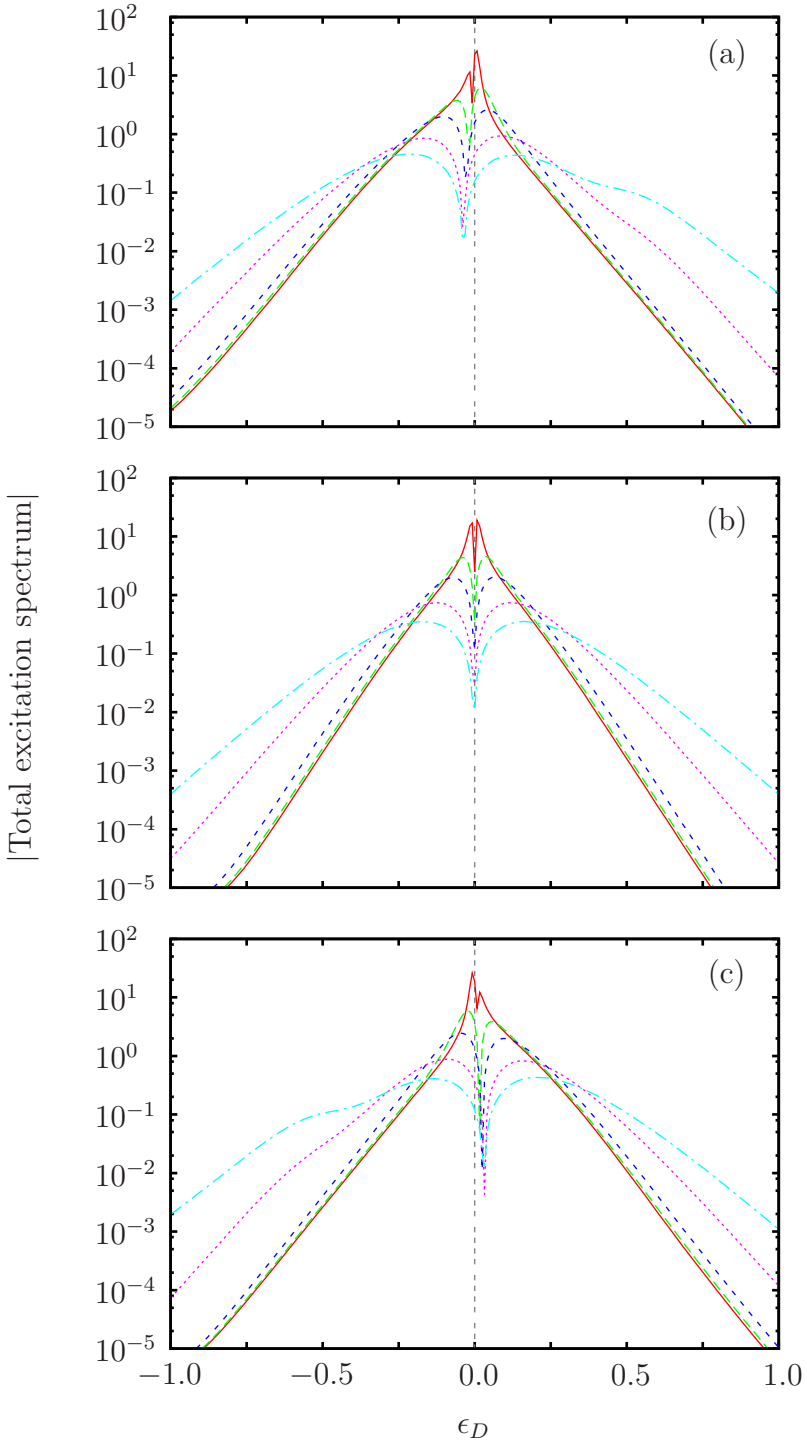


Figure 6.13: The impact on temperature on the final total excitation spectra on a logarithmic scale for the (a) $\epsilon_{aD} = -2.5$, (b) $\epsilon_{aD} = -1.5$ and (c) $\epsilon_{aD} = -0.5$ model systems. Colours denote the same thermal energies or temperatures used in figure 6.12.

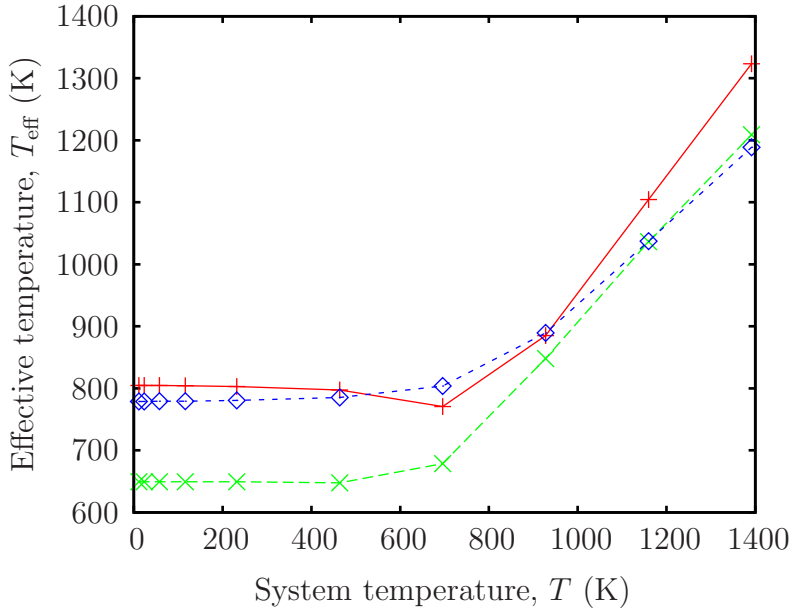


Figure 6.14: Effective temperature as a function of system temperature. Solid red lines relate to the $\epsilon_{aD} = -2.5$ system, long-dashed green lines relate to the $\epsilon_{aD} = -1.5$ system and medium-dashed blue lines relate to the $\epsilon_{aD} = -0.5$ system. The scaling energy $\Gamma_0$ has been taken to be 1 eV.

ation of $T_{\text{eff}}$ with $T$ is approximately linear. At higher dimensionless speeds, $\dot{s}_D$, a similar behaviour is observed, with $T_{\text{eff}}$ constant at low system temperatures, but thermal effects appearing when $T \approx T_{\text{eff}}$.

The onset of this behaviour can be understood by considering the excitation process. The excitation of the electronic system moves electrons from one state to another – at zero temperature this would only be the promotion of electrons from below the Fermi level to above it. At finite temperatures small excitations can move electrons from just above the Fermi level to further above, or from well below to just below $\epsilon_F$. We expect that the increase in the separation of the peaks of electrons and holes at higher temperatures is due to this process. The transition between the two regimes of $T_{\text{eff}}$ variation can also be understood by considering these low-energy excitations. For large system temperatures the low-energy excitations are widely spread around the Fermi energy giving a contribution to the excitation spectrum with an effective temperature which is the same as the system temperature. At these large system temperatures the high-energy excitations will also be spread over a much wider range of energies, resulting in a reduced contribution to the overall excitation spectrum. The results shown in figure 6.14 suggest that the transition between the dominance of the high-energy

and low-energy contributions to the excitation occurs when $T$ exceeds the low temperature value of $T_{\text{eff}}$.

## 6.3 Conclusions

In this chapter we have introduced the methods used to numerically compute the time-evolving and instantaneous electron distribution functions, from which the spectrum of electronic excitations can be obtained.

Through the calculations described in section 6.2.1 we have seen a number of interesting phenomena in the excitation spectra. Figures 6.3 to 6.5 show the evolution of $n_{\sigma D}^{(ex)}$ occurring primarily while the variation of the width $\Gamma_D$ is largest. Above the Fermi level the excitation spectra consist of a peak of low energy electrons extending to an exponential tail (see figure 6.6) at high energies, while below $\epsilon_F$ there are similar features in the spectra of excited holes. By changing the parameters governing the evolution of the system the balance between these features is altered. For example the $\epsilon_{aD} = -2.5$ model system excites more low-energy electrons and high-energy holes than the other model systems, while the high-energy electron and low-energy hole components are reduced. These excitations are also spin-polarised – in figure 6.7 $n_{\sigma D}^{(ex)}$ is plotted for each spin for the $\epsilon_{aD} = -1.5$ system, demonstrating that at high energies excitations are dominated by majority spin electrons and minority spin holes.

The 'node' of the excitation spectra, the point at which $\sum_\sigma n_{\sigma D}^{(ex)} = 0$, is not fixed to the Fermi level as might be expected. We have seen that the position of the node in the total excitation spectrum depends upon the position of the energy levels (figure 6.6), the speed of parameter variation (figure 6.9) and temperature (figure 6.12).

In section 6.2.2 the effect of the speed of parameter variation $\dot{s}_D$ on the excitation spectra is explored. We have observed significant variation in the shape of the exponential high-energy tails which can be represented using the effective temperature $T_{\text{eff}}$ defined in equation (6.8). Figure 6.11 shows that the dependence of $T_{\text{eff}}$ on $\dot{s}_D$ consists of two domains; at high-speed there is an approximately linear variation, while at low speeds a square-root dependence on speed appears to be more appropriate. The high-speed behaviour is consistent with that reported by Lindenblatt and Pehlke [33], but that for slow speeds is unexpected.

The impact of the system temperature on the excitation process has been explored in section 6.2.3. Close to the Fermi level the structure of the excitation spectrum, as shown in figure 6.12, changes from a $1/(\epsilon_D - \epsilon_F)$ singularity at low temperatures to a smooth variation at higher temperatures. Away from the Fermi level temperature has two effects; for surface temperatures close to, but below, the effective temperature of the excitations an enhancement of the spectrum is observed. At high temperatures thermal effects start to dominate, with the effective temperature approaching the system temperature.

We finally note that the majority of the points made in this conclusion, and indeed this chapter, are observations of the behaviour of the model with little in the way of interpretation in terms of the underlying physical processes. We have found that the structure of the electron distribution function has prevented us from attributing any particular feature of the excitation spectrum to a particular term in the electron distribution function. It has therefore not been possible to gain a strong physical insight into the excitation process.

# Appendix G: The analytic window approximation

In this appendix we use the 'analytic window' approximation, described on page 158, to obtain expressions for the $\eta \to 0^+$ limit of the final three terms in the electron distribution function $n_\sigma$.

The fifth term in $n_\sigma$, (4.25), can be written as

$$\begin{aligned} n_\sigma^{(5)}(\epsilon,t) &= \frac{2}{\pi}\mathrm{Re}\left\{p_\sigma^{(inst)}(\epsilon,t)\right\}\mathrm{PV}_\alpha\int d\epsilon'\frac{f(\epsilon')}{\epsilon-\epsilon'}\mathrm{Im}\left\{p_\sigma(\epsilon',t)\right\} \\ &\quad +\frac{2}{\pi}\int_{\epsilon-\alpha}^{\epsilon+\alpha}d\epsilon' f(\epsilon')\mathrm{Im}\left\{p_\sigma(\epsilon',t)\right\}\mathrm{Re}\left\{\frac{p_\sigma^{(inst)}(\epsilon,t)}{\epsilon-\epsilon'+i\eta}\right\}, \end{aligned} \tag{G.1}$$

where $\eta$ has been dropped from the first term as the $\mathrm{PV}_\alpha$ integral does not cover the region in which it is important. We now expand the product $f(\epsilon')p_\sigma(\epsilon',t)$ in the second term on the right-hand side as a Taylor series about $\epsilon'=\epsilon$, yielding to first order in $\alpha$

$$\begin{aligned} n_\sigma^{(5)}(\epsilon,t) &= \frac{2}{\pi}\mathrm{Re}\left\{p_\sigma^{(inst)}(\epsilon,t)\right\}\mathrm{PV}_\alpha\int d\epsilon\frac{f(\epsilon')}{\epsilon-\epsilon'}\mathrm{Im}\left\{p_\sigma(\epsilon',t)\right\} \\ &\quad +\frac{2}{\pi}\mathrm{Re}\left\{p_\sigma^{(inst)}(\epsilon,t)\int_{\epsilon-\alpha}^{\epsilon+\alpha}\frac{d\epsilon'}{\epsilon-\epsilon'+i\eta}\right\}f(\epsilon)\mathrm{Im}\left\{p_\sigma(\epsilon,t)\right\} \\ &\quad +\frac{2}{\pi}\mathrm{Re}\left\{p_\sigma^{(inst)}(\epsilon,t)\int_{\epsilon-\alpha}^{\epsilon+\alpha}d\epsilon'\frac{\epsilon-\epsilon'}{\epsilon-\epsilon'+i\eta}\right\}\frac{\partial}{\partial\epsilon}\Big[f(\epsilon)\mathrm{Im}\left\{p_\sigma(\epsilon,t)\right\}\Big]. \end{aligned} \tag{G.2}$$

The $\epsilon'$ integrals in the second and third terms of this expression can be performed analytically in the $\eta\to0^+$ limit, giving

$$\begin{aligned} \lim_{\eta\to0^+}\int_{\epsilon-\alpha}^{\epsilon+\alpha}\frac{d\epsilon'}{\epsilon-\epsilon'+i\eta} &= -\lim_{\eta\to0^+}\left[\ln(\epsilon-\epsilon'+i\eta)\right]_{\epsilon-\alpha}^{\epsilon+\alpha} \\ &= -\lim_{\eta\to0^+}\left[\frac{1}{2}\ln\left|(\epsilon-\epsilon')^2+\eta^2\right|+i\arg(\epsilon-\epsilon'+i\eta)\right]_{\epsilon-\alpha}^{\epsilon+\alpha} \\ &= -i\lim_{\eta\to0^+}\left(\arg(-\alpha+i\eta)-\arg(\alpha+i\eta)\right) \\ &= -i\pi, \end{aligned} \tag{G.3}$$

$$\lim_{\eta\to 0^+}\int_{\epsilon-\alpha}^{\epsilon+\alpha} d\epsilon' \frac{\epsilon'-\epsilon}{\epsilon-\epsilon'+i\eta} = \lim_{\eta\to 0^+}\int_{\epsilon-\alpha}^{\epsilon+\alpha} d\epsilon' \left(-1+\frac{i\eta}{\epsilon-\epsilon'+i\eta}\right) = -2\alpha. \quad \text{(G.4)}$$

On substitution of these expressions into G.2 we obtain

$$\begin{aligned} n_\sigma^{(5)}(\epsilon,t) &= 2\sqrt{\frac{\Gamma(t)}{2\pi}}\rho_{a\sigma}^{(inst)}(\epsilon,t)\mathrm{PV}_\alpha\int d\epsilon' \frac{f(\epsilon')}{\epsilon-\epsilon'}\mathrm{Im}\left\{p_\sigma(\epsilon',t)\right\} \\ &\quad +2\sqrt{\frac{2\pi}{\Gamma(t)}}(\epsilon-\bar{\epsilon}_{a\sigma}(t))\rho_{a\sigma}^{(inst)}(\epsilon,t)f(\epsilon)\mathrm{Im}\{p_\sigma(\epsilon,t)\} \\ &\quad -4\alpha\sqrt{\frac{\Gamma(t)}{2\pi}}\rho_{a\sigma}^{(inst)}(\epsilon,t)\left(\frac{df}{d\epsilon}\,\mathrm{Im}\{p_\sigma(\epsilon,t)\}+f(\epsilon)\mathrm{Im}\left\{\frac{\partial p_\sigma}{\partial\epsilon}(\epsilon,t)\right\}\right), \end{aligned} \quad \text{(G.5)}$$

where the definitions of $\rho_{a\sigma}^{(inst)}$, (4.24), and $p_\sigma^{(inst)}$, (4.26) have been used.

By using the same method an approximation for the sixth term in (4.25) can be found. $n_\sigma^{(6)}$ is expanded in a similar manner to (G.1), giving to first order in $\alpha$

$$\begin{aligned} n_\sigma^{(6)}(\epsilon,t) &= -2\sqrt{\frac{\Gamma(t)}{2\pi}}\mathrm{PV}_\alpha\int d\epsilon' \frac{f(\epsilon')}{\epsilon-\epsilon'}\mathrm{Im}\left\{q_\sigma^*(\epsilon,\epsilon',t)p_\sigma^{(inst)}(\epsilon,t)\right\} \\ &\quad -2\sqrt{\frac{\Gamma(t)}{2\pi}}\mathrm{Im}\left\{p_\sigma^{(inst)}(\epsilon,t)f(\epsilon)q_\sigma^*(\epsilon,\epsilon,t)\int_{\epsilon-\alpha}^{\epsilon+\alpha}\frac{d\epsilon'}{\epsilon-\epsilon'+i\eta}\right\} \\ &\quad -2\sqrt{\frac{\Gamma(t)}{2\pi}}\mathrm{Im}\left\{p_\sigma^{(inst)}(\epsilon,t)\frac{\partial}{\partial\epsilon'}\left[f(\epsilon')q_\sigma^*(\epsilon,\epsilon',t)\right]\Big|_{\epsilon'=\epsilon}\right. \\ &\qquad \left.\times\int_{\epsilon-\alpha}^{\epsilon+\alpha} d\epsilon'\frac{\epsilon'-\epsilon}{\epsilon-\epsilon'+i\eta}\right\}. \end{aligned} \quad \text{(G.6)}$$

The $\epsilon'$ integrals in the second and third terms in this equation are the same as those evaluated in (G.3) and (G.4), and $n_\sigma^{(6)}$ therefore becomes

$$\begin{aligned} n_\sigma^{(6)}(\epsilon,t) &= -2\sqrt{\frac{\Gamma(t)}{2\pi}}\mathrm{PV}_\alpha\int d\epsilon' \frac{f(\epsilon')}{\epsilon-\epsilon'}\mathrm{Im}\left\{q_\sigma^*(\epsilon,\epsilon',t)p_\sigma^{(inst)}(\epsilon,t)\right\} \\ &\quad +2\sqrt{2\pi\Gamma(t)}f(\epsilon)\mathrm{Re}\left\{p_\sigma^{(inst)}(\epsilon,t)q_\sigma^*(\epsilon,\epsilon,t)\right\} \\ &\quad +4\alpha\sqrt{\frac{\Gamma(t)}{2\pi}}\mathrm{Im}\left\{p_\sigma^{(inst)}(\epsilon,t)\frac{\partial}{\partial\epsilon'}\left[f(\epsilon')q_\sigma^*(\epsilon,\epsilon',t)\right]\Big|_{\epsilon'=\epsilon}\right\}. \end{aligned} \quad \text{(G.7)}$$

To complete this expansion the derivative $\frac{\partial q_\sigma(\epsilon,\epsilon',t)}{\partial\epsilon'}$ is required. Differentiation of

(4.27) gives

$$\begin{aligned}\frac{\partial q_\sigma}{\partial \epsilon'}(\epsilon,\epsilon',t) &= \int_{t_0}^{t} dt_1 \sqrt{\frac{\Gamma(t_1)}{2\pi}} \frac{\partial p_\sigma}{\partial \epsilon'}(\epsilon',t_1)\exp[i(\epsilon-\epsilon')(t_1-t)] \\ &\quad + \int_{t_0}^{t} dt_1 \sqrt{\frac{\Gamma(t_1)}{2\pi}} p_\sigma(\epsilon',t_1).-i(t_1-t)\exp[i(\epsilon-\epsilon')(t_1-t)],\end{aligned} \tag{G.8}$$

which, when evaluated at $\epsilon' = \epsilon$, becomes

$$\begin{aligned}\frac{\partial q_\sigma}{\partial \epsilon'}(\epsilon,\epsilon',t)\big|_{\epsilon'=\epsilon} &= \int_{t_0}^{t} dt_1 \sqrt{\frac{\Gamma(t_1)}{2\pi}} \left(\frac{\partial p_\sigma}{\partial \epsilon}(\epsilon,t_1) - i(t_1-t)p_\sigma(\epsilon,t_1)\right) \\ &= \int_{t_0}^{t} dt_1 \sqrt{\frac{\Gamma(t_1)}{2\pi}} \left(\frac{\partial p_\sigma}{\partial \epsilon}(\epsilon,t_1) - i(t_1-t_0)p_\sigma(\epsilon,t_1)\right) \\ &\quad + i(t-t_0)q_\sigma(\epsilon,\epsilon,t).\end{aligned} \tag{G.9}$$

The separation of the integral in this expression into two terms allows us to maintain the ability to compute the evolution of the excitation spectra. By substituting (G.9) into (G.7), we obtain our final expression for $n_\sigma^{(6)}$;

$$\begin{aligned}n_\sigma^{(6)}(\epsilon,t) &= -2\sqrt{\frac{\Gamma(t)}{2\pi}}\mathrm{PV}_\alpha \int d\epsilon' \frac{f(\epsilon')}{\epsilon-\epsilon'}\mathrm{Im}\left\{q_\sigma^*(\epsilon,\epsilon',t)p_\sigma^{(inst)}(\epsilon,t)\right\} \\ &\quad + (2\pi - 4\alpha(t-t_0))\sqrt{\frac{\Gamma(t)}{2\pi}} f(\epsilon)\mathrm{Re}\left\{q_\sigma^*(\epsilon,\epsilon,t)p_\sigma^{(inst)}(\epsilon,t)\right\} \\ &\quad + 4\alpha\sqrt{\frac{\Gamma(t)}{2\pi}}\frac{df}{d\epsilon}\,\mathrm{Im}\left\{q_\sigma^*(\epsilon,\epsilon,t)p_\sigma^{(inst)}(\epsilon,t)\right\} \\ &\quad + 4\alpha\sqrt{\frac{\Gamma(t)}{2\pi}} f(\epsilon)\mathrm{Im}\left\{p_\sigma^{(inst)}(\epsilon,t)\right. \\ &\qquad \left.\times \int_{t_0}^{t} dt_1 \sqrt{\frac{\Gamma(t_1)}{2\pi}}\left(\frac{\partial p_\sigma^*}{\partial \epsilon}(\epsilon,t_1) + i(t_1-t_0)p_\sigma^*(\epsilon,t_1)\right)\right\}.\end{aligned} \tag{G.10}$$

The final term in $n_\sigma$, (4.25), requires some manipulation before the analytic window approximation is employed due to the $1/(\epsilon-\epsilon')^2$ dependence of the

integrand. Integration of $n_\sigma^{(7)}$ by parts yields

$$\begin{aligned} n_\sigma^{(7)}(\epsilon,t) &= \frac{1}{\pi}\sqrt{\frac{\Gamma(t)}{2\pi}}\mathrm{Re}\left\{p_\sigma^{(inst)}(\epsilon,t)\left(\left[\frac{f(\epsilon')}{\epsilon-\epsilon'+i\eta}\right]_{\epsilon'_-}^{\epsilon'_+}-\int d\epsilon'\frac{df}{d\epsilon'}\frac{1}{\epsilon-\epsilon'+i\eta}\right)\right\} \\ &= -\frac{\Gamma(t)}{2\pi}.\frac{\rho_{a\sigma}^{(inst)}(\epsilon,t)}{(\epsilon-\epsilon'_-)}-\frac{1}{\pi}\sqrt{\frac{\Gamma(t)}{2\pi}}\int d\epsilon'\frac{df}{d\epsilon'}\mathrm{Re}\left\{\frac{p_\sigma^{(inst)}(\epsilon,t)}{\epsilon-\epsilon'+i\eta}\right\}, \quad \text{(G.11)} \end{aligned}$$

where $\epsilon'_+$ and $\epsilon'_-$ are the upper and lower bounds of the $\epsilon'$ integration range, and we have assumed that $f(\epsilon'_+)=0$ and $f(\epsilon'_-)=1$. The analytic window approximation can now be applied giving, to first order in $\alpha$,

$$\begin{aligned} n_\sigma^{(7)}(\epsilon,t) &= -\frac{\Gamma(t)}{2\pi}.\frac{\rho_{a\sigma}^{(inst)}(\epsilon,t)}{(\epsilon-\epsilon'_-)}-\frac{\Gamma(t)}{2\pi}\rho_{a\sigma}^{(inst)}(\epsilon,t)\mathrm{PV}_\alpha\int d\epsilon'\frac{df}{d\epsilon'}\frac{1}{\epsilon-\epsilon'} \\ &\quad -\frac{1}{\pi}\sqrt{\frac{\Gamma(t)}{2\pi}}\mathrm{Re}\left\{p_\sigma^{(inst)}(\epsilon,t)\frac{df}{d\epsilon}\int_{\epsilon-\alpha}^{\epsilon+\alpha}\frac{d\epsilon'}{\epsilon-\epsilon'+i\eta}\right\} \\ &\quad -\frac{1}{\pi}\sqrt{\frac{\Gamma(t)}{2\pi}}\mathrm{Re}\left\{p_\sigma^{(inst)}(\epsilon,t)\frac{d^2f}{d\epsilon^2}\int_{\epsilon-\alpha}^{\epsilon+\alpha}d\epsilon'\frac{\epsilon'-\epsilon}{\epsilon-\epsilon'+i\eta}\right\}. \quad \text{(G.12)} \end{aligned}$$

Combination of this expression with (G.3) and (G.4) yields our final expression for $n_\sigma^{(7)}$;

$$\begin{aligned} n_\sigma^{(7)}(\epsilon,t) &= -\frac{\Gamma(t)}{2\pi}.\frac{\rho_{a\sigma}^{(inst)}(\epsilon,t)}{(\epsilon-\epsilon'_-)}-\frac{\Gamma(t)}{2\pi}\rho_{a\sigma}^{(inst)}(\epsilon,t)\mathrm{PV}_\alpha\int d\epsilon'\frac{df}{d\epsilon'}\frac{1}{\epsilon-\epsilon'} \\ &\quad -(\epsilon-\bar{\epsilon}_{a\sigma}(t))\frac{df}{d\epsilon}\rho_{a\sigma}^{(inst)}(\epsilon,t)+\frac{\alpha\Gamma(t)}{\pi}\frac{d^2f}{d\epsilon^2}\rho_{a\sigma}^{(inst)}(\epsilon,t). \quad \text{(G.13)} \end{aligned}$$

# Chapter 7

# Case study: Hydrogen isotopes approaching copper and silver surfaces

In this chapter we use the model constructed in chapters 2 to 4 to investigate the excitation of electrons and holes in a set of real systems. Calculations of the excitation spectra for these systems will allow us to make direct comparisons with experimental results.

We have chosen to consider hydrogen isotopes approaching the (111) surfaces of copper and silver. These choices will allow direct comparisons to be made with the experiments reported by Nienhaus and co-workers [18, 20, 22, 25], as discussed in the introduction.

To obtain the parameter variations needed to simulate the H/Cu and H/Ag systems we have performed a set of density functional theory (DFT) calculations, a description of which (along with the parameter extraction procedure) is presented in section 7.1. These parameters are used in sections 7.2 and 7.3 to consider first the occupation of the adsorbate states and the energy transfer behaviour, and then the electronic excitations induced by the adsorption. In both of these sections results will be presented for hydrogen and deuterium atoms approaching copper and silver surfaces, with the latter adsorbate represented by slowing the parameter variation by a factor of $\sqrt{2}$. In section 7.3 we will use the excitation

spectra to estimate the probability of an electron being excited with sufficient energy to be detected in the thin-film Schottky diodes used by Nienhaus and co-workers to measure chemicurrents. A summary of the important results and their implications is given in section 7.4.

## 7.1 DFT calculations and parameter extraction

To use our model to simulate the adsorption of a hydrogen atom on a metal surface an appropriate set of parameters are required. In this section the method we have used to obtain the variation of the parameters of the Newns-Anderson model is described in detail for the H/Cu (111) system, with final results also presented for H/Ag (111).

We have used the DFT code CASTEP (version 3.0) [72] to perform calculations of a supercell containing a static hydrogen atom above a metal surface. The copper and silver (111) surfaces are modelled using a slab geometry consisting of five-layers of atoms, with an equivalent thickness of vacuum above. For the copper and silver surfaces the bulk lattice parameter is fixed at the experimental values of 3.614 Å and 4.085 Å respectively [73]. In each system a $2 \times 2$ in-plane supercell is used, with ultrasoft Vanderbilt pseudopotentials [74] representing the atomic cores of both the substrate atoms and the hydrogen adsorbate. The hydrogen atom is placed at a fixed altitude above an atop site of the metal surface. A Cunningham k-point set [75] consisting of 6 special points in the irreducible wedge of the surface Brillouin zone[1] is used to perform calculations in reciprocal space and a Fermi surface smearing width of 0.25 eV was applied. The Perdew, Burke and Ernzerhof (PBE) [76] exchange-correlation function was used and the plane-wave cutoffs were set to 290 eV for the copper system and 300 eV for silver.

A total of 88 calculations (60 for H/Cu and 28 for H/Ag) were performed, each consisting of a self-consistent total energy run followed by a band-structure calculation, for H-atom altitudes in the range 1-3.5 Å. The total energy calculations return the total energy and the spin-polarisation of the system, in addition to the self-consistent electron densities and potentials required to perform the band-structure calculations. By subtracting the energy of an isolated hydrogen atom and the surface slab from the total energy of the combined system the surface

[1] By symmetry this gives 54 points in the whole surface Brillouin zone.

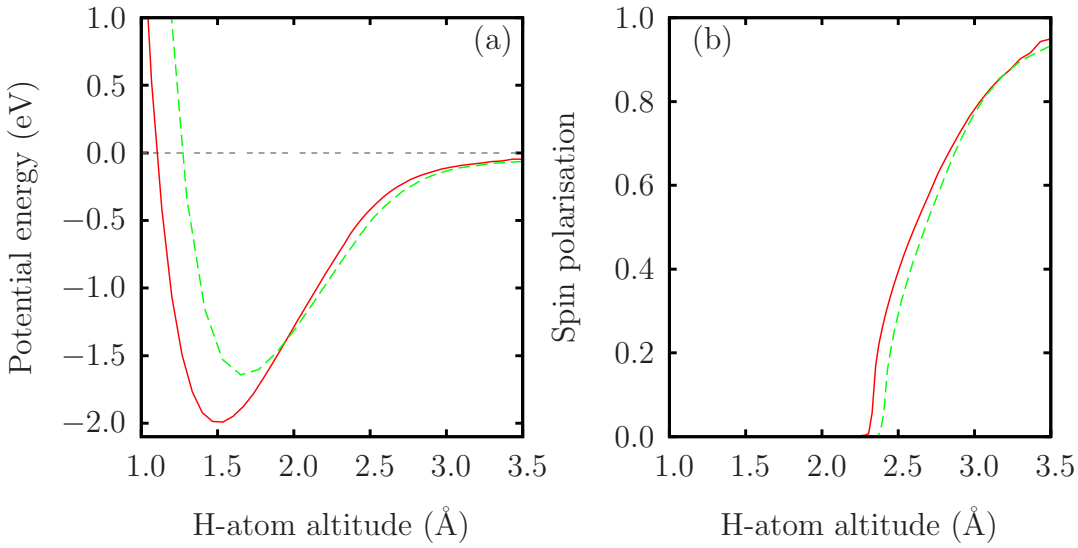


Figure 7.1: (a) Surface potential well and (b) Spin polarisation of the H/Cu (111) [solid red lines] and H/Ag (111) [dashed green lines] systems.

potential well is obtained – this is plotted, along with the spin polarisation, for both systems in figure 7.1 The two systems display similar surface potential wells, with the minimum in the H/Ag system around 0.1 Å further from the surface than for H/Cu. Both systems also display a sharp spin transition at 2.3 and 2.4 Å, for H/Cu and H/Ag respectively (see figure 7.1(b)), which has a square-root like dependence on altitude.

Following the total energy runs, band-structure calculations give details of the electronic states of each spin up to around 10 eV above the Fermi level. By weighting the results from each of the k-points appropriately and applying Gaussian smoothing with a width of 0.11 eV we obtain the projected density of states (PDOS) onto the hydrogen 1s orbital. Previous work in the literature (see for example work by Niedfeldt, Carter and Nordlander [77–79]) has also used these PDOS to investigate adsorbate-surface interactions.

The PDOS for the H/Cu system is shown for several different altitudes in figure 7.2. Far away from the surface the majority spin PDOS consists of a sharp peak with a width dominated by the Gaussian smoothing parameter (0.11 eV), while the minority resonance is significantly broader, as shown in panels (a) and (b) of figure 7.2. At lower H-atom altitudes the PDOS become broader as the strength

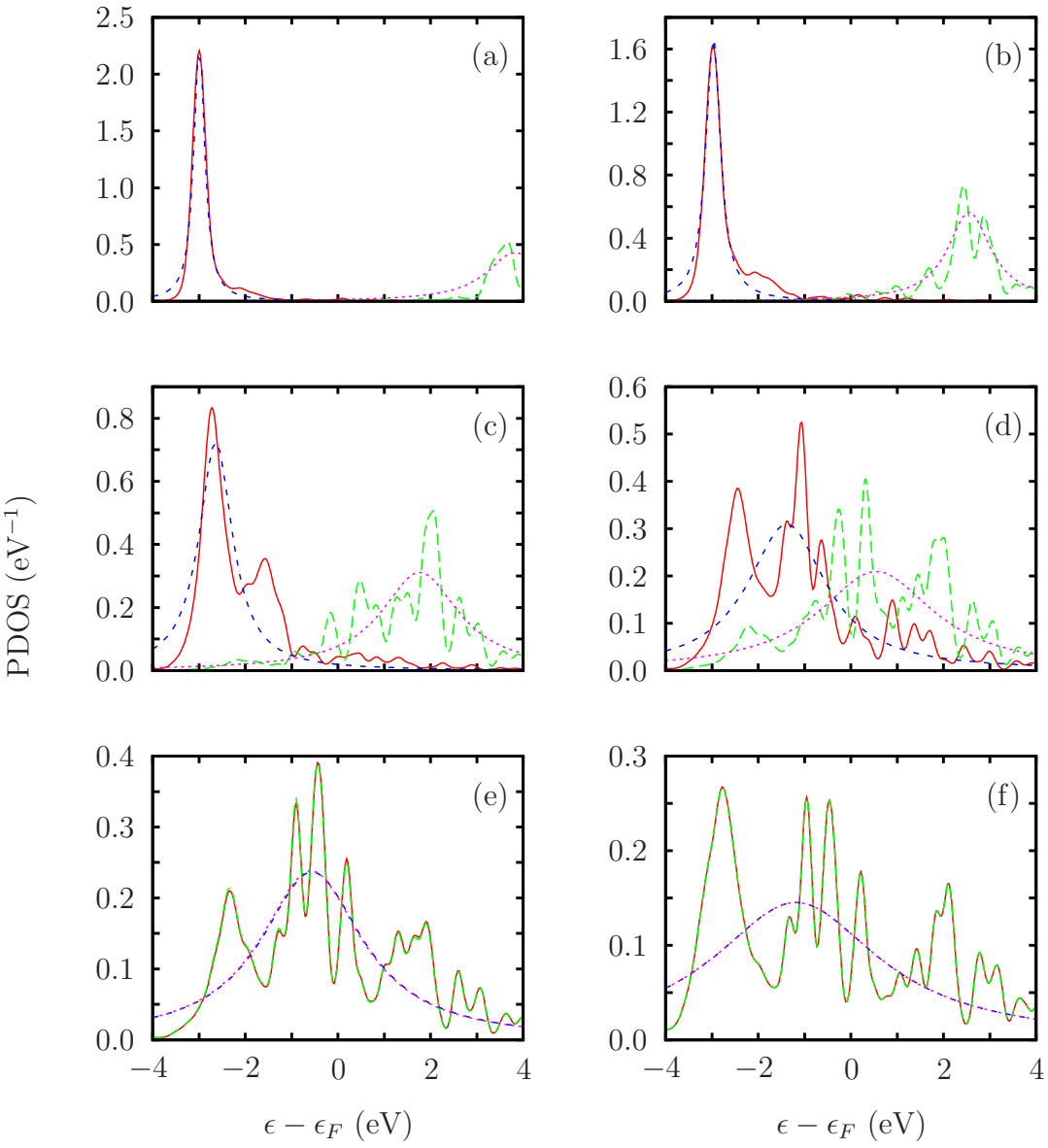


Figure 7.2: PDOS for the H/Cu(111) system for six H-atom altitudes. Panels correspond to altitudes of (a) 3.17 Å, (b) 2.90 Å, (c) 2.61 Å, (d) 2.39 Å, (e) 2.28 Å and (f) 2.00 Å. Solid red lines denote the majority spin PDOS and long-dashed green lines the minority spin PDOS. Medium-dashed blue lines and short-dashed magenta lines indicate the corresponding Lorentzian fits.

of the interaction increases, with oscillations due the to electronic structure of the surface and the finite number of states that are included in the DFT calculations. As the spin-transition is approached the PDOS for the two spins move towards the Fermi level, with the minority PDOS slightly broader than for the majority state. At a certain point, around 2.3 Å for H/Cu, the PDOS for the two spins become degenerate (see panel (e) of figure 7.2) and the spin-polarisation is lost – this is the spin-transition. Once the spin-transition is passed the PDOS broaden further as the bottom of the potential well is approached. At the lowest altitudes (see panel (f) in figure 7.2) part of the PDOS separates and shifts to lower energy – we attribute this behaviour to the adsorbate energy level falling off the bottom of the copper d-band.

The oscillatory nature of the PDOS shown in figure 7.2 is due, in part, to the finite number of k-points used in the DFT calculations. To remove the oscillatory features we could have used a larger Gaussian smoothing parameter. This would have increased the width the PDOS at high adsorbate altitudes and therefore affected the fitting procedure described below. Carrying out the fitting procedure using a larger smoothing width of 0.22 eV results in very similar parameter variations except for high-adsorbate altitudes. We therefore chose to use the small smoothing parameter (0.11 eV) to obtain more representative parameters at these high altitudes.

For each H-atom altitude the PDOS for each spin is least-squares fitted to the adiabatic resonance $\rho_{a\sigma}^{(ad)}$ of the Newns-Anderson model, (2.33), yielding values for the width $\Gamma_{\sigma}^{(fit)}$ and energy level $\bar{\epsilon}_{a\sigma}^{(fit)}$. These fits are shown in figure 7.2 along with the DFT calculated PDOS. While these fits are not perfect representations of the DFT results they do capture the essence of the interaction. Figure 7.3 shows the fitted widths and energy levels for each spin. Panel (a) shows the variation in the fitted widths of the adsorbate resonances; the variation in $\Gamma_{\sigma}^{(fit)}$ is dominated by an almost linear rise in the majority state width between 2.7 and 1.8 Å, at which point the widths for both spins reach a maximum. In panel (b) the variation of the fitted energy levels, $\bar{\epsilon}_{a\sigma}^{(fit)}$, is plotted. It can be seen how the majority and minority levels converge to just below the Fermi energy as the adsorbate passes through the spin-transition at around 2.3 Å. At low altitudes the energy levels fall away from the Fermi level rapidly as the surface is approached, with the widths also decreasing below 1.7 Å. This behaviour appears to be due to the adsorbate PDOS separating into two components at low altitude, with

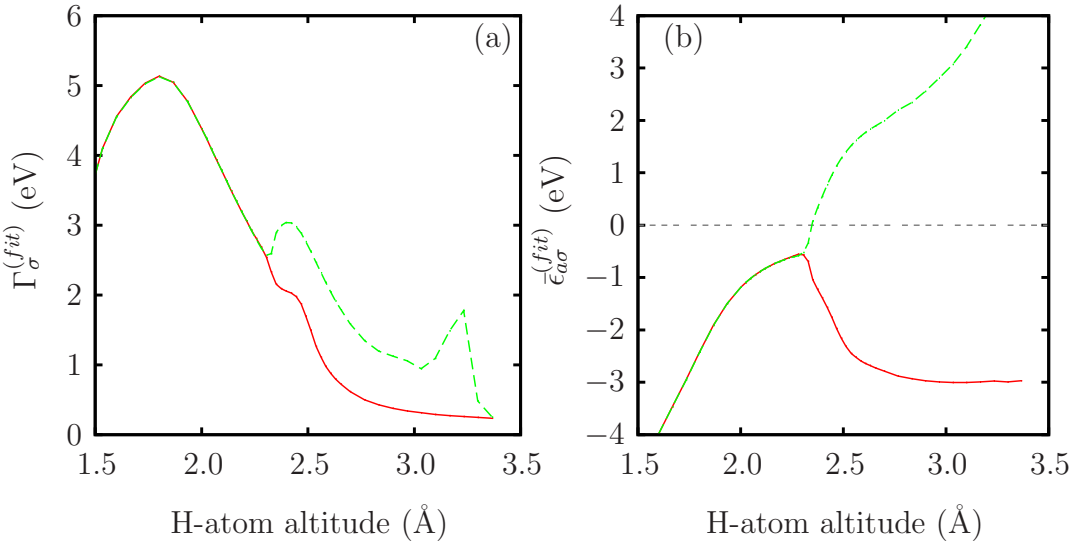


Figure 7.3: Variation of fit parameters with altitude; adsorbate resonance width $\Gamma_\sigma^{(fit)}$ (a) and energy levels $\bar{\epsilon}_{a\sigma}^{(fit)}$ (b). Solid red lines denote the majority spin results and dashed green lines the minority results.

a broad distribution around the Fermi level and a narrow distribution which grows and shifts to lower energies as the surface is approached[2] . The Newns-Anderson model, within the wide-band approximation at least, cannot imitate this variation in the electronic structure of the adsorbate PDOS, and so the fits must be considered to be less reliable and meaningful in this region.

The raw fit parameters shown in figure 7.3 can be used, with equation 2.34, to calculate the adsorbate occupations, which will be referred to as $n_{a\sigma}^{(fit)}$. The occupation of the adsorbate orbitals can also be found by integrating the PDOS generated by the DFT code CASTEP up to the Fermi level – we will refer to this quantity as $n_{a\sigma}^{(DFT)}$. In figure 7.4 these two occupation are compared for the H/Cu system under consideration. The two occupations show somewhat different behaviour; the spin-transition occurs at a lower occupation for $n_{a\sigma}^{(DFT)}$ than for $n_{a\sigma}^{(fit)}$ and the low altitude occupation shows less variation. This difference between the two sets of occupations is due to the form of the adsorbate PDOS discussed above, and the corresponding inability of the Newns-Anderson model to describe the DFT results.

[2]This narrow peak can be seen at around 3 eV below the Fermi level in panel (f) of figure 7.2.

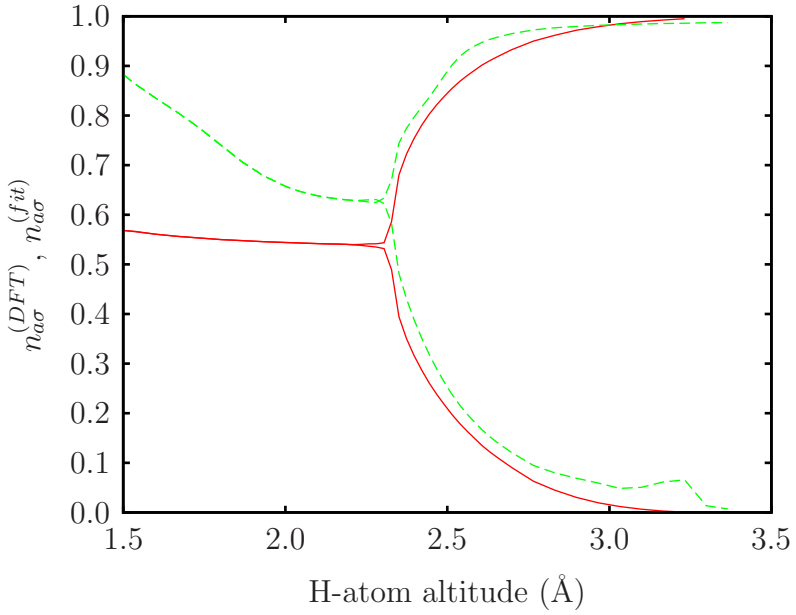


Figure 7.4: Comparison of occupations obtained directly from the calculated PDOS $n_{a\sigma}^{(DFT)}$ (solid red lines) with those resulting from $\Gamma_{\sigma}^{(fit)}$ and $\bar{\epsilon}_{a\sigma}^{(fit)}$ (dashed green lines).

In the previous chapter we saw that the evolution of the energy-levels and occupations of the model systems has a significant impact on the form of the electronic excitation spectrum. The model system with the largest occupation at and after the spin-transition, the $\epsilon_{aD} = -2.5$ model, produced a spectrum with more high-energy hole excitations than high-energy electrons (by a factor of around five). Conversely, the $\epsilon_{aD} = -0.5$ model system, which has the smallest occupation at and after the spin-transition, showed the opposite behaviour; more high-energy electrons than holes were excited. In order to obtain the right balance between the electron and hole excitations we have therefore chosen to ensure that the occupations and energy levels resulting from the parameter variations are consistent with the most reliable occupations, that is $n_{a\sigma}^{(DFT)}$.

To obtain this behaviour we have developed a procedure which ensures that the variation of $\epsilon_a$ and $\Gamma$, and the value of $U$, are consistent with the occupations $n_{a\sigma}^{(DFT)}$. This procedure is not straightforward and is described in appendix H.

The parameter variations are approximated using error functions, yielding

$$\frac{\Gamma}{\text{eV}} = -8.020\times10^{-5} + 2.805\ \text{erfc}\left(1.796\left(\frac{s}{\text{Å}} - 2.352\right)\right), \tag{7.1}$$

$$\frac{\epsilon_a}{\text{eV}} = -2.872 - 0.263\ \text{erfc}\left(3.717\left(\frac{s}{\text{Å}} - 1.729\right)\right), \tag{7.2}$$

$$U = 4.827\ \text{eV}, \tag{7.3}$$

where erfc is the complementary error function and $s$ is the altitude of the H-atom. The error function has been chosen to represent $\Gamma$ as it has an approximately linear variation half-way between maximum and minimum values, together with a smooth exponential tail at high altitudes. We also use the error function to represent the $\epsilon_a$ variation for simplicity. These parameters, the energy levels $\bar{\epsilon}_{a\sigma}^{(ad)}$ and the corresponding occupations are compared to the raw fit data in figure 7.5. The error function representation of $\Gamma$, as shown in panel (a), is similar in form to the raw fit data, but with little variation close to 1 and 4 Å. In panel (b) the effective energy levels resulting from the parameters described above are compared directly to the raw fit results. This plot shows two main differences between the energy levels from the raw fits and from the procedure to obtain consistent occupations. At high altitudes the variation in the minority level cannot be fitted with a constant value for $U$, as discussed in appendix H. At low altitudes the rapid fall in $\bar{\epsilon}_{a\sigma}^{(fit)}$ as the surface is approached cannot be matched whilst maintaining consistency with $n_{a\sigma}^{(DFT)}$. The $\epsilon_a$ variation generated by the consistency procedure is approximately constant close to and above the spin-transition with variation occurring primarily below 2 Å. From these results we can see that the majority of the behaviour of the system, up to and including the spin-transition, is driven by the variation in interaction strength – seen here in the variation in $\Gamma$.

While the fitted and processed energy levels, $\bar{\epsilon}_{a\sigma}^{(fit)}$ and $\bar{\epsilon}_{a\sigma}^{(ad)}$ respectively, show very different behaviour close to the surface, we note that the majority of energy-transfer and evolution of the electronic excitation spectrum occurs when the time-dependent energy levels are significantly different to their adiabatic counterparts (see chapters 5 and 6). Calculations of the time-evolving adsorbate level occupations for the parameter variations shown in figure 7.5 show that differences from the adiabatic state are small ( $10^{-3}$) by the time the adsorbate reaches 1.8 Å. The difference in the energy level behaviour close to the surface should not therefore have a significant impact on the non-adiabatic behaviour of the system.

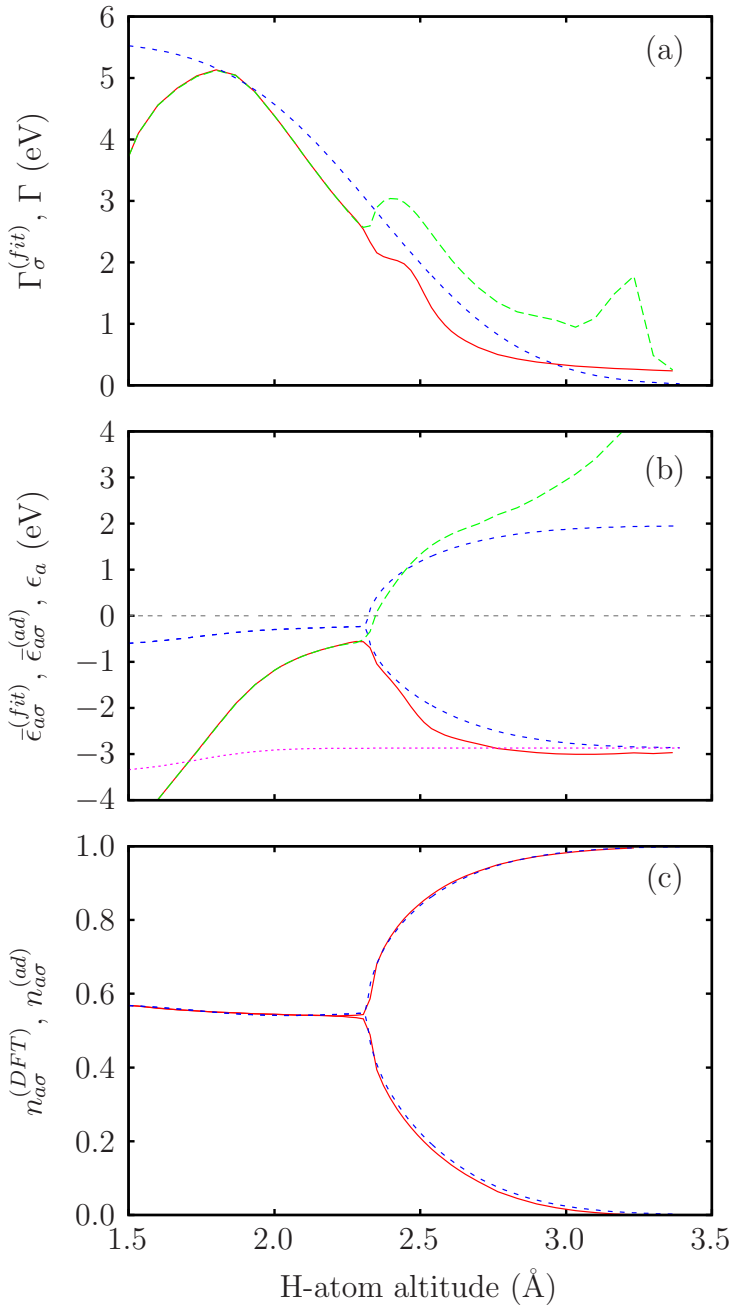


Figure 7.5: Comparison of processed parameters to initial fit results and DFT occupations. Panel (a) compares the error function fitted $\Gamma$ (medium-dashed blue line) to the fitted majority and minority spin resonance widths (solid red and long-dashed green blue lines respectively) from figure 7.3(a). Panel (b) compares the energy levels calculated from the error function parameter variation (medium-dashed blue red lines) to the fit results shown in figure 7.3(b) (solid red and long-dashed green lines for majority and minority spin). The short dashed magenta line in panel (b) denotes the function used to represent the $\epsilon_a$ variation. In panel (c) the occupations calculated from the error function fits (medium-dashed blue lines) and those calculated directly from the PDOSs (solid red lines) are plotted.

Panel (c) of figure 7.5 shows that the adiabatic occupations, calculated from the parameter variations in equations (7.1) to (7.3), are very similar to $n_{a\sigma}^{(DFT)}$. We are therefore confident that this set of parameters will give representative results for the charge and energy transfer behaviour and the spectrum of electronic excitations.

By following the same procedure we have also obtained the set of parameters required to simulate the H/Ag system. The variations of the width $\Gamma$ and the bare adsorbate energy level $\epsilon_a$ are again modelled using error functions, yielding

$$\frac{\Gamma}{\text{eV}} = -0.00175 + 2.944 \text{ erfc}\left(1.514\left(\frac{s}{\text{Å}} - 2.396\right)\right), \tag{7.4}$$

$$\frac{\epsilon_a}{\text{eV}} = -2.774 - 0.430 \text{ erfc}\left(4.076\left(\frac{s}{\text{Å}} - 1.901\right)\right), \tag{7.5}$$

$$U = 4.574 \text{ eV}. \tag{7.6}$$

These parameter variations are plotted, along with the results of the raw fits, in figure 7.6. The interaction between a hydrogen atom and the silver surface appears to be similar in form to that seen in the H/Cu system; the width of the resonances increases from a small value beyond 3-3.5 Å to around 6 eV by the bottom of the potential well (see panel (a)). The energy level variation is also similar to the H/Cu system, but with the initial levels slightly closer together and the final, degenerate level is a little further below the Fermi level. In panel (c) of figure 7.6 the occupations calculated from the raw fit parameters are again seen to deviate significantly from $n_{a\sigma}^{(DFT)}$ in the region around the spin-transition, with the occupations resulting from the processed parameters significantly closer.

The sets of parameter variations for H/Cu and H/Ag we will supply to the Newns-Anderson model are directly compared in figure 7.7. The widths, panel (a), are similar with the H/Ag system having a larger, but slightly less steep, rise in $\Gamma$ as the surface is approached. From panel (b) we can see that the effective energy levels of the H-atom above the copper surface are spaced slightly further apart at high altitudes than for the silver surface, while the low-altitude, degenerate level varies more in the H/Ag system. However, panel (c) shows that these differences only have a small effect on the variation of the adsorbate level occupations, with the H/Ag system passing through the spin-transition less than 0.05 Å further from the surface than the H/Cu system.

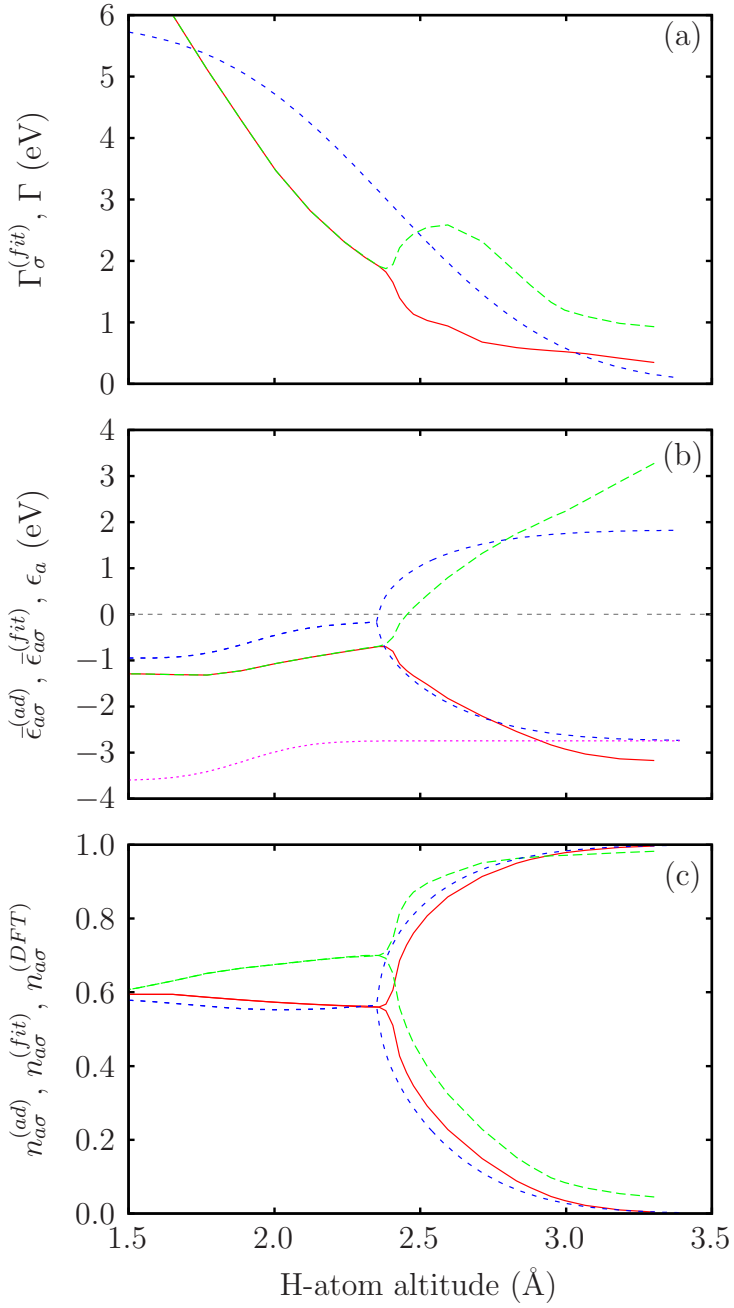


Figure 7.6: Comparison of processed parameters to initial fit results and DFT occupations. Panel (a) compares the error function fitted $\Gamma$ (medium-dashed blue line) to the fitted majority and minority spin resonance widths (solid red and long-dashed green lines respectively). Panel (b) compares the energy levels calculated from the error function parameter variation (medium-dashed blue lines) to the raw fit results shown in figure 7.3(b) (solid red and long-dashed green lines form majority and minority spin respectively). The short-dashed magenta line in panel (b) represents the function used to represent the $\epsilon_a$ variation. In panel (c) the occupations calculated from the error function fits (medium-dashed blue lines), $n_{a\sigma}^{(DFT)}$ (solid-red lines) and those calculated directly from the PDOSs (long-dashed green lines) are plotted.

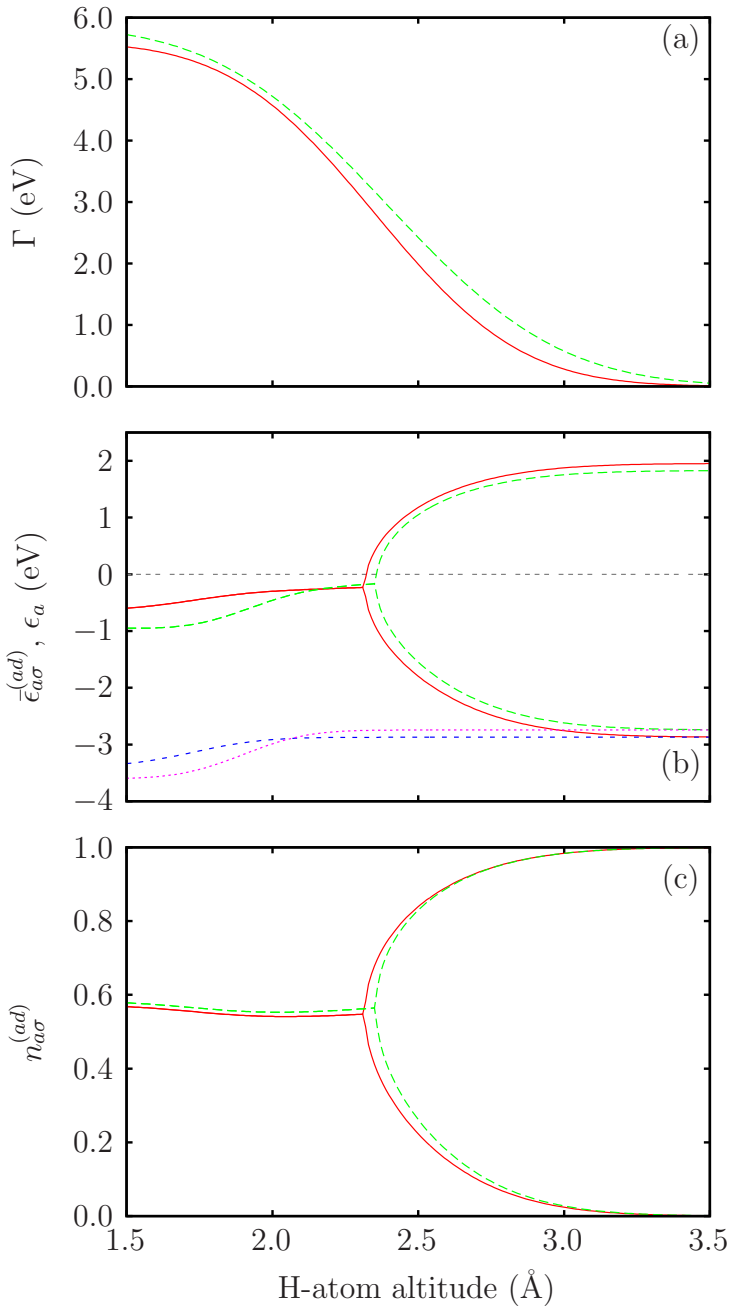


Figure 7.7: Comparison of processed parameters for the H/Cu (solid red lines) and H/Ag (dashed green lines) systems. Panel (a) shows the resonance width variation and (b) shows the effective adsorbate energy level variation, with the bare adsorbate energy levels denoted by short-dashed blue and dotted magenta lines for the H/Cu and and H/Ag systems respectively. Panel (c) shows the adiabatic occupation variation.

Before these parameters can be used to drive our model a relationship between altitude and time needs to be established. We choose to consider a very simple adsorbate motion; the adsorbate starts at an altitude of 4 Å and moves at constant velocity towards the surface until an altitude of 1 Å is reached. The speed of the adsorbate is determined using the potential energy of the system, as plotted in figure 7.1(a), at the spin-transition. We find this energy is 0.717 eV for the H/Cu system and 0.691 eV for the H/Ag system, which equates to speeds of 0.117 Å $\text{fs}^{-1}$ and 0.115 Å $\text{fs}^{-1}$ respectively. It is important to note that this simplistic model of the adsorption process only considers a single approach of the adsorbate to the surface. A more realistic model would see the adsorbate oscillating back and forth in the surface potential well as it slowly loses energy. However, our main reason for using the Newns-Anderson model is that it can describe the spin-transition, which has been neglected in previous work, and we therefore concentrate on the first approach of the adsorbate to the surface.

As the electronic structure of deuterium is identical to its lighter isotope the parameter variations extracted in this section can be applied to the D/Cu and D/Ag systems by reducing the approach velocities quoted above by a factor of $\sqrt{2}$. This will allow us to produce quantitative estimates of the magnitude of the isotope effect which can be directly compared to experimental data.

The final step we take before performing calculations is to de-dimensionalise the parameter variation, as described in sections 5.1 and 6.1. $\Gamma_0$, the scaling energy, is set to 3 eV for both systems, and the scale length $s_0$ is taken to be 1 Å. All quantities reported in this chapter will be converted to real units before presentation.

Other parameters used to perform the numerical computations presented in the following sections are: a 320,001 point energy grid covering the range $-60$ to 60 eV for calculating energy integrals and a time step of approximately $2 \times 10^{-3}$ fs. The analytic window half-width $\alpha$, used to evaluate several terms in $n_\sigma$, is again taken to be one grid-spacing ($3.75 \times 10^{-4}$ eV).

## 7.2 Occupations and energy transfer

By using the parameters constructed in the previous section we now present results for four model systems; hydrogen or deuterium atoms approaching the

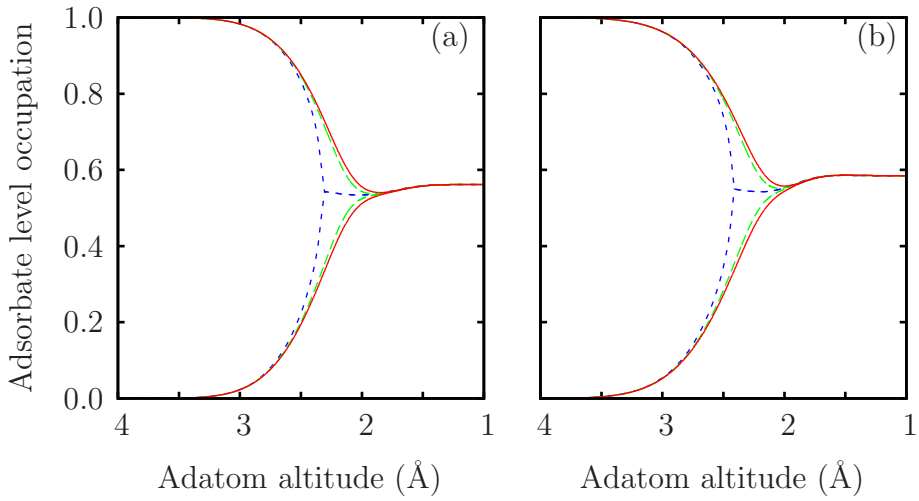


Figure 7.8: Variation of the adsorbate level occupation for hydrogen and deuterium approaching (a) copper and (b) silver surfaces. In each case medium-dashed blue lines denote the adiabatic occupations, solid red lines the time-dependent occupations of a hydrogen atom and long-dashed green lines the time-dependent deuterium occupations.

atop site of either the copper or silver (111) surface.

Figure 7.8 shows the variation of the adsorbate level occupations with altitude for the four systems. To maintain consistency with the calculations presented in chapters 5 and 6 the abscissa is reversed compared to the previous figures in this chapter. The two panels in this figure, showing results for the copper and silver surfaces, display very similar behaviour; the hydrogen atoms overshoot the spin-transitions and de-polarise below 2 Å (in both cases the spin-polarisation, $n_{a\uparrow} - n_{a\downarrow}$, is below $10^{-4}$ by the bottom of the potential wells). The curves for deuterium atoms (long-dashed green lines in figure 7.8) are a little closer to the adiabatic results than for its lighter isotope in the region around the spin-transition, but the polarisation is roughly two orders of magnitude smaller at the bottom of the potential well. We also note that the results shown in figure 7.8 are similar to the symmetric $\epsilon_{aD} = -1.5$ model system considered in the previous chapter.

The non-adiabatic energy transfer rate $\dot{E}_{non-ad}$, calculated from equation (3.17), is plotted for the four systems in figure 7.9. The energy transfer rates for H-atoms approaching the two surfaces are similar in form to each other and to that for the

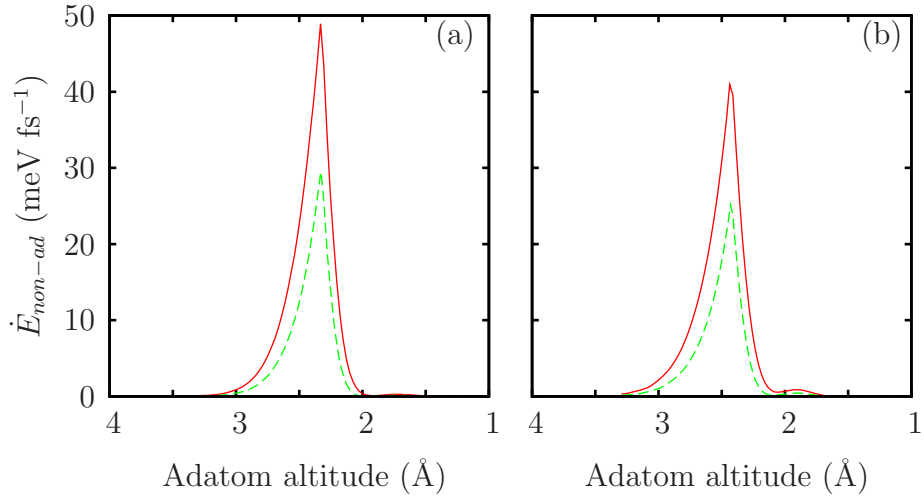


Figure 7.9: Non-adiabatic energy transfer rate variation for hydrogen and deuterium approaching (a) copper and (b) silver surfaces. In each case solid red lines denote the results for hydrogen adsorption and long-dashed green lines those for deuterium.

$\epsilon_{aD} = -1.5$ model system considered in chapter 5 (see figure 5.8(c)). The energy transfer rate for the silver system exhibits a slightly smaller peak transfer rate at the spin-transition, 41 meV fs$^{-1}$, in comparison to that for copper, 49 meV fs$^{-1}$. In panel (b) of figure 7.9 there is also a small peak in $\dot{E}_{non-ad}$, for both systems, just below 2 Å – this occurs during the same range of altitudes as the change in $\epsilon_a$ (see figure 7.7(b)). A similar feature does exist in the energy transfer rates for the H/Cu system. However, its magnitude is approximately three times smaller and therefore is not apparent on the scales used. We attribute this difference to the larger variation of $\epsilon_a$ for the silver surface. The energy transfer rates for D/Cu and D/Ag show similar behaviour to those for hydrogen atoms, but with smaller magnitudes (approximately 40% smaller close to the spin-transition).

Integration of these energy transfer rates over time yields the total energy transfer for the single pass through the spin-transition under consideration. By using the same method described in chapter 5 we obtain total energy transfers of 126 and 97 meV for the H/Cu and D/Cu systems respectively. For the silver surface the total energy transfer is found to be 117 meV for hydrogen atoms and 90 meV for deuterium. These results are consistent with calculations for the H/Al system investigated by Lindenblatt and Pehlke [34], who found the energy transfer during

| System | Effective temperature (K) | |
|---|---|---|
| | Electrons | Holes |
| H/Cu | 1246 | 1254 |
| D/Cu | 1040 | 1030 |
| H/Ag | 1210 | 1226 |
| D/Ag | 1005 | 1018 |

Table 7.1: Table of effective temperatures for electrons and holes for the spectra plotted in figure 7.10. Errors due to fitting suggest uncertainties of approximately $\pm 10$ K for each temperature. All calculations are performed for a surface temperature of 350 K.

a single approach to the surface to be around 0.1 eV.

## 7.3 Excitation spectra and chemicurrents

In this section we present excitation spectra for the four systems under consideration, and make direct comparisons to the chemicurrent experiments of Nienhaus and co-workers [18, 25]

In figure 7.10 the total excitation spectrum for a single pass through the spin-transition is plotted for each of the adsorbate-surface combinations. The time-evolution of these spectra is very similar in nature to the $\epsilon_{aD} = -1.5$ model system explored in chapter 6 and is therefore not presented here. Panels (a) and (b) of figure 7.10 show very similar spectra for the two substrates, with the results for deuterium only slightly smaller than for hydrogen close to the Fermi level. Away from the Fermi level the differences between the adsorbates is best presented on a logarithmic scale (see panels (c) and (d)). The high-energy tails of these distributions are exponential in nature and, as discussed in the previous chapter (see page 174), this behaviour can be described using the 'effective temperature' $T_{\text{eff}}$. The effective temperatures for the high-energy tails are tabulated in table 7.1. The temperatures for the excited electrons are slightly smaller, between 8 and 16 K, than for holes. However, the isotope effect is significant, with differences in $T_{\text{eff}}$ of approximately 200 K for both the copper and silver surfaces. The effective temperatures shown in table 7.1 are similar to values of around 1000 K obtained by Lindenblatt and Pehlke [33] in their unpolarised time-dependent DFT calculations of the H/Al system.

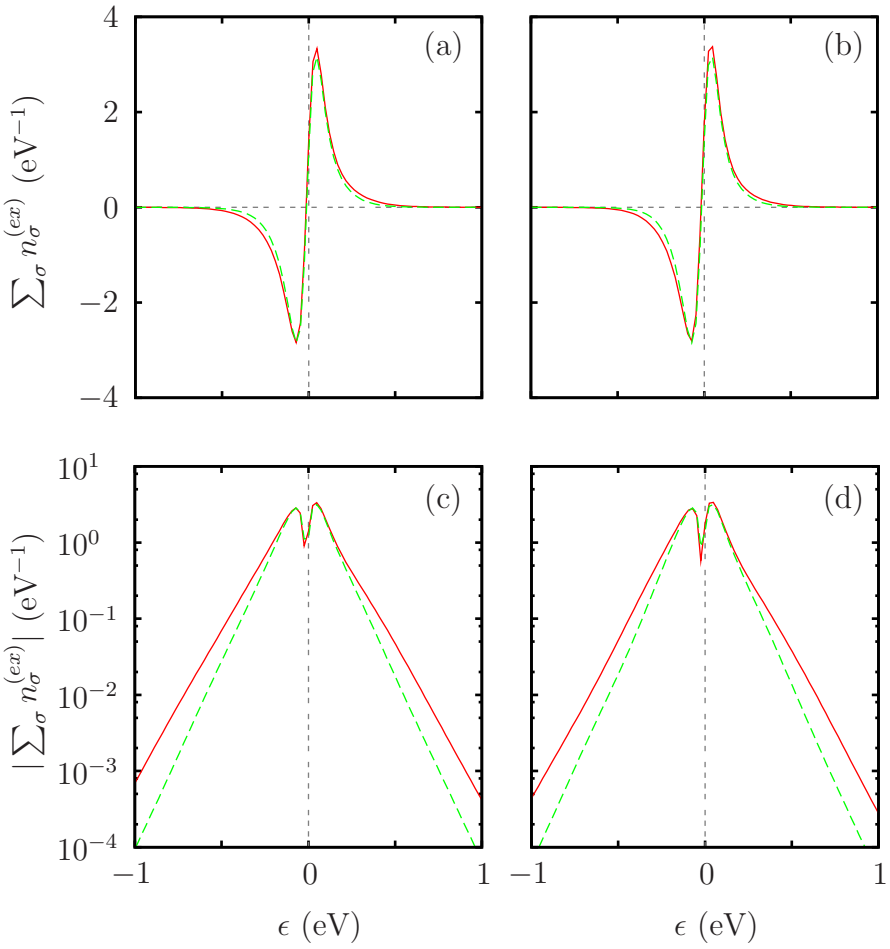


Figure 7.10: Total excitation spectra for hydrogen (solid red lines) and deuterium (dashed green lines) atoms approaching copper [(a) and (c)] and silver [(b) and (d)] surfaces. Panels (c) and (d) show the same data as (a) and (b), but on a logarithmic scale. A temperature of 350 Kelvin is used to allow the features close to the Fermi level to be seen.

The excitation spectra plotted for all four systems are similar to the $\epsilon_{aD} = -1.5$ model system used to demonstrate our model in chapter 6. As seen for the model system, the excitation spectra have very similar high-energy tails for both electrons and holes, with the 'node' of the spectra close to the Fermi level. The majority and minority-spin components of each of the excitation spectra are not presented here as these distributions are similar to those shown in figure 6.7 on page 171.

In section 6.2.2 we demonstrated that the dependence of $T_{\text{eff}}$ on the speed of the adsorbate can be separated into two domains; a square-root dependence on the rate of variation at low speed, and a linear dependence at high speed. Comparison of the results for the different isotopes suggests that both the hydrogen and deuterium calculations for both surfaces are in the low speed domain.

We now seek to compare our results to experimental data. As discussed in section 1.1.1, Nienhaus and co-workers [18] have used thin-film Schottky diodes to measure a chemically-induced current, or chemicurrent. These devices consist of a 70-100 Å thick metal film deposited on top of a doped silicon wafer, with contacts to the film and the back of the wafer used for making current measurements. At the silicon-metal film interface there is a Schottky barrier over which electrons or holes must be excited to register a chemicurrent. To make direct comparisons to experimental data we must therefore calculate the probability of exciting an electron or hole through the film and over the Schottky barrier. Gadzuk [38] and Nienhaus [80] have both described this process in terms of a multiple step model, taking into account excitation generation, attenuation in the metal film, and transmission across the Schottky barrier.

We will use a more simple description of this process. The attenuation factor $a$ is defined as the probability that an electron, or hole, of energy $\epsilon$ crosses a film of thickness $D$ with sufficient momentum perpendicular to the surface to cross a Schottky barrier of height $\epsilon_S$ at the other side. The mean-free-path of the excited electron or hole, $\lambda$, is assumed to be independent of energy. The attenuation factor then becomes

$$a(\epsilon, \epsilon_S) = \frac{1}{2\pi} \int_0^{2\pi} d\phi \int_0^{\theta_c} d\theta \sin(\theta) \exp\left[-\frac{D}{\lambda \cos(\theta)}\right], \tag{7.7}$$

where $\theta$ is the angle to the surface normal, $\phi$ is the angle in the plane of the

surface, and $\theta_c$ is the angle above which the excitation will not have enough momentum perpendicular to the surface to cross the Schottky barrier. $\theta_c$ can easily be found to be

$$\theta_c = \cos^{-1}\left(\sqrt{\frac{\epsilon_S}{\epsilon}}\right). \tag{7.8}$$

In writing down these expressions we have made a number of additional assumptions; there is no preference for the direction of propagation of the excitations within the metal, the metal has a uniform thickness and the barrier height $\epsilon_S$ is uniform throughout the device. The transmission probability of an electron with sufficient momentum perpendicular to the surface to cross the Schottky barrier is also assumed to be unity.

In appendix I an analytic expression for the attenuation factor is obtained by performing the angular integrals in (7.7), yielding (I.1);

$$\begin{aligned} a(\epsilon,\epsilon_S) &= \exp\left[-\frac{D}{\lambda}\right] - \sqrt{\frac{\epsilon_S}{\epsilon}}\exp\left[-\frac{D}{\lambda}\sqrt{\frac{\epsilon}{\epsilon_S}}\right] \\ &\quad -\frac{D}{\lambda}\left[\mathrm{E}_1\left(\frac{D}{\lambda}\right) - \mathrm{E}_1\left(\frac{D}{\lambda}\sqrt{\frac{\epsilon}{\epsilon_S}}\right)\right]. \end{aligned} \tag{7.9}$$

The probability of exciting an electron or hole such that it can be measured by a device with a Schottky barrier of height $\epsilon_S$ is therefore

$$P_e(\epsilon > \epsilon_S) = \sum_\sigma \int_{\epsilon_S}^{\infty} d\epsilon\; n_\sigma^{(ex)}(\epsilon,t) a(\epsilon,\epsilon_S), \tag{7.10a}$$

$$P_h(\epsilon > \epsilon_S) = \sum_\sigma \int_{\epsilon_S}^{\infty} d\epsilon\; |n_\sigma^{(ex)}(-\epsilon,t)| a(\epsilon,\epsilon_S), \tag{7.10b}$$

for electrons and holes respectively. To perform the integrals in (7.10) we require values for $\lambda$ and $D$. The value of $\lambda$ in the copper film was estimated by Nienhaus and co-workers [22] to be around 100 Å and was measured in the silver film to be approximately 200 Å (Krix and co-workers [25]). Typical film thicknesses are in the range 60-100 Å. These values, the excitation spectra in figure 7.10 and (7.10) can now be used to estimate the probability of an electron or hole being detected in a thin-film Schottky diode following a single approach of an adsorbate to the surface.

Figure 7.11 shows the probabilities of electrons and holes being detected in a thin-

film Schottky diode for the four systems under consideration. The variation of the barrier-crossing probabilities are again found to be approximately exponential at high energies, with results for deuterium almost an order of magnitude smaller than for hydrogen for both electrons and holes above a barrier height of 0.6 eV.

It is important to emphasise here that these calculations are for a single passage of the adsorbate through the spin-transition to the minimum of the surface potential well. However, these results compare well to results reported by Nienhaus et al. [18]; for Cu/n-Si Schottky diodes[3] with barrier heights in the range 0.55-0.6 eV, $1.5\times10^{-4}$ electrons per incident atom were observed. From our calculations we find the probability of exciting an electron over barrier heights in this range is between $1.0\times10^{-4}$ and $0.6\times10^{-4}$. More recent experiments by Krix, Nünthel and Nienhaus [25] using Ag/p-Si devices with barrier heights in the region of 0.46 eV measured $4.0\times10^{-4}$ electrons per incident hydrogen atom. From figure 7.11(c) we find the probability of crossing such a barrier to be approximately $4.5\times10^{-4}$. These results suggest that a significant fraction of the observed chemicurrent could be excited by the first approach of the adsorbate to the surface as it passes through the spin-transition.

Similar estimates of the magnitude of the chemicurrent have also been reported by Trail and co-workers [28, 29], who used a nearly-adiabatic friction based description of the excitation process (see section 1.2.1 for a description). Their calculations, in which the spin-transition was removed in an arbitrary manner, suggest that the behaviour of the system close to the spin-transition is not of primary importance to the generation of electronic excitations (frictional effects from the region at and below the potential minimum were found to dominate). However, in contradiction to their work our results show that non-adiabatic effects at the spin-transition can also explain the chemicurrent measurements. We conclude that a full description of the electronic excitation process should be a combination of non- and nearly-adiabatic theories covering the entire adsorption trajectory.

The roughly exponential dependence of the probability of measuring an excited electron or hole on the height of the Schottky barrier allows us to characterise these plots by another effective temperature. Table 7.2 summarises the temper-

[3]Devices constructed using n-doped silicon detect hot electrons and those with p-doped silicon detect hot holes.

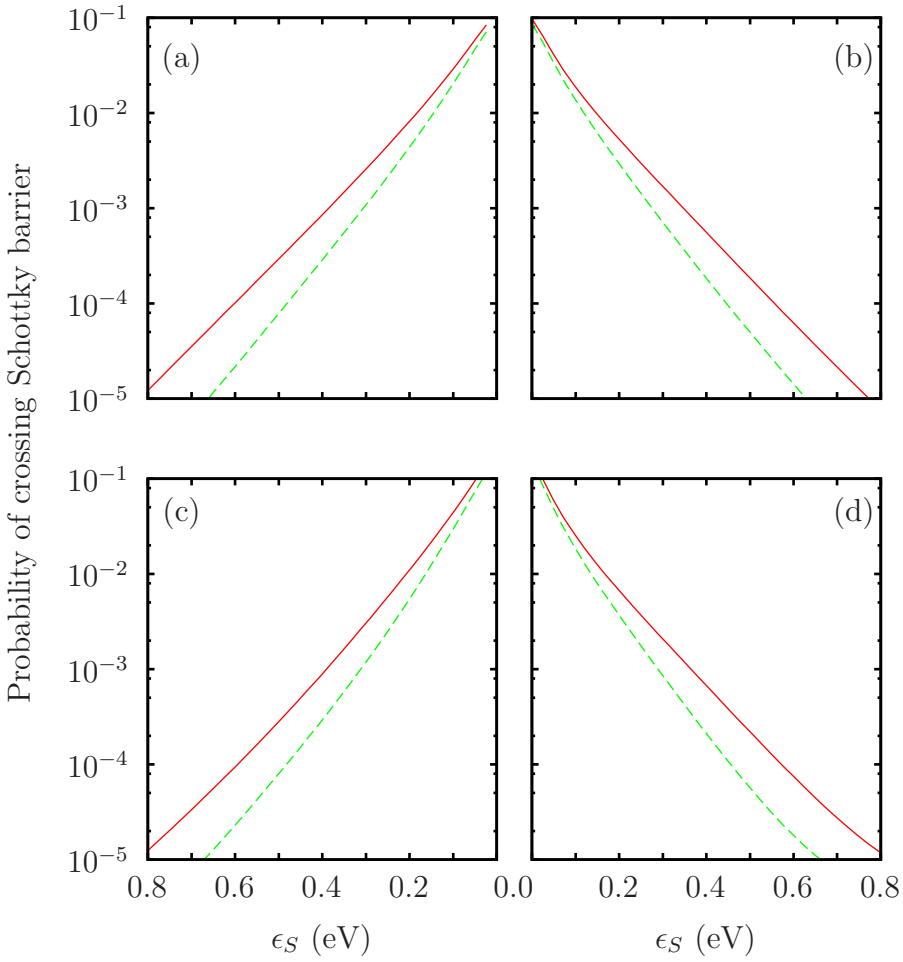


Figure 7.11: Estimates of the probability of exciting an electron at the surface with enough energy to traverse a 75 Å thick metal film and cross a Schottky barrier of height $\epsilon_S$. Panels (a) and (b) show the probabilities for hydrogen (solid red lines) and deuterium (dashed green lines) approaching a copper surface for holes and electrons respectively. Panels (c) and (d) show the same data, but for a silver surface. A surface temperature of 350 K is used for these calculations. $\lambda$ is assumed to be 100 Å and 200 Å for the copper and silver surfaces respectively.

| System | Chemicurrent temperature (K) | | Chemicurrent ratio |
|---|---|---|---|
| | Electrons | Holes | Electrons:holes |
| H/Cu | 1085 | 1086 | 1:1.57 |
| D/Cu | 906 | 902 | 1:1.56 |
| H/Ag | 1021 | 1004 | 1:1.27 |
| D/Ag | 918 | 915 | 1:1.35 |

Table 7.2: Table of chemicurrent effective temperatures for electrons and holes for the results plotted in figure 7.11 along with the ratio of electron to hole chemicurrents for a barrier height of 0.5 eV. Errors due to fitting suggest uncertainties of approximately ±20 K for each temperature. All calculations were performed using a surface temperature of 350 K.

atures obtained from least-squares fitting. The difference between the isotopes is smaller for the chemicurrent temperatures than for the spectra (see table 7.1), with a slightly smaller effect for the silver surface compared to copper. The ratio of the electron and hole chemicurrents for a given barrier height is also shown in table 7.2, showing larger ratios for the copper surface than for silver.

In the previous chapter, section 6.2.3, we demonstrated that the temperature of the system can have a significant effect on the excitation spectra. This behaviour will also have an effect on the probability of detecting an excitation – this is demonstrated in figure 7.12 for the H/Cu system. The system temperatures used here (175 K, 350 K and 700 K) are below the effective temperature of the excitation and we do not therefore see changes in the slope of the chemicurrent probabilities. There is, however, an increase in the magnitude of the barrier crossing probabilities, with the results for $T$=700 K and 350 K approximately 50% and 6% larger than the 175 K results respectively.

The recent experiments performed by Krix, Nünthel and Nienhaus [25] have compared the chemicurrents excited by hydrogen and deuterium. By using an Ag/p-Si diode with a Schottky barrier height of $\epsilon_S = 0.46$ eV, they observed chemicurrents for hydrogen atoms which were approximately 3.7 times larger than for deuterium. The corresponding ratios derived from our calculations are plotted for both metal surfaces at different system temperatures in figure 7.13.

The H:D ratios shown in figure 7.13 show a number of interesting features. First, the H:D ratios increase with barrier height in a simple fashion. Second, the system temperature has a substantial impact with higher temperatures reducing

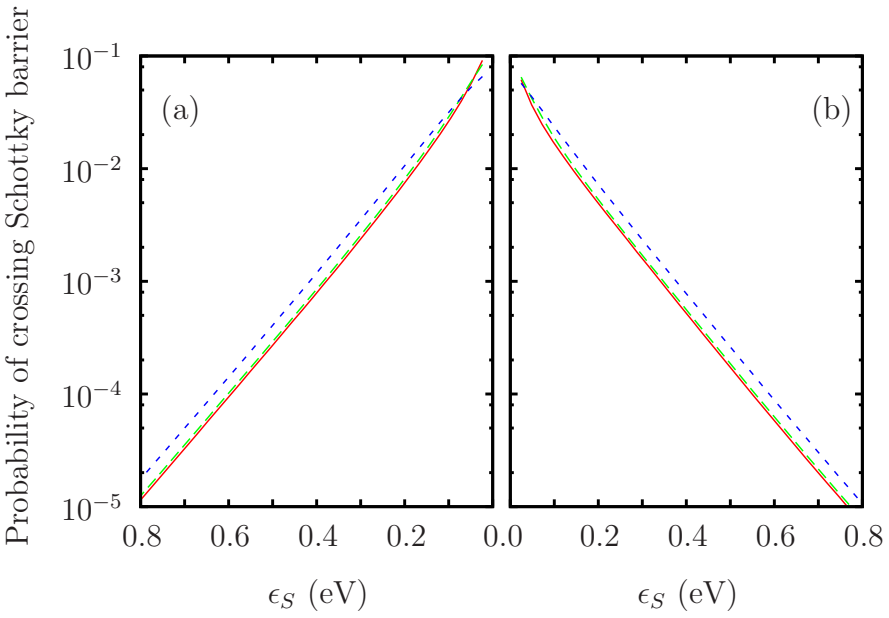


Figure 7.12: The impact of system temperature on the probability of an incident hydrogen atom exciting a hole (a) or an electron (b) over a Schottky barrier of height $\epsilon_S$ after traversing a 75 Å thick copper film. Different colours denote different surface temperatures; solid red = 175 K, long-dashed green = 350 K and medium dashed blue = 700 K.

the ratio of H:D results. For holes being excited through a silver film over a barrier height of 0.46 eV (see panel (c) in figure 7.13) our model suggests an H:D ratio of 3.4:1 for $T = 175$ K, 3.3:1 for $T = 350$ K and 2.7:1 for $T = 700$ K. The lower temperature results show good agreement with the experimental data, which was obtained at a substrate temperature of 100 K.

Krix, Nünthel and Nienhaus [25] have also used an expression presented by Lindenblatt and Pehlke [33] to relate the magnitude of the isotope effect to the effective chemicurrent temperature. This expression is obtained by approximating the dependence of the chemicurrent on the Schottky barrier height by the exponential $A\exp(-\epsilon_S/k_B T_{\text{chemi}})$. The logarithm of the ratio of the chemicurrents for H:D is therefore

$$\ln\left(\frac{P_H(\epsilon > \epsilon_S)}{P_D(\epsilon > \epsilon_S)}\right) = \ln\left(\frac{A_H}{A_D}\right) + \frac{\epsilon_S}{k_B T^H_{\text{chemi}}}\left(\frac{T^H_{\text{chemi}}}{T^D_{\text{chemi}}} - 1\right), \qquad (7.11)$$

where $P_H$ and $P_D$ are the electron or hole detection probabilities for hydrogen and deuterium adsorbates, respectively. $A_H$ and $A_D$ are the pre-factors of the exponentials for the two isotopes, which are assumed to be identical. Lindenblatt and Pehlke use the relationship $T_{\text{eff}} \propto m^{-1/2}$ where $m$ is the adsorbate mass,

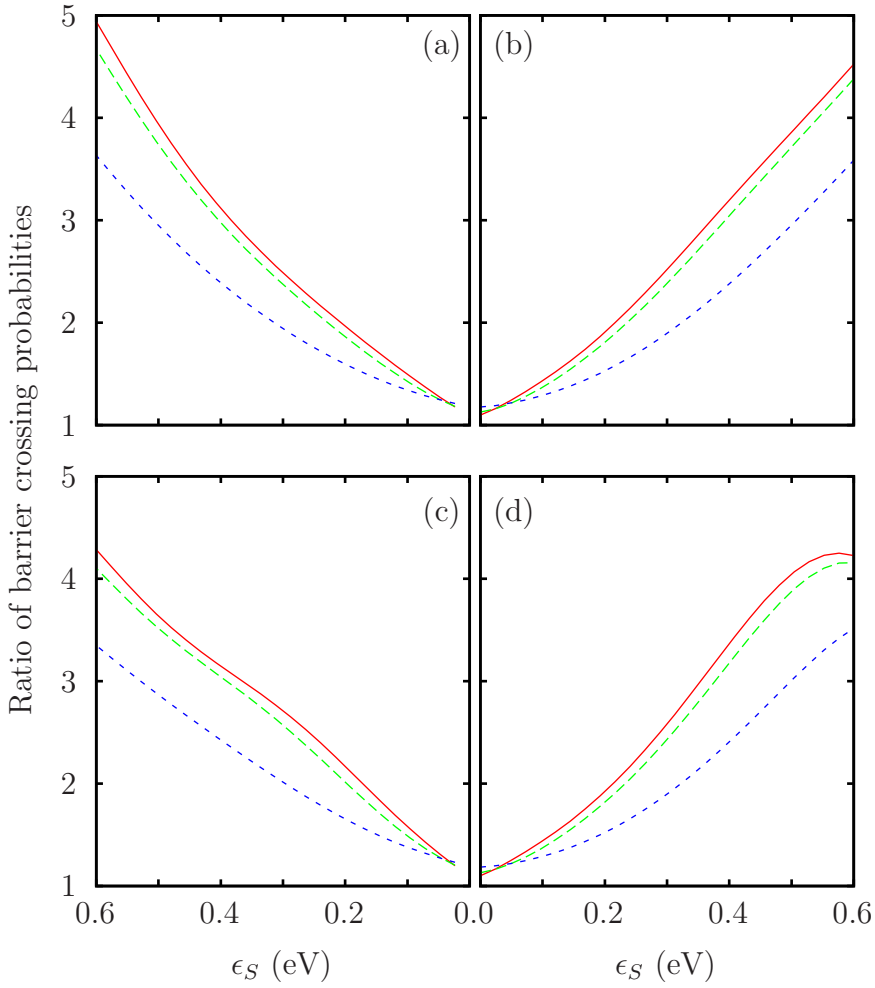


Figure 7.13: Estimates of the ratio of barrier crossing probabilities for hydrogen to deuterium atoms incident on copper [(a) and (b)] and silver [(c) and (d)] surfaces. Panels (a) and (c) show this ratio for hole excitations while (b) and (d) relate to electron excitations. Different lines denote different system temperatures – solid red = 175K, long-dashed green = 350K and medium-dashed blue = 700K.

which is derived from the forced oscillator model. This suggests that (7.11) can be re-expressed as

$$\ln\left(\frac{P_H(\epsilon > \epsilon_S)}{P_D(\epsilon > \epsilon_S)}\right) = \frac{\epsilon_S}{k_B T^H_{\text{chemi}}}\left(\sqrt{\frac{m_D}{m_H}} - 1\right), \tag{7.12}$$

which, using the experimental data and the adsorbate masses, Krix and co-workers evaluate to give $T^H_{\text{chemi}} = 1690 \pm 300$ K.

However, in section 6.2.2 we saw two domains in the variation of the effective temperature with speed; at high speeds $T_{\text{eff}}$ is proportional to the speed, while at slow speeds a square-root dependence on speed is observed. This second domain is equivalent to a $T_{\text{eff}} \propto m^{-1/4}$ variation. Comparison of the effective and chemicurrent temperatures for the two isotopes suggests that the slow-speed behaviour is dominant here, as discussed above. This suggests that the following expression is more appropriate for the experimental data;

$$\ln\left(\frac{P_H(\epsilon > \epsilon_S)}{P_D(\epsilon > \epsilon_S)}\right) = \frac{\epsilon_S}{k_B T^H_{\text{chemi}}}\left(\sqrt[4]{\frac{m_D}{m_H}} - 1\right). \tag{7.13}$$

By combining this expression with the experimental parameters reported by Krix and co-workers we find a chemicurrent temperature of 770 ± 150 K, which is substantially closer to that obtained from our model (1004 K, see table 7.2).

## 7.4 Conclusions

In this chapter we have applied our Newns-Anderson model to investigate the electronic excitations generated by the adsorption of hydrogen and deuterium atoms on the copper and silver surfaces. We have presented a method by which a suitable set of parameters for the Newns-Anderson model can be extracted from DFT calculations. These parameter sets have been used to drive the time-dependent model constructed in chapters 2 to 4 through a single approach of each adsorbate to the metal surfaces. The results obtained for the adsorbate level occupations, non-adiabatic energy transfer rates and the electronic excitation spectra closely resemble those of the symmetric $\epsilon_{aD} = -1.5$ model system considered in chapter 6. The effective temperature $T_{\text{eff}}$, which describes the variation of the excitation spectra with energy, has been calculated yielding similar values to the time-dependent DFT calculations reported by Lindenblatt and Pehlke [33] for the H/Al system.

By analysing a simple model of the propagation of electronic excitations in a metal film we have been able to make quantitative predictions of the chemicurrent excited by the single approach of an adsorbate for comparison with the experiments of Nienhaus and co-workers. The magnitudes of the chemicurrents obtained from our calculations are in broad agreement with experimental results. We have investigated the isotope effect, the difference between chemicurrents induced by the adsorption of hydrogen and deuterium atoms, finding a H:D ratio of 3.4:1 in excellent agreement with that reported by Krix and co-workers, 3.7±0.7:1, [25].

The results we have presented in this chapter have all been based on a single approach of an adsorbate to a metal surface. This is not truly representative of the entire adsorption process, which consists of a series of damped oscillations in the surface potential well (the damping arises due to energy transfer away from the adsorbate). However, the fact that we find chemicurrents which are consistent with experimental data indicates that a significant fraction of the measured current may arise from a single passage of the adsorbate through the spin-transition. In the light of this it is interesting to note that the largest chemicurrents for all the adsorbates investigated by Gergen, Nienhaus and co-workers [20] were found for spin-polarised atoms and molecules, i.e. H, O, NO, $NO_2$.

# Appendix H: DFT Parameter consistency procedure

In section 7.1 we plotted fit parameters, figures 7.3 and 7.6, extracted from DFT generated PDOS. This appendix describes the method used to extract simple parameter variations from these data, which can then be used to drive our time-dependent model. We have chosen to take the spin-state populations calculated directly from the DFT generated PDOS as the most reliable measure of the system behaviour, and the fit parameters $\Gamma_\sigma^{(fit)}$ and $\bar{\epsilon}_{a\sigma}^{(fit)}$ therefore need to be modified to be consistent with this behaviour. Much of the method described here is somewhat arbitrary – our justification for this is pragmatic; this approach appears to give reasonable results for the two systems under investigation. The steps of this procedure will be demonstrated using data for the H/Cu system.

Before any processing takes place the variation in the fitted widths $\Gamma_\sigma^{(fit)}$ is stopped below either the potential well minimum (1.5Å for H/Cu) or the maximum in the width. The widths and energy levels obtained are then used to determine the variation of $\Gamma$ and $\epsilon_a$, and the value of $U$; a consistency procedure is followed to impose the required occupations on the parameters. To impose this consistency the ($\Gamma_\sigma^{(fit)}$,$\bar{\epsilon}_{a\sigma}^{(fit)}$) combination needs to be modified – we replace this combination with ($\Gamma_\sigma^{(mod)}$, $\bar{\epsilon}_{a\sigma}^{(mod)}$), which has the correct occupation, where the difference

$$(\Gamma_\sigma^{(fit)} - \Gamma_\sigma^{(mod)})^2 + (\bar{\epsilon}_{a\sigma}^{(fit)} - \bar{\epsilon}_{a\sigma}^{(mod)})^2, \tag{H.1}$$

is minimised. This choice of the quantity to minimise is arbitrary, but it does not appear to place more importance on the fitted widths or energy levels. Figure 7.14 compares the raw fit results to the modified parameters.

As the minority energy level in both the H/Cu and H/Ag systems shifts to higher energy with increasing altitude above 3 Å it is difficult to find a set of parameters which describe both majority and minority spin levels well. We have chosen to base the rest of the parameter extraction procedure on the majority spin resonance width, the majority spin energy level, and the DFT occupations $n_{a\sigma}^{(DFT)}$ of both spins.

We now extract the variation of the bare adsorbate level $\epsilon_a$ and $U$ from the

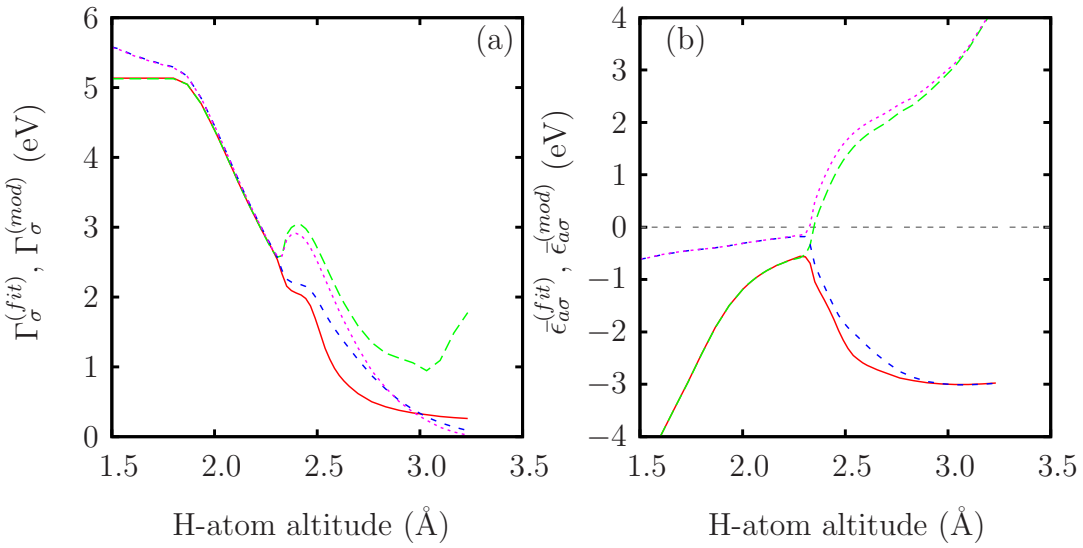


Figure 7.14: Comparison of raw to modified variations for the resonance widths (a) and energy levels (b) for the H/Cu system. Solid red and long-dashed green lines denote raw fit results of majority and minority spin respectively, while medium-dashed blue and short-dashed magenta lines relate to the modified results.

behaviour of the majority energy level. At altitudes above around 2.8 Å the minority level shifts rapidly away from the Fermi level, while the majority level is roughly constant at $-3$ eV. This behaviour is impossible to model with a constant value for $U$, and the $\epsilon_a$ variation is therefore extracted exclusively from the majority level. $\epsilon_a$ is modelled using an error function variation, the parameters of which (along with the value of $U$) are found by minimising

$$\sum_{s_i} \left[ \bar{\epsilon}_{a\uparrow}^{(mod)}(s_i) - \left( \epsilon_a(s_i) + U n_{a\downarrow}^{(DFT)} \right) \right]^2 , \tag{H.2}$$

where $s_i$ are the altitudes of the set of DFT calculations (20 were used for H/Ag and 40 for H/Cu) and $\epsilon_a(s)$ is of the form

$$\epsilon_a(s_i) = a + b \, \mathrm{erfc}\left(c(s_i - d)\right) , \tag{H.3}$$

where $a$, $b$, $c$ and $d$ are constants.

The width $\Gamma^{(mod)}$ is fitted to the function

$$\Gamma(s) = a' + b' \text{ erfc}\left(c'(s - d')\right), \tag{H.4}$$

subject to the requirement that both $\Gamma$ and the derivative $d\Gamma/ds$ are small at an altitude of 4 Å.

$\epsilon_a$, (H.3), $\Gamma$, (H.4) and the value of $U$ are then combined with the velocity of the adsorbate (chosen to be constant for the calculations performed in this chapter) to give the time-variation required by the model.

# Appendix I: Calculation of chemicurrents from $n_\sigma^{(ex)}$

The attenuation factor for electron or hole excitations, of energy $\epsilon$, crossing a metal film of thickness $D$ with sufficient momentum perpendicular to the Schottky barrier of height $\epsilon_S$ is expressed in (7.7) as

$$a(\epsilon, \epsilon_S) \;=\; \frac{1}{2\pi}\int_0^{2\pi} d\phi \int_0^{\theta_c} d\theta \sin(\theta) \exp\left[-\frac{D}{\lambda\cos(\theta)}\right]. \tag{I.1}$$

In this expression $\lambda$ is the mean-free-path of electrons, which is assumed to be independent of energy $\epsilon$. The angles $\theta$ and $\phi$ are the angle to the surface normal (within the metal) and the angle in the plane of the surface, respectively. $\theta_c$ is the angle at which an excitation of energy $\epsilon$ will not have sufficient momentum perpendicular to the metal-silicon interface to cross the Schottky barrier. $\theta_c$ is defined in (7.8) as

$$\cos(\theta_c) = \sqrt{\frac{\epsilon_S}{\epsilon}}. \tag{I.2}$$

Evaluation of the $\phi$ integral is trivial, but the $\theta$ integral requires a little more work. By using the substitution $x = 1/\cos(\theta)$ (I.1) can be rewritten as:

$$a(\epsilon, \epsilon_S) = \int_1^{x_c} dx \frac{\exp\left[-Dx/\lambda\right]}{x^2}, \tag{I.3}$$

where $x_c = 1/\cos(\theta_c)$. On integration by parts (I.3) yields

$$\begin{aligned} a(\epsilon, \epsilon_S) &= \left[-\frac{\exp[-Dx/\lambda]}{x}\right]_1^{x_c} - \frac{D}{\lambda}\int_1^{x_c} dx \frac{\exp[-Dx/\lambda]}{x}, \\ &= \exp\left[\frac{D}{\lambda}\right] - \frac{1}{x_c}\exp\left[\frac{Dx_c}{\lambda}\right] - \frac{D}{\lambda}\int_1^{x_c} dx \frac{\exp[-Dx/\lambda]}{x}. \end{aligned} \tag{I.4}$$

The remaining integral in this expression can be related to the first exponential integral, defined by Arfken [81] as

$$\mathrm{E}_1(t) = \int_t^{\infty} du \frac{\exp[-u]}{u}. \tag{I.5}$$

As there is a simple series approximation for this function it is convenient to rewrite the remaining integral in (I.4), yielding

$$\begin{aligned} \int_1^{x_c} dx \frac{\exp[-Dx/\lambda]}{x} &= \int_1^{\infty} dx \frac{\exp[-Dx/\lambda]}{x} - \int_{x_c}^{\infty} dx \frac{\exp[-Dx/\lambda]}{x} \\ &= \int_{D/\lambda}^{\infty} dy \frac{\exp[-y]}{y} - \int_{Dx_c/\lambda}^{\infty} dy \frac{\exp[-y]}{y} \\ &= \mathrm{E}_1\left(\frac{D}{\lambda}\right) - \mathrm{E}_1\left(\frac{Dx_c}{\lambda}\right), \end{aligned} \tag{I.6}$$

where we have used the substitution $y = Dx/\lambda$. By recalling the relationship between $x_c$, $\theta_c$ and the energies $\epsilon$ and $\epsilon_S$ the attenuation factor $a$ becomes

$$\begin{aligned} a(\epsilon, \epsilon_S) &= \exp\left[-\frac{D}{\lambda}\right] - \sqrt{\frac{\epsilon_S}{\epsilon}}\exp\left[-\frac{D}{\lambda}\sqrt{\frac{\epsilon}{\epsilon_S}}\right] \\ &\quad -\frac{D}{\lambda}\left[\mathrm{E}_1\left(\frac{D}{\lambda}\right) - \mathrm{E}_1\left(\frac{D}{\lambda}\sqrt{\frac{\epsilon}{\epsilon_S}}\right)\right]. \end{aligned} \tag{I.7}$$

# Chapter 8

# Conclusions

In this thesis we have derived and demonstrated a model describing the electronic excitation of a metal surface induced by interactions with an adsorbate orbital. The major results and the conclusions drawn in this work, along with some suggested areas for future research, will be discussed in this chapter.

In chapters 2 to 4 we used the time-dependent, mean-field Newns-Anderson model to construct expressions describing the charge and energy transfer between an adsorbate and a surface, along with the spectrum of electronic excitations generated by this transfer. Results for the adsorbate level occupation and the nearly-adiabatic energy transfer rate are similar to previous work in the literature, but the spectrum of electronic excitations is entirely new. We note here that the expressions for the adsorbate level occupations, the energy transfer rates and the electronic excitation spectrum are all expressed in terms of three parameters; the bare adsorbate energy level, $\epsilon_a$, the width of the adsorbate resonance, $\Gamma$, and the intra-adsorbate Coulomb repulsion energy, $U$. Our model includes time-dependence in both $\epsilon_a$ and $\Gamma$, with $U$ held constant.

In chapters 5 and 6 we have presented numerical calculations of the time-evolution of the adsorbate level occupations, the adsorbate-surface energy transfer rates, and the electronic excitation spectra. These quantities have been computed for three model systems describing slightly different adsorbate-surface interactions – they differ only in the position of the bare adsorbate energy level $\epsilon_a$. For each system the effects of the rate of parameter variation, which can be associated

with an adsorbate 'speed', and temperature have been considered.

The adiabatic model of the adsorbate level occupations displays a sharp spin-transition between two distinct energy levels and a degenerate state. The position of this spin-transition depends on the parameters of the model in question, with the spin-transition occurring for a smaller value of $\Gamma$ in asymmetric systems, those with one level initially closer to the Fermi level. In the time-evolving model, the adiabatic behaviour is overshot by the time-evolving system with the adsorbate de-polarising later. The magnitude of this overshoot is determined by the speed of the adsorbate, i.e. the rate of variation of the parameters which drive the evolution of the system. At slow speeds the region in which the difference between the adiabatic and time-dependent occupations is significant is smaller, but at the spin-transition there is always an overshoot. The sharp nature of the spin-transition implies an infinite rate of adiabatic charge transfer between adsorbate and surface which the time-evolving model cannot achieve, irrespective of the rate of evolution. We would therefore expect some non-adiabatic effects in any system which experiences a spin-transition.

The non-adiabatic energy transfer rate, investigated in section 5.3, was calculated, yielding a peak at the same point as the spin-transition. At slow speeds the non-adiabatic results approach the nearly-adiabatic energy transfer rate, with deviations seen only close to the adiabatic spin-transition point where the time-dependent system cannot follow the adiabatic behaviour.

The spectrum of electronic excitations, investigated in chapter 6, shows a number of features which require comment. Calculations of the evolution of the excitation spectra for the three model systems considered in chapter 5 demonstrate that the majority of the evolution occurs in a short window around the adiabatic spin-transition point. The final spectra consist of a peak just above the Fermi level with an exponential tail stretching to high energies made up predominantly of majority spin electrons, while below the Fermi level there are similar features for holes with minority spin excitations dominating. Different energy level configurations change the balance between the components of the excitation spectra. Systems which transfer charge to the surface generate larger high-energy electron excitations, while charge transfer to the adsorbate enhances the high-energy hole distribution.

The exponential tails of the excitation spectra lend themselves to a description in terms of a Boltzmann factor with an 'effective temperature', $T_{\text{eff}}$, determining the shape of the tail. These effective temperatures have been calculated for the three model systems at a range of adsorbate speeds. At high speeds the variation of $T_{\text{eff}}$ with the speed of the parameter variation is linear, in agreement with the work of Lindenblatt, Pehlke and co-workers [33]. However, at slower speeds the effective temperature follows a square-root dependence on speed. The existence of two domains for this effective temperature variation suggests a different interpretation of recent experimental results as discussed below. We are unsure of the origin of this two domain behaviour.

Thermal effects on the excitation process have been considered in chapters 5 and 6. The adsorbate level occupations and the energy transfer rates show little dependence on temperature, with only small differences between results at zero and several thousand Kelvin. The excitation spectra on the other hand are sensitive to the temperature of the system. At low temperature the excitation spectra develops a $(\epsilon - \epsilon_F)^{-1}$ like behaviour close to the Fermi level. At high temperatures this feature is smeared out into a smooth variation across the Fermi level, while at higher energies the exponential tails of the excitation spectra are enhanced. Above a threshold point of $T \approx T_{\text{eff}}$ thermal effects determine the shape of the high-energy tails of the excitation spectra. We attribute this behaviour to the availability of electrons above the Fermi level at high system temperatures, from which electrons can be excited to higher energies with the same energy input. A similar argument holds for the variation in the hole excitation spectrum.

A striking feature of the adsorbate level occupations and the electronic excitation spectrum is the symmetry in the behaviour of electrons and holes. If the energy levels for a given system are reflected in the Fermi level, the resulting time-evolution will be the same, but with the spins of the states reversed and electrons replaced by holes.

The final chapter of results in this thesis, chapter 7, applies our model to the adsorption of hydrogen isotopes on the copper and silver (111) surfaces. A set of simple parameter variations describing the interaction of a hydrogen atom with each of these surfaces was extracted from density functional theory calculations. These parameters were then used to drive our model through a single approach

to each surface for hydrogen and deuterium adsorbates[1].

The total non-adiabatic energy transfer was in the range 90-130 meV for each system, with values for H-atoms approximately 30% larger than for the heavier isotope. The excitation spectra, for the single approach to the surface under consideration, again show approximately exponential high-energy tails with effective temperatures in the region of 1200 K for H-atom calculations and 1000 K for D-atoms.

Recent experiments by Nienhaus and coworkers [18, 25] have directly observed electronic excitations generated by the adsorption of hydrogen and deuterium atoms on a metal film making up part of a thin-film Schottky diode. By taking into account angular effects and the attenuation of the electronic signal in a thin-metal film we have used our calculations to make direct comparisons with these experiments. The numbers of electrons excited over barrier heights similar to those measured in the aforementioned experiments are in broad agreement with experimental values.

Krix, Nünthel and Nienhaus [25] have recently reported a ratio of 3.7±0.7:1 for chemicurrents generated by hydrogen atoms to deuterium atoms using Ag/p-Si Schottky diodes. Our calculations suggest an isotopic ratio of 3.4:1 for these systems in good agreement with the experimental result. This isotope ratio has also been used by Krix and co-workers to obtain an effective temperature of $T_{\text{chemi}}$ = 1680 ± 300 K for the generation of chemicurrents by hydrogen atoms. The analysis used to obtain this value, reported by Lindenblatt and Pehlke [33], assumes that $T_{\text{chemi}}$ is proportional to $m^{-1/2}$, where $m$ is the adsorbate mass. This behaviour can be extracted from the forced oscillator model used by Trail and co-workers [28, 29], and is consistent with the time-dependent DFT calculations performed by Lindenblatt and Pehlke. We find that $T_{\text{chemi}}$ scales with $m^{-1/4}$ for the H/Cu and H/Ag systems, suggesting that an effective chemicurrent temperature of $T_{\text{chemi}}$ = 770 ± 150 K is more appropriate for the isotope ratio reported by Krix and co-workers. This value is much closer to the value of $T_{\text{chemi}}$ obtained from our calculations for the H/Ag system; 1004 K.

[1]The parameters for the interaction of deuterium were taken to be the same as for hydrogen, but were slowed down by a factor of $\sqrt{2}$ to account for the larger mass.

The work we have presented here suggests a number of avenues of further research. It is not obvious from the model systems considered in chapter 6 what the most important factors in the generation of electronic excitations are. Is the rate at which the adsorbate resonances broaden the principle driver of the excitation process? How important is the behaviour of the adsorbate energy levels? A broader study of the dependence of our model on the parameters $\epsilon_a$, $U$ and $\Gamma$ than that presented here may give further insight into the process of electronic excitation in the adsorption process.

In chapter 3 we have been able to take the nearly-adiabatic limit of the non-adiabatic energy transfer rate, yielding an expression that, when valid, gives some insight into the energy transfer process. Our attempts to perform a similar expansion of the electronic excitation spectrum have failed due to the presence of terms which grow continuously in time, preventing the use of slow-variation approximations. It has therefore not been possible to obtain the same insight for the excitation spectrum as for energy transfer. Trail and co-workers [29] have shown that a nearly-adiabatic, friction-based description of energy transfer is consistent with the forced oscillator model. It would be reasonable to expect the slow-variation limit of our excitation spectrum to approach that obtained from the forced oscillator model. A direct comparison of the excitation spectra from the two models for slowly-evolving systems would allow the validity of the nearly-adiabatic approximation to be assessed.

The work we have performed in chapter 7 has only considered a single approach of an adsorbate to the surface. In a real adsorption event the adsorbate will oscillate back and forth in the surface potential well, losing energy with each oscillation. Such an event could be considered by periodically varying the parameters $\Gamma$ and $\epsilon_a$ to simulate the movement of the adsorbate above the surface. A slow decay in the amplitude of the parameter variation could also be used to imitate the loss of energy to the surface. This procedure would however be difficult to perform with our current methods because numerical accuracy is difficult to maintain over long calculations. It would also be interesting to address one question; does the adsorbate, as described by our model, re-polarise as it passes the adiabatic spin-transition while moving away from the surface? This would indicate whether the single pass through the spin-transition that we have simulated is the dominant contribution to the electronic excitation process.

Perhaps the most crude approximation used in our analysis is the wide-band approximation, which assumes that the surface with which the adsorbate is interacting consists of a featureless, infinite band of metallic states. Real metals do not have this infinite band of states and it would therefore be useful to investigate the impact of surface electronic structure on the excitation spectra. In an ideal world we would use a first principles technique, such as time-dependent DFT to investigate such systems. However, current state-of-the-art DFT methods require significant computational effort, which makes it very difficult to investigate a wide range of systems, particularly those that include transition metals. It may therefore be more instructive to use less rigorous techniques. One method which is theoretically straightforward, but includes some features of the electronic structure of the metal surface and adsorbate is the time-dependent tight-binding method used by Todorov [82]. In the tight-binding approximation the electronic wave-functions are constructed from a linear combination of atomic orbitals. Time-independent tight-binding methods have been found to be useful for modelling a large range of systems, including those with d-orbitals. Generalisation of this time-dependent formalism should provide a more realistic description of the adsorption process. It would then be possible for a wider range of molecular adsorbates to be investigated, such as the NO/Au system for which exo-electron emission has been observed [26,27] and chemicurrent excitation in the O/Ag and NO/Ag systems [20, 21].

# References


[1] C. B. Duke. "The birth and evolution of surface science: Child of the union of science and technology." Proc. Natl. Acad. Sci. U. S. A, **100**, 3858 (2003).

[2] G. R. Darling and S. Holloway. "The dissociation of diatomic molecules at surfaces." Rep. Prog. Phys., **58**, 1595 (1995).

[3] T. Greber. "Charge-transfer induced particle emission in gas surface reactions." Surf. Sci. Rep., **28**(1-2), 1 (1997).

[4] A. Groß. "Reactions at surfaces studied by ab initio dynamics calculations." Surf. Sci. Rep., **32**, 291 (1998).

[5] R. G. Parr and W. Yang. *Density-functional theory of atoms and molecules*. Oxford University Press New York (1989).

[6] M. Born and R. Oppenheimer. "On the quantum theory of molecules." Ann. Phys. (Berlin), **84**, 457 (1927).

[7] A. M. Wodtke, J. C. Tully and D. J. Auerbach. "Electronically non-adiabatic interactions of molecules at metal surfaces: Can we trust the Born-Oppenheimer approximation for surface chemistry?" Int. Rev. Phys. Chem., **23**(4), 513 (2004).

[8] P. W. Anderson. "Infrared catastrophe in Fermi gases with local scattering potentials." Phys. Rev. Lett., **18**(24), 1049 (1967).

[9] J. K. Nørskov, D. M. Newns and B. I. Lundqvist. "Molecular orbital description of surface chemiluminescence." Surf. Sci., **80**, 179 (1979).

[10] A. Zangwill. *Physics at surfaces*. Cambridge University Press (1988).

[11] H. Metiu and J. W. Gadzuk. "Theory of rate processes at metal surfaces. II. The role of substrate electronic excitations." J. Chem. Phys., **74**(4), 2641 (1981).

[12] H. J. Krebs and H. Lüth. "Evidence for two different adsorption sites of CO on Pt(111) from infrared reflection spectroscopy." Appl. Phys. A: Mater. Sci. Process., **14**(4), 337 (1977).

[13] B. N. J. Persson and M. Persson. "Vibrational lifetime for CO adsorbed on Cu (100)." Solid State Commun., **36**(2), 175 (1980).

[14] B. N. J. Persson and M. Persson. "Damping of vibrations in molecules adsorbed on a metal surface." Surf. Sci., **97**(2), 609 (1980).

[15] M. Gostein, W. Watts and G. O. Sitz. "Vibrational relaxation of $H_2(\nu = 1, J = 1)$ on Pd (111)." Phys. Rev. Lett., **79**(15), 2891 (1997).

[16] E. Watts, G. O. Sitz, D. A. McCormack, G. J. Kroes, R. A. Olsen, J. A. Groeneveld, J. N. P. Van Stralen, E. J. Baerends and R. C. Mowrey. "Rovibrationally inelastic scattering of ($\nu$=1, j=1) $H_2$ from Cu(100): Experiment and theory." J. Chem. Phys., **114**(1), 495 (2001).

[17] L. C. Shackman and G. O. Sitz. "State-to-state scattering of D[sub 2] from Cu(100) and Pd(111)." J. Chem. Phys., **123**(6), 064712 (2005).

[18] H. Nienhaus, H. S. Bergh, B. Gergen, A. Majumdar, W. H. Weinberg and E. W. McFarland. "Electron-hole pair creation at Ag and Cu surfaces by adsorption of atomic hydrogen and deuterium." Phys. Rev. Lett., **82**(2), 446 (1999).

[19] H. Nienhaus, H. S. Bergh, B. Gergen, A. Majumdar, W. H. Weinberg and E. W. McFarland. "Selective H atom sensors using ultrathin Ag/Si Schottky diodes." Appl. Phys. Lett., **74**(26), 4046 (1999).

[20] B. Gergen, H. Nienhaus, W. H. Weinberg and E. W. McFarland. "Chemically induced electronic excitations at metal surfaces." Science, **294**(5551), 2521 (2001).

[21] B. Gergen, S. J. Weyers, H. Nienhaus, W. H. Weinberg and E. W. McFarland. "Observation of excited electrons from nonadiabatic molecular reactions of NO and $O_2$ on polycrystalline Ag." Surf. Sci., **488**, 123 (2001).

[22] H. Nienhaus, B. Gergen, W. H. Weinberg and E. W. McFarland. "Detection of chemically induced hot charge carriers with ultrathin metal film Schottky contacts." Surf. Sci., **514**, 172 (2002).

[23] S. Glass and H. Nienhaus. "Continuous monitoring of Mg oxidation by internal exoemission." Phys. Rev. Lett., **93**(16), 168302 (2004).

[24] H. Nienhaus and S. Glass. "Probing the distribution of hot charge carriers generated in Mg surfaces by oxidation." Surf. Sci., **600**(18), 4285 (2006).

[25] D. Krix, R. Nünthel and H. Nienhaus. "Generation of hot charge carriers by adsorption of hydrogen and deuterium atoms on a silver surface." Phys. Rev. B, **75**, 073410 (2007).

[26] J. D. White, J. Chen, D. Matsiev, D. J. Auerbach and A. M. Wodtke. "Conversion of large-amplitude vibration to electron excitation at a metal surface." Nature, **433**(7025), 503 (2005).

[27] J. D. White, J. Chen, D. Matsiev, D. J. Auerbach and A. M. Wodtke. "Vibrationally promoted electron emission from low work-function metal surfaces." J. Chem. Phys., **124**(6), 64702 (2006).

[28] J. R. Trail, M. C. Graham, D. M. Bird, M. Persson and S. Holloway. "Energy loss of atoms at metal surfaces due to electron-hole pair excitations: First-principles theory of 'chemicurrents'." Phys. Rev. Lett., **88**(16), 166802 (2002).

[29] J. R. Trail, D. M. Bird, M. Persson and S. Holloway. "Electron-hole pair creation by atoms incident on a metal surface." J. Chem. Phys., **119**(8), 4539 (2003).

[30] J. Van Heys, M. Lindenblatt and E. Pehlke. "Molecular-dynamics simulations of non-adiabatic processes at surfaces." Phase Transitions, **78**(9), 773 (2005).

[31] M. Lindenblatt, J. Van Heys and E. Pehlke. "Molecular dynamics of nonadiabatic processes at surfaces: Chemisorption of H/Al (111)." Surf. Sci., **600**(18), 3624 (2006).

[32] M. Lindenblatt, E. Pehlke, A. Duvenbeck, B. Rethfeld and A. Wucher. "Kinetic excitation of solids: The concept of electronic friction." Nucl. Instrum. Methods Phys. Res., Sect. B, **246**(2), 333 (2006).

[33] M. Lindenblatt and E. Pehlke. "Time-dependent density-functional molecular-dynamics study of the isotope effect in chemicurrents." Surf. Sci., **600**(23), 5068 (2006).

[34] M. Lindenblatt and E. Pehlke. "Ab initio simulation of the spin transition during chemisorption: H/Al (111)." Phys. Rev. Lett., **97**(21), 216101 (2006).

[35] P. W. Anderson. "Localized magnetic states in metals." Phys. Rev., **124**(1), 41 (1961).

[36] D. M. Newns. "Self-consistent model of hydrogen chemisorption." Phys. Rev., **178**(3), 1123 (1969).

[37] S. M. Sze. *Physics of semiconductor devices*. Wiley, New York, 2nd edition (1981).

[38] J. W. Gadzuk. "On the detection of chemically-induced hot electrons in surface processes: from X-ray edges to Schottky barriers." J. Phys. Chem. B, **106**, 8265 (2002).

[39] B. Mildner, E. Hasselbrink and D. Diesing. "Electronic excitations induced by surface reactions of H and D on gold." Chem. Phys. Lett., **432**, 133 (2006).

[40] B. Roldan-Cuenya, H. Nienhaus and E. W. McFarland. "Chemically induced charge carrier production and transport in Pd/ $SiO_2$/ n-Si (111) metal-oxide-semiconductor Schottky diodes." Phys. Rev. B, **70**(11), 115322 (2004).

[41] Y. Huang, A. M. Wodtke, H. Hou, C. T. Rettner and D. J. Auerbach. "Observation of vibrational excitation and deexcitation for NO (v= 2) scattering from Au (111): evidence for electron-hole pair mediated energy transfer." Phys. Rev. Lett., **84**(13), 2985 (2000).

[42] Y. Huang, C. T. Rettner, D. J. Auerbach and A. M. Wodtke. "Vibrational promotion of electron transfer." Science, **290**(5489), 111 (2000).

[43] E. G. d'Agliano, P. Kumar, W. Schaich and H. Suhl. "Brownian motion model of the interactions between chemical species and metallic electrons: Bootstrap derivation and parameter evaluation." Phys. Rev. B, **11**(6), 2122 (1975).

[44] A. Blandin, A. Nourtier and D. W. Hone. "Localized time-dependent perturbations in metals–Formalism and simple examples." J. Phys. (Paris), **37**(4), 369 (1976).

[45] J. R. Trail, M. C. Graham and D. M. Bird. "Electronic damping of molecular motion at metal surfaces." Comp. Phys. Comm., **137**(1), 163 (2001).

[46] B. Hellsing and M. Persson. "Electronic damping of atomic and molecular vibrations at metal surfaces." Phys. Scr., **29**, 360 (1984).

[47] M. Head-Gordon and J. C. Tully. "Molecular dynamics with electronic frictions." J. Chem. Phys., **103**(23), 10137 (1995).

[48] A. C. Luntz, M. Persson and G. O. Sitz. "Theoretical evidence for nonadiabatic vibrational deexcitation in $H_2$ ($D_2$) state-to-state scattering from Cu(100)." J. Chem. Phys., **124**(9), 091101 (2006).

[49] K. Schönhammer and O. Gunnarsson. "Localized dynamic perturbations in metals." Z. Phys. B: Condens. Matter, **38**(2), 127 (1980).

[50] R. Brako and D. M. Newns. "Slowly varying time-dependent local perturbations in metals: a new approach." J. Phys. C: Solid State Phys., **14**(21), 3065 (1981).

[51] R. Brako and D. M. Newns. "Theory of electronic processes in atom scattering from surfaces." Rep. Prog. Phys., **52**(6), 655 (1989).

[52] A. Yoshimori and K. Makoshi. "Time-dependent Newns-Anderson model." Prog. Surf. Sci., **21**(3), 251 (1986).

[53] A. C. Hewson. *The Kondo problem to heavy fermions.* Cambridge University Press (1997).

[54] D. C. Langreth and P. Nordlander. "Derivation of a master equation for charge-transfer processes in atom-surface collisions." Phys. Rev. B, **43**(4), 2541 (1991).

[55] H. Shao, D. C. Langreth and P. Nordlander. "Many-body theory for charge transfer in atom-surface collisions." Phys. Rev. B, **49**(19), 13929 (1994).

[56] H. Shao, P. Nordlander and D. C. Langreth. "Nonadiabatic effects in charge transfer in atom-surface scattering." Phys. Rev. B, **52**(4), 2988 (1995).

[57] K. Makoshi, H. Kawai and A. Yoshimori. "Charge transfer in Hartree-Fock approximation of time-dependent Anderson model." J. Phys. Soc. Jpn., **53**(8), 2441 (1984).

[58] A. Yoshimori, K. Makoshi and H. Kawai. *Dynamical processes and ordering on solid surfaces*, volume 59 of *Springer Series in Solid-State Sciences*, pages 74–80. Springer-Verlag (1985).

[59] D. M. Bird, M. Persson, J. R. Trail and S. Holloway. "Dynamics of the spin transition in the adsorption of hydrogen atoms on metals." Surf. Sci., **566-568**, 761 (2004).

[60] M. S. Mizielinski, D. M. Bird, M. Persson and S. Holloway. "Electronic nonadiabatic effects in the adsorption of hydrogen atoms on simple metals." J. Chem. Phys., **122**(8), 084710 (2005).

[61] M. S. Mizielinski, D. M. Bird, M. Persson and S. Holloway. "Spectrum of electronic excitations due to the adsorption of atoms on metal surfaces." J. Chem. Phys., **126**(3), 034705 (2007).

[62] B. L. Burrows and A. T. Amos. "Wide-band approximation in the theories of charge transfer during ion-surface scattering." Phys. Rev. B, **49**(8), 5182 (1994).

[63] M. Plihal and D. C. Langreth. "Role of intra-adsorbate Coulomb correlations in energy transfer at metal surfaces." Phys. Rev. B, **58**(4), 2191 (1998).

[64] R. Brako and D. M. Newns. "Charge exchange in atom–surface scattering: Thermal versus quantum mechanical non-adiabaticity." Surf. Sci., **108**(2), 253 (1981).

[65] S. Doniach and E. H. Sondheimer. *Green's functions for solid state physicists*. Imperial College Press (1998).

[66] L. I. Schiff. *Quantum mechanics*. McGrawHill Book Company, 3rd edition (1968).

[67] A. Nourtier. "Friction coefficient of atoms near a metal surface." J. Phys. (Paris), **38**(5), 479 (1977).

[68] R. Baierlein. *Thermal physics*. Cambridge University Press (1999).

[69] E. N. Economou. *Green's functions in quantum physics.* Springer Series in Solid State Sciences (1990).

[70] W. H. Press, B. P. Flannery, S. A. Teukolsky and W. T. Vetterling. *Numerical recipes in FORTRAN 77: The art of scientific computing.* Cambridge University Press (1992).

[71] C. Kittel. *Introduction to solid state physics.* Wiley New York (1996).

[72] M. D. Segall, P. J. D. Lindan, M. J. Probert, C. J. Pickard, P. J. Hasnip, S. J. Clark and M. C. Payne. "First-principles simulation: ideas, illustrations and the CASTEP code." J. Phys.: Condens. Matter, **14**(11), 2717 (2002).

[73] D. R. Lide and F. H. P. R., editors. *CRC handbook of chemistry and physics.* CRC Press, Inc. (1994).

[74] D. Vanderbilt. "Soft self-consistent pseudopotentials in a generalized eigenvalue formalism." Phys. Rev. B, **41**(11), 7892 (1990).

[75] S. L. Cunningham. "Special points in the two-dimensional Brillouin zone." Phys. Rev. B, **10**(12), 4988 (1974).

[76] J. P. Perdew, K. Burke and M. Ernzerhof. "Generalized gradient approximation made simple." Phys. Rev. Lett., **77**(18), 3865 (1996).

[77] K. Niedfeldt, E. A. Carter and P. Nordlander. "First principles resonance widths for Li near an Al(001) surface: Predictions of scattered ion neutralization probabilities." J. Chem. Phys., **121**(8), 3751 (2004).

[78] K. Niedfeldt, P. Nordlander and E. A. Carter. "Mechanism of enhanced broadening of the ionization level of Li outside transition metal surfaces." Phys. Rev. B, **74**(11), 115109 (2006).

[79] K. Niedfeldt, P. Nordlander and E. A. Carter. "Prediction of structure-dependent charge transfer rates for a Li atom outside a Si(001) surface." Surf. Sci. Lett., **601**(5), L29 (2007).

[80] H. Nienhaus. "Electronic excitations by chemical reactions on metal surfaces." Surf. Sci. Rep., **45**(1-2), 1 (2002).

[81] G. B. Arfken and H. J. Weber. *Mathematical methods for physicists.* Harcourt Academic Press, 5th edition (2001).

[82] T. N. Todorov. "Time-dependent tight binding." J. Phys.: Condens. Matter, **13**(45), 10125 (2001).